Assessment of the water quality in an urban environment

A case study from Torshovdalen (Oslo, Norway)

Ingrid Emilsen Kristiansen

Master Thesis in Geosciences

Geochemistry and Mineralogy

60 credits

Department of Geosciences

Faculty of Mathematics and Natural Sciences

UNIVERSITY OF OSLO

March 2019

Assessment of the water quality in an urban environment.

A case study from Torshovdalen (Oslo, Norway)

Ingrid Emilsen Kristiansen

Master Thesis in Geosciences

Geochemistry and Mineralogy

60 credits

Department of Geosciences

Faculty of Mathematics and Natural Sciences

UNIVERSITY OF OSLO

March 2019

2019

Assessment of the water quality in an urban environment. A case study from Torshovdalen (Oslo, Norway)

Ingrid Emilsen Kristiansen

http://www.duo.uio.no/

Trykk: Reprosentralen, Universitetet i Oslo

Abstract

Oslo is one of many cities that is facing new challenges in handling urban runoff water. In recent years, climate changes have led to extreme weather events and increased rainfall. In urban settings, these events lead to the generation of large volume of surface runoff in short time periods which demand innovative solutions in what regards stormwater management. The Stormwater Management Strategy for Oslo, adopted in 2014, aims to reduce the risk of flooding and contribute to the achievement of a blue-green city where surface waterways are actively used and an important component of the urban landscape.

At present, Torshovbekken water way runs in pipelines below the valley profile of Torshovdalen and is, therefore, a part of a combined sewage system where urban runoff and sewage are led into the same pipeline before processing at a sewage treatment plant. The capacity of culverted waterways is often limited. During periods with heavy rainfall, culverted waterways (combined sewage systems) can be overloaded, resulting in flood events, damage of infrastructure and sewage overflow. The stormwater related problems in the area surrounding Torshovdalen have motivated an interdisciplinary student project led by The Agency of Water and Wastewater, City of Oslo. This master thesis has, as an integral part of the project, been focused on the water quality in Torshovbekken watershed, including natural and anthropogenic inputs. To assess the water quality and identify the change in water chemistry from rainwater to groundwater, several water and sediment samples were analyzed and compared. The samples reveal a change in the water chemistry, starting with a highly diluted sodium-chloride type of rainwater, and evolving into a calcium-chloride type of water in an ephemeral spring, open waterways and groundwater. The results from the groundwater were also used to evaluate the distribution of major and trace elements from the Cambro-Silurian bedrock, showing that dissolution and weathering of minerals highly affect the groundwater quality. Additionally, leachate from old seawater and anthropogenic inputs are important factors contributing to the chemical composition of the groundwater. Sediments samples collected in Torshovdalen were used to assess the geochemical processes that occur in the unsaturated zone and providing information regarding the mineralogy and chemistry of the bedrock. The consequence of intensive rainfall and increasing volume of runoff water due to seasonal climate changes in an urban environment has been evaluated by collecting water samples during dry and wet periods. These samples were analyzed for Escherichia coli (*E. coli*), a bacteria used as an indicator for recent faecal contamination. Results show that the highest values of *E. coli*, in Akerselva, are detected shortly after heavy rainfall, which can be linked to overloaded sewage systems and sewage leaking.

Acknowledgments

First and foremost, I would like to thank my main supervisor Clara Sena, University of Oslo, for her guidance. I have really enjoyed our meetings and I am truly grateful to have you as my supervisor. Thank you for motivating me, giving me very good and constructive feedback and sharing your enormous knowledge! I would also like to thank my co-supervisors Julia Kvitsjøen (The Agency of Water and Wastewater, VAV) and Anja Sundal (University of Oslo) for all the help during the last year and for always being supportive and giving me the opportunity to be a part of the project!

A big thank you to all the friendly, helpful and kind professors and staff at the Department of Geoscience. Firstly, I must express a special thanks to Mufak Said Naoroz for helping me with the chemical analysis and Thanusha Naidoo for all the help I got before running the XRF and XRD machine, I really enjoyed working with the two of you. Thank you for always smiling and laughing, and for making the lab-work easy and fun at the same time! Also, many thanks to Magnus Kristoffersen for help with the QICPMS analyses.

I would also like to thank all the interesting people I have met at VAV. Thanks to Karl Friedrich Eckner for giving me guidance and knowledge about *E. coli* analysis and Anna- Lena Beschorner for sharing her experience and knowledge regarding the water quality in Akerselva. I must also thank Tharan Furgursen for continuously giving me advice and sharing her passion regarding the topic.

Thanks to NGI, especially Tor Overskeid and Audun Dalene Bjerga, for the installation of the three groundwater wells in Torshovdalen, the geophysical borehole logging and the laboratory work.

I must also express a special thanks to my good friend, Maria Uglum, for the excellent teamwork and support the last two years at the University of Oslo.

A big thank you to my fellow student friends for daily support and all the amazing people in the running group BUL!

Finally, I want to thank my family and friends. Thank you for always motivating and supporting me and showing your interest in my work. I truly appreciate all you have done for me!

Petter, you have been, and still are, fantastic! Thank you for always having my back.

Everyone, thank you so much!

Ingrid Emilsen Kristiansen, March 2019

Table of contents

Abstract ... **iii**

Acknowledgments ... **v**

Table of contents ... **vii**

List of figures ... **xi**

List of tables ... **xvi**

List of equations ... **xviii**

1. Introduction ... **1**

1.1. Thesis outline ... 2

1.2. Aim of study ... 2

2. Study area ... **3**

2.1. Geographical location ... 3

2.2. Geological background ... 4

2.3. Torshovdalen and Torshovbekken watershed ... 7

3. Theoretical background ... **9**

3.1. The hydrological cycle ... 9

3.2. Urban hydrology ... 10

3.2.1. Climate ... 12

3.2.2. Water quality ... 14

3.2.3. Escherichia coli as an indicator of faecal contamination ... 16

4. Materials and methods ... **19**

4.1. Field-methods ... 19

4.1.1. Collecting sample material ... 19

4.1.2. Drilling of groundwater wells and geophysical logging ... 22

4.1.3. Hydrochemical field parameters; pH, temperature, electrical conductivity ... 24

4.1.4. In-situ infiltration tests ... 25

4.2. Methods applied for water analysis ... 26

4.2.1. Alkalinity ... 26

4.2.2. Ion chromatography 27
4.2.3. Determination of soluble silicate 28
4.2.4. Quadrupole Inductively Coupled Plasma Mass Spectrometer 29
4.2.5. Extraction of dissolved species in the unsaturated zone 29
4.2.6. Colilert – 18 30
4.3. Methods applied for sediment analysis 31
4.3.1. Loss on ignition 32
4.3.2. X-ray fluorescence (XRF) 33
4.3.3. X-ray diffraction (XRD) 34
4.3.4. Grain size distribution 37
5. Results 39
5.1. Sampling campaigns 39
5.2. Water chemistry characterization 40
5.2.1. Rainwater 44
5.2.2. Grefsen 46
5.2.3. Akerselva 49
5.2.4. Torshovdalen - Ephemeral spring 53
5.2.5. Torshovdalen – The unsaturated zone 55
5.2.6. Torshovdalen - Groundwater wells 59
5.2.7. Bivariate analysis 61
5.3. Bacterial characterizations 63
5.3.1. Grefsen 64
5.3.2. Akerselva 64
5.3.3. Torshovdalen – ephemeral spring 65
5.3.4. Torshovdalen - Groundwater 66
5.4. Physical and chemical properties of the soil and sediments 67
5.4.1. XRD Bulk mineralogy 67
5.4.2. Major element geochemistry 71

5.4.3. Clay fraction XRD 74
5.4.4. Infiltration test and grain size distribution 78
5.5. Geophysical borehole logging 82
6. Discussion 85
6.1. Rainwater 85
6.1.1. Water chemistry characterization 85
6.2. Surface water – Grefsen and Akerselva 87
6.2.1. Major inorganic ions 87
6.2.2. Trace elements 90
6.2.3. Field parameters 91
6.2.4. Bacterial characterization 92
6.3. Subsurface water – Ephemeral spring 93
6.3.1. Major inorganic ions 93
6.3.2. Trace elements 96
6.3.3. Field parameters 96
6.3.4. Bacterial characterization 97
6.4. Unsaturated zone 99
6.4.1. Major inorganic ions, mineralogy and geochemistry 99
6.4.2. Trace elements 101
6.5. Groundwater 102
6.5.1. Weathering and dissolution of minerals 104
6.5.2. Effect of old seawater 105
6.5.3. Anthropogenic sources 105
6.5.4. Trace elements 106
6.5.5. Field parameters 107
6.5.6. Bacterial characterization 108
6.6. Bivariate analysis of water samples 109
6.7. Geophysical logging 111

6.8. Daylighting of Torshovbekken 111

7. Conclusion 113

7.1. Recommendations for further work 115

References 117

Appendix A: Groundwater wells 127

Appendix B: Chemical data of water samples 131

Appendix C: XRD analysis 141

Appendix D: XRF data 153

Appendix E: Unsaturated zone 157

List of figures

Figure 2.1. Map showing the location of the study area, Oslo (Norway).The photo is modified in QGIS. 3

Figure 2.2. Simplified geological map of the Oslo area. The study area (marked with a red cycle) is located in the Lower Palaeozoic sediments (Bjørnlykke, 2004). 4

Figure 2.3. Stratigraphy of the Lower Palaeozoic of the Oslo Area (Bjørnlykke, 2004). 6

Figure 2.4. Map showing Torshovbekken watershed in Oslo. The river Torshovbekken was originally a tributary of Akerselva but is today a part of the combined sewage system. 7

Figure 3.1. The global hydrological cycle describes the storage and circulation of water between the biosphere, atmosphere, lithosphere and the hydrosphere. From Pidwirny (2006). 10

Figure 3.2. Demonstration of how urbanization affects the infiltration and runoff. An increasing amount of impervious surface area results in a higher volume of runoff water, lower evaporation and infiltration. From County (1999). 11

Figure 3.3. The urban water cycle is strongly influenced by human made activities, resulting in air pollution, leaching from landfills, septic tanks and sewage systems, agriculture etc. From Marsalek et al. (2014) 12

Figure 3.4. The Stormwater three-step Approach,including;1) catch and infiltrate, 2) delay and retain and 3) safe floodways. The figure is modified from Miljødirektoratet (2016) 13

Figure 3.5: a) Daylighting of Hovinbekken and b) Teglveksdammen. Photos from Gulde (2017). 14

Figure 3.6. a) Sørenga is located in the southern part of Oslo, very close to the river mount of Akerselva, b) the area is popular for bathing during the summer, from (Roald, 2018). 16

Figure 4.1. Maps showing the location of where the water samples were collected. A3 (from Akerselva) is monitored by VAV. G1 is located close to the hiking path to Grefsenkollen. W1, W2 and T1 are located in Torshovdalen, while A1, A2 and A3 represent water samples from Akerselva. 20

Figure 4.2. Sediment samples were collected from an auger, here showing the auger from well W2. Photo a) taken by Sena, C, photo b) taken by Kristiansen, I). 22

Figure 4.3. Map of the installed groundwater wells in Torshovdalen (W1, W2 and W3). Geophysical borehole logging was performed in holes drilled close to W1 and W3. Sediment samples were taken from each location. 23

Figure 4.4. Configuration of ion chromatography. From Naoroz (2016b). 27

Figure 4.5. a) Formation of o-nitrophenol (b) and 4-methylumbelliferone. From IDEXX (2006). 30

Figure 4.6. Overview of an X-ray tube where the X-rays are generated. The electrons are directed towards the target in a high-voltage vacuum, and X-rays are generated as the electrons collide with the target. From Leng (2009). 35

Figure 5.1. Registered precipitation during the water sampling period from 01.05.2018 – 15.11.2018, together with average daily air temperature. The data are registered at Blindern, Oslo (eklima.met.no). 40

Figure 5.2. Bulk chemical composition of water samples plotted in a Piper diagram. As seen in the diamond shaped diagram, most of the samples are of calcium-chloride type. The rainwater contains more sodium, potassium and magnesium, and the sample from Grefsen contains more calcium compared to the other samples. 43

Figure 5.3. Results of the trace element analysis (QICPMS) of the water samples from Akerselva (A1-2, A2-2), Torshovdalen (ephemeral spring T1-2 and groundwater wells W3-1, W3-2, W1-1) and Grefsen (G1-1). 44

Figure 5.4. Cation and anion concentration in rainwater (R1) collected 21.09.2018. Chloride and sodium are the dominating cation and anion. 44

Figure 5.5. Temperature, pH and EC in rainwater (R1) collected 21.09.2018. 45

Figure 5.6. Average cation and anion concentration in precipitation, measured at Norwegian stations in 2017 (the results are modified from Aas (2018) and compared to the result obtained from Blindern 21.09.2018). 46

Figure 5.7. Cation and anion concentration in the stream located in Grefsen (G1-1 and G1-2). Calcium and sodium were the dominating cations. Chloride and sulphate were the dominating anions. 47

Figure 5.8. Temperature, pH and electrical conductivity (EC on the secondary axis) in a water stream located in Grefsen (G1-1 and G1-2). 47

Figure 5.9. Trace element analysis from Grefsen (G1-1). Strontium, iron and aluminium are the dominant elements. 48

Figure 5.10. Water samples was collected from the sampling point A1 and A2 in Akerselva. A3 is the location of were VAV collects weekly samples for E. coli analysis. 49

Figure 5.11. Cation and anion concentration in Akerselva at location A1 in the three sampling campaigns. Chloride and calcium are the dominant ions. The samples from 12.11.18 show a higher concentration for all elements. 50

Figure 5.12. Cation and anion concentration in Akerselva at location A2 in the three sampling campaigns. Chloride and calcium are the dominant ions. The samples from 12.11.18 show a higher concentration for all elements. 50

Figure 5.13. pH, EC (electrical conductivity) and temperature measured in the water during three sampling campaigns in Akerselva and Torshovdalen (10.05.2018; A1-1, A2-1, T1-1. 23.05.2018; A1-2, A2-2, T1-2. 12.11.2018; A1-3, A2-3, T1-3). 51

Figure 5.14. Trace element analysis of samples from Akerselva on the 23rd May 2018. Aluminium, iron and strontium are the dominant trace elements. 52

Figure 5.15. Cation and anion concentration from the ephemeral spring in Torshovdalen (T1) in the three sampling campaigns. T1-1 was collected 10.05.2018, T1-2 was collected 23.05.2018 and T1-3 was collected 12.11.2018. Chloride, calcium and sodium are the dominant ions. 53

Figure 5.16. Trace element analysis from the ephemeral spring in Torshovdalen (T1-2). Strontium, zinc, iron and boron are the dominant elements. 54

Figure 5.17. Chemical composition of major cations and anions in the unsaturated zone in Torshovdalen, given in mg/g of dry sediments. The samples collected from each location (W1, W2 and W3) are plotted stratigraphically. 56

Figure 5.18. Chemical composition of trace elements in the unsaturated zone in from groundwater well W1 in Torshovdalen. All elements are given in µg/g dry weight of sediments. The concentration of manganese (Mn) in the water sample W1-L2.5 is divided by 10. 57

Figure 5.19. Chemical composition of trace elements in the unsaturated zone in from groundwater well W3 in Torshovdalen. All elements are given in µg/g dry weight of sediments. The concentration of manganese (Mn) in the water sample W3-L4 is divided by 10. 58

Figure 5.20. Chemical composition of trace elements in the unsaturated zone in from groundwater well W1 in Torshovdalen. All elements are given in µg/g dry weight of sediments. 58

Figure 5.21. Water samples representing the groundwater was collected from the well W1 and W3 (the samples W3-1 and W3-2). Three samples were also taken from the ephemeral spring (T1-1, T1-2 and T1-3), described in section 5.2.4. 59

Figure 5.22. Cation and anion concentration in groundwater wells from Torshovdalen, W1 and W3. Sodium and calcium are the dominating cations, and chloride and sulphate the dominating anions. 60

Figure 5.23. Temperature, pH and EC (secondary axis) measured in groundwater wells from Torshovdalen, W1 and W3. 60

Figure 5.24. Trace element analysis from the groundwater wells (W1 and W3) in Torshovdalen. Strontium, iron and manganese are the dominant elements. 61

Figure 5.25. Scatter plot between (a) Na vs Cl (b) Ca cs Cl (c) K vs Fe (d) Na vs As (e) Ca vs As (f) Cl vs As (g) Na vs Ca (h) Mg vs Sr (i) Mn vs Sr. 62

Figure 5.26. The concentration of E. coli bacteria/100mL water sample, at A3, weekly since February 19th – November 5, 2018. Highest measured concentration was achieved on September 10, 2018, concomitant with high precipitation rate. The precipitation reflects the amount registered 24 hours before the water samples were collected. 64

Figure 5.27. The concentration of E. coli bacteria/100mL water sample, at A1 and A2. Highest concentration from both locations were achieved June 18, 2018, together with heavy rainfall the last 24 hours. The precipitation reflects the amount registered 24 hours before the water samples were collected. 65

Figure 5.28. The concentration of E.coli bacteria/100 mL water sample from the ephemeral spring in Torshovdalen (T1). Opposite trend, compared to Akerselva, are observed as the lowest concentration was measured after heavy rainfall during the 24 hours that preceded the water sample collection. 66

Figure 5.29. Weight % of the bulk composition from the loose sediments and bedrock in well W1. The samples are plotted stratigraphically are colored according to different facies associations. 68

Figure 5.30. Weight % of the bulk composition from the loose sediments and bedrock in well W2. The samples are plotted stratigraphically are colored according to different facies associations. 69

Figure 5.31. Weight % of the bulk composition from the loose sediments in section W3. The samples are plotted stratigraphically are colored according to different facies associations. 69

Figure 5.32. Major element geochemistry obtained from XRF analysis in the ten sediment samples collected from the groundwater wells W1, W2 and W3, in Torshovdalen 72

Figure 5.33. Overview of the trace elements (mg/L) obtained from XRF analysis of press pellets. From the graph, it is possible to see that there are some differences regarding the concentration of each element, but all samples have a relatively similar trend. 73

Figure 5.34. Sample W2-L1: X-ray diffraction analysis of the clay fraction, identified peak pattern fits into Illite and chlorite. Black = untreated, red = ethylene glycol treatment, grey = heated at 350 °C, green = heated at 550 °C 75

Figure 5.35. Sample W3-L4: X-ray diffraction analysis of the clay fraction, identified peak pattern fits into Illite and chlorit. Black = untreated, red = ethylene glycol treatment, grey = heated at 350 °C, green = heated at 550 °C 76

Figure 5.36. Map showing an overview of Torshovdalen with the location of eleven in-situ infiltration tests 78

Figure 5.37. Infiltration capacity measured in Torshovdalen. ”Round” is used to explain when the cylinder is emptied and filled up with water again. 79

Figure 5.38. Grain size distribution from the upper 10 cm of the soil at TD1, TD2 and TD3 (all located in the northern part of Torshovdalen. 80

Figure 5.39. Grain size distribution from the upper 10 cm of the soil at TD4 and TD6 (both located in the middle of Torshovdalen. 80

Figure 5.40. Grain size distribution from the upper 10 cm of the soil at TD9 and TD11 (both located in the southern part of Torshovdalen. 81

Figure 5.41. Geophysical borehole logging near well 1. A change in the resistivity and the natural gamma ray are observed at 7.5, 8, 9 and 10 meters below the surface. The logging was performed by NGI on the 14.09.2018, and includes; Optical Televiewer, Acoustic Televiewer, Natural gamma ray, Resistivity and Caliper. 83

Figure 5.42. Geophysical borehole logging near well 3. A peak is observed around 16-17 meters depth and a fracture in the bedrock is observed at 18.5 meters below the surface. The logging was performed by NGI on the 14.09.2018, and includes; Optical Televiewer, Acoustic Televiewer, Natural gamma ray, Resistivity and Caliper 84

Figure 6.1. The change in water chemistry from rainwater to the stream in Grefsen (G1-1 and G1-2) and the river Akerselva from the samplingpoint A2;A2-1, A2-2 and A2-3). The concentration of major cations and anions are significantly higher in the stream in Grefsen compared to Akerselva. Silica was not measured for the rainwater sample R1.Note the different scale on the y-axis. 88

Figure 6.2. The change in the water quality from the rainwater to the ephemeral spring is due to several processes, resulting in a high concentration of the major cations and anions in the ephemeral spring. A change in the concentration was observed in samples T1-3, collected after heavy rainfall on the 11.12.2018. Akerselva, located downstream is made up of rainwater, subsurface water and groundwater. 94

Figure 6.3. Location of the observed pipe line (yellow line) in Torshovdalen, close to the ephemeral spring (T1). W1, W2 and W3 show the location of the installed groundwater wells. Several combined sewage system pipelines are located in and near Torshovdalen (red line). Information regarding the sewage system pipelines in Torshovdalen and the surrounding area are modified from the Agency for Water and Sewerage in Oslo municipality. Photo of the pipeline was taken by Uglum, M. 98

Figure 6.4. The change from rainwater to groundwater involves several processes in the soil which may affect the concentration of the groundwater. As seen in the figure, the concentration from the ephemeral spring to the groundwater increase, which can be due to various processes. The unsaturated zone is not shown graphically in the figure as the concentrations are calculated (c.f. section 4.2.5.) and significantly lower compared to the other water samples (c.f. section 5.2.5.). 103

List of tables

Table 3.1. Classification of bathing water in saltwater. MPN = Most probable number. 17

Table 3.2. Classification of bathing water in freshwater. MPN = Most probable number. 17

Table 4.1. The water samples are divided into five groups with different sample codes. The codes are used when explaining the analysis and results. Groundwater samples from the well W2 were not collected and analyzed due to bentonite contamination. Coordinates are in UTM Zone 32N, ETRS89 datum. 21

Table 4.2. Overview of the sediment samples taken during the installation of three groundwater wells in Torshovdalen, together with the dates for the collection of each water samples 21

Table 4.3. Overview of the sediment samples prepared and analyzed for LOI, XRF. XRD and XRD Clay fraction. Depth below the surface is given in meters, indicating the depth of the collected sediment samples. 32

Table 5.1. Three sampling campaigns were done in Akerselva (A1 and A2) and Torshovdalen (T1). 39

Table 5.2: A total of 23 water samples have been analyzed and grouped into 4 groups based on the location. 40

Table 5.3. Total sum of cations (Sum +) and anions (Sum -) in meq/L, and the calculated electrical balance (E.B.) 41

Table 5.4. The depth in meters below the surface of each sample collected from the unsaturated zone during the drilling operation of the groundwater wells in Torshovdalen. 55

Table 5.5. Overview of the sampling points, minimum, maximum and average concentration (E. coli/100mL) and the number of measurements done at each sampling point. Results from A3 are measured by VAV. 63

Table 5.6. Overview of the soil and sediment samples collected in Torshovdalen, in September 2018. The depth is in meters below the surface 67

Table 5.7. Summary of the mineralogical composition of the sediment samples taken from the three wells drilled in Torshovdalen. The values are in weight %..... 70

Table 5.8. Estimated loss on ignition (%), gravimetric water content (%) and organic matter (%) for the 10 sediment samples collected in the wells frilled in Torshovdalen. The depth of the sampling points is also given..... 74

Table 5.9. Chemical composition (wt%) of the clay fraction of samples W2-L1 and W3-L4, as well as the calculated loss on ignition (%). 77

Table 5.10. Grain size distribution obtained from undisturbed sediments at depth 4.22m, 5.29m and 6.47m, analyzed at NGI laboratory. 81

List of equations

Eq. 3.1 9

Eq. 3.2 15

Eq. 4.1 25

Eq. 4.2 25

Eq. 4.3 26

Eq. 4.4 28

Eq. 4.5 30

Eq. 4.6 32

Eq. 4.7 33

Eq. 4.8 33

Eq. 4.9 35

1. Introduction

In the 1980s, several rivers and waterways in Oslo were enclosed in culverts and pipes. By closing the waterways, the polluted river water was covered and transported away from the urban setting. It also increased the area available for the development of housing and industrial buildings, etc. In some areas, the rivers became a part of the sewage system, a so-called combined sewage system designed to receive both stormwater and wastewater (Oslo Municipality, 2015). The trend where rivers and waterways were enclosed in pipes was reversed by the end of the 1990s due to the climate changes which made Oslo more vulnerable to the risk of flooding during heavy rainfall events.

In an urban setting, intense rainfall events lead to the generation of large volumes of surface runoff in short periods which requires innovative solutions for stormwater management. The increased amount of urban runoff from, e.g. highways, parking, industrial and agricultural areas can also result in increased supply of nutrients and pollutants that could have a negative impact on water quality.

Today, Torshovbekken, a relatively small stream, flows in a combined sewage pipe that is led into a wastewater treatment plant. Originally, this stream was a tributary of the river Akerselva which runs in an open waterway through Oslo. The Agency of Water and Wastewater (VAV), in the City of Oslo, has created an interdisciplinary project, led by Julia Kvitsjøen. The project consists of students from different academic disciplines, working with stormwater related problems within Torshovbekken watershed. Daylighting of Torshovbekken is one possible solution which can reduce the flooding events, especially in the area surrounding Torshovdalen

Daylighting of rivers and waterways (also known as deculverting) entails re-directing some or all of a waterway that was formerly buried in culverts or pipes (Pinkham, 2000). In Oslo, daylighting is an integral part of the city's climate change adaption plan, that is expected to reduce the risk of flooding during rain events. Daylighting of waterways in urban settings requires a comprehensive study of the quality, quantity and flow patterns of the urban runoff, infiltration water and groundwater before and after the opening of waterways.

Despite the importance of stormwater management in an urban area, few studies have investigated the water quality and how it is affected by increased urbanization and climate changes, in the city of Oslo. Therefore, as an integral part of the interdisciplinary project created by VAV, the master thesis presented here focuses on the water quality within the Torshovbekken watershed and attempts to highlight the importance of water quality monitoring and geochemical characterization of sediments in an urban area. In order to assess the water quality, several field campaigns were conducted between May and November 2018 and three groundwater observation wells were drilled in Torshovdalen. It is hoped that this study will contribute to a better understanding of the urban water cycle and provide VAV with information regarding the water quality in an urban area, which can be used in the process of daylighting

waterways is Oslo. The information will also be vital if daylighting of Torshovbekken is considered in the future.

1.1. Thesis outline

This thesis is composed of seven themed chapters. The second chapter (Study area) gives an overview of the geological setting and location of the study area. This chapter also provides an introduction of Torshovdalen and Torshovbekken watershed.

The third chapter (Theoretical background) presents the relevant theory.

The fourth chapter (Materials and methods) is concerned with the methodology used in this study, including the collection of sample material, field parameters, and the drilling and geophysical logging of groundwater wells in Torshovdalen. Subsequently, a description of the methods applied to water and sediment analysis is given.

The fifth chapter (Results) presents the findings of the research which are interpreted, compared and evaluated in chapter six (Discussion).

The conclusions are presented in chapter seven (Conclusion), along with recommendations for further work.

Supplementary information to this thesis is given in the Appendices A to E.

- Appendix A: Groundwater wells
- Appendix B: Chemical data of water samples
- Appendix C: XRD data
- Appendix D: XRF data
- Appendix E: The unsaturated zone

1.2. Aim of study

The main objectives of this study are to:

- Assess the water quality of the urban runoff, infiltration water and groundwater, including natural and anthropogenic inputs, and identify the change in water chemistry from rainwater to groundwater in an urban area.
- Assess the geochemical processes in the unsaturated zone.
- Observe how the Cambro-Silurian bedrock in Oslo affect the distribution of major and trace elements in the groundwater.
- Identify changes in *E. coli* concentration as a result of natural and anthropogenic inputs.

2. Study area

2.1. Geographical location

The studied area, Torshovdalen, is a valley in the southeastern part of Norway, Oslo (Figure 2.1). Oslo is a small town compared to global standards, with a population of approximately 680 000, living in the municipality of Oslo (SSB, 2018). The overall area of the municipality of Oslo is 453.7 km^2, but only one third (approximately 150 km^2) is urbanized areas. The surrounding area is the so-called "Oslomarka", an area dominated by forests and lakes and, protected against urban development (Eriksson et al., 2016b, Reimann et al., 2009).

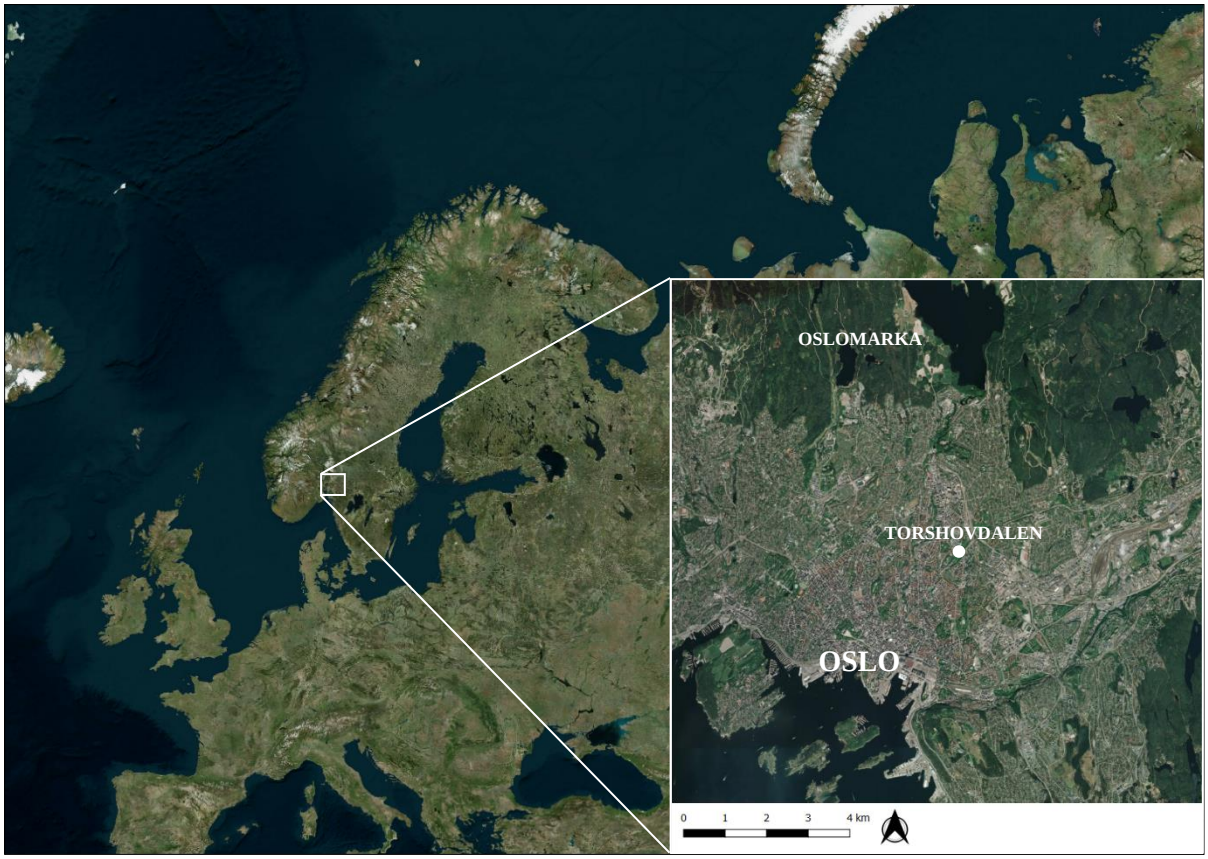

Figure 2.1. Map showing the location of the study area, Oslo (Norway).The photo is modified in QGIS.

2.2. Geological background

The city of Oslo is located at the northern end of the Oslo Fjord, in the Oslo Graben, which formed during Carboniferous-Permian time (Olaussen et al., 1994). Lower Paleozoic sedimentary and exposed Permian magmatic rocks are preserved in the Oslo graben, whereas the surrounding areas consist of Precambrian rocks (Neumann et al., 1992) (Figure 2.2). The Lower Paleozoic sedimentary rocks in Oslo is dominated by marine clay, shale and limestone. Depth to bedrock varies from 0 to 100 meters, with the deepest areas, where the depth to bedrock has been measured to be 94 meters, are in the southern part of Oslo (Eriksson et al., 2016a).

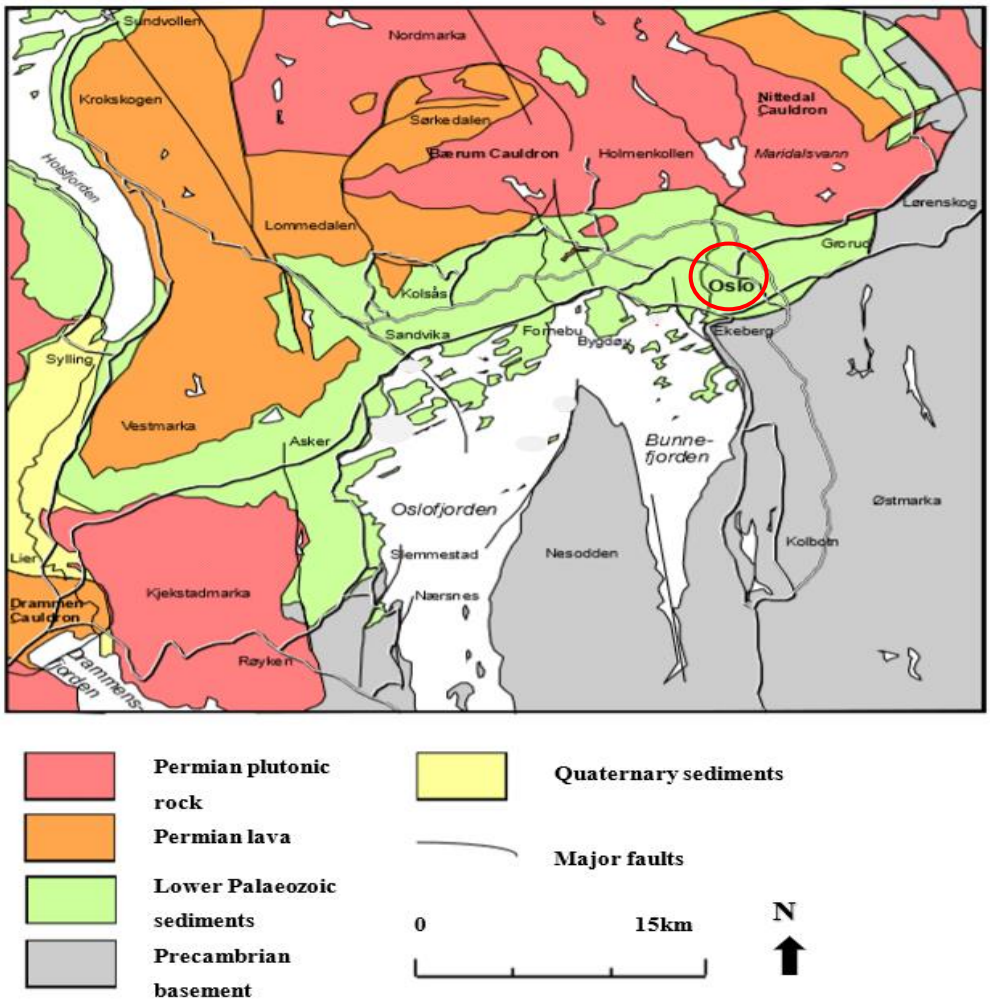

Figure 2.2. Simplified geological map of the Oslo area. The study area (marked with a red cycle) is located in the Lower Palaeozoic sediments (Bjørnlykke, 2004).

The Precambrian basement rock is overlain by a Lower Palaeozoic marine sedimentary sequence from Middle Cambrian to late Silurian (Figure 2.3). The Lower Palaeozoic sequence started with a transgression in Middle Cambrian. During this period, a shallow epicontinental sea formed and existed on the stable craton and covered much of the Precambrian bedrock, until the late Silurian Caledonian Orogeny started (Bjørlykke, 1974). Most sediments from Cambrian, Ordovician and Silurian (Lower Paleozoic) were deposited when the sea covered the land area. The main graben forming period in the Oslo Region was followed with extensive volcanism and rifting (Larsen et al., 2008), which resulted in the deposition of intrusive and magmatic rocks in the northern part of Oslo, often bordering to the Cambro-Silurian sedimentary rocks. A thin sequence of continental and partly also marine sediments from late Carboniferous can be found overlying the Cambro-Silurian sediments, although quaternary deposits formed during and after the retreat of the last glaciation (Holocene) were the last deposited sediments in the Oslo Region. The deposition from this period is terminal moraines and glacial-marine coarse to fine sediments (Bjørlykke, 2004). It is also important to mention that the top layer in Oslo is strongly influenced by anthropogenic activities.

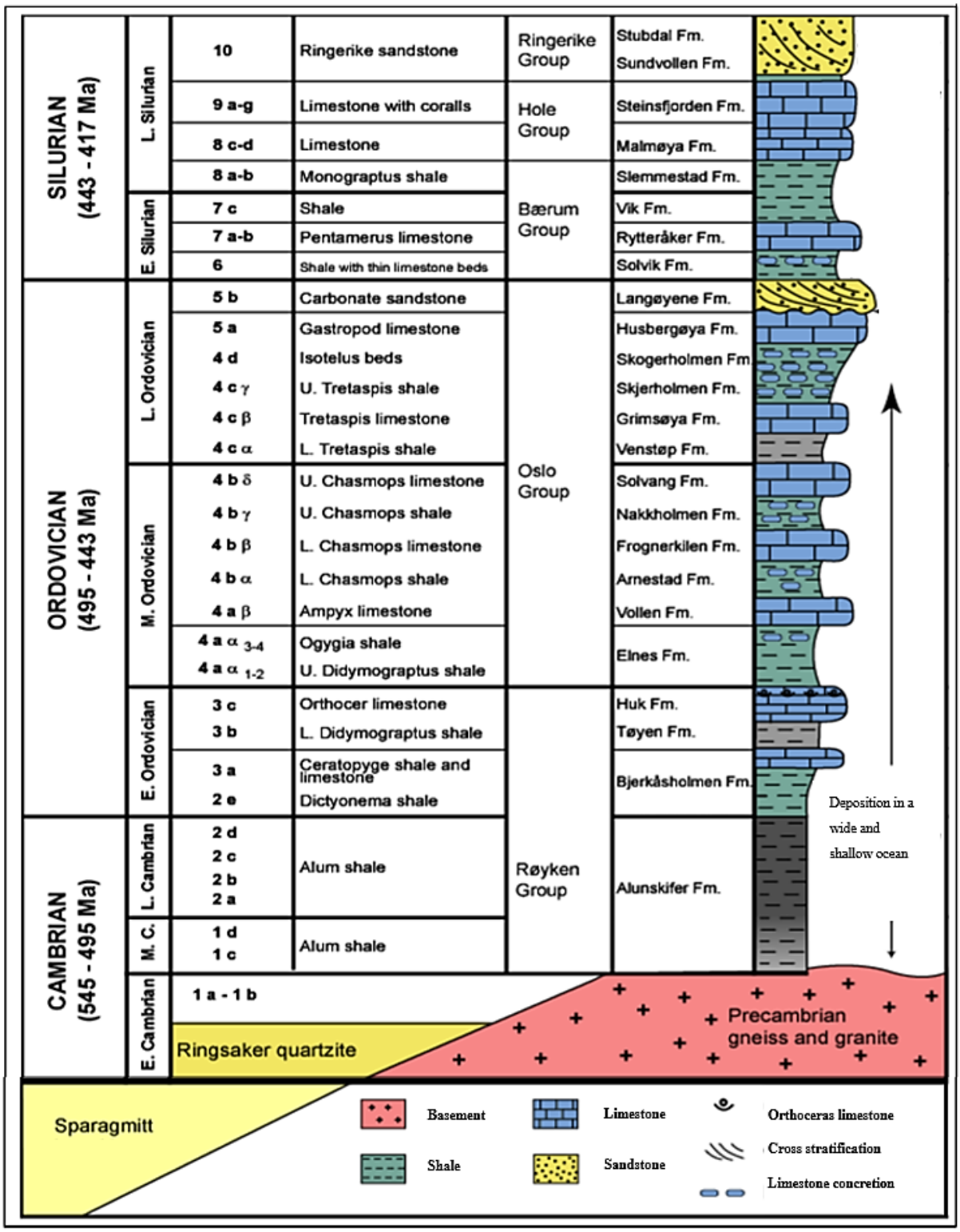

Figure 2.3. Stratigraphy of the Lower Palaeozoic of the Oslo Area (Bjørnlykke, 2004).

2.3. Torshovdalen and Torshovbekken watershed

In this study, the Cambro-Silurian succession is of main interest as is represents the rocks that occur in Torshovbekken watershed (Figure 2.4).

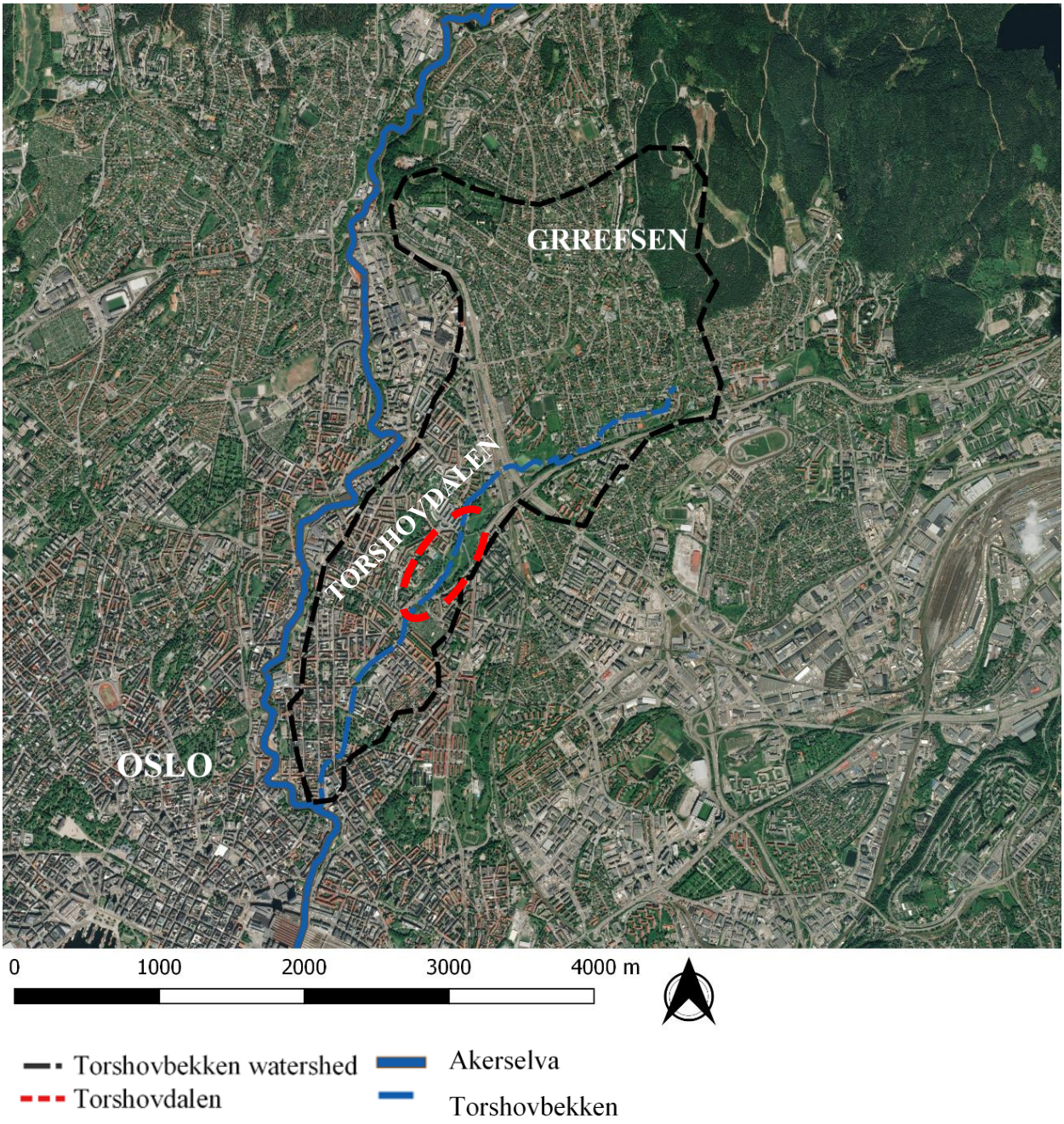

Figure 2.4. Map showing Torshovbekken watershed in Oslo. The river Torshovbekken was originally a tributary of Akerselva but is today a part of the combined sewage system.

Torshovdalen is a green recreational area in the central part of Oslo, the capital of Norway. It is an elongated park in Oslo with a gentle southwest dipping direction. The park mainly consists of weathered and anthropogenic material that is covering the Cambro-Silurian strata, a part of the Elnes and Vollen formation (Figure 2.3), dominated by limestone and shale (Bruton et al., 2010). Large parts of the Cambro-Silurian strata in the area consist of nodular limestones which are made up of limestone concretions in a matrix of calcareous shale. The concretions are formed by precipitation of calcite in the sediment pores right underneath the ocean floor (Bjørlykke, 2012, Bjørlykke, 2004). There are some variation in the thickness of the unconsolidated Quaternary and anthropogenic sediments in the valley. In the middle and northern part of Torshovdalen, depth to bedrock is about 2 to 4 meters. In the southern part of the valley, depth to bedrock is about 12 meters, indicate an increasing depth in the loose Quaternary and anthropogenic sediments towards the southern part of the area.

This section has attempted to provide a summary of the geological background in Torshovdalen and the surrounding area. The chapter that follows presents the theoretical background of this study.

3. Theoretical background

3.1. The hydrological cycle

The global hydrological cycle (also referred to as the water cycle), as seen in Figure 3.1, describes the circulation of water between the biosphere, atmosphere, lithosphere and the hydrosphere (Pidwirny, 2006). The rate of change in water stored in an area, such as a watershed, and the circulation of water between these storages can be defined by a water balance equation. The equation is typically studied over time within a watershed, as changes in the water budget can be used to assess the effects of seasonal changes and human activities on the water resources (Healy et al., 2007). A basic water budget for a small watershed and the underlying unsaturated and saturated zone can be expressed as (Healy, 2010):

$$P + Q_{in} = ET + \Delta S + Q_{out} \qquad \textit{Eq. 3.1}$$

Where P is precipitation, Q_{in} is surface and subsurface water flow into the watershed, ET is evapotranspiration, ΔS is the change in water storage and Q_{out} is surface and subsurface water flow out of the watershed (Healy, 2010, Healy and Cook, 2002).

Water can be temporarily stored in several places, e.g. the atmosphere, oceans, lakes, rivers, glaciers, snowfields, the unsaturated zone and groundwater aquifers. The circulation between these storage compartments is mostly driven by solar energy and gravity, including processes such as precipitation, evapotranspiration, condensation infiltration, snowmelt and runoff (Marsalek et al., 2014). Some of the precipitated waters will partly infiltrate into the unsaturated zone and percolate through, before reaching the saturated zone.

The unsaturated zone is the area between the land surface and the saturated zone and constitutes the part of the soil profile where the water content is less than the soil porosity (Nielsen et al., 1986). The unsaturated zone includes the surface soil, the unsaturated subsurface material containing partially weathered soil, mineral and organic matter, and a transiently inundated capillary fringe (Holden and Fierer, 2005). It is a vital zone in the subsurface as it involves both hydrological and biogeochemical processes, including evaporation, infiltration, groundwater recharge, soil moisture storage, and soil erosion. Biochemically, the unsaturated zone constitutes the primary zone of interaction between soil material and precipitation (Phillips and Castro, 2003). It might also serve as a buffer for runoff and erosion through its potential to absorb water infiltration from rainfall and runoff (Nielsen et al., 1986). Some part of the rainwater might also infiltrate into the soil surface and move laterally through the upper soil horizons towards the streams as ephemeral, shallow, perched groundwater above the main groundwater table, also referred as the subsurface runoff or interflow (Glazovsky and Zaitseva, 2009).

As the rainwater reaches the ocean, either through the groundwater, as precipitation or in stream flow, the hydrological cycle is completed.

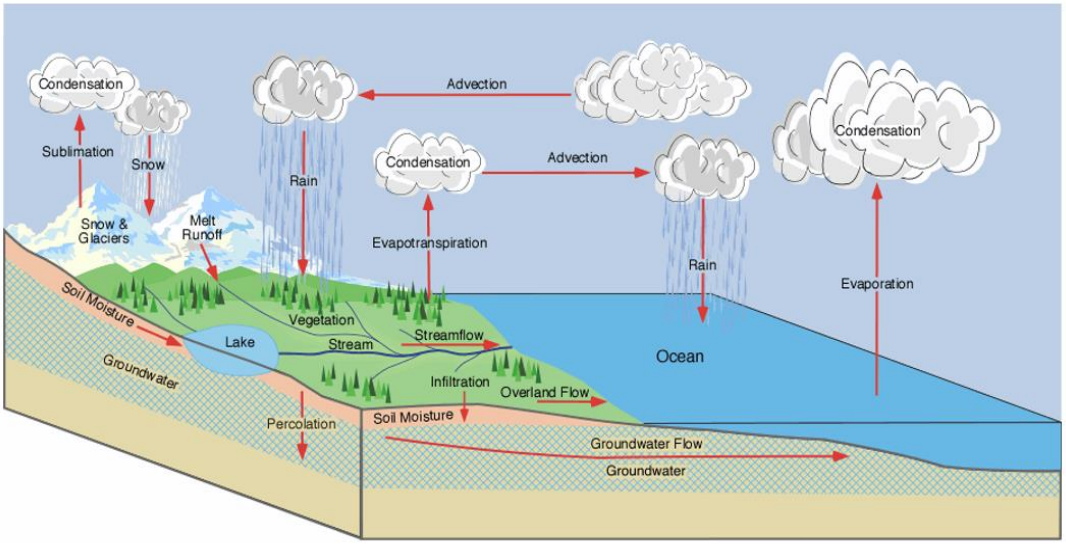

Figure 3.1. The global hydrological cycle describes the storage and circulation of water between the biosphere, atmosphere, lithosphere and the hydrosphere. From Pidwirny (2006).

3.2. Urban hydrology

Urbanization is a worldwide trend, with more than 50% of the world's population living in cities (UN, 2018). The process of urbanization affects the catchment hydrology, resulting in an increased area of impervious surfaces which limits infiltration and thus increases the volume of surface runoff dramatically (Fletcher et al., 2013) (Figure 3.2). When the infiltration capacity decreases, the groundwater recharge will also decrease, resulting in a lowering of the groundwater level (Pitt et al., 2002). Lowering of the groundwater levels can trigger differential compaction of clayey sediments which, in turn, affects the stability of the soil, buildings and infrastructure. The weight bearing capacity of the land is dependent upon its lithology as well as the groundwater in the pores of the loose sediments. As the groundwater pressure drops, the pore pressure is lowered, resulting in compression of the loose sediments due to a loss of buoyant force (Ewing and Vepraskas, 2006, NGU, 2017). This process is called primary subsidence. Secondary subsidence is caused by several processes in the soil, including microbial decomposition of organic debris, as a consequence of lowering the groundwater level and increased air filled pores (Ewing and Vepraskas, 2006). Consequently, monitoring the groundwater level in an urban environment is important for the city's infrastructure and for frequently assess the groundwater quality.

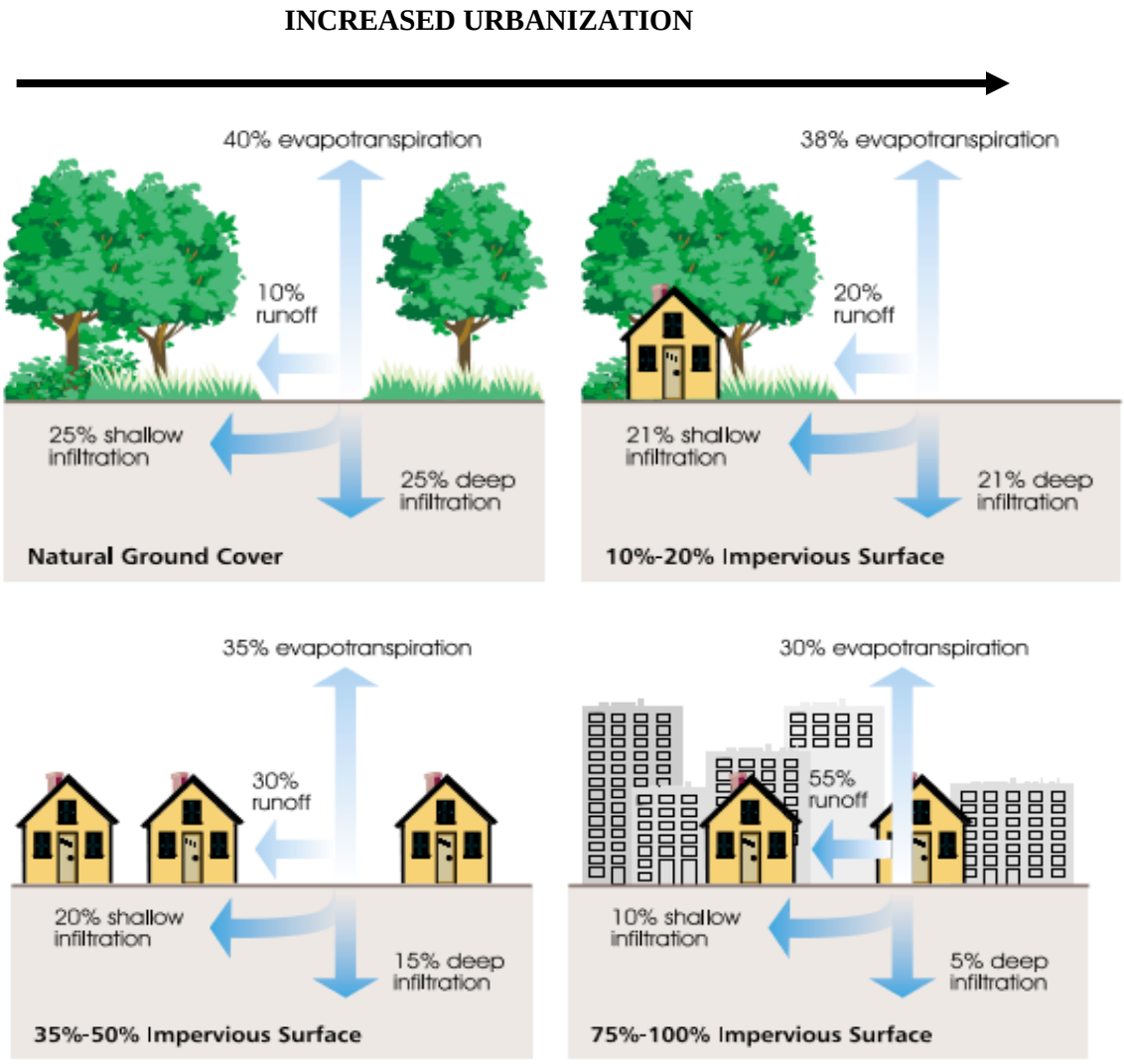

Figure 3.2. Demonstration of how urbanization affects the infiltration and runoff. An increasing amount of impervious surface area results in a higher volume of runoff water, lower evaporation and infiltration. From County (1999).

As shown in Figure 3.3, the hydrological cycle is significantly modified by urbanization, resulting in a more complex hydrological cycle – the urban hydrological cycle. Urban hydrology is, according to Mayhew (2015), the study of the consistent transformation of hydrological regimes that results from urban development. It is a special case of hydrology applied for cities and other areas with a very high level of human interference with natural processes causing impacts in the natural water cycle, both regarding quantity and quality (Niemczynowicz, 1999).

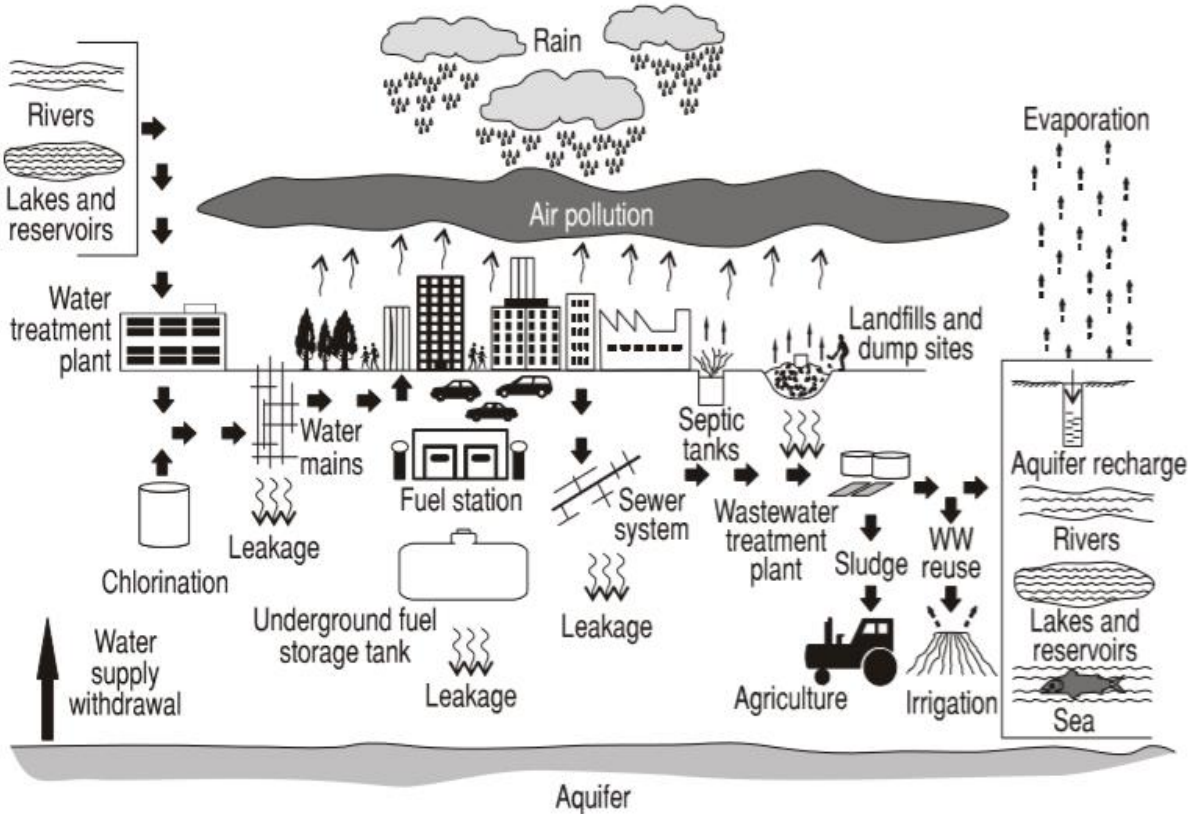

Figure 3.3. The urban water cycle is strongly influenced by human made activities, resulting in air pollution, leaching from landfills, septic tanks and sewage systems, agriculture etc. From Marsalek et al. (2014)

3.2.1. Climate

Climate is defined as the long-term behavior of the weather in a region (Marsalek et al., 2014), and a change in the climate can have significant impacts on the environment. A report from Hanssen-Bauer et al. (2015) confirms that the average precipitation (mm/year) in Norway has increased by 18 percent since 1900 until today, with the most significant increase happening in the period after 1980. Extreme rainfall events in Norway are also expected to increase up to 2050 (Torgersen et al., 2014). More frequent and intensive rainfall as a consequence of the climate changes, together with the increasing amount of impervious surface area due to urbanization, have led to an increasing amount of runoff water (Becker et al., 2016).

An increase in the amount and intensity of rain has also resulted in a higher load on the existing drainage and sewage system in Oslo (Torgersen et al., 2014). The system was designed for a specific maximum flow rate based on the knowledge about the climate conditions at the point in time when they were designed (NOU, 2010), which does not meet the increasing water volumes in Oslo today (Torgersen et al., 2014). As a consequence, several municipalities have experienced problems related to water damage

and sewage overflow due to the limited capacity in the pipelines, increased urbanization and precipitation (NOU, 2010)

In this context, the municipality of Oslo has established a stormwater management strategy, based on a three-step approach (S3SA) (Lindholm et al., 2008). The strategy defines how to handle stormwater related problems and reduce the amount of runoff going into the combined sewage system (Figure 3.4). S3SA is a technique used to manage the stormwater through three steps: (1) catch and infiltrate, (2) delay and retain and (3) safe floodways (Becker et al., 2016, Lindholm, 2008). Daylighting rivers and waterways is a part of the third step – creating safe floodways, and results in numerous benefits, including increased hydraulic capacity for flood control and the removal of water from combined sewage systems. The latter is important, as it can result in fewer sewage overflows, as well as improvement of the water quality. Daylighting also provides improved recreational space, reconnecting us with nature (Trice, 2013).

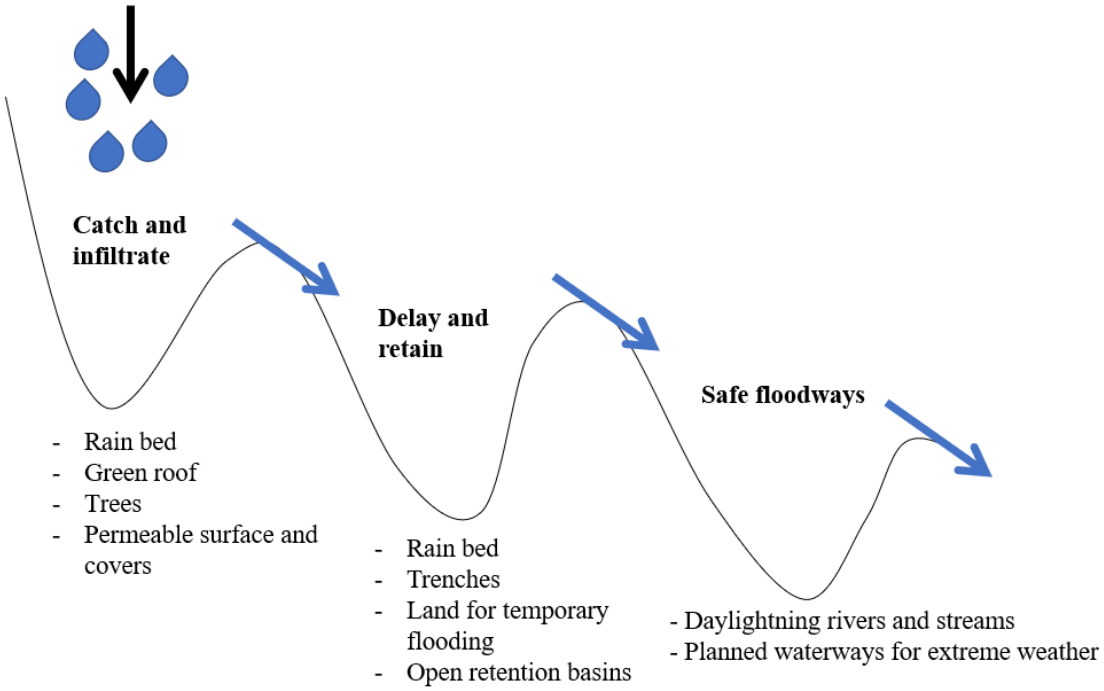

Figure 3.4. The Stormwater three-step Approach,including;1) catch and infiltrate, 2) delay and retain and 3) safe floodways. The figure is modified from Miljødirektoratet (2016)

Daylighting waterways are often costly and can be challenging in dense urban areas due to existing buildings and infrastructure. In the city of Oslo, two successful projects are Hovinbekken and Teglverksdammen. Daylighting of the river Hovinbekken and the pond Tegleverksdammen were completed in 2017 (Figure 3.5). Approximately 650 meters of the Hovinbekken stream was reopened, while Teglveksdammen was designed and constructed as a natural cleaning system with sedimentation basins and shallow water with dense vegetation (Oslo Municipality, 2015).

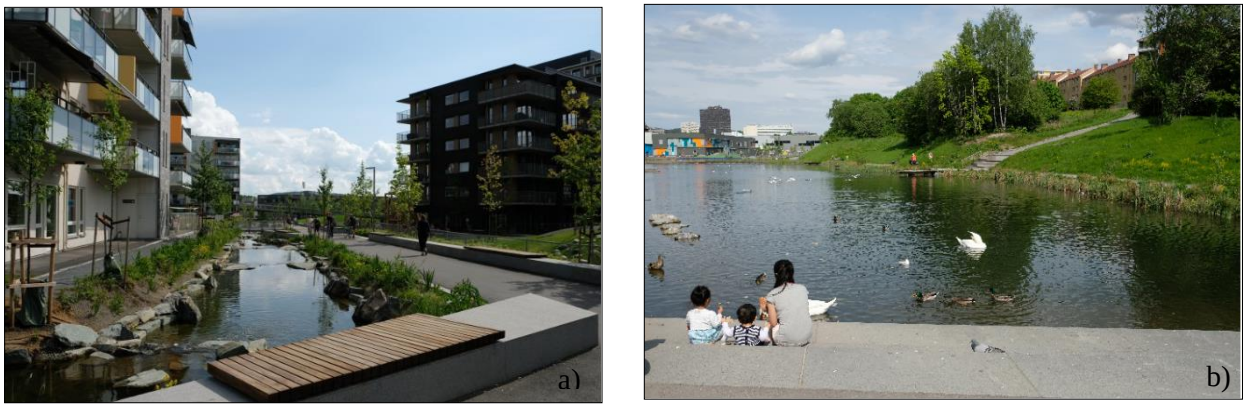

Figure 3.5: a) Daylighting of Hovinbekken and b) Teglveksdammen. Photos from Gulde (2017).

3.2.2. Water quality

Rivers, groundwater and runoff, contain a chemical signature of the catchment land use, climate and geology, reflecting several processes that are affecting the water composition and quality. The signatures are also strongly influenced by the urban landscape and the composition of materials, in addition to the activities that occur on impervious surfaces due to human activities (Davies et al., 2010).

The change in hydrology induced by urbanization has proven to affect water chemistry and quality. Water quality in urban areas is often degraded as a result of increased generation of pollutants, through land use and human activity (Fletcher et al., 2013). Runoff from urban construction areas may be chemically influenced by materials such as concrete, cement and asphalt. Additionally, salting of roads during the winter season provides a source of chloride and sodium in rivers, runoff and groundwater. The road salt may also contain small amounts of calcium, magnesium, sulphate and potassium (Amundsen et al., 2012, Reimann et al., 2009).

Rainwater is the source of most groundwater, rivers, streams and runoff. Continental rainwater is dominated by oceanic vapor and does resemble strongly diluted rain. The rainwater composition is, however, not just distilled water, but contains a component of marine and terrestrially derived salts, modified in recent time by natural and anthropogenic dust and gases (Appelo and Postma, 2005, Reimann et al., 2009). As the rain is transported over land, the air masses and clouds pick up this continental dust and gases which modifies the composition of rainwater (Appelo and Postma, 2005).

Numerous processes in the soil may affect the concentration of the rainwater before it turns into groundwater. If rain falls on an impervious surface, such as a road, the rainwater will be influenced by, for example, nutrients and pollution from highways, parking and agricultural areas, all having a negative impact on the water quality. As a result, the chemistry changes, and more organic micropollutants and, to some extent, heavy metals might be transported by the rainwater on impervious surfaces as runoff. If the rain falls on the soil, different processes in the unsaturated will affect the concentration of solutes before it reaches, and becomes a part of, the groundwater. Processes that may occur and affect the concentration of solutes in the unsaturated zone are evapotranspiration which concentrates the solutes, dissolution of gases (such as carbon dioxide from organic matter decomposition), dry-deposited dust particles, weathering of minerals and ion exchange. Ion exchange reactions between dissolved cations and those sorbed to mineral surfaces can change the water chemistry when the infiltration water differs from the porewater and groundwater (Appelo and Postma, 2005). A typical scenario is the infiltration of rainfall or runoff containing dissolved salt (NaCl) into the unsaturated zone. As the water is infiltrating, an exchange of cations take place (Appelo and Postma, 2005);

$$Na^+ + \frac{1}{2}Ca - X_2 \rightarrow Na - X + \frac{1}{2}Ca^{2+} \qquad \textit{Eq. 3.2}$$

Where X is the soil exchanger.

In the reaction (Eq. 3.2) Na^+ is taken up by the exchanger and Ca^{2+} is released (Appelo and Postma, 2005). The exchanger is often clay minerals or organic material.

Some of the processes that occur as the rain falls on the soil can improve the water quality of the infiltrating water. Urban runoff is often strongly influenced by pollution from human activity such as traffic. By retaining contaminants through different biochemical processes, the soil can enhance the quality of infiltration water (Cassiani et al., 2006). The soil can adsorb suspended solids, nutrients, metals and organic compounds from the percolating water through filtration, biological degradation and ion exchange (Marsalek et al., 2014). Nevertheless, under varying hydrochemical conditions, the contaminants accumulated in the soil can be leached and, therefore, become a source of pollution to the infiltrating water. The chemical composition of groundwater will, consequently, reflect the rainwater and urban runoff chemistry and processes in the unsaturated zone (Banks et al., 1998a). Weathering and dissolution of silicate and carbonate are also among the most important processes taking place along the flow paths and resulting in a change of the groundwater composition (Jørgensen et al., 1991).

3.2.3. Escherichia coli as an indicator of faecal contamination

The rainfall, runoff and surface water in Torshovbekken watershed will find its way downwards to Akerselva and eventually end up in the Oslo fjord, close to Sørenga (Figure 3.6). Sørenga is a popular bathing area during the summer in Oslo, and it is therefore essential to provide good hygienic bathing water quality in the Inner Oslo fjord.

Figure 3.6. a) Sørenga is located in the southern part of Oslo, very close to the river mount of Akerselva, b) the area is popular for bathing during the summer, from (Roald, 2018).

Contamination of water with fecal bacteria is a common and persistent problem, impacting the public health (Ishii and Sadowsky, 2008). Within the fecal indicator bacteria, Escherichia coli (*E. coli)* is the most appropriate measure of fecal contamination in the natural environment of water and soils as it reveals some new pollution with faecal matter (Paruch, 2011). *E. coli* is naturally present in the intestinal tracts of warm-blooded animals and is released into the environment through deposition of fecal

material. In the natural environment, individual *E. coli* can be found at concentrations of $1x10^9$/g of fecal matter (Ishii and Sadowsky, 2008).

E. coli is a rod-shaped, gram-negative, gammaproteobacterium, and is a member of the fecal coliform group of bacteria. Once *E. coli* is released from their primary host (warm-blooded animals) through fecal droppings, most of the released bacteria die due to the lack of nutrients and other environmental factors, i.e. low temperature and absence of sunlight (Blaustein et al., 2013). Some of the bacteria may survive for an extended period in the environment by becoming attached to soil, sand, sediments, or algae surfaces (Ishii and Sadowsky, 2008). The bacteria can also survive in drinking water for 4 to 12 weeks, depending on the environmental conditions, such as the temperature and microflora (Edberg et al., 2000).

The European Union (EU) bathing water directive (EU, 2006) is not implemented in Norway but is used in most of the Norwegian municipalities, including Oslo, as guidelines in their bathing water surveillance. In the guideline, *E. coli* is used as an indicator parameter for predicting microbiological health risk (Bouchalová et al., 2013). The classification of bathing water in saltwater and freshwater, based on the reports from FHI (2015) and EU (2006), are shown in Table 3.1 and Table 3.2, respectively.

Table 3.1. Classification of bathing water in saltwater. MPN = Most probable number.

Parameter	Good	Sufficient	Poor
E.coli (MPN/100 ml)	<250*	250-500*	<500**
* True if 95% of the samples give better values than specified ** True if 95% of the samples give better values than specified			

E. coli bacteria will usually survive longer in freshwater compared to saltwater which is why the limit for good water quality is different for salt- and freshwater (FHI, 2012). Observation of *E. coli* in saltwater will, therefore, in most cases, indicate recent pollution of *E.coli.*

Table 3.2. Classification of bathing water in freshwater. MPN = Most probable number.

Parameter	Good	Sufficient	Poor
E.coli (MPN/100 ml)	<500*	900*	<1000**
* True if 95% of the samples give better values than specified ** True if 95% of the samples give better values than specified			

4. Materials and methods

The chapter describes the methods and equipment used in this master thesis. Collection of water and sediment samples, in addition to in-situ infiltration tests, was done in the field, before the samples were taken to the laboratory for further analyses.

Three groundwater wells were installed in Torshovdalen in September 2018. The wells were ordered by VAV and installed by The Norwegian Geotechnical Institute (NGI). Groundwater samples were collected from the installed wells and geophysical borehole logging performed in separate boreholes.

The laboratory methods applied for water analysis consist of ion chromatography, Quadrupole Inductively Coupled Plasma Mass Spectrometer (QICPMS), determination of soluble silicates, alkalinity titration, and Colilert-18. The laboratory methods applied for sediment analysis were Loss on Ignition (LOI), X-ray fluorescence (XRF), X-ray diffraction (XRD) and grain size distribution.

4.1. Field-methods

4.1.1. Collecting sample material

The sample materials used in this study are collected field samples from Torshovbekken watershed and a rainwater sample (R1) taken from Blindern, Oslo (Figure 4.1), all taken during the year 2018. In addition, VAV has provided with continuous measurements of the *E. coli* concentration in Akerselva (from the sampling point A3 in Figure 4.1). A total of twenty-three water samples have been collected within the Torshovbekken watershed (Table 4.1), including:

- Rainwater sample (R1).
- Samples from a stream located in Grefsen (G1).
- Water samples from Akerselva (A1, A2, A3) and an ephemeral spring in Torshovdalen (T1), done in three sampling campaigns, two in May and one in November 2018.
- Groundwater samples from the wells W1 and W3 in Torshovdalen
- Porewater samples from the unsaturated zone in Torshovdalen.

Measurements performed in the field includes pH, temperature and electrical conductivity. The sample material also includes ten sediments samples from the loose unsaturated zone and the bedrock, all taken during the drilling of the groundwater wells (W1, W2 and W3) (Table 4.2). During the finalizing of W2, bentonite, used to stabilization of the well, were accidentally poured into the well. Due to this bentonite contamination, it was decided not to use water samples from the groundwater well W2.

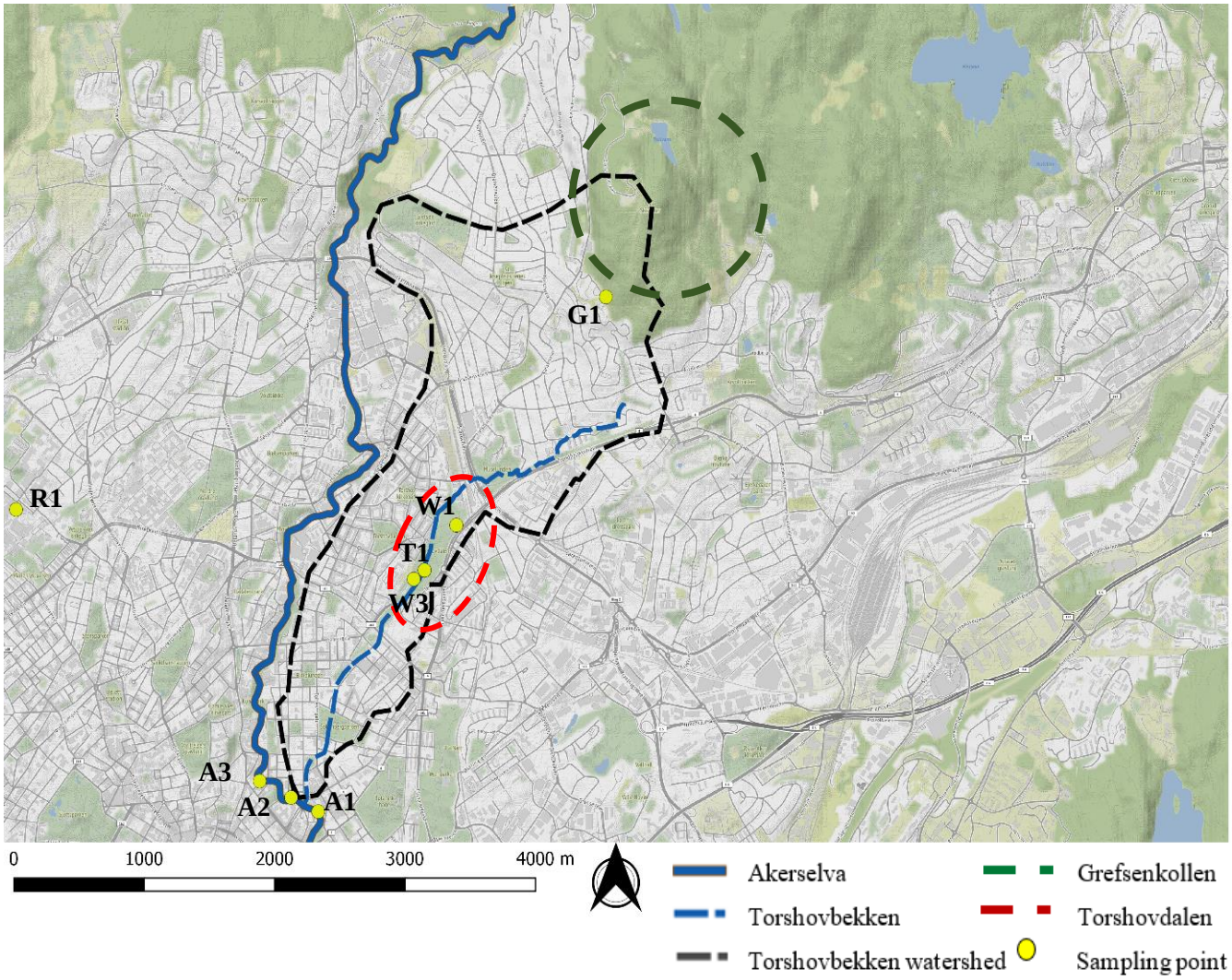

Figure 4.1. Maps showing the location of where the water samples were collected. A3 (from Akerselva) is monitored by VAV. G1 is located close to the hiking path to Grefsenkollen. W1, W2 and T1 are located in Torshovdalen, while A1, A2 and A3 represent water samples from Akerselva.

Table 4.1. The water samples are divided into five groups with different sample codes. The codes are used when explaining the analysis and results. Groundwater samples from the well W2 were not collected and analyzed due to bentonite contamination. Coordinates are in UTM Zone 32N, ETRS89 datum.

Sample group	Sample code	Coord. X	Coord. Y	Coord. Z
Akerselva	A1	598437	6643548	3
	A2	598239	6643598	4
	A3	598029	6643730	4
Ephemeral spring, Torshovdalen	T1	599261	6645305	72
Groundwater, Torshovdalen	W1	599485	6645614	102
	W2	599250	6645402	72
	W3	599170	6645217	61
Grefsen	G1	600583	6647309	234
Rainwater	R1	596167	6645702	78

Conduction of the sediment samples was done September 4 to 6, 2018, using a 1.5 m long manual auger with a diameter of 0.8 m (Figure 4.2). Fragments of bedrock flushed to the surface during drilling were collected for XRF and XRD analysis. Hollow cylinders of 80 cm length and 72 mm diameter were used to obtain three undisturbed sediment sections from Well 3. The location of the groundwater wells is shown in Figure 4.3.

Table 4.2. Overview of the sediment samples taken during the installation of three groundwater wells in Torshovdalen, together with the dates for the collection of each water samples

Date	Sample code
04.09.2018	W2-L1; W2- B1; W2-B4
05.09.2018	W1-L1.5; W1-L2.5; W1-L3.5; W1-B1; W1-B1.5; W1-B4
06.09.2018	W3-L3

Figure 4.2. Sediment samples were collected from an auger, here showing the auger from well W2. Photo a) taken by Sena, C, photo b) taken by Kristiansen, I).

4.1.2. Drilling of groundwater wells and geophysical logging

NGI performed the drilling operation of three separate groundwater wells in Torshovdalen on September 4 to 6, 2018 (Figure 4.3). A GM100GT-2008 drilling rig with a 76 mm bore crone was used to install the groundwater well W2 and W3. For the groundwater well W1, NGI used a Sonic drilling-CRD-T rig with a 102 mm bore crone. Solid PVC (polyvinyl chloride) pipes and filtered PVC pipes were used to configure the wells. Manholes covering the installation of the groundwater wells were used to finalize all three wells. Figures displaying the well configurations are given in Appendix A2.

The geophysical logging was also performed by NGI, in a separate borehole close to the northern (W1) and southern (W3) groundwater well (Figure 4.3).

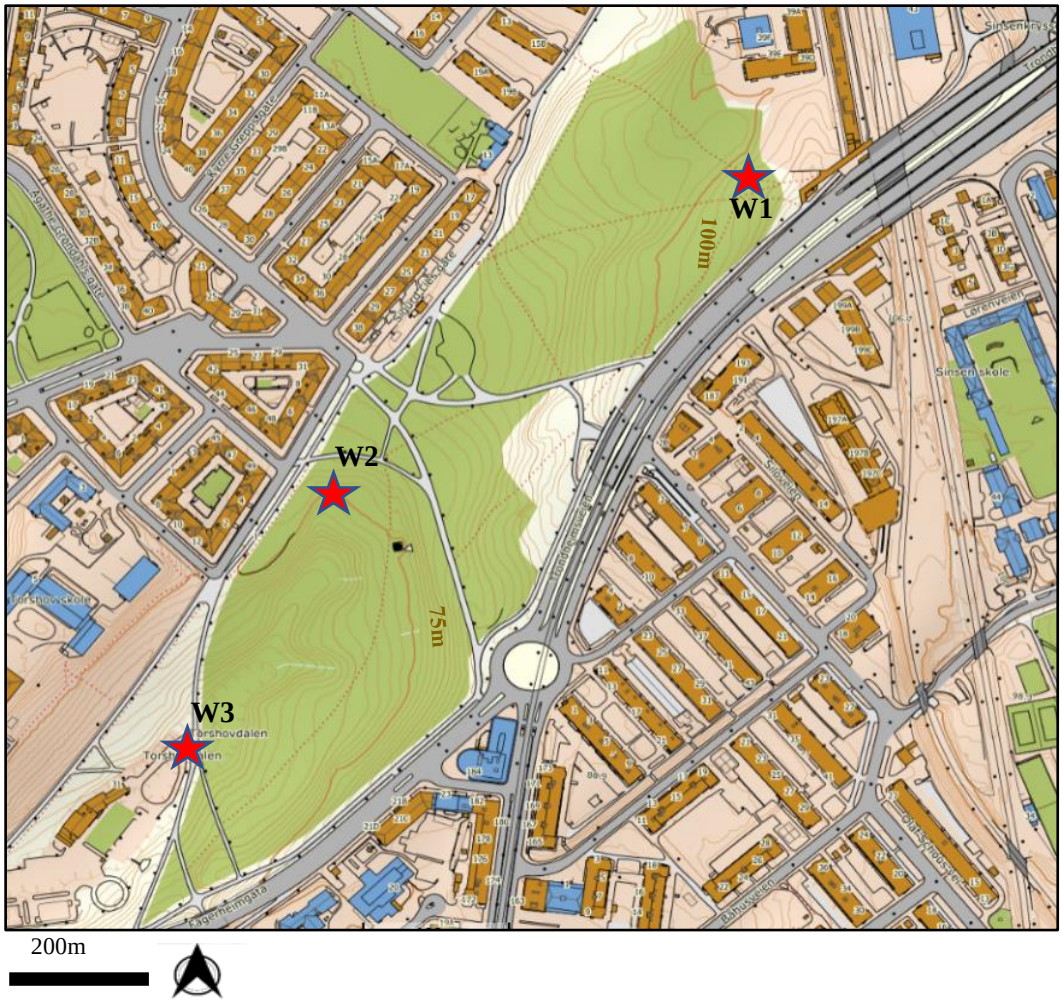

Figure 4.3. Map of the installed groundwater wells in Torshovdalen (W1, W2 and W3). Geophysical borehole logging was performed in holes drilled close to W1 and W3. Sediment samples were taken from each location.

Caliper log

The caliper log provides a single continuous log of borehole diameter and is used to observe fractures or small changes in the borehole diameter caused by variations in the rock hardness (Elvebakk, 2010).

Acoustic and optical televiewer

Imaging with acoustic and optical televiewer results in continuous and oriented 360° views of the borehole wall. From acoustic and optical televiewer the character, relation and orientation of lithologic and structural planar features can be identified (Williams and Johnson, 2004).

In the acoustic televiewer, an ultrasonic pulse is sent towards the borehole wall where the travel time and reflected amplitude of the sound pulse is detected. The borehole must be filled with water, although the water does not need to be clear to get a good image of the borehole using the acoustic televiewer (NGU, 2016).

The optical televiewer (OPTV) uses a ring of lights to illuminate the borehole and a digital camera. The camera measures the intensity of the color spectrum in red, green, and blue (Williams and Johnson, 2004). The method may be performed in both air-or water-filled boreholes and demands clear water. OPTV images allow for direct viewing of the lithology, foliation and bedding planes.

Natural gamma radiation log

Natural gamma is a radiometric log which uses the natural radioactivity produced by the unstable elements ^{238}U, ^{232}Th and ^{40}K (Kearey et al., 2013). From the logging, it is possible to gain information about the geology in the area as well as the mineralogical distribution in the bedrock (Elvebakk, 2011). The natural gamma radiation log measures radioactivity originating within a few decimeters of the borehole (Kearey et al., 2013). The measuring unit for gamma log is cps (counts per second).

Electrical resistivity logging

The electrical resistivity of a material is defined by Kearley et al. (2013) as the resistance, in ohms, between the opposite faces of a unit cube. Different materials have different abilities to resist the flow of electricity (Asquith and Krygowski, 2004). The majority of rock-forming minerals (such as silicates and carbonates) is non-conductive while formation water is relative conductive. Therefore, the electrical resistivity of a rock depends on the porosity, type and amount of fluid (water saturation), water salinity and the kind of rock (Asquith and Krygowski, 2004). The measured electrical resistivity can be used in bedrock identification, and the measuring unit for resistivity is ohm-meters (Asquith and Krygowski, 2004).

4.1.3. Hydrochemical field parameters; pH, temperature, electrical conductivity

Water samples were measured for pH, temperature and electrical conductivity (EC).

pH is an essential parameter in determining the mineral saturation state and solute-mineral interaction in the hydrogeological environment (Basberg et al., 1998). As the groundwater is brought up to the surface and in contact with the atmosphere, oxygen is established, and oxidation of elements like Fe^{2+} and H_2S might affect the pH. The pH may also increase due to degassing of CO_2, resulting in precipitation of carbonates and hydroxides (Appelo and Postma, 2005, Frengstad et al., 2001).

The pH was measured in the field, using an Orion (Model 250A) pH meter. When measuring the pH in Torshovdalen (ephemeral spring and groundwater) the electrodes were placed in a clean distilled plastic bucket to create a continuous flow of the water and to obtain normal conditions.

The electrical conductivity (EC) is a measure of the ability of a water to conduct electricity, or in other words, an indirect measure of the water salinity (Sundaram et al., 2009). The electrical conductivity is strongly dependent upon the ionic composition of the water. Chloride and sodium are the two most

common ions influencing the electrical conductivity, especially in the groundwater, although other ions can also contribute to salinity (i.e. magnesium and calcium) (Sundaram et al., 2009)

For EC values up to around 1500 µS/cm, the following relationship is valid at 25 °(Appelo and Postma, 2005) ;

$$\sum anions(meq/l) = \sum cations(meq/l) = \frac{EC}{100}(\mu S/cm) \qquad \textit{Eq. 4.1}$$

The electrical conductivity and temperature were measured using a Phenomenal PC5000H (VWR) instrument. The temperature exerts a significant influence on biological activity and growth and water chemistry. The rate of chemical reactions increases typically at high temperature, and the dissolution of minerals from the host-rock will normally increase in higher water temperature, often resulting in a higher EC (Perlman, 2016).

4.1.4. In-situ infiltration tests

Infiltration is the hydrological process in which water from rainfall, snow melting, irrigation or other water sources, enter the underlying material due to gravity and capillary suction in the soil (Becker, 2016, Gulliver and Anderson, 2008). There are several methods to assess the infiltration rate of the soil. The two most common methods used for measuring the infiltration in the upper part of the soil are Modified Philip-Dunes Infiltrometer (MPD) and Double-Ring Infiltrometer (DR) (Solheim et al., 2017). MPD is the method applied in this thesis as it is a simple method, has sufficient accuracy and numerous measurements can be done at the same time. Also, the method is not expensive in term of cost and small volumes of water are required to perform the test (Ahmed et al., 2011a, Ahmed et al., 2011b, Muñoz-Carpena et al., 2002).

MPD infiltrometer consists of a cylinder which is inserted into the soil surface and filled with water. The cylinders must normally be re-filled with water up to several times at locations with higher infiltration capacity. It is recommended to do at least five reading during the infiltration test. The infiltration rate is estimated as a change in water level over time, and can be calculated using the following equation (Solheim et al., 2017):

$$Infiltation\ rate = \frac{\Delta h}{\Delta t} \qquad \textit{Eq. 4.2}$$

where Δh is change in height (inside the waterfilled cylinder), and Δt is change in time (seconds).

The infiltration water will have a horizontal movement in the surface soil, which results in an overestimate of the infiltration capacity. A correction factor, depending on the soil type, can be used to adjust for the horizontal movement. The infiltration rate should be multiplied with 0.6 for fine sediments (silt and clay), and 0.8 for coarse grain sediments (sand) (Solheim et al., 2017).

4.2. Methods applied for water analysis

4.2.1. Alkalinity

According to Appelo and Postma (2005), the alkalinity of a water sample is equal to the number of equivalents of all dissociated weak acid and is the water's capacity to resist changes in pH. The alkalinity of a water sample is, therefore, an expression of how much acid that can be buffered by the solution. Usually, only the carbonate ions are of quantitative importance for the measured alkalinity, but phosphoric acid and other weak acids may also contribute to some extent (Appelo and Postma, 2005). In areas where leachate from waste site might occur, organic acids are essential. Since carbonate ions are of quantitative importance for the measured alkalinity, the following simplification for alkalinity, Alk, is equal to:

$$Alk = \left[m_{HCO_3^-}\right] + [2\, m_{CO_3^{2-}}] \qquad \textit{Eq. 4.3}$$

When pH is below 8.3, the carbonate (CO_3^{2-}) contribution is lower than 1%. In that case, only bicarbonate (HCO_3^-) is of importance (Appelo and Postma, 2005).

Autotitration

The alkalinity of a water sample is generally determined by titration with H_2SO_4 or HCl solution of known normality. In this study, titration with HCl was used. All water samples have been titrated in the laboratory, within a maximum of 24 hours after they were taken in the field, using a TT 80 Titrator. The instrument produces a continuous stream of HCl solution, which is directed into a known volume of the water sample, towards an endpoint where pH is about 4.5. The volume of added HCl and the changes in pH are registered by a PHM 82 Standard pH meter connected to a computer to directly obtain a curve.

4.2.2. Ion chromatography

Ion chromatography is a method used to separate the different constituents in a water sample and to determine the concentration of major cations and anions (Naoroz, 2016b). Before the ion chromatography was conducted, all water samples were filtered through 0.45 µm disposable filters into plastic bottles, marked with date and location, and kept in a dark and cold storage (refrigerator, 7-8 °C). Nitric acid (HNO_3) was added to the water samples collected for cation analysis. All samples have been analyzed for both cations and anions using a Dionex ICS – 2000 Ion Chromatography System (ICS-2000). The system consists of a liquid eluent, a high-pressure pump, a sample injector, a guard and separator column, a chemical suppressor, a conductivity cell and a data collection system (Naoroz, 2016a) (Figure 4.4). The ion chromatography system is calibrated using a standard solution before running a sample.

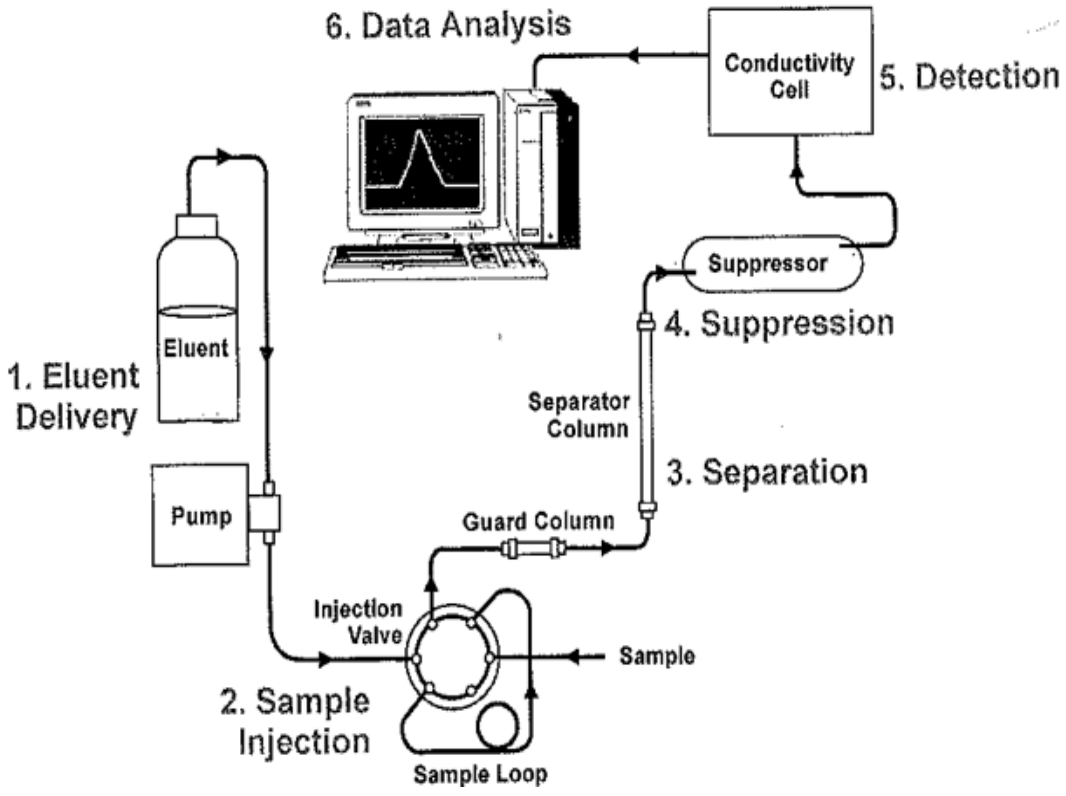

Figure 4.4. Configuration of ion chromatography. From Naoroz (2016b).

For the anions, the water sample is injected into a flowing stream of potassium hydroxide eluent while an electrolytically generated Methanesulphonic Acid (MSA) is used for cations. The ions emerge from the separator column (Figure 4.4) in a fixed order given by their size, shape, and charge before the sample is passed through a conductivity suppressor device and into a conductivity detector. Then, the ions are separated into discrete bands based on their affinity for the exchange sites of the resin. The data emerge as a chromatogram, and the absolute concentration of each ion (expressed in ppm, parts per million) in the sample is determined by using external standard with a known solution (Naoroz, 2016a).

The accuracy of the analysis for ion concentration can be estimated based on the electrical balance (E.B), a principle of electro-neutrality in water. The electrical balance is often used to judge the validity and quality of water analysis since the sum of positive and negative charges in the water should be equal. The electrical balance may be estimated as follows (Appelo and Postma, 2005):

$$Electrical\ balance\ (E.B.,\%) = \frac{Sum\ cations + Sum\ anions}{Sum\ cations - Sum\ anions}\ X\ 100 \qquad \textit{Eq. 4.4}$$

Cations and anions are expressed as meq/L and inserted with their charge sign.

In this thesis, the following anions and cations were measured; F^-, Cl^-, SO_4^{2-}, Br^-, NO_3^-, PO_4^{3-}, Na^+, K^+, Mg^{2+} and Ca^{2+}. These ions were, in addition to HCO_3^- used in the electrical balance.

Standard deviations corresponding for each of the elements varied between 0 – 7.5 % and are listed in Appendix B2.

Mufak Said Naoroz performed the analyses at the Department of Geosciences at the University of Oslo.

4.2.3. Determination of soluble silicate

A Seal AutoAnalyzer (AA3) instrument was used to determine the amount of soluble silicate (SiO_2) in selected water samples. The instrument is an automated analyzer using a flow technique called continuous flow analysis (CFA). CFA is a constant stream of reagents divided by air bubbles into discrete segments in which chemical reactions occur (Naoroz, 2017). The measurement relies on the fact that the intensity of the colored silica compound and its light absorbance is proportional to the sample concentration, with a standard deviation of 1.07 % (Appendix B3). The output of the system comes in peaks with specific heights, which are compared to standard measured under the same conditions (Naoroz, 2017).

Mufak Said Naoroz performed the analyses at the Department of Geosciences at the University of Oslo.

4.2.4. Quadrupole Inductively Coupled Plasma Mass Spectrometer

Mass spectrometry represents several analytical methods to separate and measure charged atoms and molecules and gives a quantitative analysis of trace elements in water samples. The Quadrupole Inductively Coupled Plasma Mass Spectrometer (QICPMS) was used in this study, a mass spectrometry consisting of an ion source, a quadrupole mass analyser, a detection system and a high-temperature argon plasma source to generate ions (Andersen, 2017).

The sample is pumped into the sample introduction system before it is directed into the base of the plasma as aerosols. As the sample reaches the analytical zone of the plasma, it exists as excited atoms and ions, representing the elemental composition of the sample (Thomas, 2001). A quadrupole mass analyser is used in QICPMS, consisting of four parallel rods for separation of the ions based on their mass to charge (m/z) ratio (Andersen, 2017). A detection system catches and counts the received ions before passing the information through the computer system. The concentration of each element is calibrated and calculated based on a standard sample.

Magnus Kristoffersen performed the analyses at the Department of Geosciences at the University of Oslo. A Bruker Aurora elite, equipped with a Cetac ASX-250 autosampler and an ESI oneFAST sample introduction system, in addition to an acid of 1% single distilled nitric acid (HNO_3), was used to perform the analyzes. The analyzed isotopes were: ^{11}B, ^{27}Al, ^{53}Cr, ^{55}Mn, ^{60}Ni, ^{65}Cu, ^{66}Zn, ^{88}Sr, $^{206,207,208}Pb$ (analyzed in He collision gas mode) and ^{57}Fe, ^{75}As, ^{78}Se, (analyzed in H reaction gas mode). Standard deviation together with a detection limit for each element is displayed in Appendix B4-B5.

In advance of the QICPMS analysis, all water samples were filtered through 0.45 µm disposable filters into plastic bottles, marked with date and location, and kept in a dark and cold storage (refrigerator, 7-8 °C). Nitric acid (HNO_3) was added to the water samples collected for QICPMS. Filtration was done to remove sediments and particulate matter and to prevent microbial reactions altering the sample.

4.2.5. Extraction of dissolved species in the unsaturated zone

To understand the chemical transport in the unsaturated zone, the water composition of the porewater were obtained from sediment samples collected during the drilling in Torshovdalen September 4th to 6th 2018. The first step was to dry the sediments samples at 80 °C for 24 hours. Then, the samples were dispersed in deionized water (40ml), using a sample shaker for 2 hours, before the samples were stored for approximately 70 hours at room temperature. Afterwards, the sediment samples were centrifuged at 3000 rounds/minute for 10 minutes followed by filtration through 0.45 µm syringe filters. The filters were used to extract the leachate that was further analyzed for major cations and anions by ion chromatography (see section 4.2.2 for details).

The results from the ion chromatography of the leachate were used to calculate the in-situ concentration of the different ionic species present in the porewater (species, expressed in milligram or microgram per gram of dry sediment weight (mg,µg/g dry weight)) in the unsaturated zone (*Eq. 4.5*);

$$Species\left(\frac{mg,\mu g}{g}dry\ weight\right)=\frac{C*V}{m_d} \qquad \textit{Eq. 4.5}$$

Where C is the concentration of a given species in the leachate extracted from the centrifuged sediment samples (mg, ug/L), V is the amount of deionized water (mL) added to the sediment sample, and m_d is the dry weight of the sediment sample (g).

4.2.6. Colilert – 18

In this study, Colilert 18/Quanti- Tray*2000, a simple, fast and efficient method, was used to detect and count both Escherichia coli *(E. coli)* and coliform bacteria in the water samples.

The method is a combination of an enzyme-based detection test and the Most Probable Number (MPN) technique (Paruch, 2011), and is based on specific bacterial enzymes. Coliforms use their β-galactosidase enzyme to metabolize *ortho*-nitrophenyl-β-D-galactopyranoside (ONPG), which produces the yellow-colored product *o*-nitrophenol. *E. coli* uses their β-glucurinidase to metabolize 4-methyl-umbelliferyl- β-D-glucuronide (MUG), which results in the formation of the fluorescent product 4-methyl-umbelliferone (Eckner, 1998, IDEXX, 2006, Hakalehto et al., 2013) (Figure 4.5).

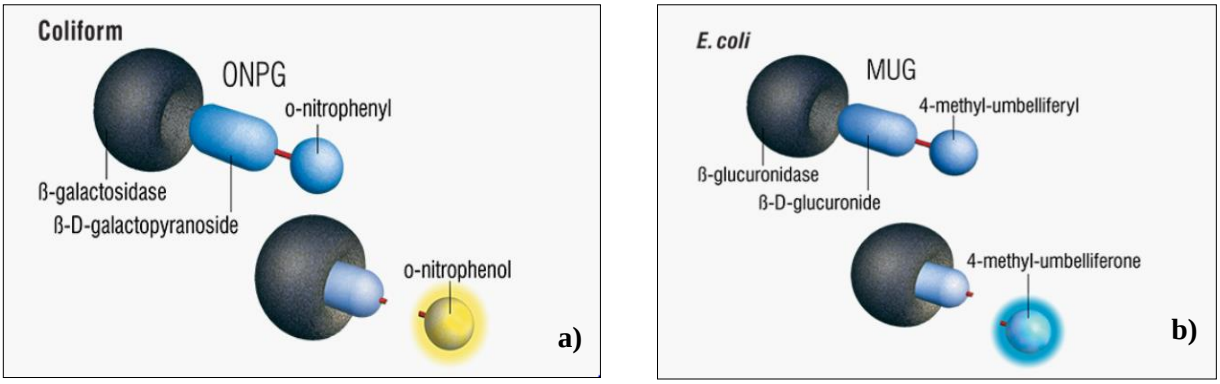

Figure 4.5. a) Formation of o-nitrophenol (b) and 4-methylumbelliferone. From IDEXX (2006).

The water samples were diluted in 99 mL and 90 mL of distilled water, always resulting in 100 mL of water (either a mixture of distilled and sample water or 100 mL of only the sample water), and then shaken by hand. A prepacked Colilert-18 reagent was added in all water samples, containing both distilled water and sampled water. The mixtures were shaken by hand another 3-5 minutes to dissolve the reagent. The prepared reagent mixtures were poured into sterile Quanti-Tray 2000^{TM} before it was sealed in an INDEX Quanti-Tray Sealer (Eckner, 1998). The sealed trays had to be incubated at 35 ± 0.5°C for 18 hours (Paruch, 2011). After incubation, coliform bacteria represent the number of yellow wells, while counting the fluorescing wells gave the amount of *E. coli*. By using a most-probable-number (MPN) table the number of coliforms and *E.coli* was calculated (Eckner, 1998).

As a part of the monitoring tasks undertaken by the Agency for Water and Sewerage (VAV) in Oslo municipality, *E. coli* concentration in Akerselva (sampling point A3, Figure 4.1) has been continuously analyzed in the period February to November 2018. In addition, water samples from the ephemeral spring in Torshovdalen (T1), as well as two other locations in Akerselva (A1 and A2), the groundwater (W3) and stream in Grefsen (G1), were analyzed for *E. coli* and coliform bacteria (Figure 4.1).

4.3. Methods applied for sediment analysis

After collecting the sediment samples in the field (Table 4.2), preparation of the samples was done according to the requirements for the machines used for sediment analysis. The sediment samples were the basis for grain size distribution, XRF and XRD. Loss on ignition (LOI) was applied to prepare the samples for XRF analysis of major elements. Table 4.3 gives an overview of all samples prepared for LOI, XRF and XRD analysis. The samples are marked with “W” according to which groundwater well they are representing (W1, W2 or W3). “L” stands for loose sediments, indicating that the sample is taken above bedrock, while “B” states that the samples are from the bedrock. The numbers followed by “L” and “B” represent the approximate depth below the surface where the sediment samples were collected.

Table 4.3. Overview of the sediment samples prepared and analyzed for LOI, XRF. XRD and XRD Clay fraction. Depth below the surface is given in meters, indicating the depth of the collected sediment samples.

Sediment sample	LOI	XRF	XRD	XRD Clay fraction	Depth below the surface (m)
W1-L1.5	√	√	√	-	0 – 1.5
W1-L2.5	√	√	√	-	1.5 – 2-5
W1-L3.5	√	√	√	-	2.5 – 3.5
W1-B1	√	√	√	-	3.5
W1-B1.5	√	√	√	-	4 – 5
W1-B4	√	√	√	-	0 – 1
W2-L1	√	√	√	√	3 – 4
W2-B1	√	√	√	-	4 – 5
W2-B4	√	√	√	-	4 - 5
W3-L4	√	√	√	√	3.5 – 4.5

4.3.1. Loss on ignition

Loss on ignition (LOI) was used to determine the water, organic and carbonate content of the sediment samples collected in Torshovdalen, September 4th to 6th ,2018.

In the first reaction (Eq. 4.6), the samples were oven-dried overnight at approximately 110°C, a temperature high enough to eliminate "free" forms of water and sufficiently low not to cause a significant loss of organic matter and unstable salts by volatilization (Pansu and Gautheyrou, 2006).

$$Water\ \% = \frac{DW - DW_{110}}{DW} * 100 \qquad \textit{Eq. 4.6}$$

In equation 4.5, water (%) is the water content in the sediment sample, DW is the weight of the air-dried sample and DW_{110} is the dry weight of the sample heated at 110 °C.

In the second reaction (Eq. 4.7), all samples were heated at 550°C for 4 hours making the organic matter oxidized to carbon dioxide and ash.

$$OM\ \% = \frac{DW_{110} - DW_{550}}{DW_{110}} * 100 \qquad \textit{Eq. 4.7}$$

Where OM represents the organic matter as a percentage at 550°C, DW_{110} is the weight of the sample before combustion and DW_{550} is the weight of the sample after heating at 550 °C for 4 hours (Heiri et al., 2001).

In the third reaction (Eq. 4.8), samples were heated to 1100°C for 2 hours. The weight loss between 550-1100°C is the amount of carbon dioxide evolved from carbonate minerals (Dean, 1974).

$$LOI\ \% = \frac{DW_{110} - DW_{1100}}{DW_{110}} * 100 \qquad \textit{Eq. 4.8}$$

Where LOI is the percentage of loss on ignition at 1100 °C and DW_{1100} is the weight of the sample after heating at 1100 °C.

The sample weight was measured before and after each reaction in order to determine the weight loss (Heiri et al., 2001) and porcelain crucibles were used in all stages.

4.3.2. X-ray fluorescence (XRF)

Wavelength-dispersive X-ray fluorescence spectrometry (WDXRF) is an analytical technique to determine major and trace element chemistry of rock samples (Rollinson, 2014). It is a non - destructive, rapid method, and large numbers of precise analyses are made in a relatively short period. Additionally, the method is accurate, does not require much of sample preparation and is good for quantitative and qualitative analysis of the elemental composition. The WDXRF method was chosen since it has a wider elemental range compared to energy dispersive system (EDXRF) and can measure all elements from beryllium to uranium (Brouwer, 2006).

The method is based on the analysis of characteristic X-rays emitted from the sample after illuminated by high energy X-rays (Brouwer, 2006). These X-rays have wavelengths characteristic of the elements present in the analyzed sediment sample, and each element produces a set of characteristic fluorescent X-rays unique for that specific element. Elemental composition of the sediment samples is determined by measuring the intensities emitted from these characteristic X-rays, and the chemical composition of the samples is calibrated based on standards with known proportions composition.

Thanusha Naidoo, at the University of Oslo, performed the analysis of the sediments identified in Table 4.3, using a *PANalytical Axiox*^{MAx} Minerals with 4kW Rh-tube at the Department of Geosciences at the University of Oslo.

Sample preparation

Sample preparation is an important step before analysing with XRF and XRD (c.f. section 4.3.3.) data. In order to obtain accurate and precise results, the sample must be homogenous, have an even grain size and a random grain orientation.

All samples were collected during the installation of the groundwater wells in Torshovdalen (September 4-6, 2018) (Figure 4.3). The first steps in sample preparation are equal for both XRD and XRF; The sediment material was dried at 80 °C for 24 hours. Subsequently, the samples were crushed to a powder using a swing mill and an agate mortar. The swing mil was cleaned with water and dried with ethanol between each sample. The next step for the XRF samples was to create fusion beads for major elements and pressed powder pellets for trace elements.

Fusion bead

Fusion (glass) beads were prepared for XRF-analysis of major elements. 0.6000g ± 0.0005 of the heated sample material was mixed with 6.000g ± 0.0006 of flux. The flux used, a FluXana, is a mixture containing 66.5 % Lithiumtetraborate and 33.5 % Lithiummetaborate. An ammonium iodide tablet was added as a releasing agent. The mixture was poured into a platinum crucible and placed in a *PANalytical Eagon 2* automatic fusion bead maker, creating the fusion beads.

Pressed powder pellet

The pressed powder pellets were prepared for XRF-analysis of trace elements. 12g of the sample and 3g of wax was mixed togheter. The mixture was compressed into circular pellets using *Eagon2*, a mechanical device that applied a weight of 20 tons.

4.3.3. X-ray diffraction (XRD)

X-ray diffraction (XRD) determines the crystal structure and was applied for 10 selected sediment samples (Table 4.3). The method is effective and can identify the chemical compound from a crystalline structure, making it possible to identify different compounds that have the same composition (Leng, 2009). The instrument typically consists of an X-ray tube, a sample holder, an X-ray detector, and a goniometer to measure and detect X-ray angles (Dutrow and Clark, 2016).

X-rays are generated in an X-ray tube (Figure 4.6), containing a source of electrons (the filament), two metal electrodes in a vacuum tube and the target (Leng, 2009). Due to the high voltage maintained across the two electrodes, the electrons are rapidly drawn towards the target. The X-rays are produced when

these high-speed electrons, accelerated by the high-voltage field, collide with the target (Leng, 2009). The collision results in a sudden deceleration of electrons, converting the kinetic energy of electrons to X-ray radiation. The X-ray tubes generates X-rays with a range of different wavelengths, starting from a minimum λ (wavelength), also named *continuous X-rays*, to some sharp intensity maxima at a certain wavelength, called *characteristic X-rays*. The generated X-rays are then radiated in all directions (Leng, 2010), and guided out of the tube through a window (Figure 4.6)

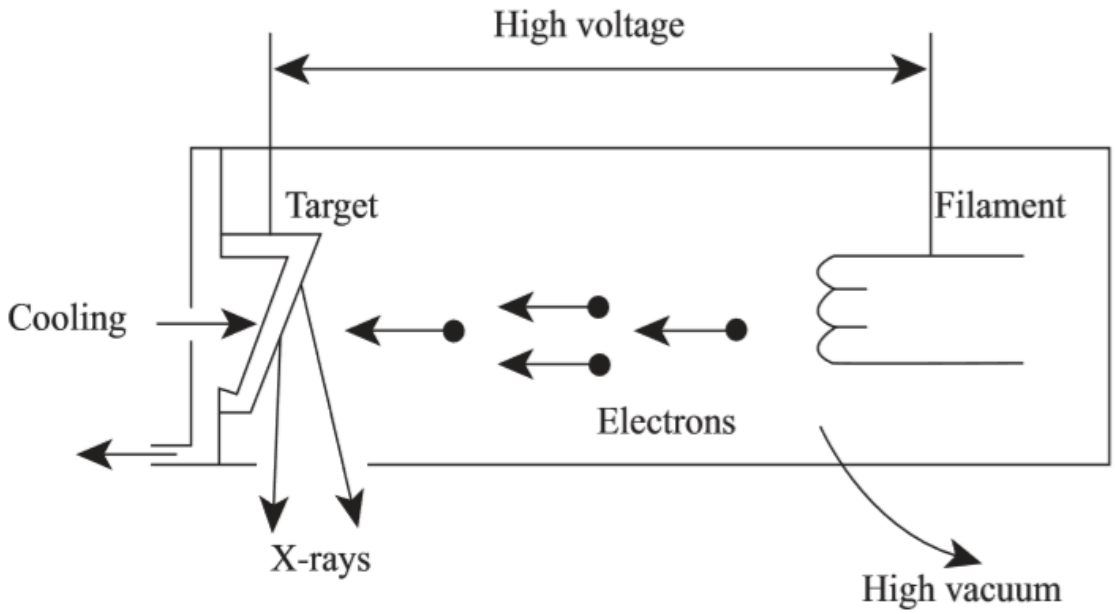

Figure 4.6. Overview of an X-ray tube where the X-rays are generated. The electrons are directed towards the target in a high-voltage vacuum, and X-rays are generated as the electrons collide with the target. From Leng (2009).

The characteristic X-rays are passed through a monochromatic filter before reaching the detector. The detector and the x-ray tube are rotating in the opposite direction around the sample, allowing the X-ray detector to detect a wide range of angles at the same time (Leng, 2010). The interaction of the incident beam (X-ray) with the sample produces constructive interference described by Bragg's law (Dutrow and Clark, 2016);

$$n\lambda = 2dsin\theta \qquad \textit{Eq. 4.9}$$

Where n is the order of reflection, λ is the wavelength of the electromagnetic radiation, d is the interplanar spacing of the crystal and θ is the angle of the incident beam. As the sample and detector are rotated in the opposite direction, the intensity of the reflected X-rays is recorded.

When the geometry of the incident X-rays strikes the sample and satisfies Bragg's law, constructive interference and a peak occur (Dutrow and Clark, 2016). The X-ray signals are detected and processed by a detector, converting the signal to a readable count rate (Dutrow and Clark, 2016).

Thanusha Naidoo, at the University of Oslo, performed the analysis, using a Bruker D8 Advance diffractometer with a Lynxeye 1-dimensional position-sensitive detector (PSD) and CuKα radiation (λ = 0.154 nm) operated at 40mA and 40kV.

Sample preparation for bulk analysis

After crushing the samples (c.f. section 4.3.2.) (Table 4.3), the next step of preparing was to utilize the *McCrone* micronizing mill, a wet crushing tool consisting of 48 agate elements. The mill is capable of minimising the grain size and homogenize the sample. 3 grams of the rock powder was milled in 7-10 ml ethanol for 10 minutes. After air-drying all samples at 60 °C for 24 hours, two samples were taken for further clay fraction analysis. For the other 10 samples, the powders were mounted on a specific sample holder for randomly oriented whole-rock analysis, with a step size of 0.01º from 2º to 65º (2θ) at a count time of 0.3 s (2θ).

The XRD results were obtained as diffractograms in .raw files. The files were first opened in *DIFFRAC.EVA* for qualitative analysis of bulk samples using calculated pattern profiles and the *search/match*-tool for phase analysis. *Profex* was used for quantitative analysis of the 10 bulk samples.

Clay fraction (XRD)

Two clay samples were analyzed using an XRD clay fraction method (W2-L1 and W3-L4). After air-drying the sample at 60°C for 24 hours, the sample was mixed with 200 ml of sodium carbonate (Na_2CO_3). The mixture underwent a 10 min in the ultrasonic in order to accelerate the dispersion of clay particles, and then left in the laboratory for 24 hours. The next day, 600 mL of distilled water was added, before leaving the mixture in the ultrasonic for another 10 minutes. The following step was to filter the clay fraction samples in a vacuum suction through a 0.45 µm filter. Approximately 150 mL of each solution got through the filter. The filtered samples were placed on silica glass slides and put in aluminium holders for the clay fraction XRD analysis.

In the first clay fraction XRD run, the samples were analyzed air-dried. In the second run, the samples had been dried in the oven at 50 °C for 24 hours and then treated with ethylene glycol vapor. Ethylene glycol is a treatment used to expand swelling clays. Then, the sample was put in the oven at 350 °C for 1 hour, before measured (representing the third run). The clay samples were taken back in the oven at 550° C for another 1 hour before measured one last time (fourth run). The heat treatments at different temperatures are used to identify clay minerals by reveling change in crystal structure spacing or loss of the structure (Poppe et al., 2001), peak position, shape and intensity after each treatment. A total of four diffractograms were created for each clay sample. By comparing the diffractograms, it is possible to

gain information about the clay mineral. A clay mineral identification flow diagram table (Appendix C1) was used to determine the clay minerals present in the samples.

4.3.4. Grain size distribution

In order to determine the grain size of the material gathered from the location where the infiltration tests were performed, a grain size distribution of the upper 10 cm of the surface soil was conducted in the laboratory. In addition, NGI performed three grain size distribution analysis from each cylinder taken during the installation of the groundwater well W3 (Figure 4.3).

Sieving was used to remove coarse sand, and a laser diffraction was applied to determine the amount of silt and clay. The Beckman Coulter LS13 measures the size distribution of particles suspended in a liquid, or as in this case, in dry powder form, by using the principles of light scattering. The LS13 measures the pattern of light scattered by the particles in the sample, called a scattering pattern. Each particle size has its own characteristic scattering pattern (Coulter, 2011). The individual scattering patterns from all moving particles in the sample cell are superimposed, creating a single composite scattering pattern representing the contributions from all the particle sizes in the sample cell (Coulter, 2011)

Fred Wegner at The Norwegian Water Resources and Energy Directorate (NVE) performed the grain distribution from samples collected the in-situ infiltration tests by laser diffraction. Samples conducted from the cylinder taken at W3 was performed at NGI laboratory.

5. Results

The results in the following chapter are divided into five sub-chapters. First, the different sampling campaigns are presented, followed by the water chemistry characterisation, including major ions, soluble silicates, trace elements and field parameters (pH, EC and temperature). The third subchapter presents the bacterial characterisation from the stream in Grefsen, Akerselva, the ephemeral spring and groundwater in Torshovdalen. Then, physical and chemical properties of the soil and sediments are given based on results obtained from XRD, XRF, infiltration test and grain size distribution analysis. Finally, results from the geophysical borehole logging performed in Torshovdalen during the installation of the groundwater wells are presented.

5.1. Sampling campaigns

Three sampling campaigns were done in Akerselva and Torshovdalen, in the year 2018, which are listed in Table 5.1 (the location of the sampling points is shown in Figure 4.1).

Table 5.1. Three sampling campaigns were done in Akerselva (A1 and A2) and Torshovdalen (T1).

Date	**Akerselva, river water**		**Torshovdalen, ephemeral spring (T1)**
	A1	**A2**	
10.05.2018	A1-1	A2-1	T1-1
23.05.2018	A1-2	A2-2	T1-2
12.11.2018	A1-3	A2-3	T1-3

Additionally, three groundwater samples were collected from the drilled wells in Torshovdalen after flushing and stabilization, in the year 2018; one sample on September 26 and October 10 in well W3 (W3-1 and W3-2, respectively), and one sample on October 10 in well W1 (W1-1) (Figure 4.1). Two samples were also collected from the upper area of Torshovbekken watershed, Grefsen (Figure 4.1); one sample on the September 22 (G1-1) and on the November 12 (G1-2), both in the year 2018. One sample representing the rainwater (R1) was collected on the September 21, 2018. The sampling campaigns were done under different weather conditions, resulting in water samples from dry and wet periods within the hydrological year. Figure 5.1 shows the air temperature (°C) and precipitation (mm/day) that were registered in Blindern in the period May 1 to November 15, 2018.

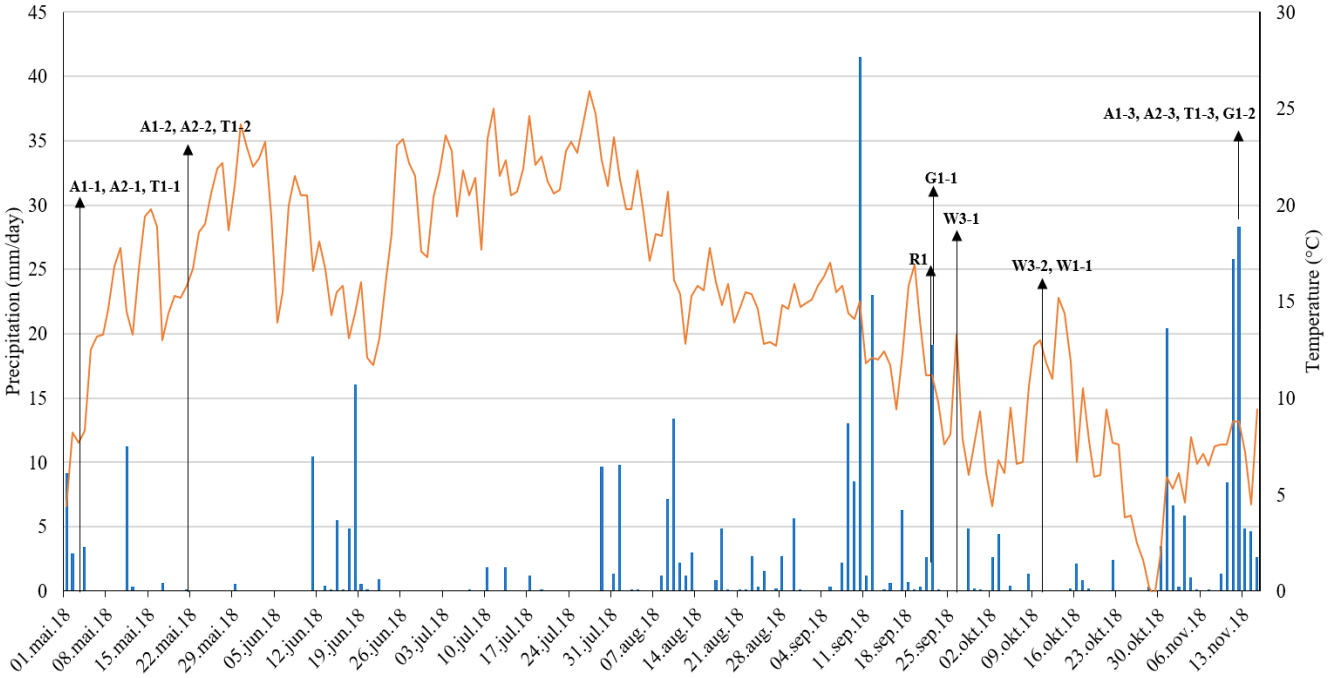

Figure 5.1. Registered precipitation during the water sampling period from 01.05.2018 – 15.11.2018, together with average daily air temperature. The data are registered at Blindern, Oslo (eklima.met.no).

5.2. Water chemistry characterization

The water samples are described in the following section, based on data gathered in the field and analyzed by ion chromatography, QICPMS, alkalinity, determination of soluble silicate and the extraction of dissolved species in the unsaturated zone. The samples have been studied individually before assembled into six groups based on the location of the water sample (Table 5.2). The analytical data of the water chemistry characterization is given in Appendix B1-B5.

Table 5.2: A total of 23 water samples have been analyzed and grouped into 4 groups based on the location.

Group		**Water sample**
Rainwater		R1
Grefsen		G1-1; G1-2
Akerselva		A1-1; A1-2; A1-3; A2-1; A2-2; A2-3
Torshovdalen	Ephemeral spring	T1-1; T1-2; T1-3
	Porewater analysis (unsaturated zone)	W1-L1.5; W1-L2.5; W1-L3.5; W2-L1; W2-L2; W3-L1; W3-L2; W3-L4
	Groundwater wells	W1-1; W3-1; W3-2

The accuracy of the analysis for ion concentration was calculated using equation 4.4, and were based on the following cations; Na^+, K^+, Mg^{2+}, Ca^{2+}, and anions: Cl^-, HCO_3^-, SO_4^{2-}, NO_3^-, F^-, Br^- and PO_4^{3-}, all analyzed by ion chromatography (c.f. section 4.2.2 for more details). e

A difference in E.B. of up to 2% is considered to be an excellent analysis. Errors up to 5 % are acceptable (Appelo and Postma, 2005), especially in very diluted water samples which is the case in some of the samples analyzed in this project. The E.B. obtained in the water samples collected in this thesis are in the range of -3.5 to 4.8 % (Table 5.3), which is acceptable and indicates an accurate chemical analysis.

The results of the E.B. calculations presented in Table 5.3 shows that the lowest concentration of the major cations and anions were found in the samples from Akerselva (A1, A2, A3) and in the rainwater (R1). Slightly higher concentration of the major ions was found in the stream located in Grefsen (G1), followed by water samples collected from the groundwater wells (W1 and W3). The highest concentrations of cations and anions were measured in the ephemeral spring in Torshovdalen (T1).

Table 5.3. Total sum of cations (Sum +) and anions (Sum -) in meq/L, and the calculated electrical balance (E.B.)

Date	Sample	Sum +	Sum -	E.B (%)
10.05.2018	A1-1	0.370	-0.341	3.980
23.05.2018	A1-2	0.420	-0.385	4.394
12.11.2018	A1-3	0.609	-0.633	-1.887
10.05.2018	A2-1	0.347	-0.359	-1.664
23.05.2018	A2-2	0.399	-0.359	0.925
12.11.2018	A2-3	0.613	-0.573	3.297
10.05.2018	T1-1	20.632	-20.254	0.925
23.05.2018	T1-2	21.297	-22.382	-2.485
12.11.2018	T1-3	17.277	-16.021	3.774
22.09.2018	G1-1	2.493	-2.318	3.652
12.11.2018	G1-2	2.477	-2.341	2.821
21.09.2018	R1	0.185	-0.168	4.769
26.09.2018	W3-1	13.718	-14.041	-1.163
10.10.2018	W3-2	15.165	-15.335	-0.555
10.10.2018	W1	4.125	-4.421	-3.469

Analysis of the major ions from Akerselva, Grefsen, groundwater in Torshovdalen and rainwater are plotted in a Piper diagram (Figure 5.2). This type of plot is used to understand the chemical character of water and the relationships between dissolved ionic constituents (Tiwari and Singh, 2014). The diagram contains two triangular charts for depicting the proportions of cations and anions (expressed in percentage of total anion and cation, in mg/l), giving the relative concentration of total cations or anions. From the triangular diagrams, the points are projected to the diamond-shaped diagram (Appelo and Postma, 2005).

Based on the distribution of cations and anions in the water samples (Figure 5.2), all samples, except rainwater, can be classified as calcium-chloride water type. Some deviations do occur, especially in the cations' triangle. Samples from Akerselva, the ephemeral spring and the groundwater in Torshovdalen are showing a "no dominant" cation type, while the samples from Grefsen (G1-1 and G1-2) are plotted towards the left corner, indicating a calcium dominant type. Sample from the rainwater also shows some deviation with a decrease of Ca^{2+} compared to samples from Akerselva and the groundwater. The rainwater is still located within the "no dominant" cation type, although an enrichment in Na^{+}, K^{+} and Mg^{2+} is observed. Regarding the anion composition, all samples are plotted towards the right corner in the triangle, reflecting a clear dominance of chloride.

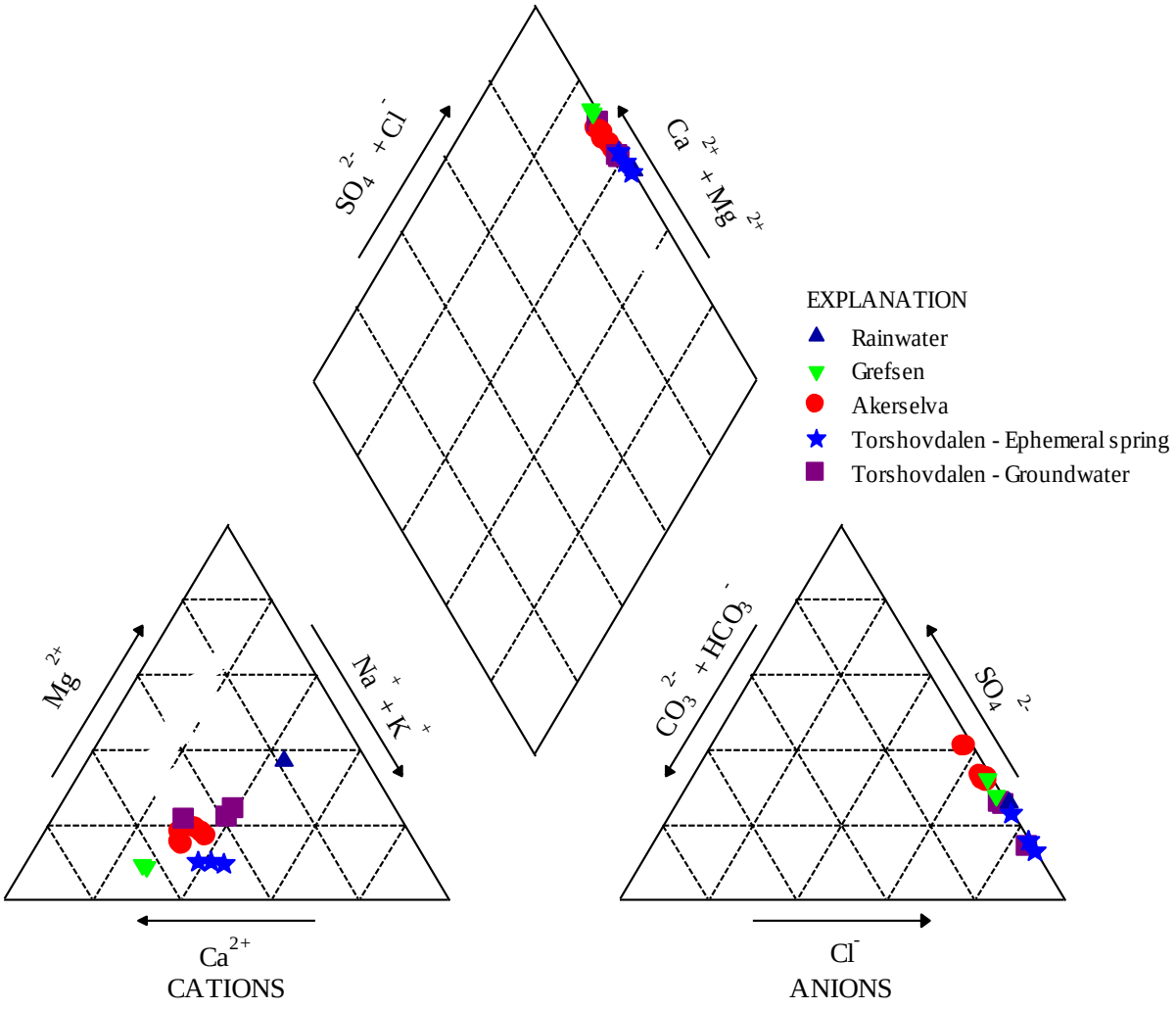

Figure 5.2. Bulk chemical composition of water samples plotted in a Piper diagram. As seen in the diamond shaped diagram, most of the samples are of calcium-chloride type. The rainwater contains more sodium, potassium and magnesium, and the sample from Grefsen contains more calcium compared to the other samples.

Results assembled from QICPMS are shown in Figure 5.3. As seen in the figure, all samples have a relatively similar trend regarding the concentration of each trace element. The ephemeral spring in Torshovdalen (T-2) together with water samples gathered from the newly installed groundwater wells (W3-1, W3-2 and W1-1) in the same area shows some deviations compared to the other water samples. High concentration of Zn is found in T1-2 and W3-2. In general, all samples contain a higher concentration of aluminium (Al), manganese (Mn), iron (Fe) and strontium (Sr). Further description of the different water samples are given in the next sections.

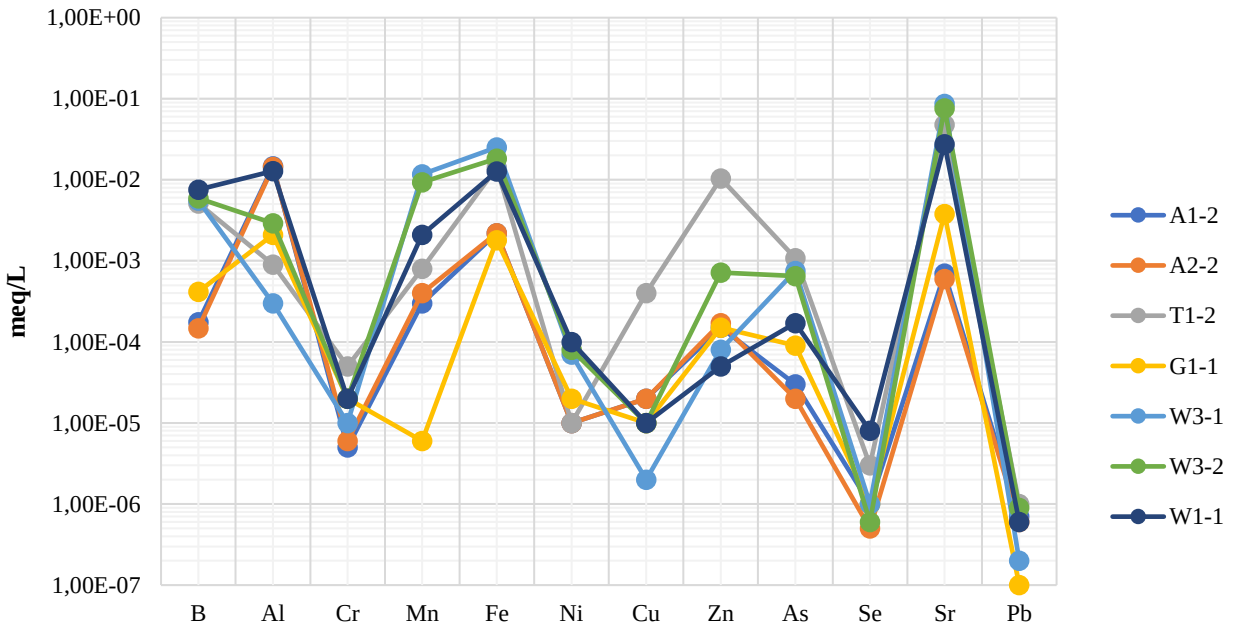

Figure 5.3. Results of the trace element analysis (QICPMS) of the water samples from Akerselva (A1-2, A2-2), Torshovdalen (ephemeral spring T1-2 and groundwater wells W3-1, W3-2, W1-1) and Grefsen (G1-1).

5.2.1. Rainwater

The rainwater sample was collected on September 21, 2018 (the sample R1). 2.6 mm precipitation was registered at Blindern at this date, resulting in enough water to perform ion chromatography and measure the pH. The alkalinity was calculated by using the equation 4.1. The analysis of major cations and anions can be seen in Figure 5.4. The values in sample R1 generally show low concentrations compared to the samples from Torshovbekken watershed, with sodium and chloride as the dominating cation and anion.

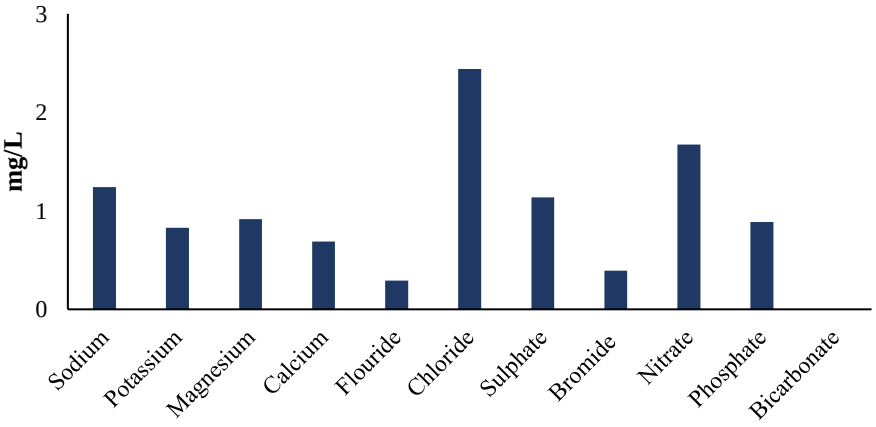

Figure 5.4. Cation and anion concentration in rainwater (R1) collected 21.09.2018. Chloride and sodium are the dominating cation and anion.

pH was measured to 6.4 in sample R1 (Figure 5.5), and the electrical conductivity was calculated to be 18.5 µg/L (Eq. 4.1). The temperature measured was 7.2 °C, but there are some uncertainties to this value as the temperature was not measured in situ, but in the laboratory, approximately 10 min after the sample was brought inside. The air temperature registered at Blindern that day was 11.2°C.

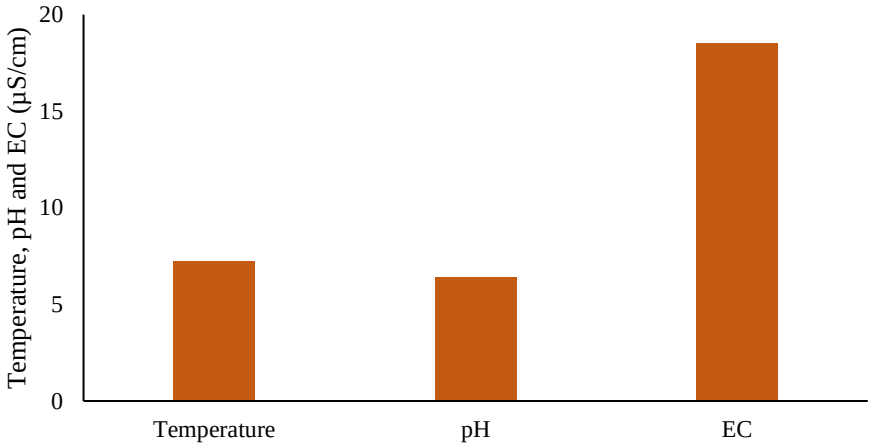

Figure 5.5. Temperature, pH and EC in rainwater (R1) collected 21.09.2018.

In Figure 5.6, results of the average concentration of inorganic ions in rainwater from selected Norwegian rainwater stations are given in context to the result obtained at Blinder on September 21, 2018. The results are modified from a report by Aas (2018). Phosphate and fluoride are not included in the report, but they were analysed in the sample R1 at the University of Oslo. Sodium and chloride are the dominant cation and anion in all rainwater samples (Figure 5.6), even though the concentration varies. Birkene and Blindern have approximately similar concentrations regarding sodium and chloride, and for the other inorganic ions, the highest concentrations are measured in Blindern.

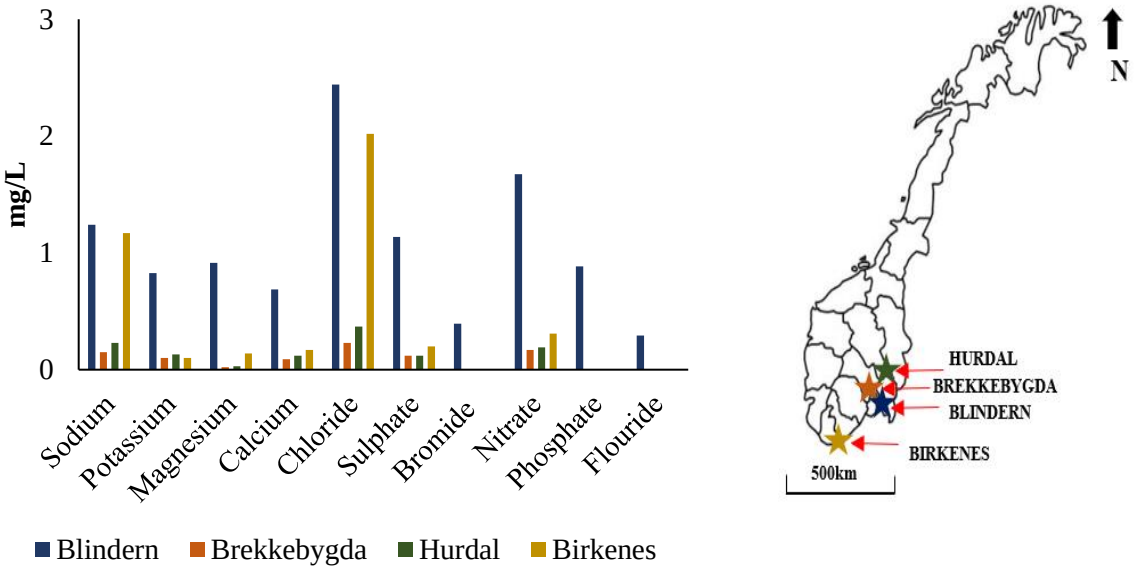

Figure 5.6. Average cation and anion concentration in precipitation, measured at Norwegian stations in 2017 (the results are modified from Aas (2018) and compared to the result obtained from Blindern 21.09.2018).

5.2.2. Grefsen

Two samples were collected in a water stream located in Grefsen, taken on September 22 (G1-1) and November 12 (G1-2) (Figure 4.1). The stream was dry during the summer due to high temperatures and little precipitation, which is why both samples were collected during the Autumn 2018.

The results of major elements analysis are given in Figure 5.7, showing that chloride is the dominant anion followed by sulphate, and calcium the dominating cation, followed by sodium. Similar results were gathered from the two sampling dates, even though the sample G1-2 was collected after a period with heavy rainfall. The concentration of soluble silicates in sample G1-1 was 9.6 mg/L.

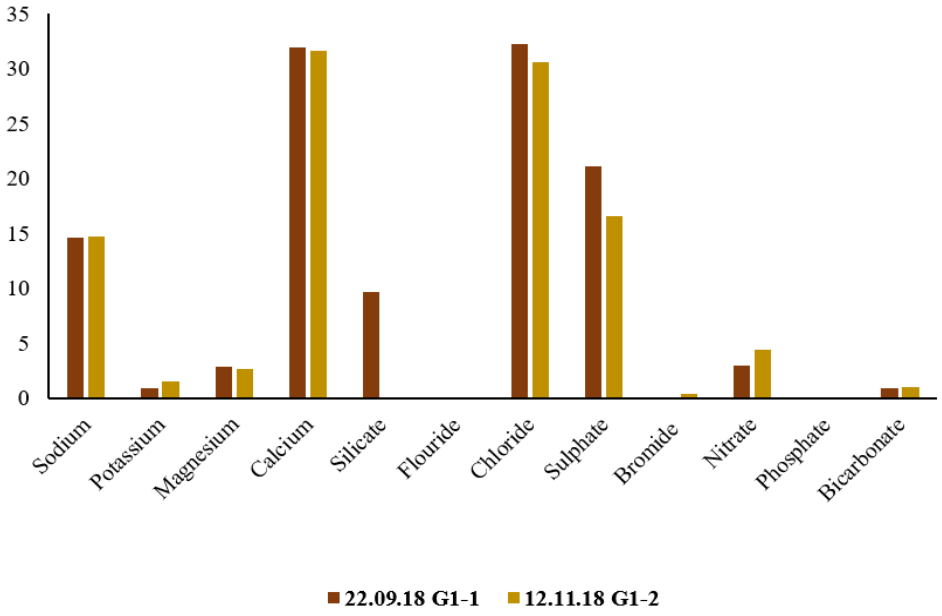

Figure 5.7. Cation and anion concentration in the stream located in Grefsen (G1-1 and G1-2). Calcium and sodium were the dominating cations. Chloride and sulphate were the dominating anions.

Small variations in G1-1 and G1-2 were also observed in both temperature and EC. The temperature varied between 6.7 to 8.2 °C and the EC between 229 to 246 µS/cm. pH obtained in the two samples G1-1 and G1-2 was 7.30 and 7.75, respectively (Figure 5.8).

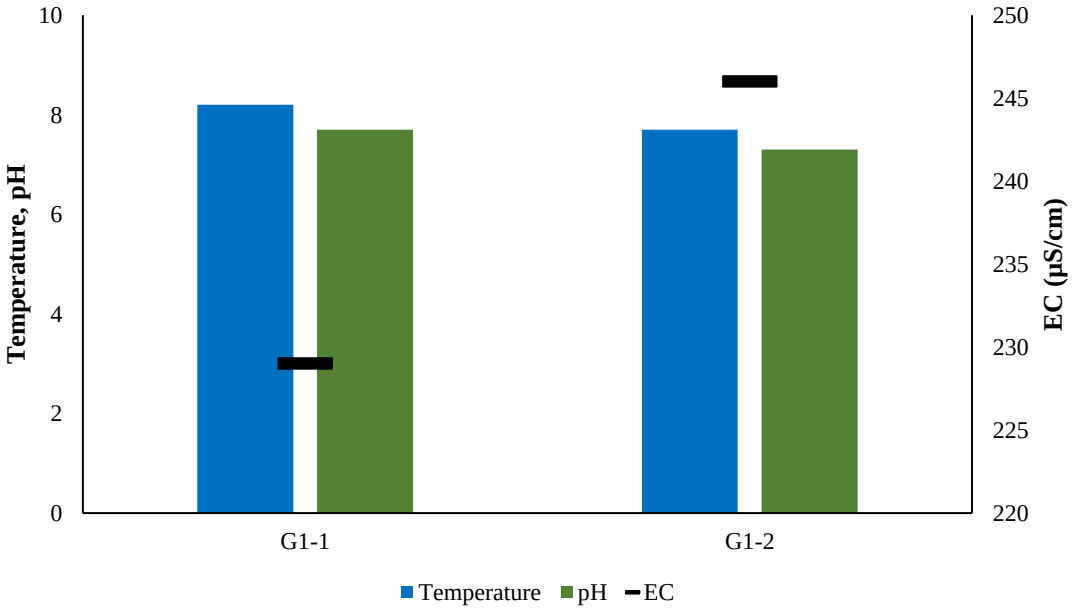

Figure 5.8. Temperature, pH and electrical conductivity (EC on the secondary axis) in a water stream located in Grefsen (G1-1 and G1-2).

The trace element results from sample G1-1 are presented in Figure 5.9. Strontium is the trace element with the highest concentration (169 µg/L) followed by iron, aluminium and boron. Other components showed concentration < 5µg/L.

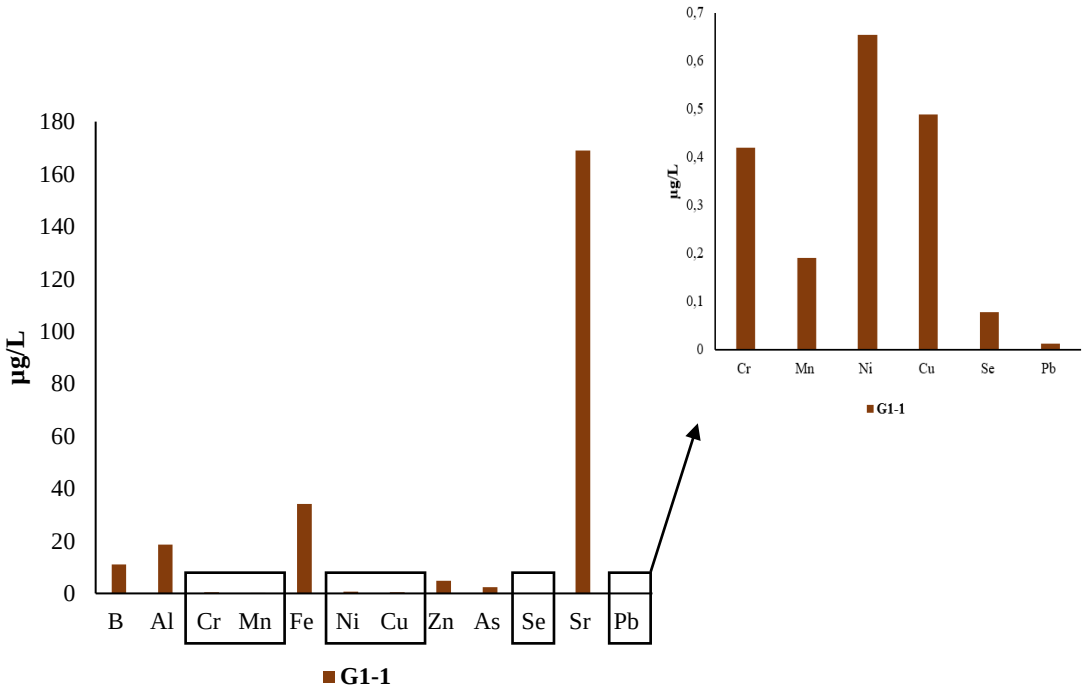

Figure 5.9. Trace element analysis from Grefsen (G1-1). Strontium, iron and aluminium are the dominant elements.

5.2.3. Akerselva

Three sampling campaigns were done in Akerselva and Torshovdalen, in the year 2018 (Table 5.1). The third sampling campaign (November 12) was done after heavy rainfall (Figure 5.1). The results from the ephemeral spring in Torshovdalen (T1) are given in the section 5.2.4. However, the field parameters from Akerselva and the ephemeral spring are displayed together in Figure 5.13 as they were measured during the same field campaigns. Location of the sampling points in Akerselva are shown in Figure 5.10 below.

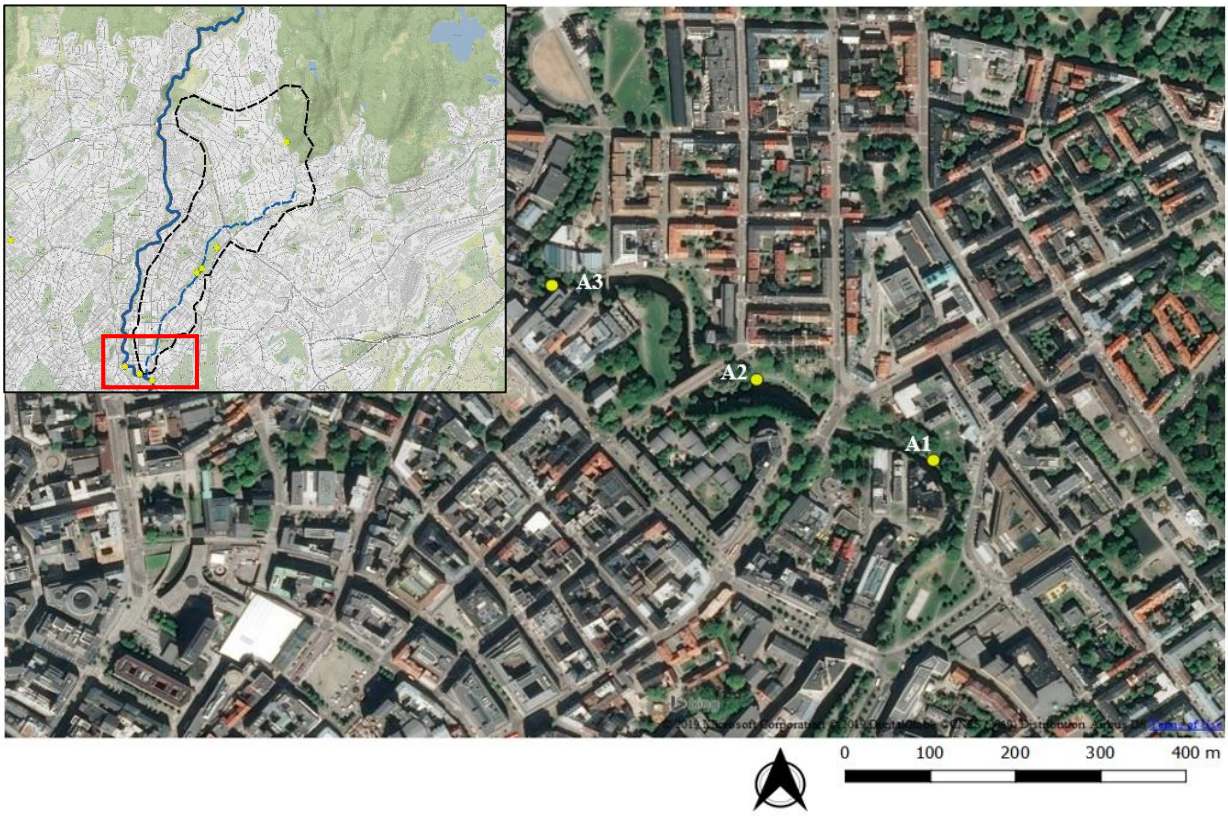

Figure 5.10. Water samples was collected from the sampling point A1 and A2 in Akerselva. A3 is the location of were VAV collects weekly samples for E. coli analysis.

As seen in Figure 5.11 and Figure 5.12, similar results have been obtained at the two locations (A1 and A2) in Akerselva. The dominate anion was chloride, followed by sulphate, in all six samples. The cation chemistry shows that calcium and sodium were the dominating cations, with values far higher that potassium and magnesium. A higher concentration of almost all elements, except for silicate and phosphorus, is found in the two samples (A1-3 and A2-3) collected on November 12, after a heavy rainfall (Figure 5.1). The concentration of soluble silicates in the water samples from Akerselva (A1-2 and A2-2), where approximately 3.4 mg/L for both samples.

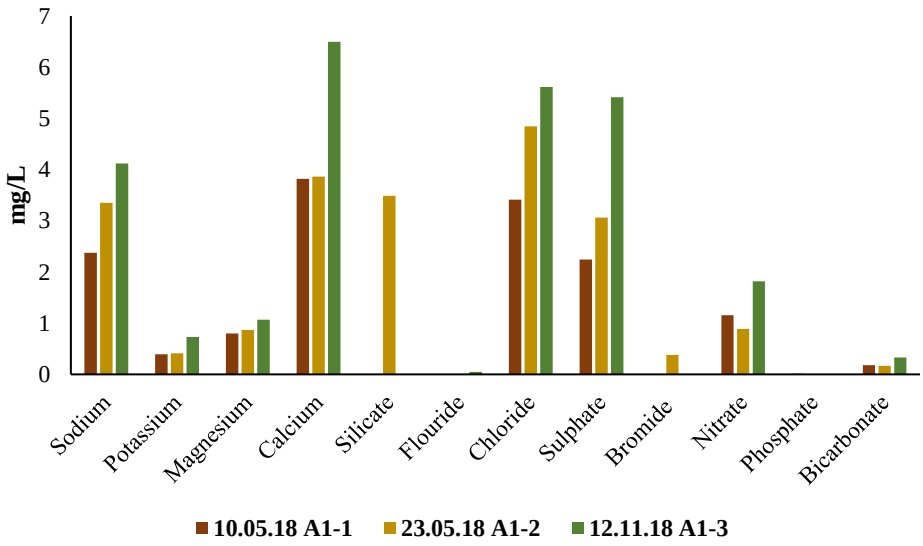

Figure 5.11. Cation and anion concentration in Akerselva at location A1 in the three sampling campaigns. Chloride and calcium are the dominant ions. The samples from 12.11.18 show a higher concentration for all elements.

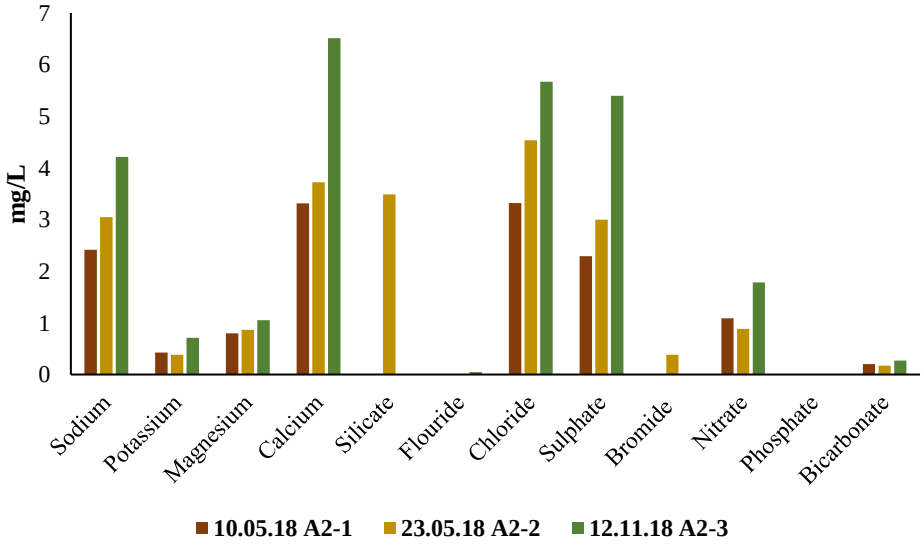

Figure 5.12. Cation and anion concentration in Akerselva at location A2 in the three sampling campaigns. Chloride and calcium are the dominant ions. The samples from 12.11.18 show a higher concentration for all elements.

The pH, electrical conductivity (EC) and water temperature measured during the three sampling campaigns are seen in Figure 5.13.

A pH value between 6.8-7.5 was measured from all water samples collected in Akerselva. The highest temperature was measured on May 23, 2018, from A1, A2 and T1. On this day, the highest electrical conductivity in the ephemeral spring (T1) was also measured, while the highest EC in the sampling points A1 and A2 was measured on November 12.

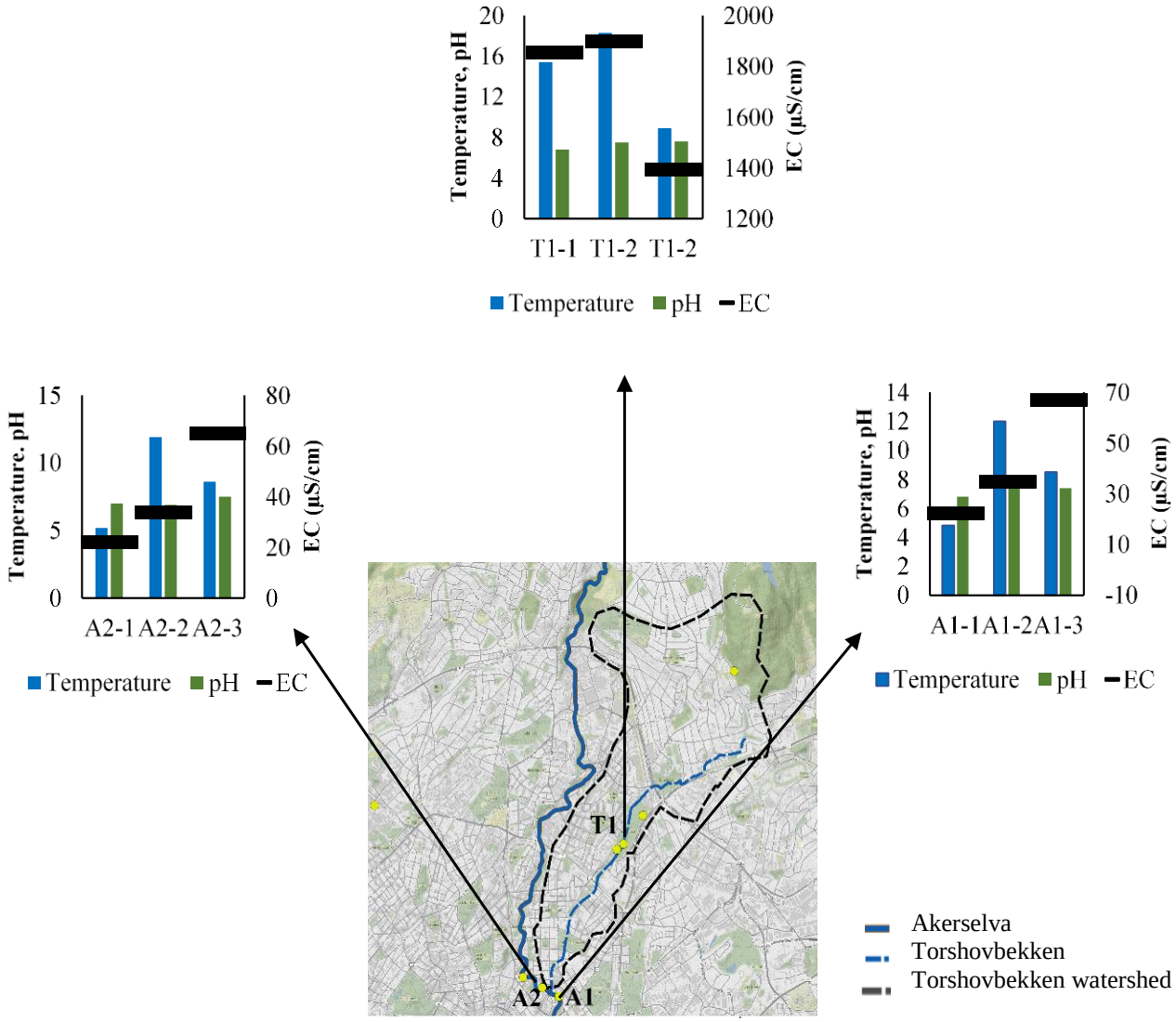

Figure 5.13. pH, EC (electrical conductivity) and temperature measured in the water during three sampling campaigns in Akerselva and Torshovdalen (10.05.2018; A1-1, A2-1, T1-1. 23.05.2018; A1-2, A2-2, T1-2. 12.11.2018; A1-3, A2-3, T1-3).

From the trace element analysis (Figure 5.14), aluminium, iron and strontium are the elements which stand out with the highest concentrations, with values of 132, 41.9 and 31 µg/L respectively. Boron and selenium are not included since they occur at concentrations below the detection limit of the instrument used. The detection limit for each element is 7.11 and 0.103 µg/L, respectively.

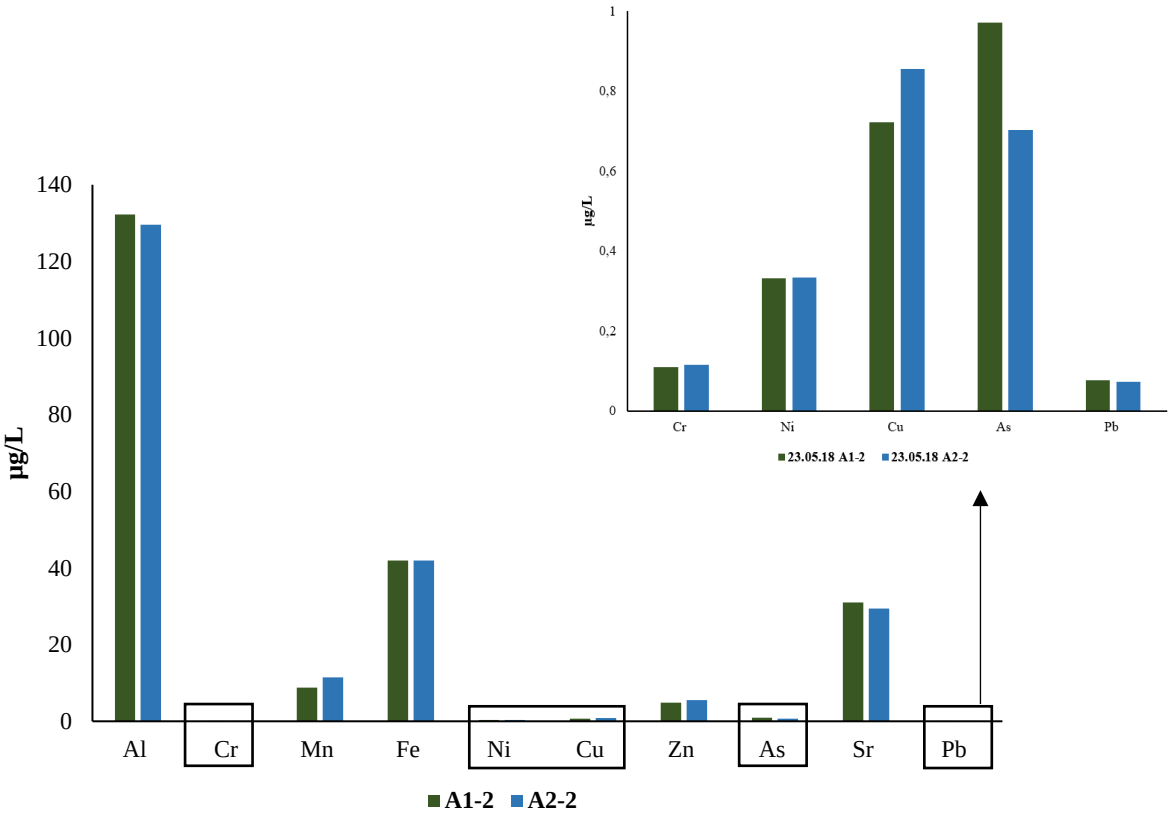

Figure 5.14. Trace element analysis of samples from Akerselva on the 23rd May 2018. Aluminium, iron and strontium are the dominant trace elements.

5.2.4. Torshovdalen - Ephemeral spring

The ion chemistry from the ephemeral spring in Torshovdalen (T1) (Figure 4.1) shows that chloride and sulphate are the dominant anions followed by nitrate and bicarbonate (Figure 5.15). Sodium and calcium are the dominating cations analyzed in the samples. All elements showed significantly higher values compared to the other samples collected within Torshovbekken watershed, i.e. Akerselva and Grefsen. The concentration of soluble silicate in the sample T1-2 was 9.3 mg/L. The pH measured from the ephemeral spring varied between 6.8 – 7.5, the same as the results obtained in Akerselva (Figure 5.13). The electrical conductivity in the ephemeral spring (T1) stands out due to high values, ranging between 1850 to 1900 µS/cm. The temperature was also higher in the ephemeral spring with values between 8.4 to 15 °C (Figure 5.13).

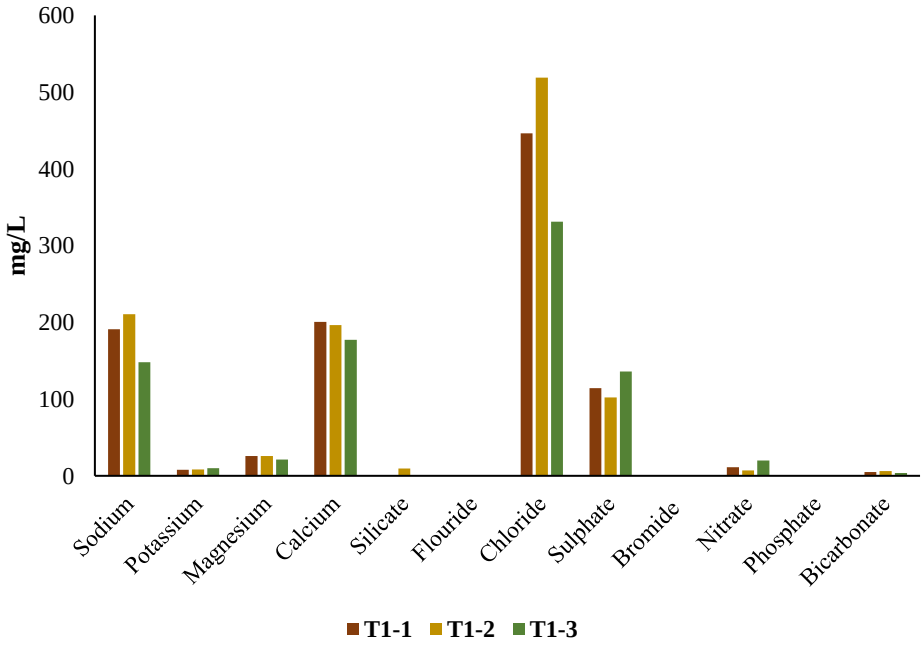

Figure 5.15. Cation and anion concentration from the ephemeral spring in Torshovdalen (T1) in the three sampling campaigns. T1-1 was collected 10.05.2018, T1-2 was collected 23.05.2018 and T1-3 was collected 12.11.2018. Chloride, calcium and sodium are the dominant ions.

From the trace element analysis of sample T1-2 (Figure 5.16), the element with the highest concentrations was strontium followed by zinc, iron and boron, with values of 2097.7, 329.4, 265.3 and 136.8 µg/L respectively. Other elements were at concentrations < 50 µg/L.

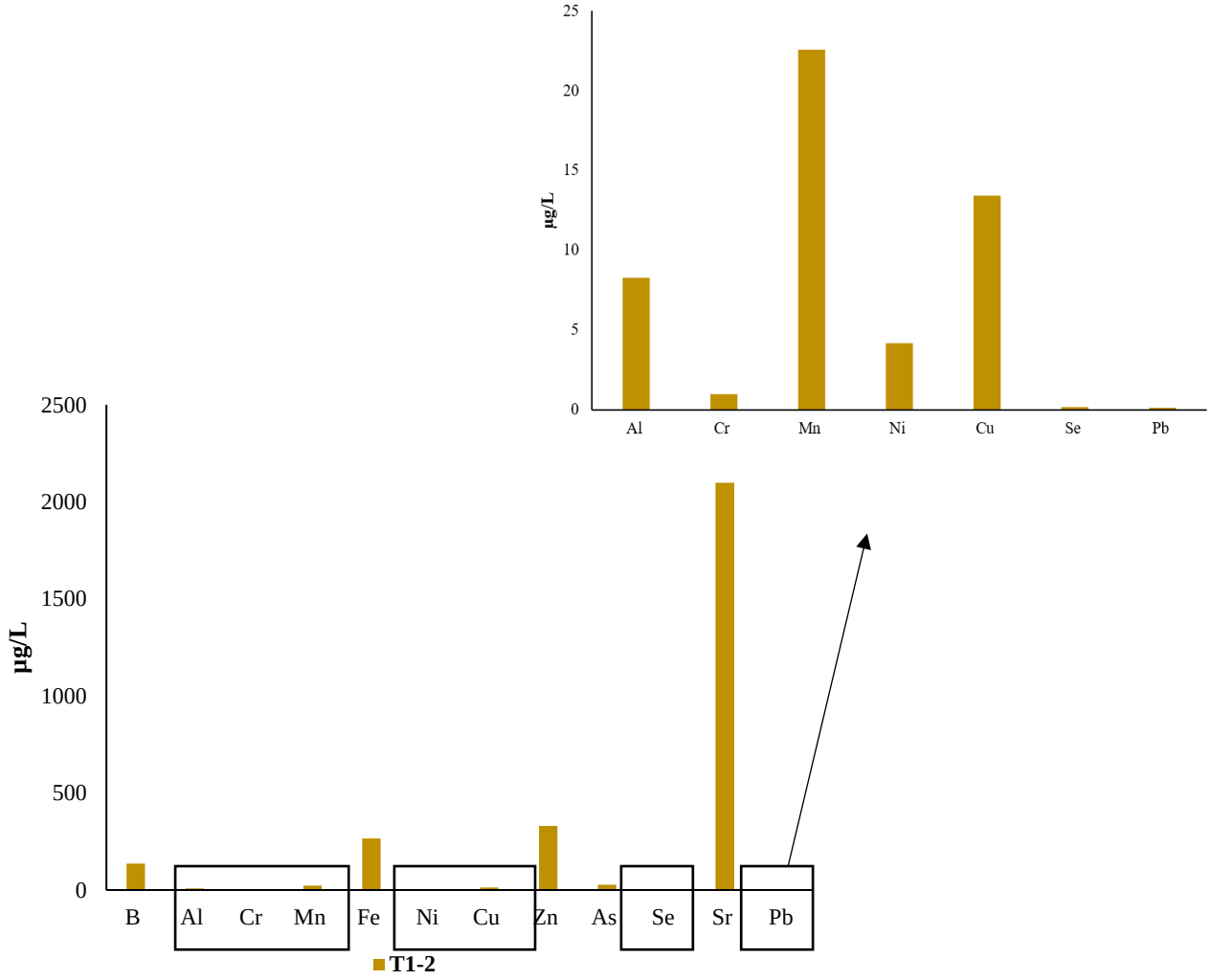

Figure 5.16. Trace element analysis from the ephemeral spring in Torshovdalen (T1-2). Strontium, zinc, iron and boron are the dominant elements.

5.2.5. Torshovdalen – The unsaturated zone

During the drilling operations of the groundwater wells in Torshovdalen, sediment samples were collected along the intersected unsaturated zone (Table 5.4). The result of the major element analysis (divided into cations and anions) of the porewater in the unsaturated zone is shown in Figure 5.17 where the samples are plotted stratigraphically in meters below the surface. Equation 4.5 was used to calculate the concentration of each element, resulting in a concentration expressed in mg/g (of dry sediment) for major elements, and µg/g (of dry sediments) for trace elements.

Table 5.4. The depth in meters below the surface of each sample collected from the unsaturated zone during the drilling operation of the groundwater wells in Torshovdalen.

Well W1	Depth (m)	Well W2	Depth (m)	Well W3	Depth (m)
W1-L1.5	0 – 1.5	W2-L1	0 – 1	W3-L1	0 – 1
W1-L2.5	1.5 – 2.5	W2-L2	1 – 2	W3-L2	1 – 2
W1-L3.5	2.5 – 3.5			W3-L4	3 – 4

Calcium is the dominant cation in all the samples from the unsaturated zone (Figure 5.17), with the highest concentration in the sample W3-L4 (0.44 mg/g dry weight calcium). High values of calcium were also observed in samples W3-L2, W3-L1, W2-L1 and W1-L2.5. Sample W3-L4 is also the sample with the highest content of potassium (0.078 mg/g) and magnesium (0.032 mg/g), while sample W2-L1 standout with the highest concentration of sodium (0.14 mg/g).

Sulfate is the dominant anion followed by chloride. Samples W3-L4, W3-L2 and W2-L1 contain a higher concentration of sulfate compared to the other sample. Additionally, the sample W3-L2 contained a high concentration of nitrate compared to the other sediment samples (Figure 5.17).

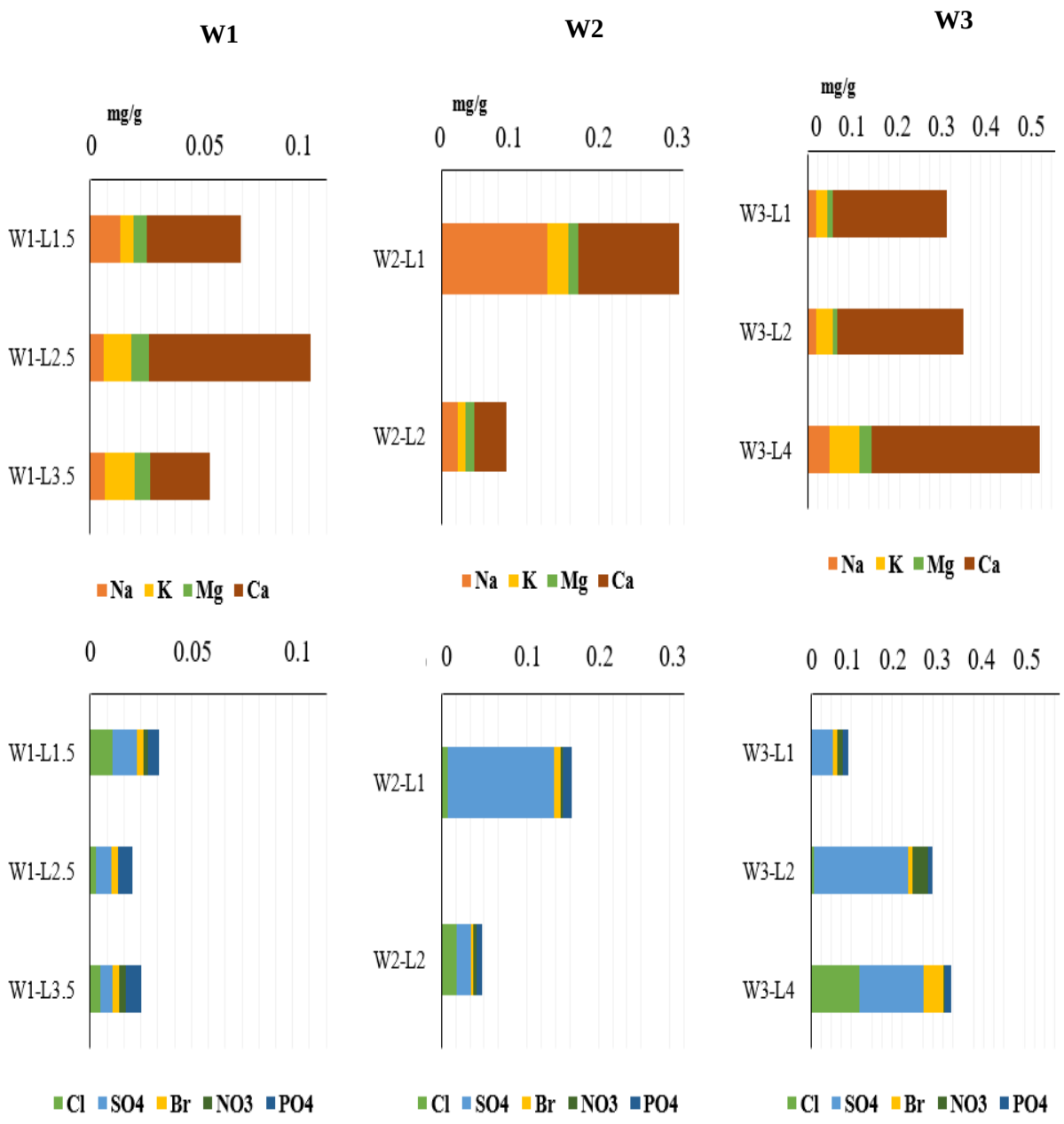

Figure 5.17. Chemical composition of major cations and anions in the unsaturated zone in Torshovdalen, given in mg/g of dry sediments. The samples collected from each location (W1, W2 and W3) are plotted stratigraphically.

Trace element results, obtained from QICPMS, are displayed stratigraphically for the three groundwater boreholes (W1, W2 and W3) in Figure 5.18, Figure 5.20 and Figure 5.19. From well W1, the sample W1-L2.5 stands out due to the high concentration of manganese (the concentration of Mn in W1.L2.5 and W3-L4 is divided by 10 in Figure 5.18 and Figure 5.19, respectively). 11.3 µg/g manganese are found in sample W1-L2.5, which is significantly higher than 1.1 and 0.5 µg/g measured in the samples W1-L.5 and W1-L3.5, respectively. Strontium, iron, and aluminium are also found in remarkable values compared to the other trace elements.

Concentrations from well W2 are generally lower compared to the wells W1 and W3. Strontium is the dominant trace element, with concentrations of 2.4 µg/g in sample W2-L1 and 2.3 µg/g in sample W2-L2, followed by iron, manganese, aluminium and boron. Manganese, together with iron, are the trace elements with the highest concentration in the two samples in well W3 (W3-L1 and W3-L4), followed by strontium and boron. All results from the extracted pore water samples are listed in Appendix E1 and E2.

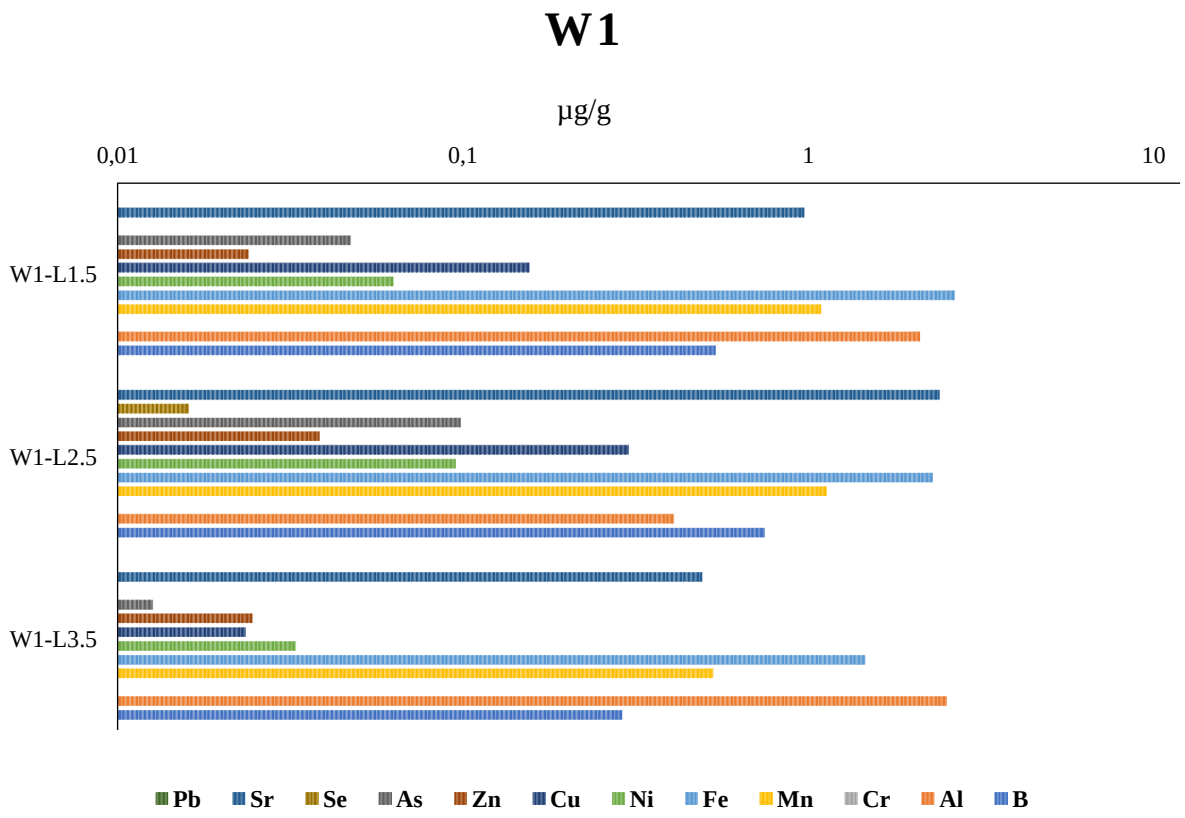

Figure 5.18. Chemical composition of trace elements in the unsaturated zone in from groundwater well W1 in Torshovdalen. All elements are given in µg/g dry weight of sediments. The concentration of manganese (Mn) in the water sample W1-L2.5 is divided by 10.

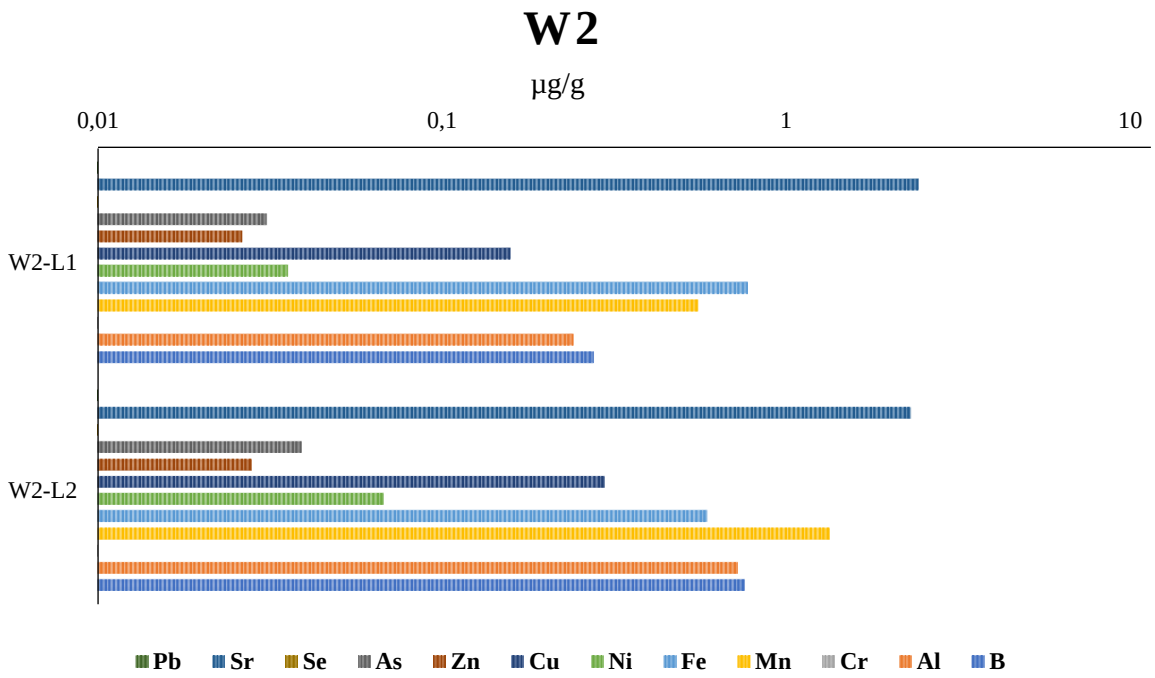

Figure 5.20. Chemical composition of trace elements in the unsaturated zone in from groundwater well W1 in Torshovdalen. All elements are given in µg/g dry weight of sediments.

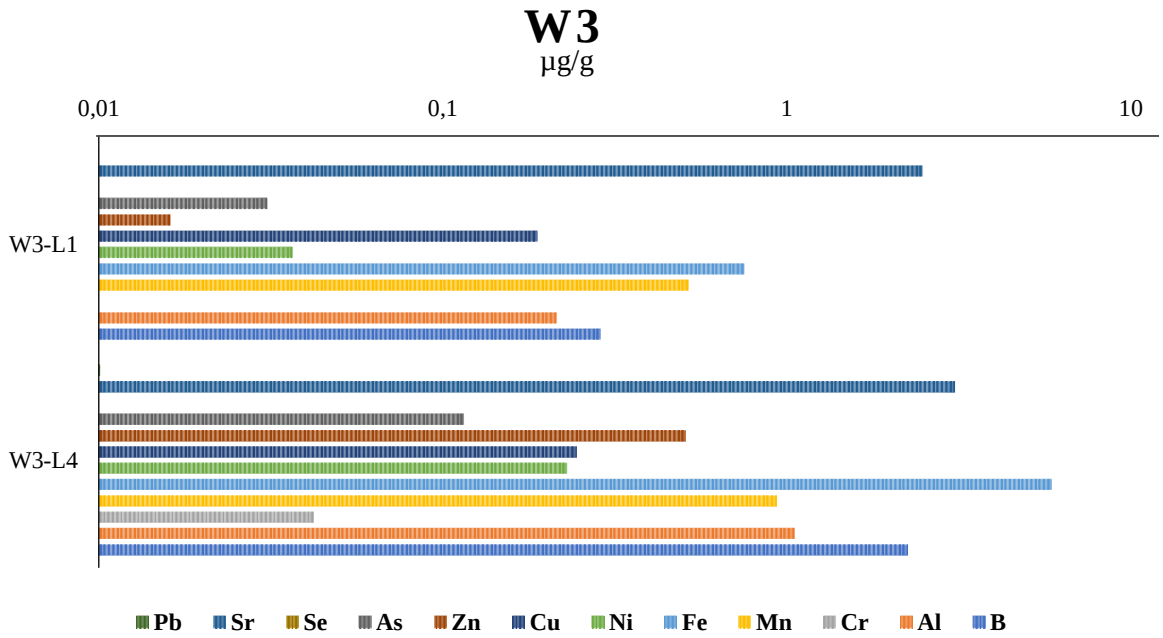

Figure 5.19. Chemical composition of trace elements in the unsaturated zone in from groundwater well W3 in Torshovdalen. All elements are given in µg/g dry weight of sediments. The concentration of manganese (Mn) in the water sample W3-L4 is divided by 10.

5.2.6. Torshovdalen - Groundwater wells

Samples were collected on the September 26 (W3-1) and October 10 (W3-2) in well W3, and one sample on October 10 in well W1 (W1-1) (Figure 5.21).

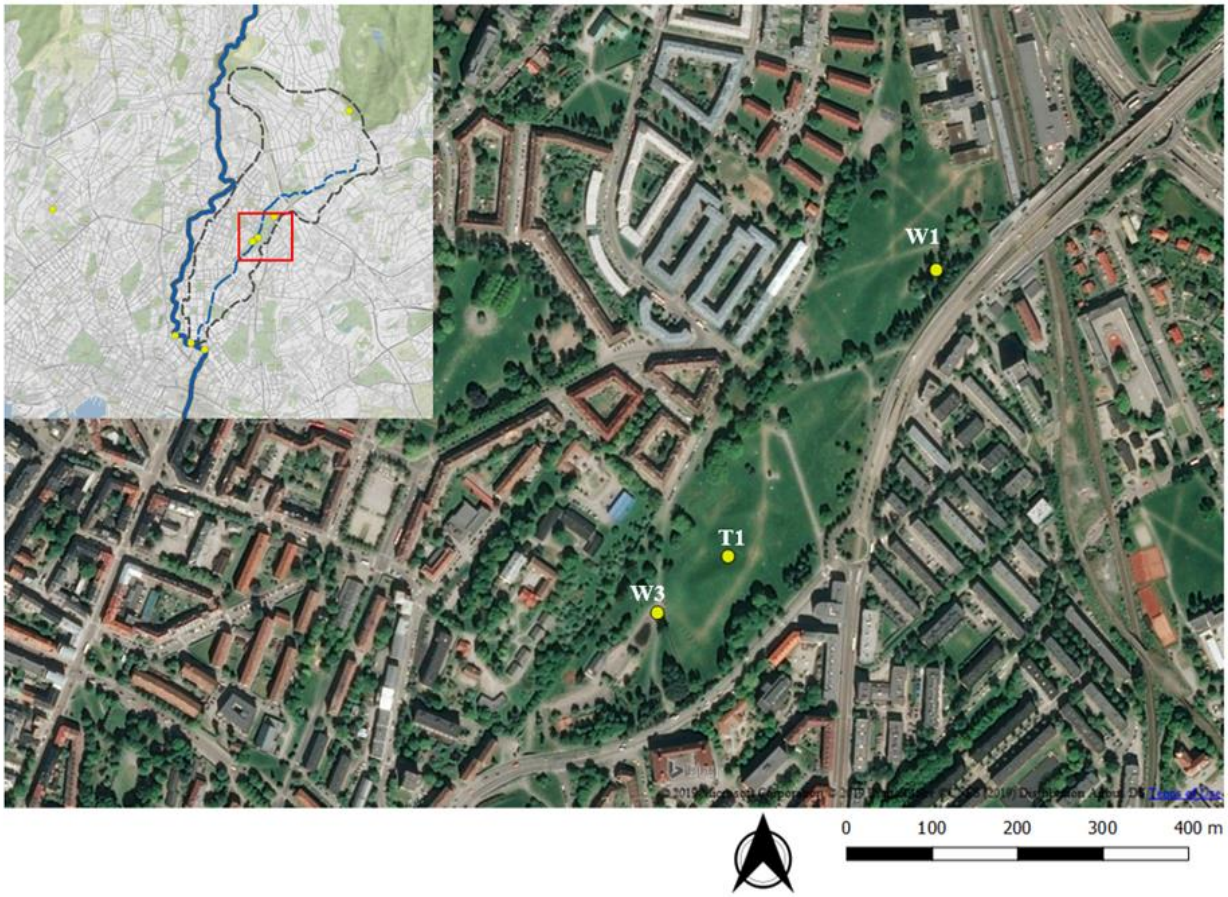

Figure 5.21. Water samples representing the groundwater was collected from the well W1 and W3 (the samples W3-1 and W3-2). Three samples were also taken from the ephemeral spring (T1-1, T1-2 and T1-3), described in section 5.2.4.

The concentration of major cations and anions in the groundwater wells drilled in Torshovdalen is given in Figure 5.22. Sodium and chloride were the cation and anion with the highest concentration in the samples W3-1 and W3-2, but also the anion sulphate and cation calcium show significant high values. As seen in Figure 5.22, all elements, except fluoride, from the sample W1-1 contained lower amounts compared to the two samples taken from the well W3. Calcium and chloride were the elements with the highest concentration in the well W1. The concentration of soluble silicates in W3-1 and W3-2 was 11.7 mg/L and 11.9 mg/L, respectively. The water sample from the northern groundwater well (W1) resulted in a lower concentration of soluble silicates compared to the samples from well W3. 5.3 mg/L soluble silicates were measured in W1-1.

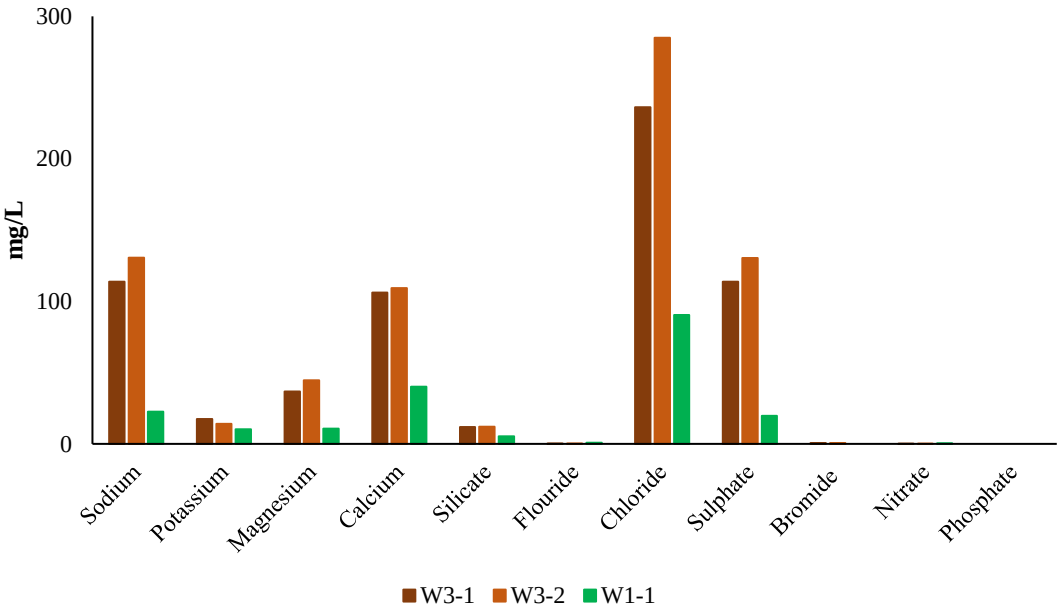

Figure 5.22. Cation and anion concentration in groundwater wells from Torshovdalen, W1 and W3. Sodium and calcium are the dominating cations, and chloride and sulphate the dominating anions.

pH of the analyzed water samples from the groundwater ranged from 7.95 to 8.08, which were the highest values obtained from water samples collected within Torshovbekken watershed. The measured EC varied from 1219 to1300 µS/cm (Figure 5.23). Regarding the temperature, small variations were observed, giving a temperature of approximately 5.5°C.

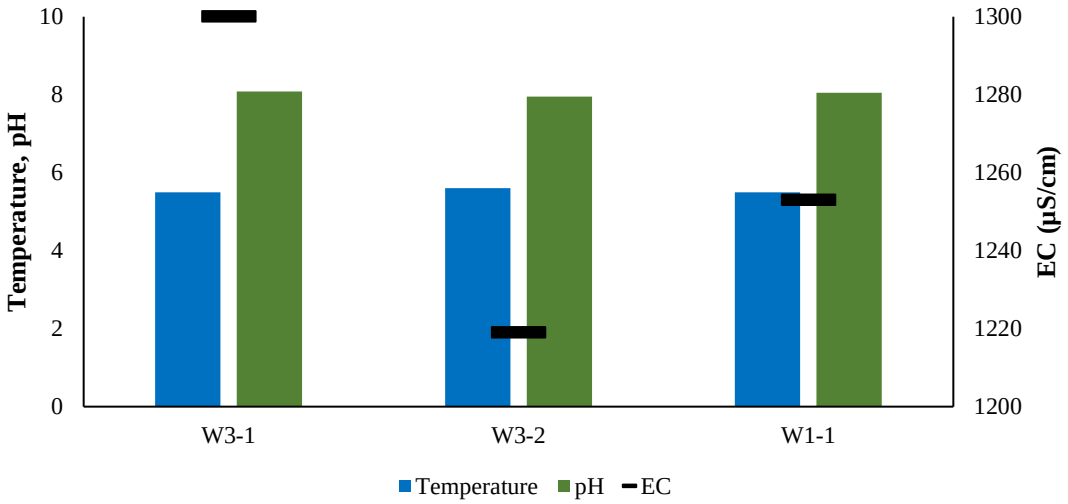

Figure 5.23. Temperature, pH and EC (secondary axis) measured in groundwater wells from Torshovdalen, W1 and W3.

The trace element analysis of the samples collected in the groundwater wells in Torshovdalen can be seen in Figure 5.24. The results are to some extent similar to the ones obtained in the samples from the ephemeral spring (T1) in Torshovdalen (Figure 5.16), except for the increase of manganese and decrease in zinc and arsenic. Strontium is still the dominate trace element in all three samples, with values in the range of 1209 to 3785 µg/L, highest concentration obtained from the samples collected in the southern groundwater well (W3-1 and W3-2). Selenium is not included due to concentrations being below the detection limit of the instrument used (0.103 µg/L).

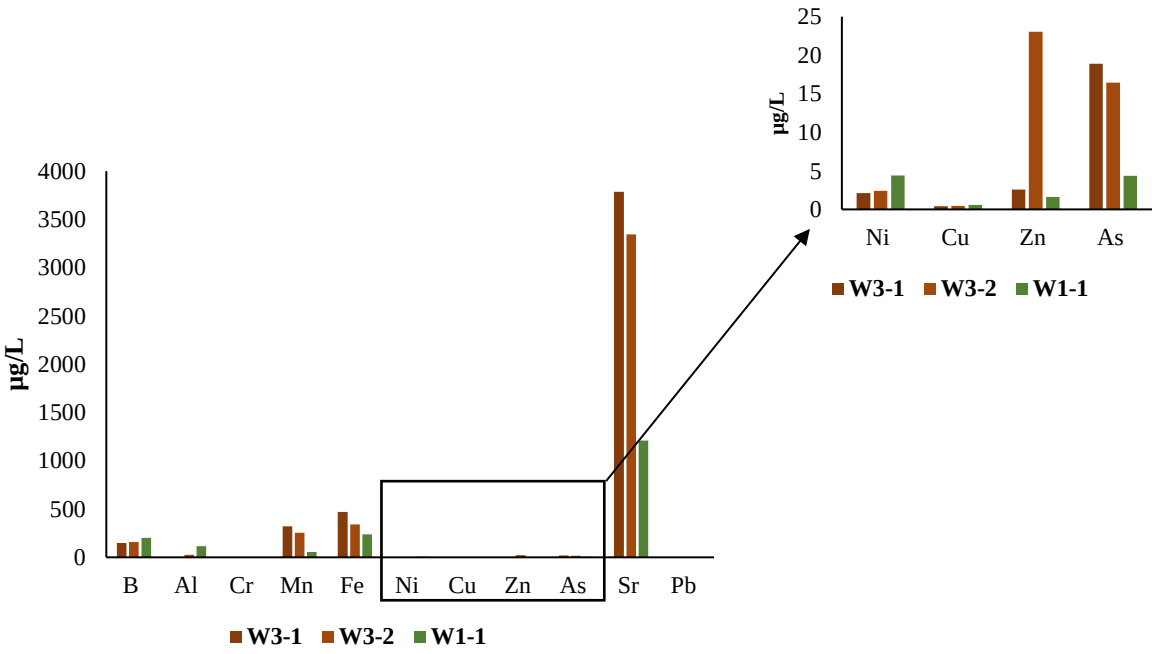

Figure 5.24. Trace element analysis from the groundwater wells (W1 and W3) in Torshovdalen. Strontium, iron and manganese are the dominant elements.

5.2.7. Bivariate analysis

Correlations between major and trace elements, together with field parameters (pH, temperature, EC), were assessed by calculating Pearson's correlation coefficient (Appendix B6). The correlations were based on results from the following water samples: A1-2, A2-2, T1-2, G1-1, W3-1, W3-2 and W1-1.

The Pearson's correlation coefficient was used to describe the degree of relation between two parameters (Asa Rani and Babu, 2008). A high correlation coefficient (>0.9 or <-0.9) indicates a good relationship (direct or inverse) between two parameters. Selected scatter plots are shown in Figure 5.25 (note the different scale), all having a positively high correlation coefficient (>0.9). Sodium, potassium, magnesium, calcium and strontium were the elements showing the highest correlation with other elements.

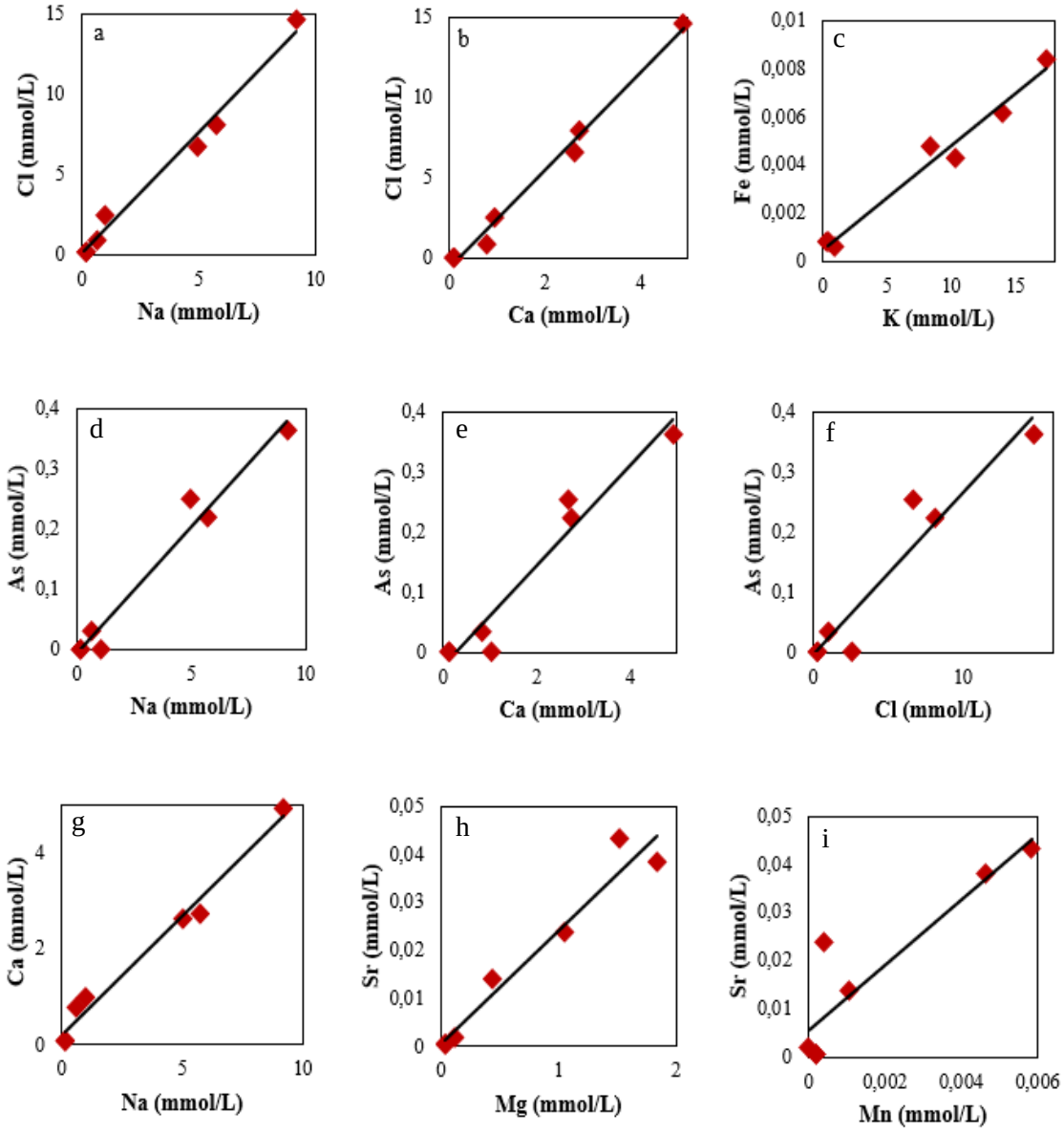

Figure 5.25. Scatter plot between (a) Na vs Cl (b) Ca cs Cl (c) K vs Fe (d) Na vs As (e) Ca vs As (f) Cl vs As (g) Na vs Ca (h) Mg vs Sr (i) Mn vs Sr.

5.3. Bacterial characterizations

The presence of *E. coli* in the environment is used as an indicator of faecal pollution. *E. coli* concentrations have been measured in the ephemeral spring in Torshovdalen (T1), in two of the groundwater wells (W1 and W3), Akerselva (A1, A2) and Grefsen (G1). Also, *E. coli* has been measured weekly since February 19, 2018 by VAV (A3) (Table 5.5). An overview of maximum, minimum and average measured *E. coli* /100 ml of a water sample, as well as the number of measurements done at each location, are presented in Table 5.5 below. As observed in the table, somewhat similar results are found in all three locations in Akerselva, with slightly higher values at A1. The ephemeral spring in Torshovdalen (T1) stands out as the sampling point with the highest average concentration of *E. coli* bacteria, while the lowest concentrations are found in the groundwater (W1 and W3). Low values were also measured in the small stream in Grefsen (G1). In Figure 5.26, Figure 5.27 and Figure 5.28 *E. coli*/100mL are shown together with measured precipitation (mm) the last 24 hours before the samples were collected, given in mm/day. All data regarding rainfall are gathered from eklima.met.no.

Table 5.5. Overview of the sampling points, minimum, maximum and average concentration (E. coli/100mL) and the number of measurements done at each sampling point. Results from A3 are measured by VAV.

Sample	Max *(date)*	Min *(date)*	Average	Number of measurements
A1	3877 *(18.06.18)*	474.5 *(30.05.18)*	2087.4	4
A2	2459.5 *(18.06.18)*	441.5 *(30.05.18)*	1048.1	4
A3	20460 *(10.09.18)*	30 *(14.05.10)*	1035.1	36
T1	7628.5 *(18.06.18)*	5 *(12.11.18)*	3705.2	5
W1	0 *(12.11.18)*	0 *(12.11.18)*	0	1
W3	0 *(12.11.18)*	0 *(12.11.18)*	0	2
G1	24 *(12.11.18)*	24 *(12.11.18)*	24	1

5.3.1. Grefsen

One sample was collected from the stream located in Grefsen (G1) (Figure 4.1). The sample was collected on November 12, after a weekend with heavy rainfall. The result from the Colilert-18 method showed a low concentration of *E.coli* bacteria in this stream, only 26 *E.coli*/100ml water sample was found.

5.3.2. Akerselva

The highest concentrations of *E. coli* bacteria were measured in Akerselva (A3 in Figure 4.1) on September 10, after heavy rainfall the last 24 hours (Figure 5.26). At this date, 20460 *E. coli*/100 ml were measured. Lowest concentration was measured May 14, after a long period without precipitation.

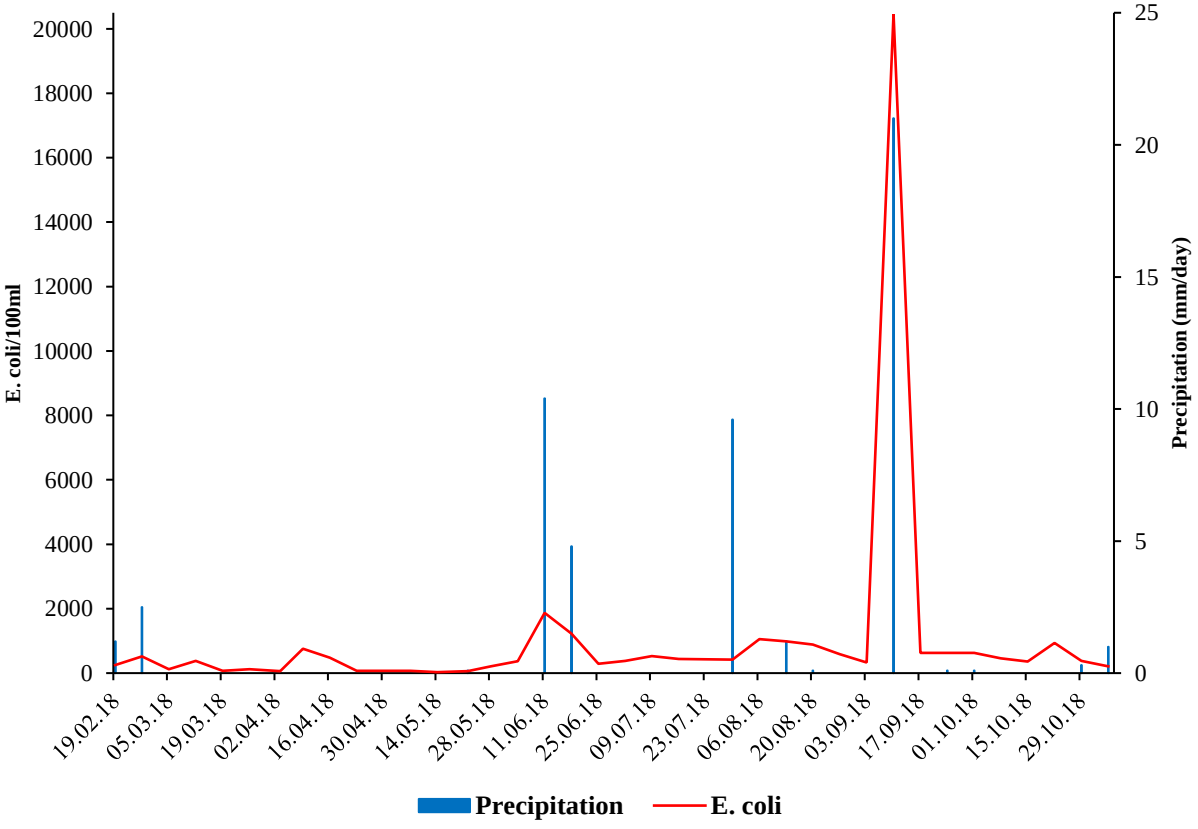

Figure 5.26. The concentration of E. coli bacteria/100mL water sample, at A3, weekly since February 19th – November 5, 2018. Highest measured concentration was achieved on September 10, 2018, concomitant with high precipitation rate. The precipitation reflects the amount registered 24 hours before the water samples were collected.

The same trends were observed in A1 and A2(Figure 5.27), where the highest concentration was measured on June 18, after 24 hours with registered precipitation. As seen in Figure 5.27, similar values were detected in A1 and A2, both having the lowest measurements taken on May 5.

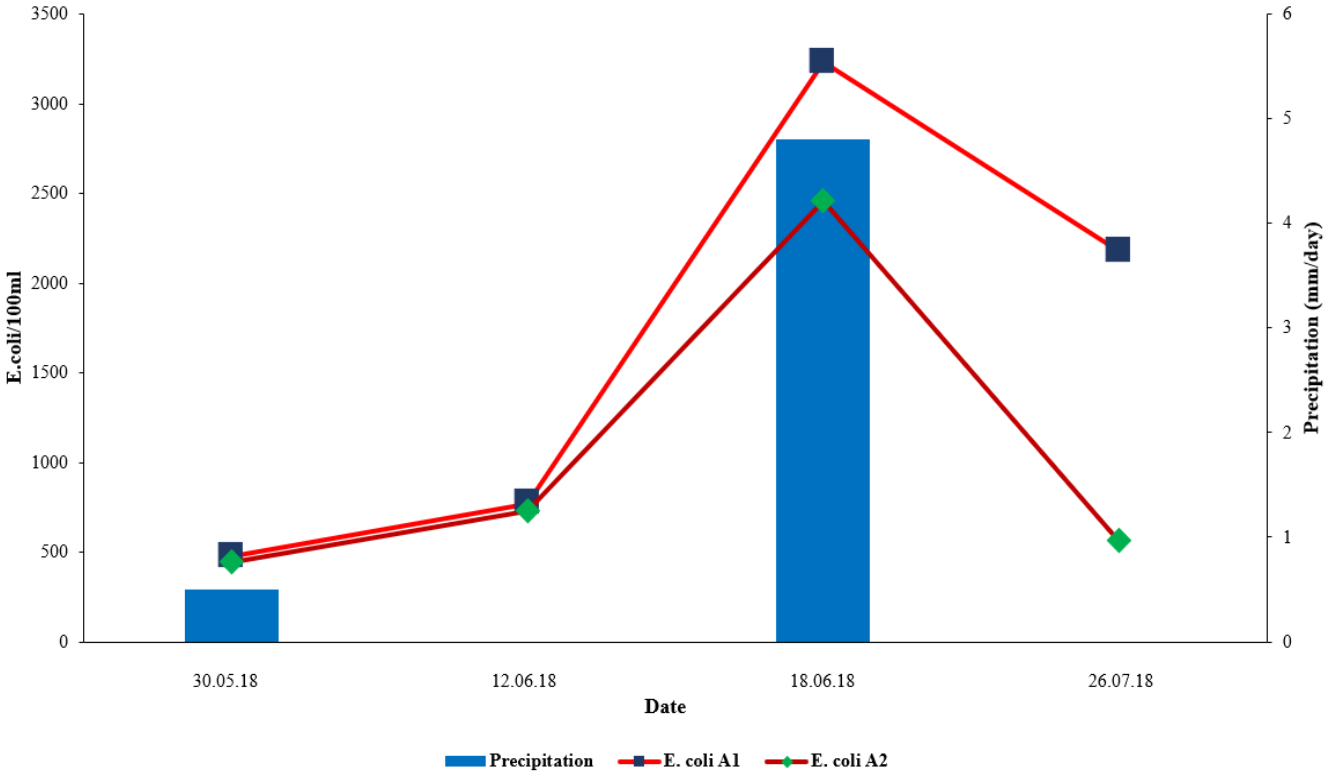

Figure 5.27. The concentration of E. coli bacteria/100mL water sample, at A1 and A2. Highest concentration from both locations were achieved June 18, 2018, together with heavy rainfall the last 24 hours. The precipitation reflects the amount registered 24 hours before the water samples were collected.

5.3.3. Torshovdalen – ephemeral spring

The lowest concentration observed in the ephemeral spring in Torshovdalen (T1) was 5.2 *E. coli*/100ml, measured on November 12, 2018, after a weekend characterized by heavy rainfall (Figure 5.28). The intensive rainfall resulted in an increasing amount of water flowing in the ephemeral spring. Results from the ephemeral spring show some deviations compared to the weekly measurments in Akerselva, as the *E. coli* concentration decreases together with an increase in precipitation. In Akerselva, the *E. coli* concentrations increases during intensive rainfall (Figure 5.26).

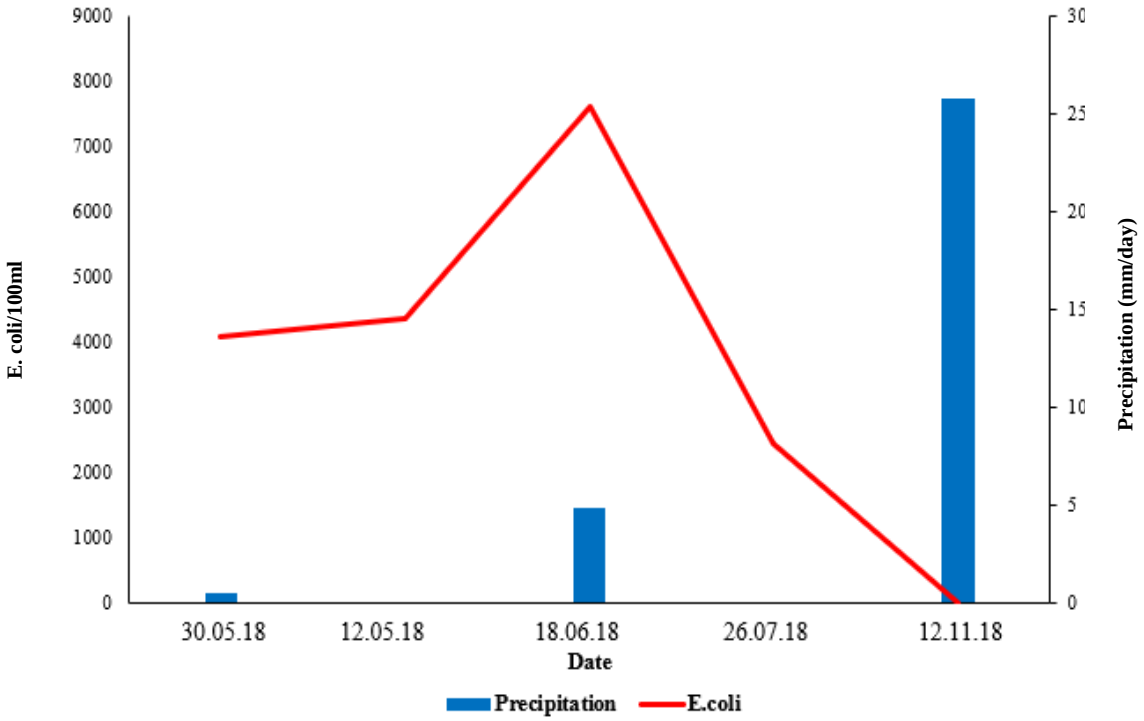

Figure 5.28. The concentration of E.coli bacteria/100 mL water sample from the ephemeral spring in Torshovdalen (T1). Opposite trend, compared to Akerselva, are observed as the lowest concentration was measured after heavy rainfall during the 24 hours that preceded the water sample collection.

5.3.4. Torshovdalen - Groundwater

Two samples were collected from well W3 and one from the well W1 in Torshovdalen. The first water sample from well W3 was collected on October 9, 2018, approximately one month after the installation, while two samples were collected on November 12, one from well W1 and one from well W3. Coliform bacteria were detected in all samples, varying between 389 to 520 coliform/100ml water sample, but none of the samples showed concentration of *E. coli* bacteria.

Since coliform bacteria contains a large group of bacteria, which may not be linked to faecal pollution, this is not included in this chapter. The results are, however, listed in the Appendix B7-B8 together with the results of the measured E. coli concentration at all sampling points. The precipitation (mm/day), before collecting the water samples are also given in Appendix B7-B8. Coliform bacteria are not measured for water samples collected by VAV at sampling point A3 in Akerselva.

5.4. Physical and chemical properties of the soil and sediments

5.4.1. XRD Bulk mineralogy

Ten XRD diffractograms were analyzed using the software *Diffract.eva* and *Profex*. The samples were collected in Torshovdalen, and include loose Quaternary sediments and lithified Palaeozoic limestone, that in this study, constitute the bedrock. Well 1 is represented by six samples, three from the loose sediments and three from the bedrock. Well 2 is represented by three samples, one from the loose sediments and two from the bedrock. Well 3 is represented by one sample from the loose sediments (Table 5.6). The complete XRD-bulk mineralogical composition of the samples is presented in Table 5.7.

Table 5.6. Overview of the soil and sediment samples collected in Torshovdalen, in September 2018. The depth is in meters below the surface

Well W1	Depth (m)	Well W2	Depth (m)	Well W3	Depth (m)
W1-L1.5	0 – 1.5	W2-L1	0 – 1	W3-L4	3 – 4
W1-L2.5	1.5 – 2.5	W2-B1	3 – 4		
W1-L3.5	2.5 – 3.5	W2-B4	4 - 5		
W1-B1	3.5				
W1-B1.5	3.5 – 4.5				
W1-B4	4 – 5				

Results from the XRD analyzes indicates that quartz, albite, calcite and muscovite are the dominant minerals in all samples, with some variations in the mineral composition with depth. K-feldspar, pyrite and kaolinite are present in some samples, although in very small amounts.

W1

Results from the six sediments samples collected as the northern groundwater well was drilled and installed, are displayed in Figure 5.29. The three samples from the loose sediments have a higher weight percent of quartz and albite, compared to samples from the bedrock, with an average content of approximately 27% quartz and 30% albite. Samples representing the bedrock were composed of approximately 20% quartz and 19% albite.

On the other hand, samples from the bedrock show a higher percentage of muscovite, calcite and chlorite, compared to the loose sediment samples from the upper part of the terrain. Sample W1-B4 stands out due to a significant amount of muscovite and chlorite, 33% and 17% respectively, and less calcite (13.5%) compared to sample W1-B1 and W1-B1.5, all representing the bedrock. Pyrite and kaolinite were only present in samples taken from the bedrock with concentration < 2%.

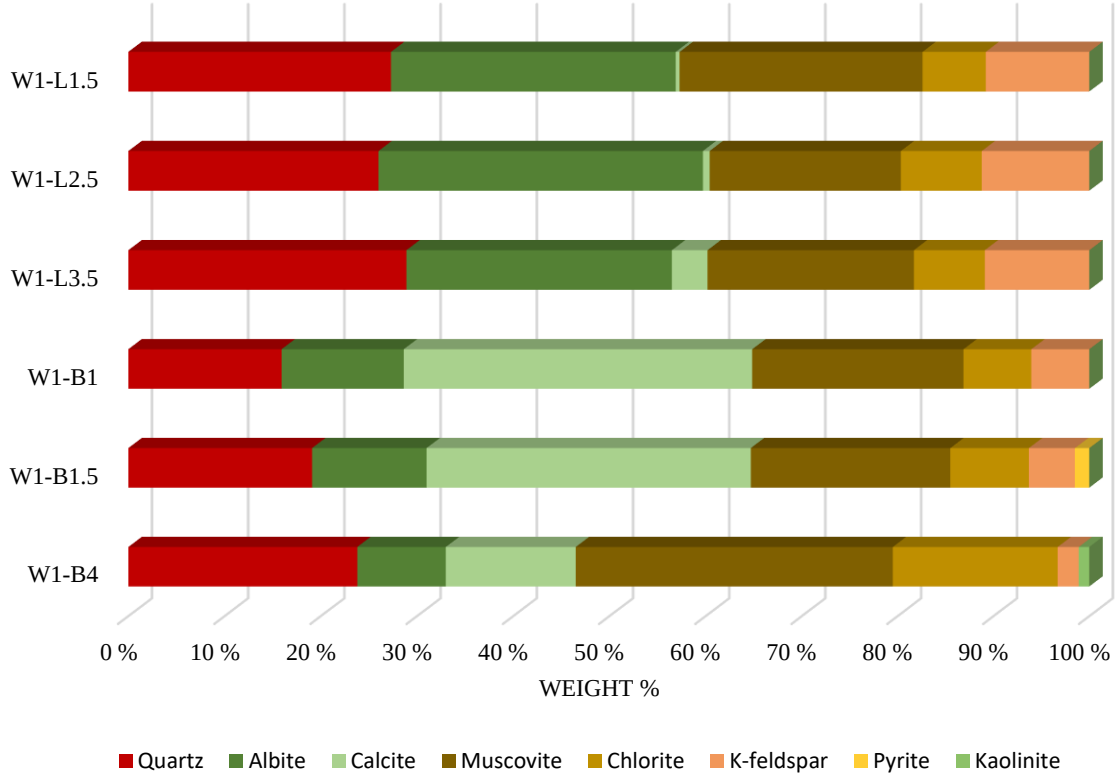

Figure 5.29. Weight % of the bulk composition from the loose sediments and bedrock in well W1. The samples are plotted stratigraphically are colored according to different facies associations.

W2

Results from the three sediments samples collected during the installation of well W2 in Torshovdalen are shown in Figure 5.30. Similar to samples from well W1, the most common minerals are quartz, albite, muscovite and chlorite. Samples representing the bedrock have a higher amount of calcite and chlorite, approximately 16% and 17%. The weight % of albite decreased with depth, from about 20% in sample W2-L1 to approximately 10 % in samples W2-B1 and W2-B4. A high amount of muscovite and albite (37% and 20.3%) and less calcite (0.1%) are found in the sample representing the loose upper soil, W2-L. Minor amounts of kaolinite are present in all samples from well W2, while pyrite is not present in any of the samples taken from this location.

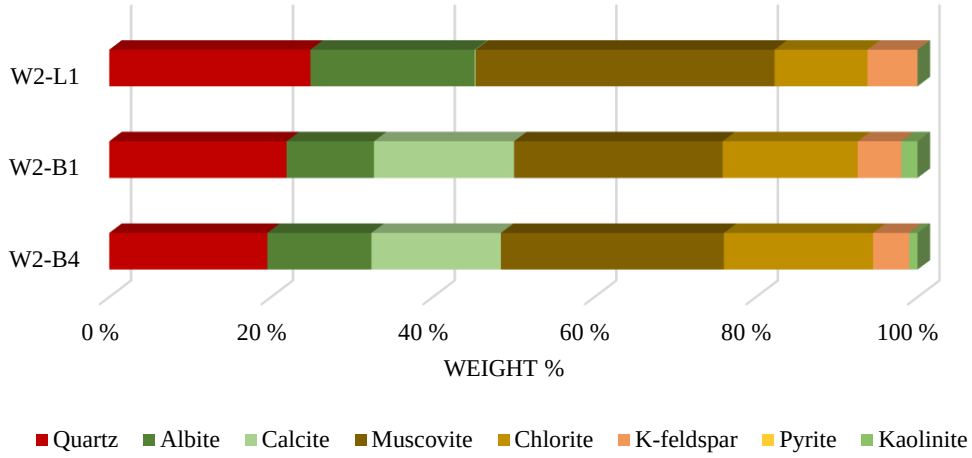

Figure 5.30. Weight % of the bulk composition from the loose sediments and bedrock in well W2. The samples are plotted stratigraphically are colored according to different facies associations.

W3

The sample gathered and analyzed from well W3 (Figure 5.31) shows significant similarities to samples from the loose sediments in well W2 (W2-L1), with quartz, albite, muscovite and chlorite as the dominating minerals, but some variations are observed. Kaolinite is present in a higher weight percent and, K-feldspar, found in samples from both W1 and W2, together with pyrite, is not detected in W3-L4.

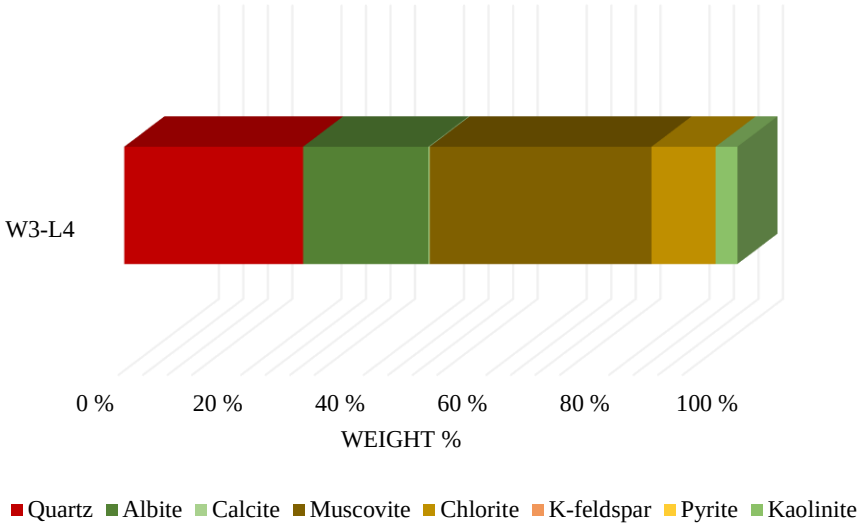

Figure 5.31. Weight % of the bulk composition from the loose sediments in section W3. The samples are plotted stratigraphically are colored according to different facies associations.

General trends

Samples from the loose sediments and bedrock collected in wells W1, W2 and W3 display relatively homogenous XRD-bulk composition, as seen in Table 5.7. Samples from the loose sediments ("L") contains more quartz and albite than the samples in bedrock, while on the other hand, an increase in the weight % of calcite is found from the bedrock. Minor pyrite and kaolinite were detected in all samples. Samples W1-B4, W2-L1 and W3-L4 stand out as the three samples with the highest weight % of muscovite. The highest amount of chlorite is found in the bedrock samples from wells W1 and W2, while the upper part of the soil in well W1 contains more k-feldspar. The diffractograms from all samples analyzed with XRD are displayed in Appendix C2-11.

Table 5.7. Summary of the mineralogical composition of the sediment samples taken from the three wells drilled in Torshovdalen. The values are in weight %.

Sample	Quartz %	Albite %	Calcite %	Muscovite %	Chlorite %	K-feldspar %	Pyrite %	Kaolinite %
W1-L1.5	27.3	29.6	0.4	25.3	6.6	10.8	0	0
W1-L2.5	26	33.7	0.7	19.92	8.4	11.2	0	0
W1-L3.5	28.9	27.6	3.7	21.5	7.4	10.9	0	0
W1-B1	15.9	12.7	36.2	22	7.1	6.1	0	0
W1-B1.5	19.1	11.9	33.7	20.8	8.2	4.8	1.5	0
W1-B4	23.8	9.2	13.5	33	17.2	2.2	0	1.1
W2-L1	24.9	20.3	0.1	37	11.5	6.2	0	0
W2-B1	21.9	10.8	17.3	25.8	16.7	5.4	0	2
W2-B4	19.5	12.9	16	27.6	18.5	4.5	0	1
W3-L4	29.2	20.4	0.2	36.1	10.5	0	0	3.5

5.4.2. Major element geochemistry

In addition to XRD analysis, a geochemical analysis was performed on the same ten samples from wells W1, W2 and W3 in Torshovdalen, analyzed for XRD. The results are displayed in Appendix D1-D3.

In general, all the samples from the upper part of the soil ("L") show a higher SiO_2 content (53-68 wt%) compared to samples from the bedrock (39-51 wt%) (Figure 5.32). The samples representing the bedrock ("B") shows a higher CaO content (9-20 wt%) compared to the loose sediments (1-3 wt%). The XRF results obtained for the content of SiO_2 and CaO corroborate the findings previously reported from the XRD results; e.g. the loose sediments are richer in quartz and other silicate minerals, while the bedrock sediments are richer in calcite. The amount of Al_2O_3 is relatively similar in all samples, ranging from 11.4 wt% in sample W1-B1 to 18.1 wt% in sample W2-L1, showing a slightly higher amount in samples representing the loose sediments. Fe_2O_3 and K_2O are found in the range of 3.7-8.8 wt% and 3.0-4.3 wt% respectively.

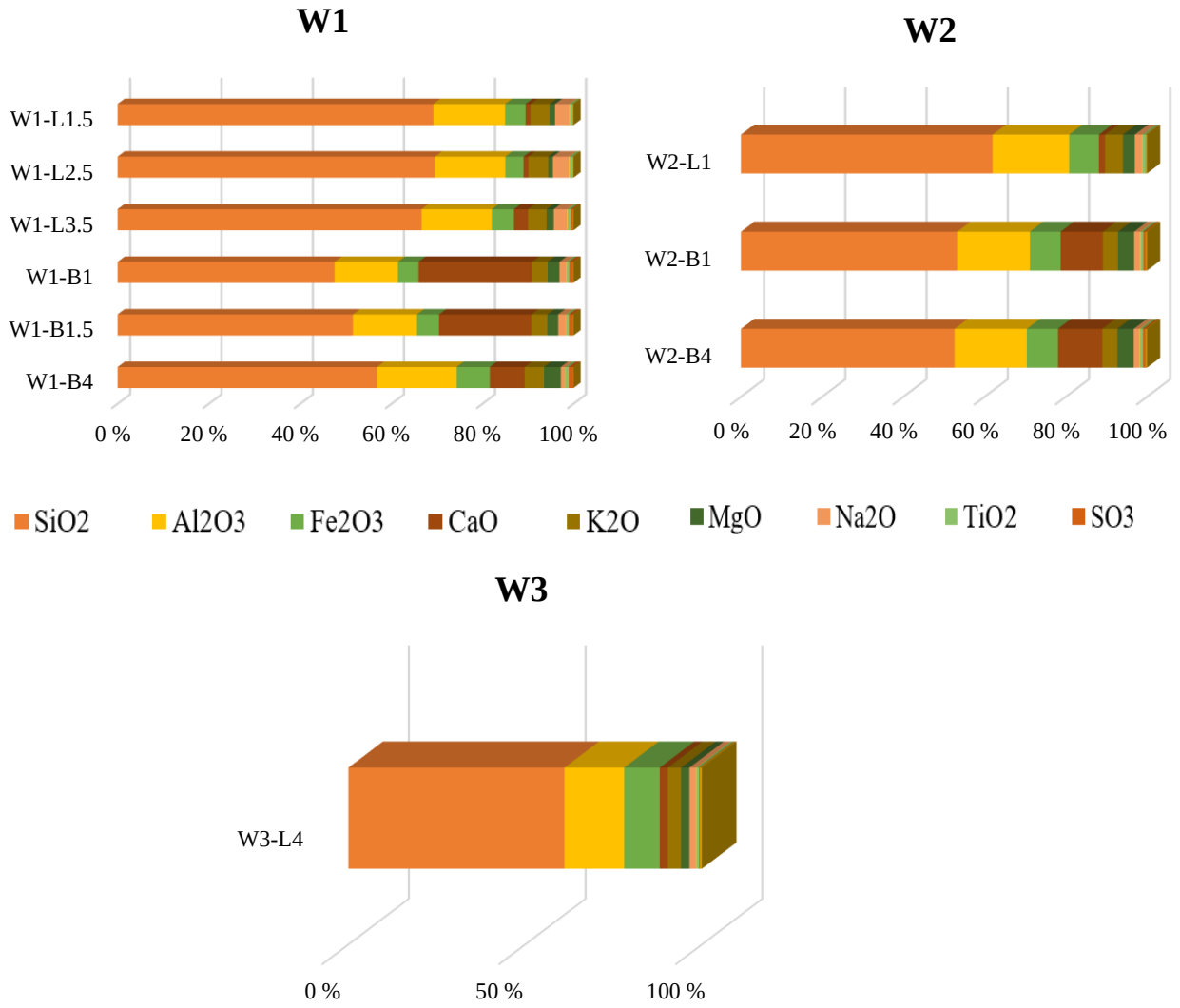

Figure 5.32. Major element geochemistry obtained from XRF analysis in the ten sediment samples collected from the groundwater wells W1, W2 and W3, in Torshovdalen

Figure 5.33 below shows the trace elements (expressed in mg/L) obtained from XRF analysis of the pressed powder pellets. The same trend is observed in almost all samples, with barium and phosphorus as the elements with highest concentrations and tantalum, ytterbium and molybdenum as the elements with the lowest concentration. Sample W1-B4 stands out as the sample with a lower concentration of samarium compared to the other samples, and sample W1-B1.5 with the lowest concentration of tantalum. The samples W2-L1 and W3-L4 were not analyzed for trace elements due to lack of sample material.

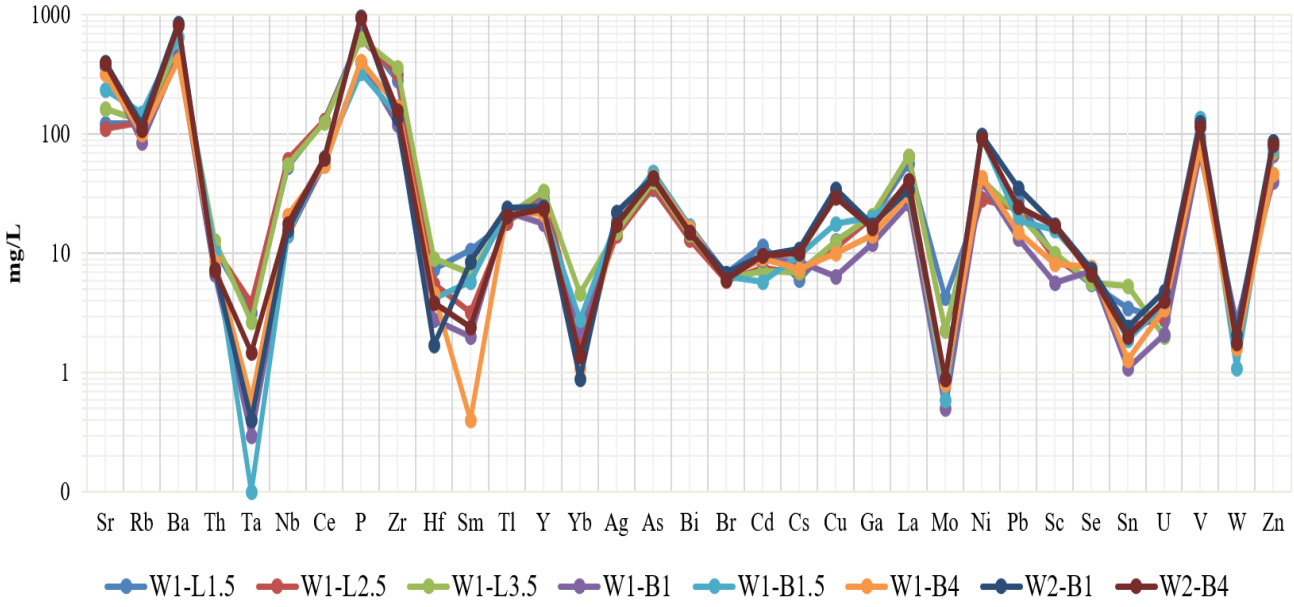

Figure 5.33. Overview of the trace elements (mg/L) obtained from XRF analysis of press pellets. From the graph, it is possible to see that there are some differences regarding the concentration of each element, but all samples have a relatively similar trend.

During the preparation of the sediment samples for XRF analysis, the loss on ignition (%) (LOI), the gravimetric water content (%) and the content of organic matter (OM) (%), were calculated (Table 5.8). A significant difference in LOI (1.9 – 18.8%) were found in the samples. Samples from the loose sediments ("L") showed a low LOI value, indicating less organic material and carbonate content compared to the bedrock. A comparison of LOI, XRD and XRF results reveals that there might be a correlation between the calcite content and LOI, as all samples from the bedrock have a higher amount of calcite and CaO, and thus, a higher LOI. The water content was low in every sample, with a slightly decreasing of the water content with depth. All samples, except W3-L4 had a low content of organic matter.

Table 5.8. Estimated loss on ignition (%), gravimetric water content (%) and organic matter (%) for the 10 sediment samples collected in the wells frilled in Torshovdalen. The depth of the sampling points is also given.

Sample	Loss on ignition (%)	Water content (%)	Organic matter (%)	Depth below the surface (m)
W1-L1.5	1.9	1	1.9	0 – 1-5
W1-L2.5	1.4	0.7	1	2.5 – 2.5
W1-L3.5	3.1	0.7	1.9	2.5 – 3.5
W1-B1	18.8	0.5	0.9	3.5
W1-B1.5	15.1	0.3	1.3	3.5 – 4.5
W1-B4	8.6	0.3	2.3	4 – 5
W2-L1	3.7	1	2.5	0 – 1
W2-B1	10.7	0.6	1.9	3 – 4
W2-B4	10.8	0.5	2.4	4 – 5
W3-L4	12.5	1.5	11	3.5 – 4.5

5.4.3. Clay fraction XRD

Two XRD clay mineral analysis were performed for the samples W2-L1 and W3-L4, collected in Torshovdalen. As described in section 4.3.3, four diffractograms were created for each clay sample after the different treatments, as seen in Figure 5.34 and Figure 5.35. The identification of the different clay minerals was done by comparing "*d*" values (Nayak and Singh, 2007) and by using a "clay mineral identification flow diagram" (Appendix C1).

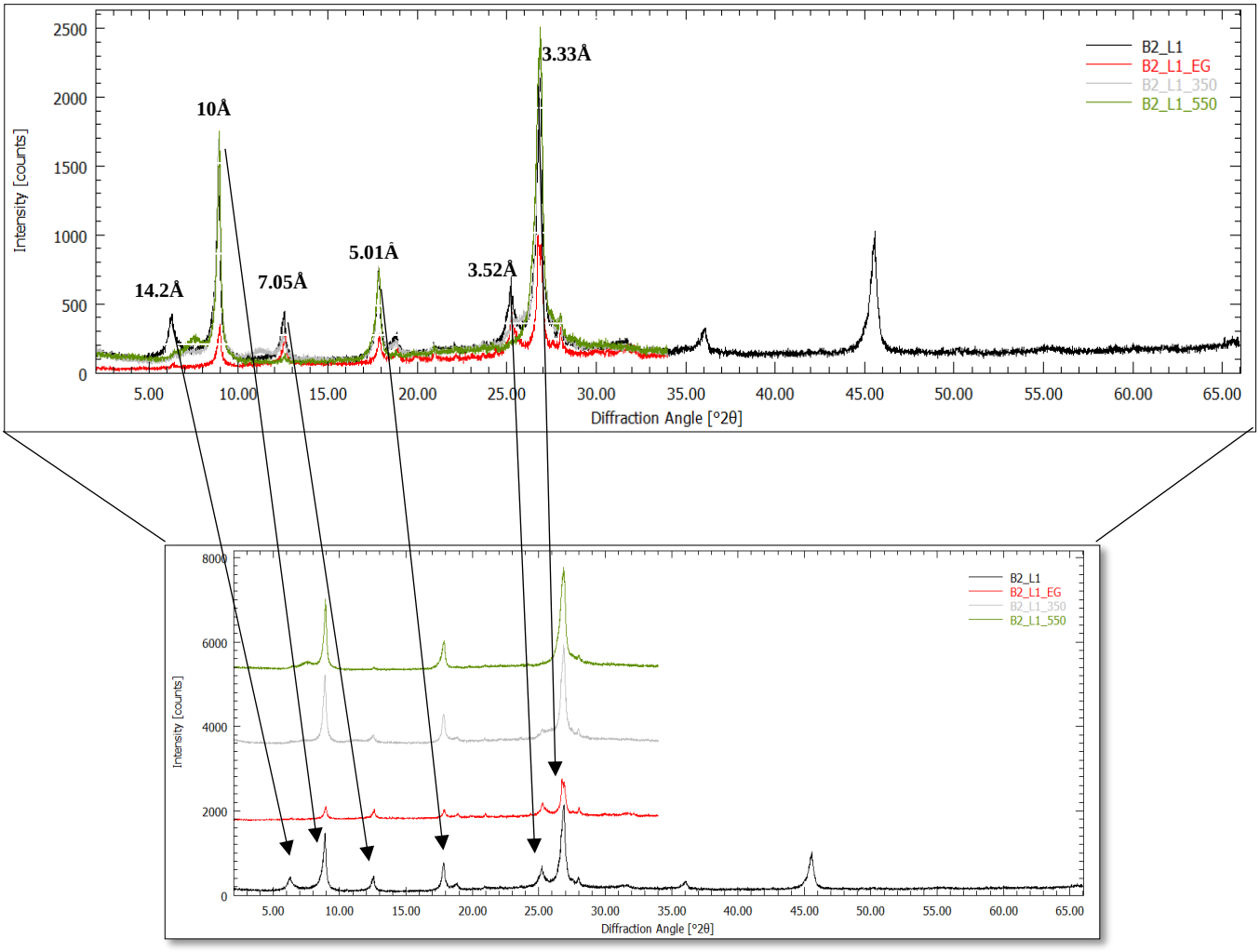

Figure 5.34. Sample W2-L1: X-ray diffraction analysis of the clay fraction, identified peak pattern fits into Illite and chlorite. Black = untreated, red = ethylene glycol treatment, grey = heated at 350 °C, green = heated at 550 °C

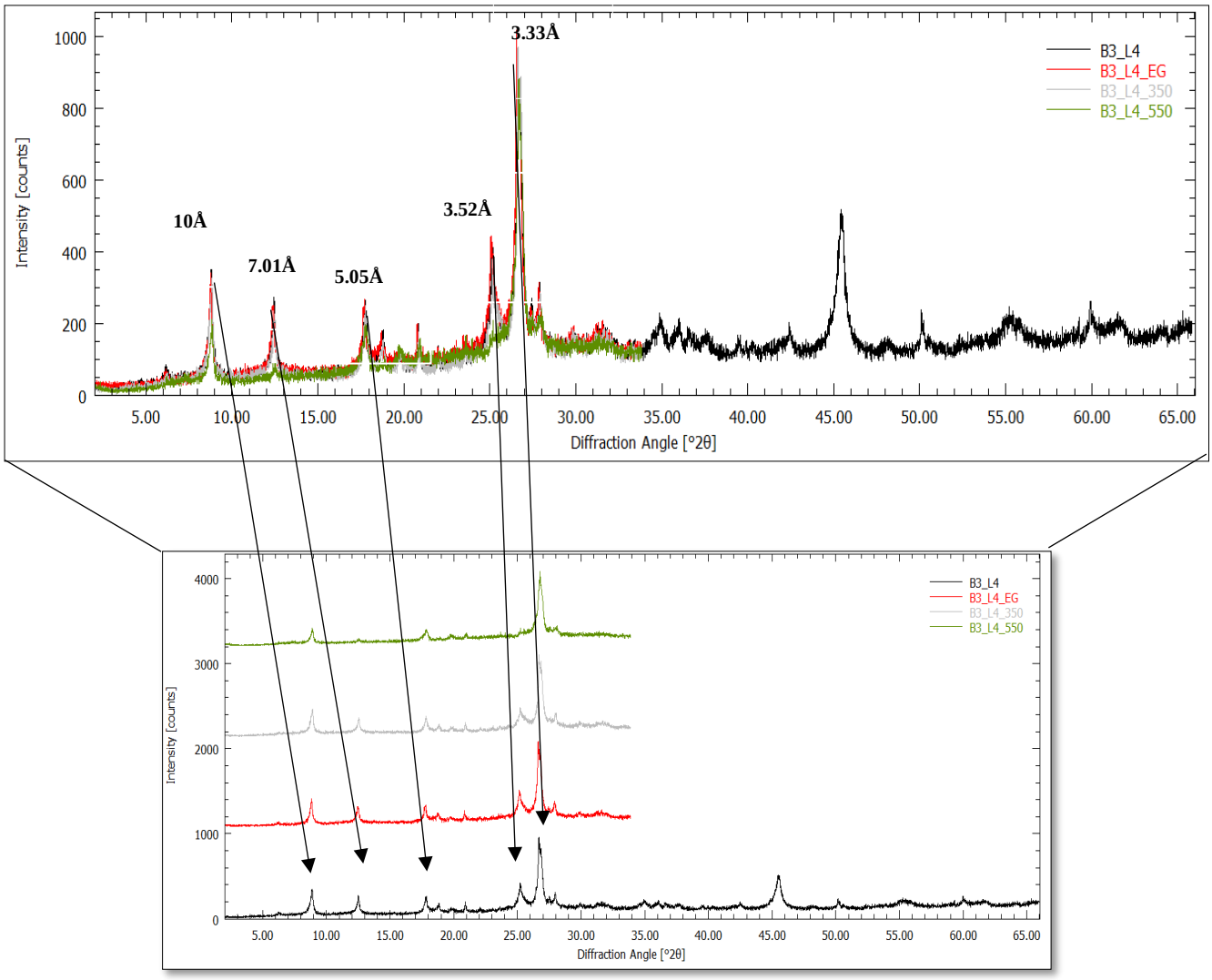

Figure 5.35. Sample W3-L4: X-ray diffraction analysis of the clay fraction, identified peak pattern fits into Illite and chlorit. Black = untreated, red = ethylene glycol treatment, grey = heated at 350 °C, green = heated at 550 °C

From the diffractograms, the presence of illite was determined based on the identification of a peak located at 2θ angle of 10Å and 3.33Å, observed in both samples. A smaller peak observed at 5.01/5.05Å was also used as an indicator of illite. The peak at 10Å collapsed in sample W2-L1 after treated with ethylene glycol, (Figure 5.34), while in the sample W3-L4, the peak is less intense and there is no collapse after ethylene glycol treatment (Figure 5.35).

Chlorite is determined by the presence of a peak at 7Å where no change is observed until it collapsed after heating the samples at 550 °C (green diffractogram in Figure 5.34 and Figure 5.35). A peak at around 14.2Å is also characteristic for chlorite, which is found in sample W2-L1, while in the sample from W3-L4, this chlorite peak is barely visible.

Both samples have a peak at 3.52Å (Figure 5.34 and Figure 5.35), indicating that kaolinite is present in the samples.

Significant quantities of silica, iron and alumina are found in both samples (Table 5.9). The LOI values for W2-L1 and W3-L4 are respectively 3.74% and 12.46%. Despite a high LOI value for W3-L4, the CaO content in the sample is rather low (1.9 wt%).

Table 5.9. Chemical composition (wt%) of the clay fraction of samples W2-L1 and W3-L4, as well as the calculated loss on ignition (%).

Sample	**LOI**	**SiO_2**	**Al_2O_3**	**Fe_2O_3**	**CaO**	**K_2O**	**MgO**	**Na_2O**	**MnO**	**TiO_2**
W2-L1	3.7	59.6	18.1	7.1	1.6	4.3	2.8	1.7	0.2	0.8
W3-L4	12.5	53.4	14.8	8.8	1.9	3.3	2.1	1.6	0.1	0.6

5.4.4. Infiltration test and grain size distribution

Infiltration tests were conducted at eleven different locations in Torshovdalen (Figure 5.36).

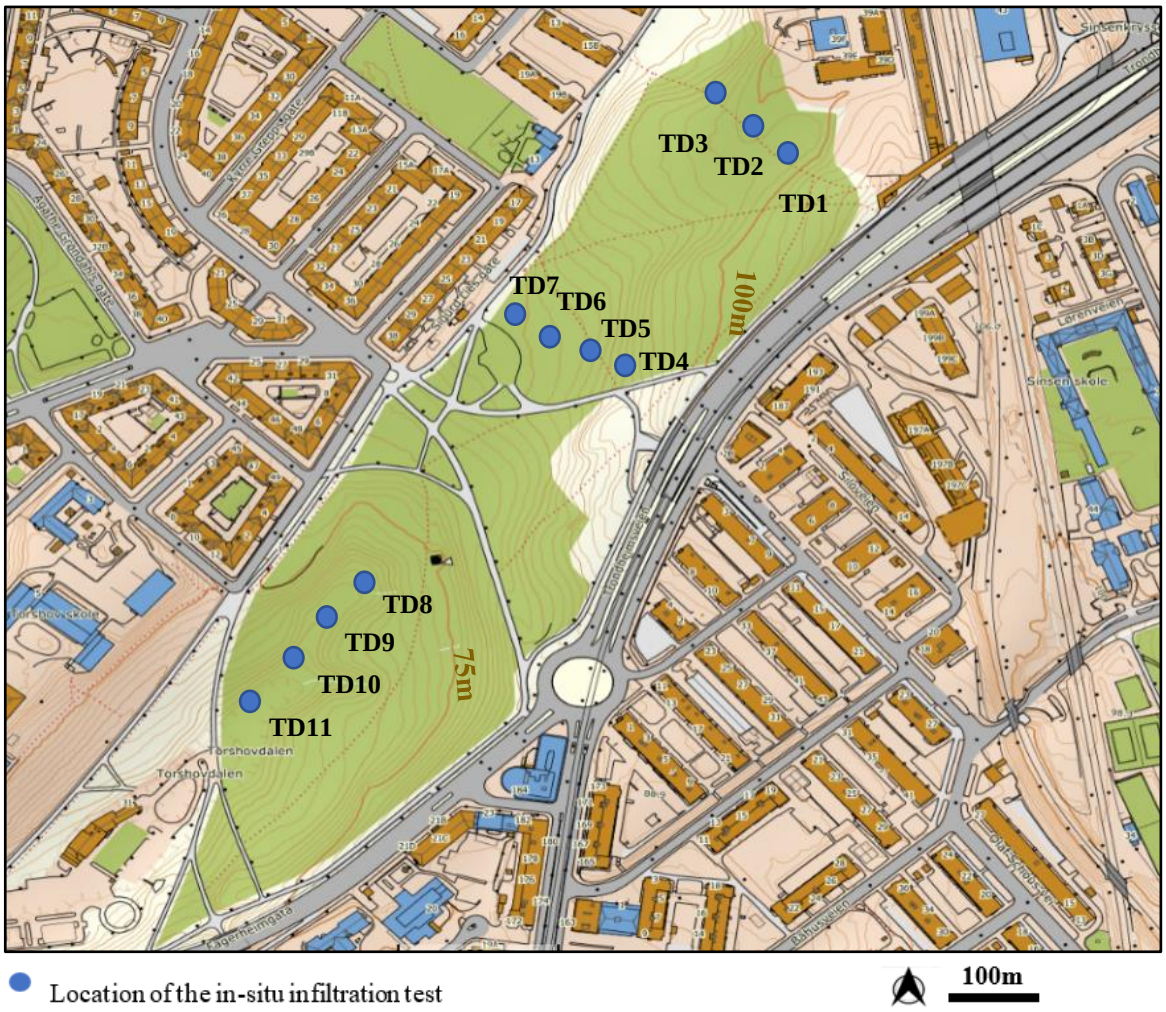

Figure 5.36. Map showing an overview of Torshovdalen with the location of eleven in-situ infiltration tests

Three infiltration tests were conducted in the northern part of Torshovdalen (TD1, TD2 and TD3), resulting in an average infiltration capacity of 31.5 cm/h. Four infiltration tests were complete in the middle part of Torshovdalen (TD4, TD5, TD6 and TD7), resulting in an average infiltration capacity of 29 cm/h. The lowest infiltration capacity was found in the southern part of Torshovdalen, where four additional infiltration tests were done (TD8, TD9, TD10 and TD11), resulting in an average infiltration capacity of 11.25 cm/h. A correction factor of 0.6 (given that the most of the soil is silt and clay) was used to correct for horizontal movement of the water in the unsaturated zone (Solheim et al., 2017).

From the graphs in Figure 5.37, TD6 and TD10 stand out with the lowest infiltration capacity. TD10 was taken in the southern part of Torshovdalen, while TD6 was done in the middle of the valley. Highest infiltration capacity was found in TD1, TD2 and TD3, measured in the northern part of Torshovdalen. It is important to mention that the infiltration test was done June 18 (TD1- TD 7) and 19 (TD8-TD11),

2018, which was a month characterized by high temperature (around 30°C), and little precipitation, resulting in dry surface soil.

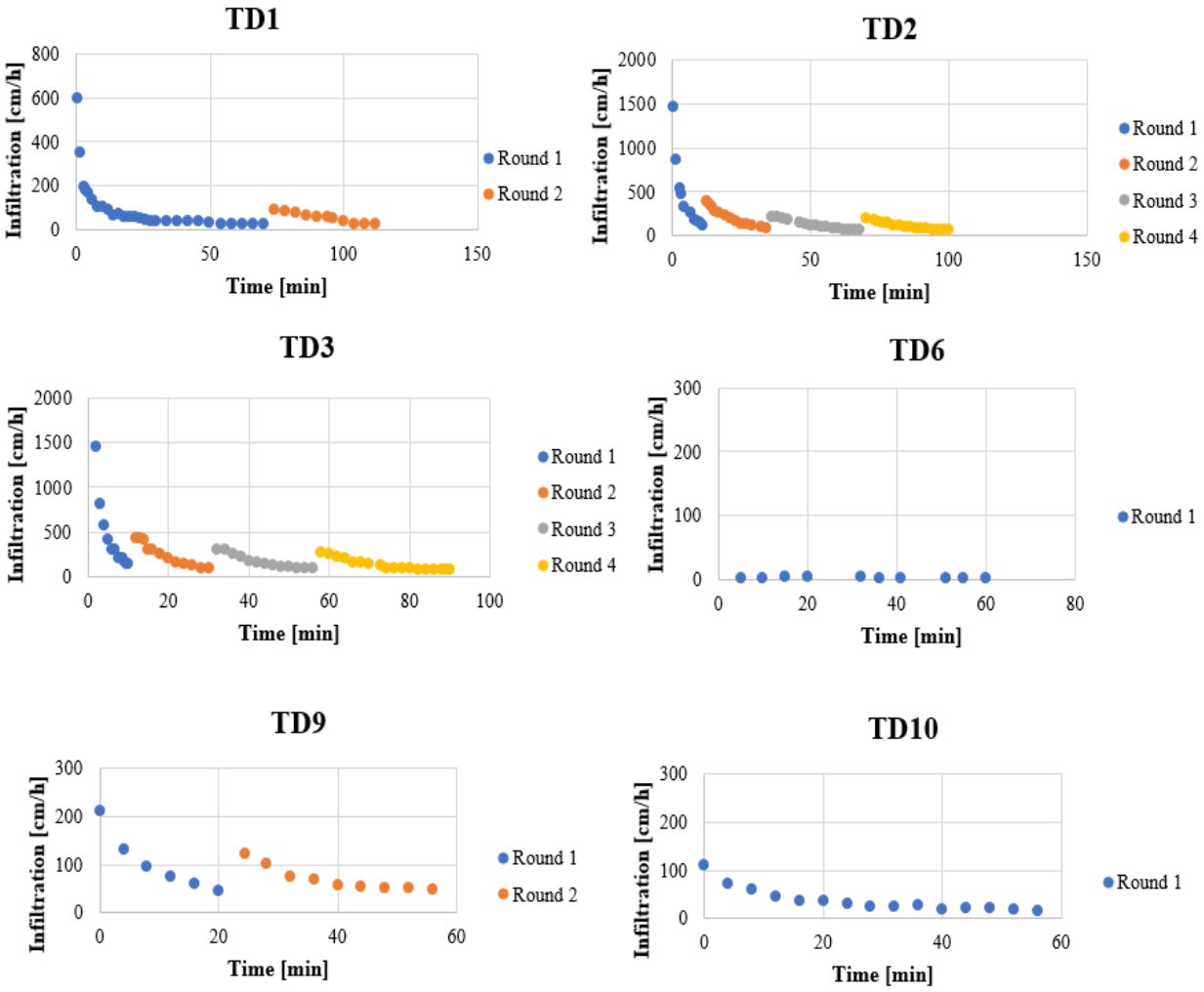

Figure 5.37. Infiltration capacity measured in Torshovdalen. "Round" is used to explain when the cylinder is emptied and filled up with water again.

Results from the grain size distribution analysis of the samples collected at TD1, TD2 and TD3 are given in Figure 5.38. Sample TD1 and TD2 show a similar trend, with approximately 5 % gravel, 20% clay, and a higher content of silt and sand. TD3, on the other hand, has a lower clay content, approximately 1%, and about 40% gravel.

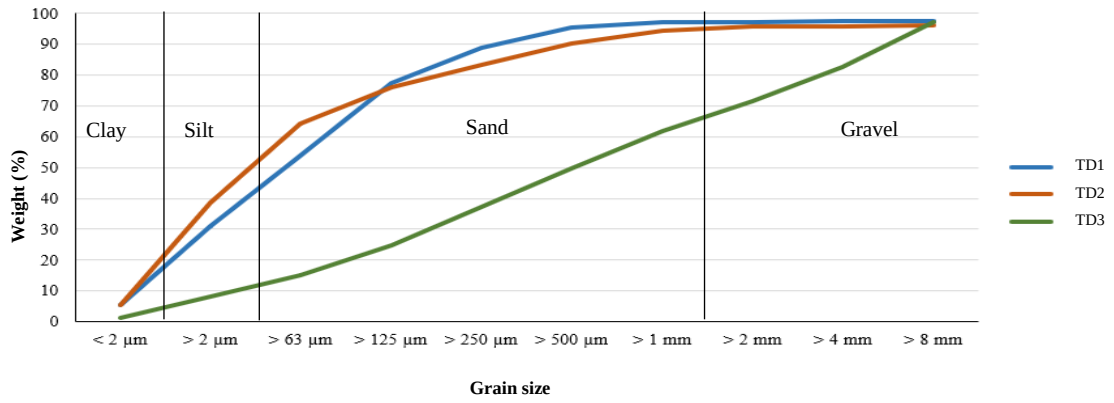

Figure 5.38. Grain size distribution from the upper 10 cm of the soil at TD1, TD2 and TD3 (all located in the northern part of Torshovdalen.

Two sediment samples were collected in the middle of Torshovdalen, where infiltration tests TD4, TD5, TD6 and TD7 were completed, for grain size distribution analysis in the laboratory (T4 and T6 in Figure 5.39). Both samples contain about 1% clay and 4-7 % silt. TD6 stands out due to the high content of gravel of approximately 65% compared to TD4 (30%).

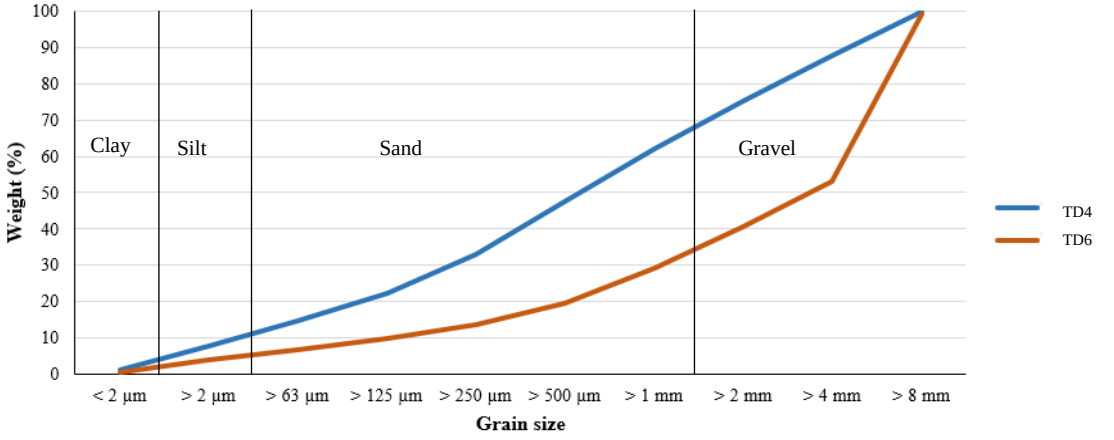

Figure 5.39. Grain size distribution from the upper 10 cm of the soil at TD4 and TD6 (both located in the middle of Torshovdalen.

Results from the grain size distribution analysis of sample TD9 and TD11 are shown in Figure 5.40 below. Both samples show low clay and silt content, respectively 1% and 6-12%. Most of the samples contained sand, but approximately 25% of the sample TD9 included gravel.

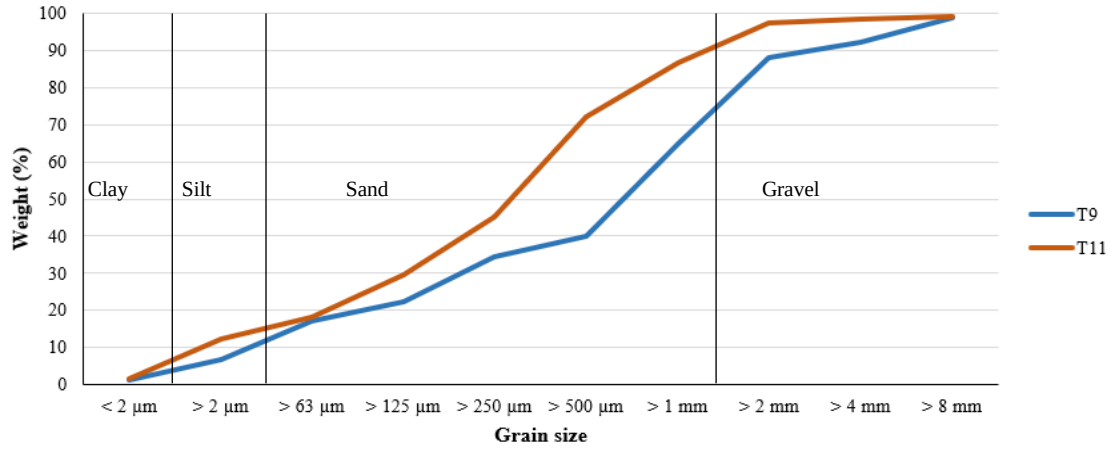

Figure 5.40. Grain size distribution from the upper 10 cm of the soil at TD9 and TD11 (both located in the southern part of Torshovdalen.

Three grain size distribution analyses were also performed from the cylinders taken during the drilling of the groundwater well W3. The analysis performed at NGI's laboratory, represents the result from the grain size distribution for undisturbed sediments at 4.22 meter, 5.29 meters and 6.47 meters depth (Table 5.10). A higher amount of silt and clay, and lower amount of gravel were found in the samples taken at greater depth by NGI compared to those taken during the infiltration tests (Figure 5.38, Figure 5.39, Figure 5.40).

Table 5.10. Grain size distribution obtained from undisturbed sediments at depth 4.22m, 5.29m and 6.47m, analyzed at NGI laboratory.

Cylinder	Depth (m)	Gravel (%)	Sand (%)	Silt (%)	Clay (%)
1	4.2	22.2	41.1	29.2	7.5
2	5.3	0	0.1	52.6	47.3
3	6.5	0	0	56.1	43.9

The results from the grain size distribution analyses are listen in Appendix E3, while the results from the infiltrations test and are listed in Appendix E4-E9.

5.5. Geophysical borehole logging

Geophysical borehole logging was conducted in a separate borehole, only a few centimetres away from well W1 and well W3, drilled by NGI on September 14, 2018. The borehole logging included; Optical Televiewer, Acoustic Televiewer, Natural gamma ray, Resistivity and Caliper.

The results from the geophysical logging near well W1 are shown in Figure 5.41, in meters below the surface. Some errors in the resistivity values are found, which is why the peaks do not correspond perfectly to the peaks found in the natural gamma ray. The resistivity values are relatively unstable, ranging from 500 – 1000 ohm. Four distinct peaks in the resistivity log are observed at approximately 7.5, 8, 9 and 10 meters, while decreasing peaks are observed in the natural gamma log at approximately the same depth.

Values from the natural gamma ray vary between 50-80 cps (counts per second). As the signal reaches bedrock, at 3.5 meters below the surface, the gamma radiation has a small increase in value and varies between 60-80 cps. An image from the borehole wall can be seen from the caliper log, showing that there are colour changes, between 7.5 and 10 meters below the terrain (as the increase in resistivity and a decrease in natural gamma ray are observed).

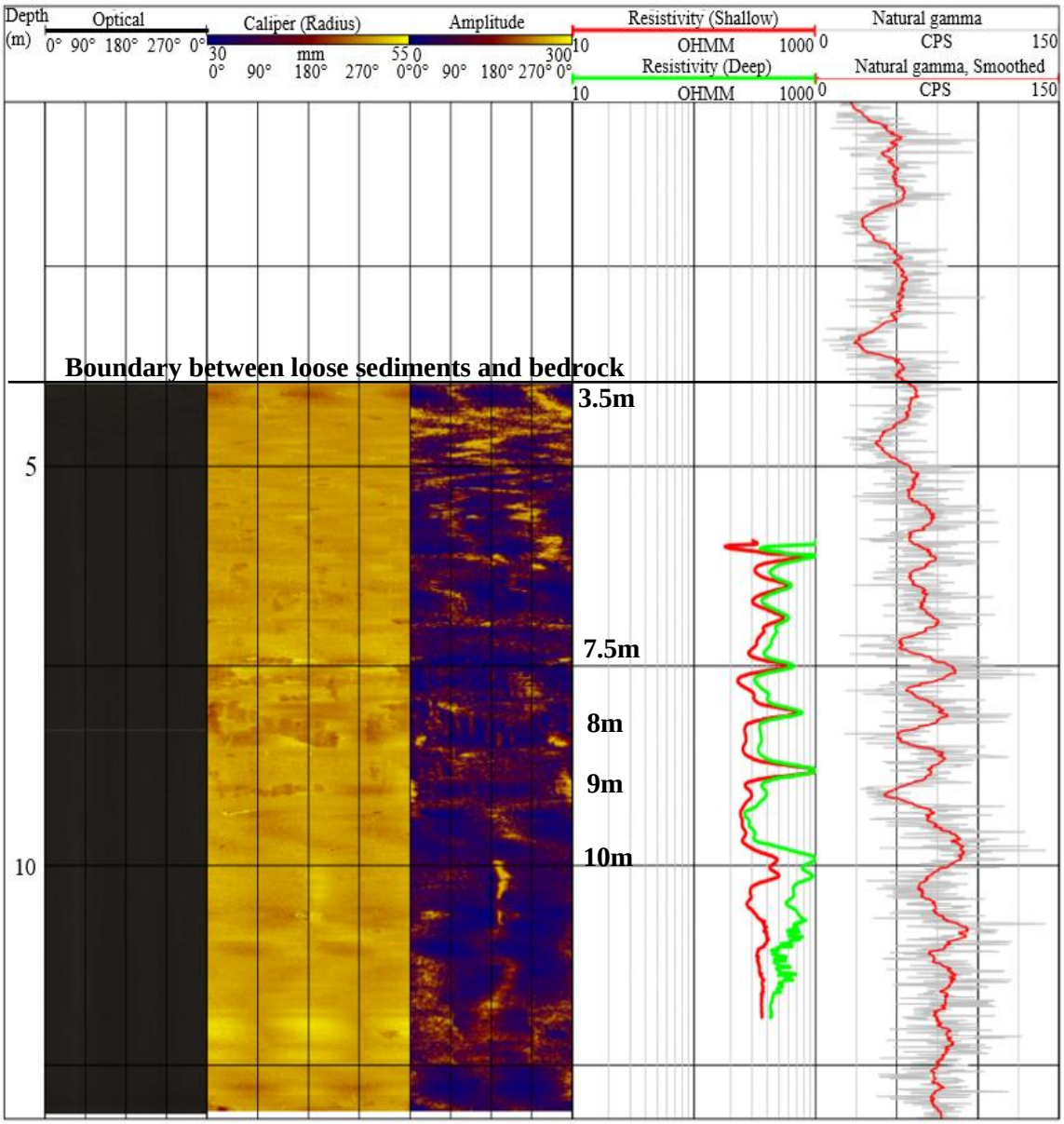

Figure 5.41. Geophysical borehole logging near well 1. A change in the resistivity and the natural gamma ray are observed at 7.5, 8, 9 and 10 meters below the surface. The logging was performed by NGI on the 14.09.2018, and includes; Optical Televiewer, Acoustic Televiewer, Natural gamma ray, Resistivity and Caliper.

The resistivity and gamma ray logs are more stable in the bedrock in well W3 (Figure 5.42) compared to well W1 (note the different scale and depth compared to well W1 in Figure 5.41). Values around 500-1000 ohm are observed for the resistivity while the results of the natural gamma ray log are approximately 75 cps in bedrock, except from a decrease seen at 16-17 meters depth (below the surface). An increase in the resistivity is found at the same depth. Colour changes in the caliper and acoustic televiewer are not so evident at 16-17 meters depth, but a very evident fracture is found at 18.5 meters below the surface. The geophysical logging gave best results in the bedrock in both wells (W1 and W3).

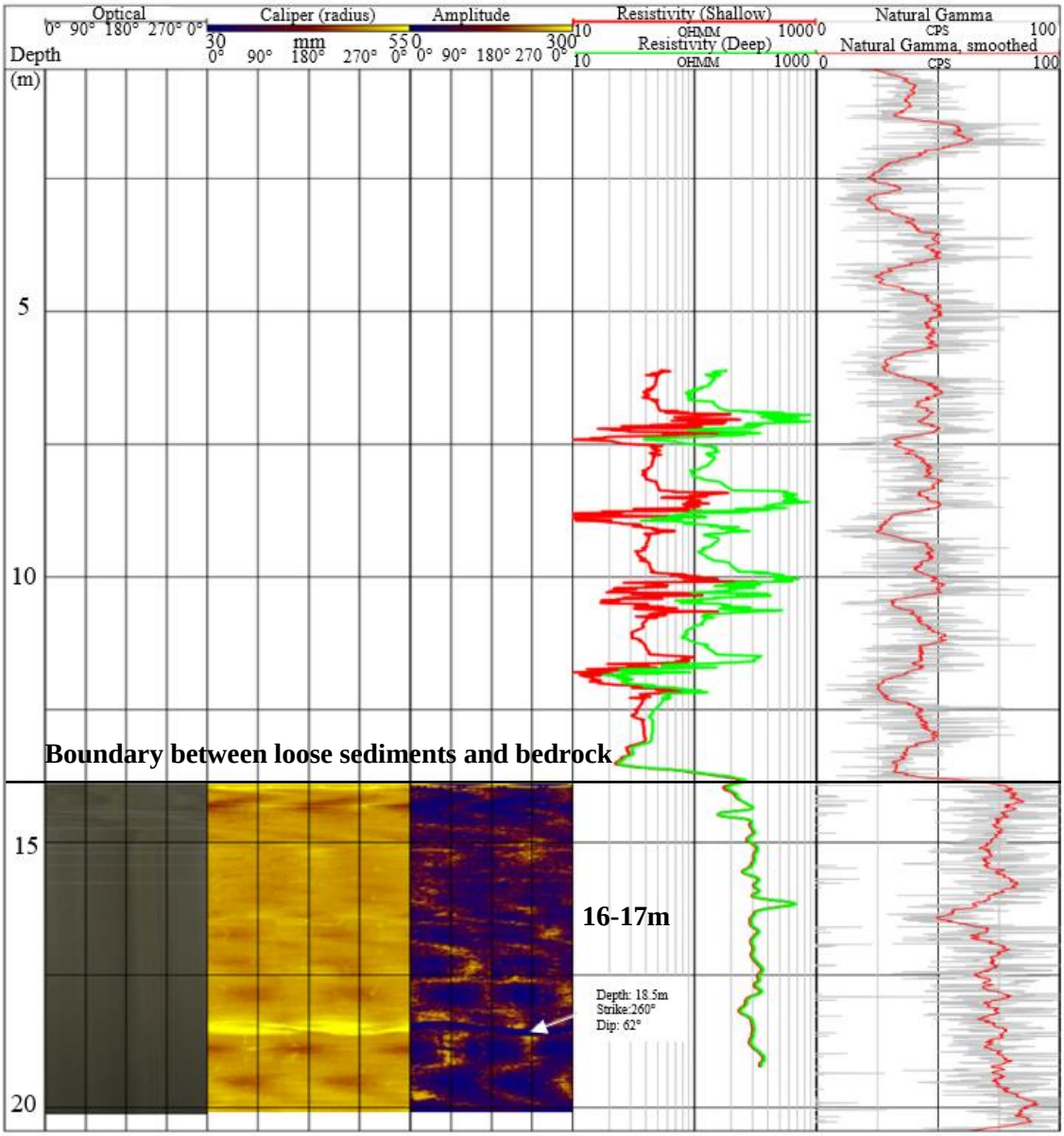

Figure 5.42. Geophysical borehole logging near well 3. A peak is observed around 16-17 meters depth and a fracture in the bedrock is observed at 18.5 meters below the surface. The logging was performed by NGI on the 14.09.2018, and includes; Optical Televiewer, Acoustic Televiewer, Natural gamma ray, Resistivity and Caliper

For the two boreholes (W1 and W3), the optical tele viewer resulted in poor images due to murky water as a consequence of lose debris filling the hole bottom, which also prevented logging of full borehole depth. It was therefore not possible to use the result from the optical televiewer. Some issues with centralization also made the amplitude log unreliable.

6. Discussion

In this chapter, the results presented in chapter five are analyzed and interpreted to better understand the chemical and bacteriological evolution from precipitation to groundwater in an urban environment. The discussion is based on water and sediments samples, in addition to geophysical logging, gathered from Torshovbekken watershed during the period May to November 2018.

First, the results from the precipitation are discussed, followed by an interpretation of the results taken from the stream in Grefsen and the river Akerselva. Then, the results from the unsaturated zone, the ephemeral spring and the installed groundwater wells in Torshovdalen are discussed. Finally, an interpretation of the bivariate analysis from the water samples and the geophysical borehole logging is presented.

Each subchapter (from rainwater to groundwater) begins with a discussion of the different geochemical processes that might affect the water quality (major ions, trace elements and field parameters) and the sediment samples. Then, the bacteriological characterization is discussed (except in the rainwater and porewater samples).

6.1. Rainwater

The precipitation sustains streams and rivers and is one of the primary sources of water in urban areas. The rainwater composition can vary from day to day, and it can also vary during a single rain event. A water sample from the first rainwater during a rain event will often contain a higher concentration of inorganic ions, compared to a sample collected later in the same event, as it takes up more dust and particles from the air. The rainwater sample (R1) discussed here was taken September 21, 2018, approximately 5-6 hours after the first raindrops were registered at Blindern, Oslo.

6.1.1. Water chemistry characterization

A relatively high concentration of all major ions was measured in the sample R1, compared to the average concentration in the precipitation registered at Hurdal, Brekkebygda and Birkene (Figure 5.6). It is important to notice that only one sample was taken in Blindern (R1), while the analytical data from Aas (2018) on the three other stations reflects an average concentration based on numerous measurements during the year 2017.

Usually, major ions in precipitation originate from natural sources, e.g. sea salt and windblown dust. Even though anthropogenic emission of inorganic compounds are considered to be relatively small compared with natural sources, they are still important when assessing the rainwater chemistry (Hellsten et al., 2017), especially in urban and agricultural settings.

Sodium and chloride dominate the rain sample (R1), indicating a sodium-chloride type of water. The primary source of these elements is usually sea salt. Typically, the concentration of sodium and chloride decreases with increasing distance from the coast. The highest concentration of both sodium and chloride was found at Blindern and Birkenes, both located near the coast (Figure 5.6). Bikenes is situated only 20 km from the Skagerrak coastline and is also the site in Norway being the most influenced by long-range transport of air pollution from Europe (Aas, 2018). Hurdal and Brekkebygda on the other hand, located further inland, contained a lower amount of both sodium and chloride.

Anthropogenic emission of HCl to the atmosphere may have increased the chloride concentration in the sample R1 since elevated anthropogenic chloride contents in precipitation are known from industrial areas (Reimann et al., 2009). Given that the water sample R1 was collected after a hot and dry summer, it is also possible that the degree of evapotranspiration resulted in a higher chloride concentration (Reimann et al., 2009).

The sample R1 also contained sulphate and nitrate. These inorganic elements may be a result of air pollution. Air pollution often originates in urban areas from sources involving traffic, fossil fuel combustion from heating and other gaseous emissions, industrial operations and gasoline evaporation (Marsalek et al., 2014). Air pollutants originating in the United Kingdom and central Europe are transported over long distances and produce highly polluted precipitation over large areas of Scandinavia (Johannessen et al., 1977). Generally, the highest concentration of nitrate and sulphate are found south and southeast of Norway (Aas, 2018).

Analysis of the sample R1 from Blindern showed a significantly higher concentration of all inorganic ions compared to Brekkebygda and Hurdal. Birkenes, on the other hand, displayed some similar results to the sample R1. The high concentration found in R1 may indicate that the sample was affected by human activities such as air pollution, which can have been enhanced by the extremely dry Summer of 2018.

The results discussed here stress the importance of monitoring rainwater composition in an urban area, in order to assess the amount of air pollution as the pollution might cause damage to both plants and animals, and it could change the chemical composition in the receiving water bodies.

6.2. Surface water – Grefsen and Akerselva

Two samples were collected from the stream located in Grefsen (G1-1 and G1-2). Normally, the stream only becomes visible after periods with rain and is a result of how precipitation sustains streams in a non-urbanized upper catchment area (close to the surface water divide). Being situated relatively central in Oslo, and that the area is a popular hiking spot, the impact of human activities and urbanization in the area should be considered as a factor influencing the water chemistry in the stream located in Grefsen.

Since Torshovbekken originally was a tributary of Akerselva, three samples were collected from the lower part of the river, close to where the Torshovbekken previously discharged into Akerselva (A1, A2 and A3). Akerselva starts northwest from Grefsen and flows in an open waterway through the urban part of Oslo, toward the Oslo fjord. Contamination from the roads and industrial waste might, therefore, occur and change the water quality. Water samples were collected during three sampling campaigns, where the last campaign, on November 12, 2018, was performed after heavy rainfall (A1-3 and A2-3).

The evolution of the water composition from precipitation to rivers and streams involves several processes, both natural and anthropogenic, which can affect the water quality. The different processes assumed to dominate the water quality of streams and rivers are discussed in the following sections.

6.2.1. Major inorganic ions

Four sampling locations (G1, A1, A2 and A3), located within Torshovbekken watershed, were chosen to represent the water quality for rivers and streams. Moving downwards from Grefsen to Akerselva, a change in the water composition is observed (Figure 6.1). The water samples from Akerselva contains a lower concentration of all major ions compared to Grefsen. The result is not surprising as Akerselva is assumed to be more diluted throughout the year since water is constantly flowing down the river, which is not the case in Grefsen. The difference in water chemistry from Grefsen to Akerselva is, however, likely to arise from the interrelationship between lithology, landscape, land-use, and climate-related factors, i.e. different evaporation rates and precipitation.

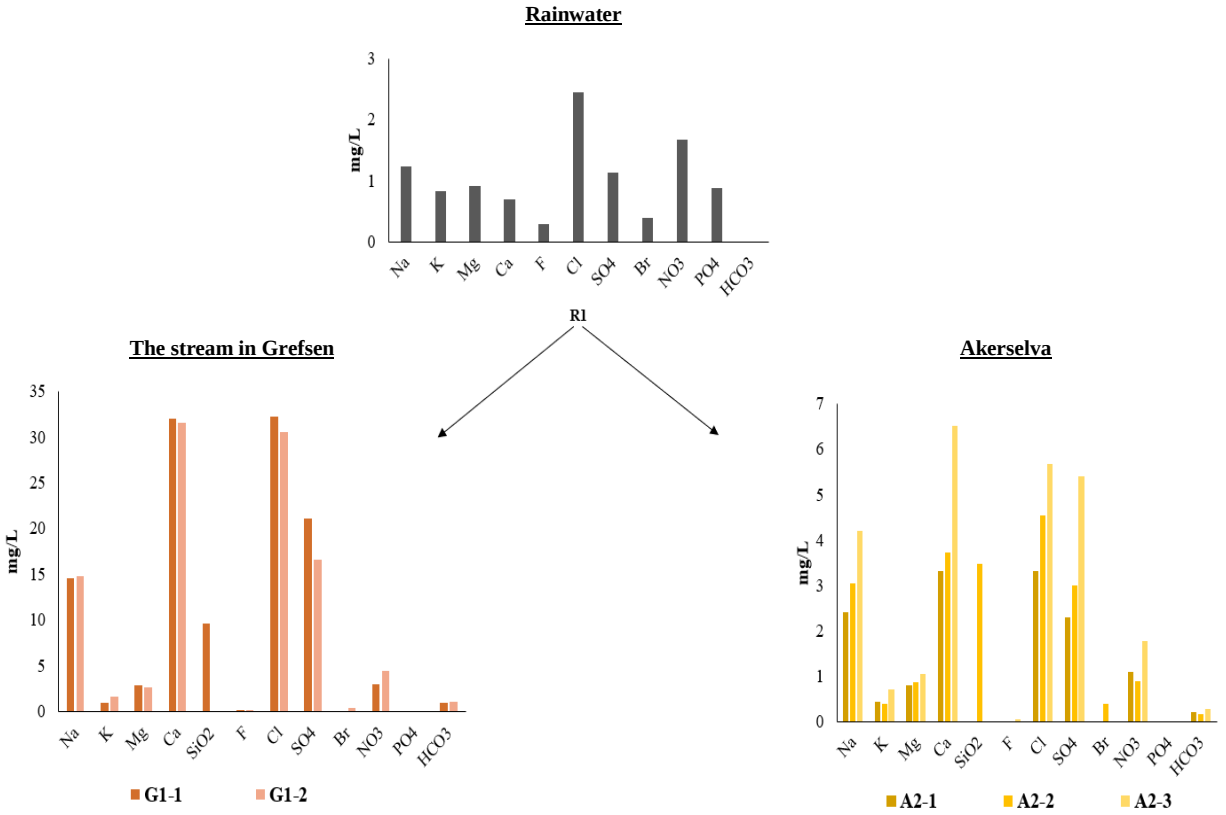

Figure 6.1. The change in water chemistry from rainwater to the stream in Grefsen (G1-1 and G1-2) and the river Akerselva from the samplingpoint A2;A2-1, A2-2 and A2-3). The concentration of major cations and anions are significantly higher in the stream in Grefsen compared to Akerselva. Silica was not measured for the rainwater sample R1.Note the different scale on the y-axis.

On the basis of major ions, the samples from Grefsen (G1-1 and G1-2) and Akerselva (location A1 and A2, Figure 4.1) fall approximately in the calcium-chloride type of water, while rainwater is a sodium-chloride type with a considerable amount of magnesium (Figure 5.2). The natural factors that can affect the water chemistry of the streams could be geological sources, such as mineral weathering which adds calcium to the water.

The main natural sources of calcium in surface- and groundwater bodies are usually carbonate rocks containing calcite, and igneous rocks with calcium-containing silicates such as plagioclase and hornblende, that are dissolved by carbonic acid naturally present in rainwater and soil water (Nikanorov and Brazhnikova, 2009, Reimann et al., 2009). Cation exchange replacing sodium in the water by calcium from the clays is also a possible explanation for calcium dominating water (Reimann et al., 2009).

Further analysis of the two water samples from Grefsen (G1-1 and G1-2) revealed a relatively high concentration of sodium and chloride compared to Akerselva and the rainwater (R1). Also, a high concentration of sulphate and nitrate is observed in the samples G1-1 and G1-2.

Sodium and chloride are normally regarded as being derived from marine salts in precipitation. An enrichment of chloride and sodium in streams and rivers can also be a result of evapotranspiration of solution on vegetation surface or in the soil (Banks et al., 2001, Reimann et al., 2009). Another possible source of chloride is leaching of pore water from marine clays in the upper postglacial marine limit. However, leaching of porewater from marine clay is not seen as a valid explanation for sample G1-1 and G1-2, located above the marine limit. In this case, leaching from manure, fertilizer applications, or, simply from sewage outfalls are more likely responsible for a higher chloride concentration (Reimann et al., 2009).

Other anthropogenic sources which also may contribute to an increase of the concentration of chloride, sodium, sulphate and calcium, are urban runoff and de-icing agents, such as road salting. Both are considered as a possible source of contamination for the receiving water bodies, i.e. the river Akerselva. Two water samples (A1-3 and A2-3) were taken right after a period of intense rain. These showed a significantly higher concentration of all major ions, especially for calcium and sulphate, but also chloride, sodium and nitrate increased in concentration this day, when compared to the other sampling dates (Figure 6.1). Polluted urban runoff contributes to the contamination of rivers, as the rainwater collects sediments, dust, oils, metals, bacteria and other types of pollutants when flowing through urban areas. Building materials, e.g. concrete are also considered as a source of calcium in urban runoff water (Davies et al., 2010). A study by Zhang et al., (2013) has demonstrated that the applied road salts during the winter significantly contributes to the increasing concentration of potassium, calcium, sodium, magnesium, chloride and sulphate in urban runoff, corroborated by the results from samples A1-3 and A2-3. During the winter (usually from November/December to March in Oslo), road salting used as de-icing such as sodium chloride (NaCl) and calcium chloride ($CaCl_2$) treats snow and ice on impervious surfaces in the city. The salt inputs can increase the salinity in urban stormwater runoff (Zhang et al., 2013), resulting in increased salinity in the recharging streams and rivers. In Norway, sodium chloride is the dominant substance used as de-icing during the winter and contains approximately 40% sodium and 60% chloride (weight percent) (Amundsen et al., 2012).

The effect of road salt contamination can be connected to the increasing population and urbanization, which leads to more impervious surfaces. As the area of impervious surfaces increases, road salt is likely to increase proportionally since it requires more de-icing during the winter. The effect has been reported by Daley et al. (2009), showing that salinization of surface water is a pervasive problem in the north-eastern part of the United States, where chemical de-icing products are used on roads and highways in the winter months. The concentration of chloride and sodium in the receiving surface water can, as seen in the river Akerselva, therefore be related to the degree of urbanization, impervious surfaces, intense rainfall, and climate change.

Given that NaCl is the most used road salt, an increase in calcium and magnesium in the river and stream can also be explained by ion exchange of NaCl in the soil. The result is a washout of calcium and magnesium from the soil, and a higher amount of both elements in the runoff (Amundsen et al., 2012).

Another important finding was the increasing concentration of nitrate when compared to the rainwater sample (R1). Nitrate, in combination with high chloride concentration, is usually an indication of anthropogenic inputs, urbanization or regional atmospheric pollution. The nitrate concentration in the two samples from Grefsen, G1-1 and G1-2, was 3.04 mg/l and 4.47 mg/l, respectively. Not considering long-transported air pollution, there are few natural sources of nitrate to the environment in Norway. Agriculture and sewage, together with the use of agrochemicals, are considered to be some of the anthropogenic sources of nitrate to rivers and streams (Reimann et al., 2009). Potassium might also be derived from agrochemicals, although the concentration of potassium found in all water samples from both Grefsen and Akerselva were low (<2 mg/l) (Banks et al., 2001).

Regarding the soluble silicates, 9.65 mg/l of soluble silicates was measured in the sample G1-1 in Grefsen, while 3.48 mg/l were measured in Akerselva (A1-2 and A2-2). The rock and mineral type in contact with water is a factor that can control the concentration of silica in streams, rivers and groundwater. Large amounts of soluble silicates in water are likely to be related to volcanic rocks (Davis, 1964), corresponding to the presence of basalt and syenite in Grefsen. The relatively high concentration of soluble silicates in Grefsen (G1-1) compared to Akerselva (A1-2 and A2-2) might also be associated with the rainfall November 12, 2018, which resulted in high stream flux. Suspended silt and clay particles (containing silica) present in the runoff will expose a much larger surface area in solution compared to periods of lower discharge (or no water in the stream). Turbulent streams with a coarse bed load, such as the upper Torshovbekken catchment and stretches of Akerselva in the urban area of Oslo with waterfalls and terraces, will also fracture minerals, i.e. quartz which is the main mineral in quartzite. The process can produce strained surfaces subject to rates of dissolution much more significant than on the unstrained surface (Davis, 1964).

6.2.2. Trace elements

The dominating trace elements in Grefsen and Akerselva are strontium, iron and aluminium.

Strontium can be released into the air and water by natural processes, i.e. weathering of rocks and sea spray, but also by anthropogenic sources. Human activities such as milling, coal burning and the use of fertilizer are some anthropogenic sources for strontium in the environment (Hibbins and Staff, 2000).

In sedimentary rocks, strontium is predominantly found in carbonate rocks composed of calcite, aragonite or dolomite (Brand et al., 1998). Due to its chemical similarity to calcium, strontium often replaces calcium in carbonate and silicate minerals (Bain and Bacon, 1994). The distribution of strontium in these sedimentary rocks is controlled mainly by the extent of Sr^{2+} can substitute for Ca^{2+} in

the $CaCO_3$ lattice (Brand et al., 1998). Therefore, the presence of strontium in streams and rivers is often associated with the dissolution of calcium-bearing minerals in igneous and sedimentary rocks. Weathering of quartz, potassium-feldspar and chlorite are also natural processes leading to strontium in groundwater. Potassium-feldspar is the most common Sr-containing mineral in granite (Heier, 1962), and also found in the syenite in Grefsen. It can thus be suggested that dissolution of calcium-rich minerals and weathering of silicates are the most likely sources of strontium in the water samples collected in this study. However, strontium may also be derived from the rainwater consisting of diluted seawater (Bain and Bacon, 1994).

Aluminium is the dominant trace element in the two samples (A1-2 and A2-2) in Akerselva, with concentrations of 132.2 and 129.5µg/l, respectively. Aluminium is the third most abundant element in the soil, constituting on average 8% of the minerals (Rosseland et al., 1990). Weathering of aluminium-rich minerals, i.e. albite found in the loose sediment samples from Torshovdalen (XRD data), is therefore considered to be one of the main processes leading to a high concentration in the water samples from Akerselva. Acidic precipitation can also be related to high aluminium concentrations since acidification of catchments often leads to an elevated aluminium concentration in soil solutions, rivers and streams (Rosseland et al., 1990).

A relatively similar concentration of iron was found in the samples from Grefsen and Akerselva (in the range of 34-41 µg/l). A possible source for iron in these streams are biotite which can be found in igneous rocks and iron as an impurity in the carbonate minerals that make up the Cambro-Silurian limestones.

6.2.3. Field parameters

Average measured pH in Akerselva and Grefsen was 7.1 and 7.5, respectively, both higher than the measured pH in the precipitation. An explanation to this result might be consistent with the release of major cations by hydrolysis of minerals such as carbonates and feldspar (or other silicate minerals), or by cation exchange in the soil (Reimann et al., 2009). Chemically, these carbonate and silicate minerals act as bases, and during a water-rock interaction with these minerals, it is expected that the pH increases (Frengstad et al., 2001).

Another important finding is the different values in electrical conductivity in samples from Grefsen and Akerselva. Measured electrical conductivity was higher in Grefsen (229-246 µS/cm) than Akerselva (22.3-67 µS/cm). These results further support the idea of Akerselva being more diluted, due to the constant waterflow in the river, than the stream in Grefsen where a higher concentration of all ions was measured, especially sodium and chloride.

6.2.4. Bacterial characterization

The presence of *E. coli* bacteria in water samples are also of interest, since it is an indication of fecal contamination and may represent sewage overflows into rivers and streams or leaching from the sewage systems.

The low concentration of *E. coli* in Grefsen (G1, 26 *E. coli*/ 100ml water sample) is not surprising as the stream is mostly sustained by rainwater. However, the large amount of rain registered on the 12th of November 2018 could also have an opposite effect on the *E. coli* concentration, as a consequence of more runoff in the Grefsen area. The runoff can potentially collect and transport particles and dust, in addition to sources of faecal contamination. Natural sources of *E. coli* bacteria in the Grefsen area are dogs, deer and other animals, contributing to fecal contamination of the stream.

Based on results from Grefsen (G1), the stream is not assumed to be affected by any form of recent faecal contamination. It is important to mention that the findings may be somewhat limited due to few measurements from the stream in Grefsen (as a result of little precipitation during Summer 2018).

The concentration of *E. coli* bacteria in Akerselva is well documented, as it is part of the established monitoring tasks run by VAV. A total of 44 samples were analyzed from location A1, A2 and A3, during the period from February 2 to November 5, 2018. The average concentration based on all samples was 1385 *E. coli*/ 100 ml water sample, which is significantly higher than the concentration measured in Grefsen (G1), and classifies the river as "poor" based on EU bathing water directive classifications (EU, 2006). Possible sources of faecal contamination in Akerselva are bird dropping, and the presence of other animals in the area, e.g. dogs and cats. Sewage overflows and human activities are also potential sources of faecal contamination.

Comparison of the *E. coli* concentration to measured precipitation (mm/day) shows that there is a close association between *E. coli* bacteria and heavy rainfall. During the sampling period, the highest concentrations of *E. coli* in Akerselva were measured the same day as heavy rainfall. Since Akerselva flows through the urban part of Oslo, with a large percentage of impervious surfaces, it is likely that the rain transports faecal matter from impervious surfaces into Akerselva during the rain event.

One specific example was the extremely high concentration of *E. coli* measured from location A3 on September 10, 2018, when 21.5 mm of precipitation were registered (Figure 5.26). This finding may confirm the correlation between climate changes leading to more intensive rainfall, urbanization and sewage overflow. Culverts and pipes in Oslo do not have the capacity to handle the increased rainfall attributed to climate change, and urbanization has resulted in more impervious surfaces, all leading to a higher volume of runoff into the sewage systems and sewage overflows.

The previous section has shown that intense rainfalls, as a consequence of climate variation, together with increasing urbanization, can result in a degradation in the water quality in the river Akerselva. Due to few results from the stream in Grefsen, it is difficult to predict how the concentration of *E. coli* changes as a result of precipitation. The chapter that follows discusses the water chemistry and bacterial characterization in the ephemeral spring in Torshovdalen.

6.3. Subsurface water – Ephemeral spring

The sampling point T1 is considered to be an ephemeral spring since the water content increased and decreased proportionally with precipitation. During wet periods, the spring can act as a groundwater seepage horizon. It is also possible that the spring is fed by the groundwater, although this is difficult to confirm without further investigation of the lithological boundaries in the area. Assessing the water quality in the spring is important since it represents, to some extent, the rainwater that has infiltrated and travelled through the unsaturated zone and is likely to recharge the groundwater. Differences observed in the water quality, and the chemical composition between the ephemeral spring and the groundwater, provide a better understanding of the chemical processes and anthropogenic inputs affecting the water quality in the unsaturated zone and groundwater.

6.3.1. Major inorganic ions

The results obtained in section 5.2.4 show a significantly high concentration of all major ions, especially for sodium, calcium, chloride and sulphate compared to the rainwater, Akerselva and Grefsen (Figure 6.2).

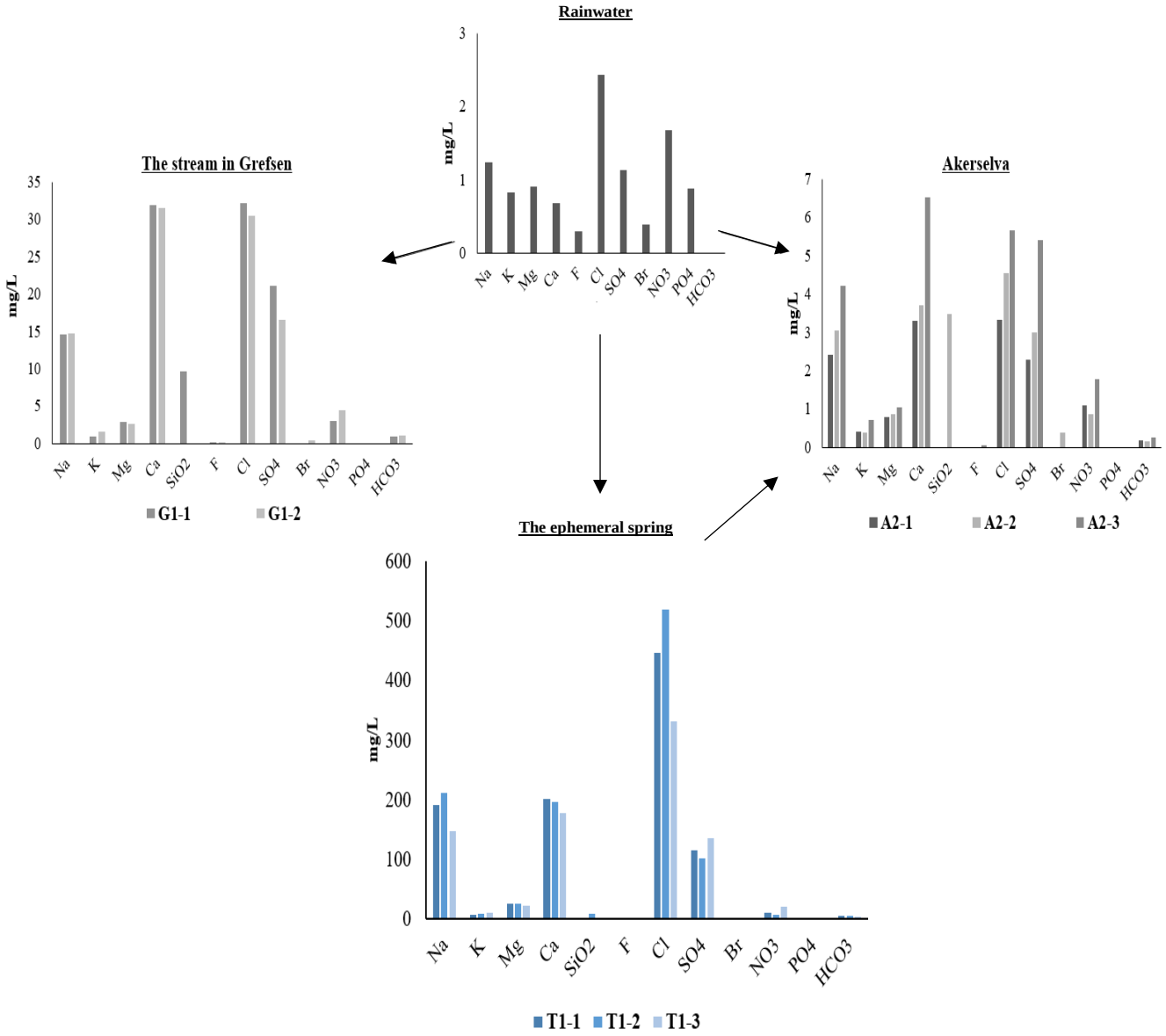

Figure 6.2. The change in the water quality from the rainwater to the ephemeral spring is due to several processes, resulting in a high concentration of the major cations and anions in the ephemeral spring. A change in the concentration was observed in samples T1-3, collected after heavy rainfall on the 11.12.2018. Akerselva, located downstream is made up of rainwater, subsurface water and groundwater.

Torshovdalen is located downhill and very close to a high traffic road, which results in polluted runoff water flowing into the soil in Torshovdalen. As already mentioned, road salting contributes to an increased concentration of K, Ca, Na, Mg, Cl and SO_4^{2-} in urban runoff (c.f. section 6.2.1), which can be a reason for the observed high concentrations. This explanation has some uncertainties due to the observation made in the sample (T1-3) taken after heavy rainfall. As seen in Akerselva (Figure 6.2), the concentration of all major ions increased after this rain event, which was not seen in the sample T1-3. Results showed that the concentration of especially sodium, calcium, and chloride decreased, and the concentration of sulphate, nitrate and potassium increased. When comparing the samples collected on November 12, 2018, from the ephemeral spring (T1-3) against Akerselva (A2-3) in Figure 6.2, it is clear that Akerselva is not only made up by rainwater but also by shallow and deep subsurface water (here represented by the ephemeral spring and groundwater wells, respectively). When the concentration of some major ions decreases in the ephemeral spring, an increase is observed in Akerselva, meaning that what is removed, in terms of inorganic elements, from the shallow subsurface (the ephemeral spring), is added to Akerselva.

A possible explanation for the decreased concentration of calcium, sodium and chloride might be that the rainwater dilutes the existing water in the ephemeral spring, resulting in lower concertation of these elements. However, the precipitation is also expected to lead to more intense runoff, which can explain the higher concentration of sulphate, potassium and nitrate. Sulphate is, as previously mentioned, found in road salt. The salt dissolves during snow melting and accumulates in the soil and unsaturated zone, where they can stay for an extended period (Amundsen et al., 2012, Provin and Pitt, 2001). Rainwater falling on the soil surface and infiltration into the unsaturated zone can lead to the dissolution of previously precipitate salts, and sulphate is released in the water that flows into the ephemeral spring. It would, however, been expected that the runoff also contributed to an increase in sodium and chloride concentration.

The increased concentration of nitrate in the sample T1-3 can be explained by nitrification. Nitrification (oxidation of NH_4 to NO_3^-) of plants and organic material increases the nitrate concentration in the surface soil. These nitrates are further transported to groundwater, or surface water as in the ephemeral spring in Torshovdalen, by the percolating water from rainfall (Reddy et al., 2011). Another possible source for the presence of inorganic nitrogen dissolved in water may be human and animal excreta, and wastewater containing urea. Urea is hydrolized to ammonia (NH_4) and carbon dioxide (CO_2) (Kreitler, 1974). Negatively charged clay minerals can adsorb NH_4 in the wastewater in the unsaturated soil, creating an unstable condition unless the zone is anaerobic. This is not the case in the unsaturated zone where the pore space is generally air-filled. NH_4 will be oxidized to NO_3^- by nitrifying bacteria during dry periods. Subsequently, the nitrate is leached out during the next rainfall (Lance, 1972). Both processes cause higher nitrate concentration.

The concentration of soluble silicates in the sample T1-2 (9.34 mg/l) was similar to the sample G1-2 (9.65 mg/l). After and during heavy rainfall, much of the runoff will travel through the upper part of the soil profile as an interflow. As the runoff and rainfall water flow through the soil, soluble silicates can be leached out (Davis, 1964). This process is likely to be the reason for higher soluble SiO_2 in the sample T1-2. Results from the XRD and XRF analysis also supports this explanation, showing that the loose sediment in Torshovdalen contained approximately 60 % SiO_2.

6.3.2. Trace elements

Regarding the trace element analysis, high concentrations of iron, zinc and strontium were measured in the sample T1-2. Road traffic and tire dust are thinkable sources for zinc in the ephemeral spring, which is considered to be profoundly affected by urban runoff. As previously explained for Akerselva and Grefsen (c.f. section 6.2.2), weathering of limestone, and to some extent shale which is relatively easily eroded, is a source for the high concentration of strontium found in the ephemeral spring in Torshovdalen. Weathering of silicates can also contribute to strontium, but these minerals are more resistant to chemical weathering and usually contain a lower amount of strontium than limestones (Palmer and Edmond, 1992).

6.3.3. Field parameters

A high electrical conductivity was measured in the samples from location T1. The result is not surprising, as the electrical conductivity is, as seen in equation 4.1, proportional to the concentration of anions and cations.

The alkalinity measured in water samples from location T1 also stands out with significantly higher values than those obtained from the other samples collected in Torshovbekken watershed. Oxidation of organic matter and root respiration in the unsaturated zone may lead to higher alkalinity in the ephemeral spring. The processes produce carbon dioxide, followed by dissolution of carbonate and weathering of silicates, both producing bicarbonate (Tiwari and Singh, 2014). The high alkalinity might support the theory that the ephemeral spring is fed mainly by groundwater which previously flowed through the limestone bedrock, containing calcium carbonate and, therefore, contribution to high alkalinity.

6.3.4. Bacterial characterization

Even though the highest concentration of *E. coli* was measured in Akerselva September 10, 2018, the average concentration was highest in the sampling point T1. This section will discuss three possible sources for the high amount of *E. coli* in Torshovdalen; animals, leachate from a sewage pipe in Torshovdalen or leachate from nearby sewage pipes. The concentration of *E. coli* has also been compared against the measured precipitation (mm/day).

The location of T1 is in the middle of Torshovdalen. Due to the sampling points location, faecal pollution from animals, especially dogs, can be a source for the high *E. coli* concentrations in the valley. By comparing the results of *E. coli* and precipitation in the ephemeral spring toward the results in Akerselva, there were some surprising observations. In Akerselva, more intensive rainfall lead to higher *E. coli* bacteria in the water sample. In the ephemeral spring, a high concentration of the bacteria was measured in all samples, except on the sample collected after heavy rainfall. This result supports the hypothesis that animals are an important source of faecal contamination in the ephemeral spring. The *E. coli* is washed away from the urban surfaces, soil and unsaturated zone and transported into the surface water bodies located downstream in the watershed (Akerselva).

Leakage from sewage pipes is another possible source for the high *E. coli* concentration. During a field campaign, a pipeline was observed close to the ephemeral spring (Figure 6.3). There are some uncertainties concerning this source of *E. coli* contamination due to lack of information regarding the pipeline.

As seen in Figure 6.3, several pipelines are located in the vicinity and uphill (to the east) from the location of T1, leading to the third source; leakage from nearby sewage pipes. The leakage could explain the high concentration of *E. coli* measured in T1 observed in May, June and July 2018. This hypothesis is also supported by the increased nitrate concentration sample T1-3, taken together with the water sample for *E. coli* analysis. Nitrates are challenging to control because the source is often diffuse; originating from agriculture, wastewater, plants, and the atmosphere (Bogárdi et al., 2013). In this urban setting, the most likely source of nitrate is leakage from sewage water.

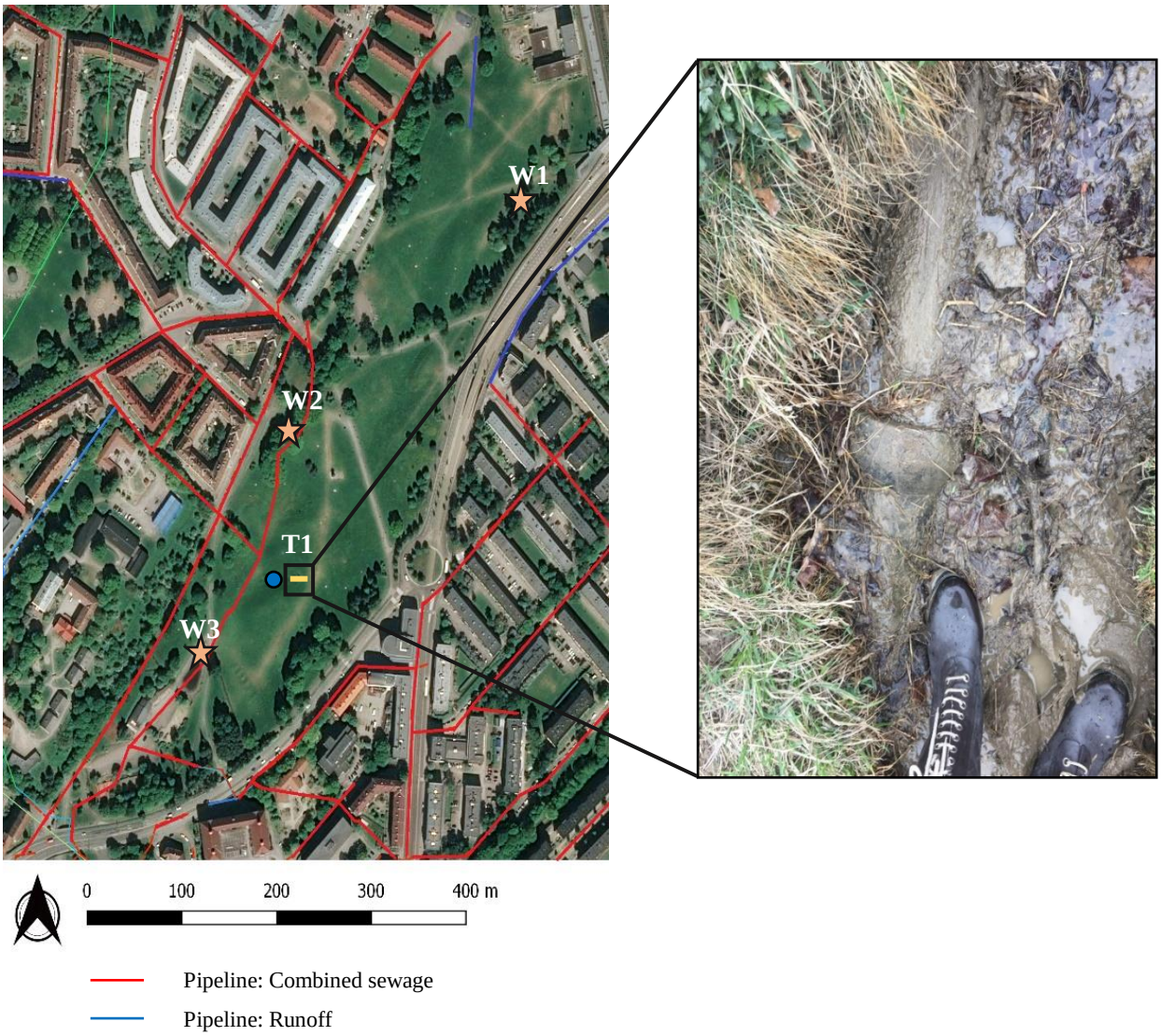

Figure 6.3. Location of the observed pipe line (yellow line) in Torshovdalen, close to the ephemeral spring (T1). W1, W2 and W3 show the location of the installed groundwater wells. Several combined sewage system pipelines are located in and near Torshovdalen (red line). Information regarding the sewage system pipelines in Torshovdalen and the surrounding area are modified from the Agency for Water and Sewerage in Oslo municipality. Photo of the pipeline was taken by Uglum, M.

Nevertheless, the sample taken for *E. coli* analysis (November 12, 2018), does not support the theory of sewage leaking from nearby pipes. If sewage water was the main source of nitrate, the concentration of *E. coli* and nitrate should increase simultaneously (or be proportional). More rainfall would typically lead to an increase in the bacteria concentration due to sewage overflow. However, the opposite occurred. While the nitrate concentration increased, the *E. coli* concentration decreased, dramatically.

The contradictory observations of *E. coli* and nitrate in this sample (T1-3) can also be explained by the different mobility of nitrate and bacteria in the soil and unsaturated zone. While bacteria are more mobile, and therefore rapidly leach into the surface water bodies after heavy rainfall, nitrate has a more unpredictable behaviour since it can be temporarily stored in the soil as precipitated nitrate salts. These nitrate salts will then be incorporated into the subsurface of interflow water during and after rainfall

events. This process is particularly efficient during rainfall events that are preceded by dry periods, which is exactly the case in the sample T1-3.

6.4. Unsaturated zone

An initial objective of the project was to identify the processes occurring in the unsaturated zone and assess the water quality by analysing a combination of water and soil samples.

Regional changes of the water quality within the aquifer are often dependent on the weathering of minerals in the unsaturated zone and the dissolution of rock minerals below the groundwater surface (Englund and Myhrstad, 1980). In this study, sediment samples from the unsaturated zone were gathered near the groundwater wells W1, W2 and W3. The results obtained from both water and sediment samples will be discussed in the following subsection.

Water samples from the unsaturated zone were not analyzed for *E. coli* bacteria, because the porewater extraction procedure (more than a day, with sediment drying steps, c.f. section 4.2.5) made them unfeasible for *E. coli* analysis. Determination of *E. coli* bacteria using the Colilert-18 method is advised to be done within a few hours and by using natural water.

6.4.1. Major inorganic ions, mineralogy and geochemistry

Based on the XRD analysis, quartz, muscovite and albite are the main minerals found in sediment samples from the unsaturated zone in Torshovdalen, followed by chlorite and potassium-feldspar. The sample W3-L4 (Figure 5.31) was the only sample from the loose sediments containing kaolinite, although the clay minerals kaolinite, chlorite and illite were determined by XRD clay fraction analysis (samples W1-L2 and W3-L4).

The results from XRD match those obtained from XRF analysis, where the dominating elements in the sample (in weight %) are; SiO_2, Al_2O_3, Fe_2O_3, K_2O and Na_2O. Each sediment samples contained a low weight percent of CaO and consequently, a low amount of calcite. These observations were also consistent with low LOI values (1.4% – 3.7%) in all sediment samples from the unsaturated zone, except for the sample W3-L4 (12.5%).

Based on the information regarding the mineralogy and chemistry in the sediment samples from the unsaturated zone, the concentration of the dissolved species in the extracted porewater showed some unexpected outcome. Porewater samples extracted from these sediment samples showed calcium and sulphate as the dominant cation and anion. The results are somewhat surprising given low concentration of calcium in the solid phase, revealed by XRF CaO data. Usually, a high concentration of calcium in

the porewater is primarily due to carbonate mineral weathering. Given the almost absence of CaO (XRF data), other sources of calcium in the sediments must be taken under consideration.

A process that can affect the water chemistry in the unsaturated zone is cation exchange. The soil usually contains abundant materials which can sorb chemicals from water. Clay minerals and organic matter are such important sorbents and exchangers. Given the low LOI values, clay minerals are probably the main sorbents in Torshovdalen. This assumption is strengthened by the results from the grain size distribution from the unsaturated zone samples. The clay-sized content increased from around 1% in the upper 10 cm of the soil towards 47 % at approximately 6.5 meters below the surface soil (based on samples near the groundwater well W3).

The clay in Torshovdalen can be either of marine or non-marine origin. If the valley is filled with non-marine clay, the clay minerals will have Ca^{2+} on the exchanger. The clay minerals in Torshovdalen may, therefore, act as cation exchangers when precipitation, containing diluted seawater (NaCl), is infiltrating into the unsaturated zone. Another possible source of calcium in the porewater can be from marine clays, which is now enriched in calcium due to the long-term weathering of calcium-containing minerals in areas upstream Torshovdalen which have transferred calcium into the subsurface water that has reacted with the marine clays. The result is an enrichment of calcium in these marine clays. Both explanations will lead to clay minerals with Ca^{2+} on the exchanger. As the water (NaCl containing rainwater or runoff) is infiltrating into the unsaturated zone, an exchange of cations can take place (c.f. section 3.2.2, Eq. 3.2). In the reaction, described by Appelo and Postma (2005) Na^{+} is taken up by the exchanger, most likely clay minerals, and Ca^{2+} is released.

Chloride is still the dominating anion in the equation 3.2, which was not the case in the water samples collected in the unsaturated zone in this study. Results showed that sulphate is the dominant anion in all samples (except sample W2-L2). Sulphate, in addition to chloride, is assumed to be derived from road salting during the winter which can accumulate in the soil and stay there for a long period. Similar to nitrate during rainfall, sulphate previously precipitated as sulphate salts in the unsaturated zone can be leached into the porewaters.

Results from the infiltration test in Torshovdalen indicate a low infiltration capacity which corroborates the predominance of fine sand, silt and clay. The grain size distribution analysis in the upper 10 cm of the soil varies from 1- 20 % clay, with a general increase of clay content with depth. The impact of clay-rich soils on the urban water cycle is two folded; on one hand surface water infiltration is hindered, while on the other hand, contaminants can be retained, contributing to the natural depuration of groundwater which, in turn, is likely to feed watercourses in downstream areas of the city. The contaminants can be retained by ion exchange or by adsorption. Since clay minerals have a large specific surface area, they can have a high cation exchange capacity (CEC), which is a quantitative measure of the ability of a mineral surface to adsorb ions (Boulding and Ginn, 2016).

6.4.2. Trace elements

Strontium, aluminium, iron and manganese are the dominant dissolved trace elements in the unsaturated zone. Strontium appears to be a common element in Torshovbekken watershed and is likely to be derived from carbonate rocks containing calcite, potassium-feldspar or human activities (c.f. section 6.2.2). Potassium-feldspar, in addition to weathering of albite and muscovite, is also an essential source for the aluminium content, although aluminium is an abundant element in the soil (Rosseland et al., 1990).

Given the low weight percentage of MnO (XRF data) in the unsaturated zone, dissolution of minerals containing manganese are probably not the main source of manganese in the ephemeral spring. The high concentration of manganese can be a result of anthropogenic sources, such as wastewater discharge and sewage sludge (Howe et al., 2004, Patil et al., 2016). Manganese oxides can play a central role in water chemistry due to their remarkable surface area and charge distributions. These properties make manganese oxides a potentially rich reservoir of adsorbed metals. Microorganisms capable of reducing manganese oxides act as a solubilizing agent of the particulate manganese oxides, triggering the release of previously adsorbed metals (Bratina et al., 1998), which also can explain the high concentration of manganese in sample T1-2.

Iron oxide minerals can be present as discrete minerals and clay particles (Oppong-Anane et al., 2018). Weathering processes, in addition to redox reactions due to post-oxic conditions, can be considered as sources of iron in the unsaturated zone (Appelo and Postma, 2005).

Based on the XRF analysis phosphorus (P) and barium (Ba), are the main trace elements from the sediment samples in the unsaturated zone, although barium was not measured from the water samples representing the unsaturated zone only

Phosphorus is a highly reactive element that is essential for life (Domagalski and Johnson, 2012). In water, phosphorus can be present as the orthophosphate ion PO_4^{3-} (measured in the water samples). From the water chemistry, only the rainwater sample contained a measurable amount of phosphorus, while a very small concentration of phosphorus was measured in the porewater samples extracted from the unsaturated zone. Erosion of rocks is normally the main source for phosphorus, although agricultural sources are also considered to be a major contribution to phosphorus in soil and water. When the ion is added to the soil, it can be retained by adsorption (clay and organic matter). However, due to limited storage capacity, phosphorus can dissolve and be leached out in the water either directly to a stream or percolate into the groundwater (Domagalski and Johnson, 2012). Since phosphorus was only detected in the rainwater and porewater samples, the concentration of phosphorus in the soil sediments and bedrock seems not to affect the water composition of the groundwater. One possible explanation is, as mentioned, that the concentration of phosphorus is adsorbed strongly by the soil. Even though phosphorus in water carries a negative charge, it can be adsorbed in the soil by clay and metal oxides, e.g. iron oxides (Domagalski and Johnson, 2012)

Barium was the other element with a significant concentration in the solid phase of the sediment samples. The element is only found in combination with others because it is very reactive, and is added to the soil through the natural process of soil formation, including the breakdown of parent rocks by weathering (Nielsen and Ladefoged, 2013). The two most common naturally occurring barium ores are barite (barium sulphate) and witherite (barium carbonate). Since the concentration of barium was only analyzed in the sediment samples, it is difficult to discuss how this element behaves and is transported under different conditions in the unsaturated zone.

6.5. Groundwater

The chemical composition in the groundwater samples varied. The two samples from groundwater well W3 (W3-1 and W3-2) contained a higher concentration of all inorganic ions compared to the sample from the groundwater well W1 (W1-1). However, with few water samples from well W1, caution must be applied when discussing the results from this well. The findings from the well W1 might not be representative of the groundwater based on the following assumptions; 1) the well might not be deep enough to reach the groundwater, 2) the water samples could present a mixture of groundwater and water used during the drilling operation.

After emptying the well volume in well W1, the water had a greyish color. This observation suggests contamination of the water, and it is reasonable to assume that drilling fluids, bentonite pellets, or casing materials, influenced the water. It is also important to mention that the flow into the groundwater well was very slow. After emptying the well, the water level raised only 1-2 cm after four hours. Consequently, the water sample W1-1 must be interpreted with caution.

The processes occurring as the subsurface water (here presented by the water collected from the ephemeral spring) percolates through the unsaturated zone affects the chemical composition of the receiving groundwater. As seen in Figure 6.4, there is a clear change in the water quality from precipitation to groundwater. When comparing the concentration of major ions in the ephemeral spring against the groundwater (Figure 6.4), it is a clear decrease in the concentration of sodium, calcium, chloride and nitrate. These changes support the explanation presented in section 6.4.1., where the high clay content in Torshovdalen are assumed to hinder surface water infiltration and retain the contaminants by ion exchange or adsorption. The main factors believed to control the quality of the groundwater in Torshovdalen will be discussed in the next pages.

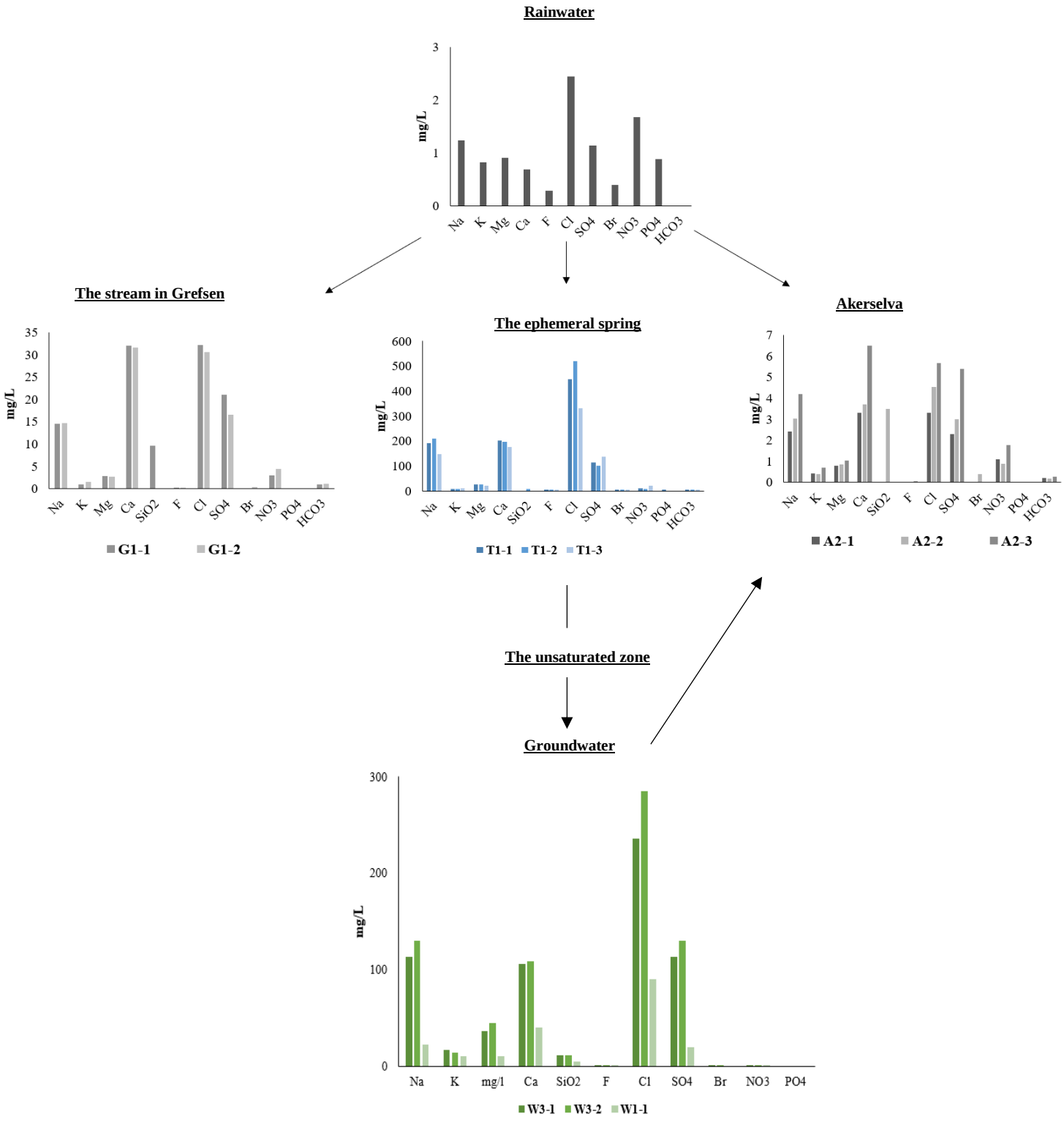

Figure 6.4. The change from rainwater to groundwater involves several processes in the soil which may affect the concentration of the groundwater. As seen in the figure, the concentration from the ephemeral spring to the groundwater increase, which can be due to various processes. The unsaturated zone is not shown graphically in the figure as the concentrations are calculated (c.f. section 4.2.5.) and significantly lower compared to the other water samples (c.f. section 5.2.5.).

6.5.1. Weathering and dissolution of minerals

An initial objective of the study was to observe how the Cambro – Silurian bedrock in Oslo affect the distribution of major and trace elements in the groundwater.

Sodium appears to be the principal cation in the two water samples from the groundwater well W3 (W3-1 and W3-2), while calcium is the main cation in the sample from W1 (W1-1). According to Englund and Myhrstad (1980), calcium is normally the main cation in groundwaters from areas above the Late-Postglacial marine limit consisting of carbonate rocks, while sodium dominates the areas below this limit. The study matches the result from samples collected from the well W3 where sodium is the dominate cation, but not for the samples from the well W1. It is important to mention that there are only small variations in the concentration of calcium and sodium in the groundwater samples from the well W3, which can be the result of several processes taking place and affecting in the groundwater composition.

Initial observations suggest that there might be a link between Cambro – Silurian bedrock and the distribution of major elements, especially calcium, in the groundwater. The Cambro-Silurian limestone in Torshovdalen, composed of calcite, is a vital source for the high content of calcium and bicarbonate in the water as it is easily weathered rocks (Hongve, 1977). These assumptions are strengthened by the interpretation of the XRD and XRF results. Interpretation showed that the weight percent of calcite in the sediment samples increased with depth, proportional to the increased amount of CaO and LOI (XRF data). These observations support the hypothesis that the Cambro-Silurian bedrock, in particularly the limestone, affects the distribution of major ions due to calcite dissolution.

Silicate weathering is a source for the high output of sodium, potassium, as well as parts of calcium and magnesium (Jørgensen et al., 1991). Weathering of silicate minerals, which are the dominant minerals in Torshovdalen, is a slow process, especially when compared to dissolution of carbonate minerals and cation exchange processes. Nevertheless, with time, silicate mineral weathering can change water chemistry (Appelo and Postma, 2005). Sodium is mainly derived from weathering of albite while weathering of potassium-feldspar, chlorite and muscovite usually are responsible for potassium and magnesium in the groundwater (Appelo and Postma, 2005, Englund and Myhrstad, 1980). The effect of the mineralogy in Torshovdalen can also be seen from the result of soluble dissolved silicates. The highest concentrations were measured in the water samples W3-1 and W3-2, indicating an active degradation of silicates minerals.

6.5.2. Effect of old seawater

Chloride was the dominant anion in all three groundwater samples. Chloride can be added to the groundwater from both natural and anthropogenic sources. Atmospheric precipitation, dissolution of salt deposits and weathering of halite are some of the major lithogenic sources for chloride in the groundwater (Tiwari and Singh, 2014). Another source can be from seawater and marine clay. Assuming that the lowermost part of the sediments was deposited below the marine limit, the groundwater might have been influenced by fossil seawater, leaching out from these marine deposits (Jørgensen et al., 1991). In this case, chloride is added to the groundwater by the long-term leaching from the pore water in marine clay (Reimann et al., 2009).

6.5.3. Anthropogenic sources

Since Torshovdalen is in an urban area in Oslo, it is important to assess anthropogenic inputs to the groundwater water quality. Septic, industrial and animal waste, fertilizers and leachate from landfill, and waste dumps are anthropogenic sources which may affect the water quality (Tiwari and Singh, 2014). Chloride is considered to be a conservative element since it is not significantly retarded by sorption, ion-exchange or precipitation in the subsurface (Sæther et al., 1992) Elevated chloride concentration in the groundwater is consequently often associated to these anthropogenic sources. Septic system leachate can be a source of groundwater salinization due to the release of sodium and chloride from human waste and water softeners into the environment (Daley et al., 2009).

Fertilizers are usually a source for nitrate contamination in the groundwater. Nitrification of reduced nitrogen (N) from fertilizers and manures generates acidity along with nitrate (NO_3^-) (Böhlke, 2002). Given the relatively low nitrate concentration in the groundwater in Torshovdalen, agricultural contamination from fertilizers is likely not a significant anthropogenic source of groundwater contamination in this area.

Another anthropogenic source which influences the groundwater quality in Torshovdalen is road salting (c.f. section 6.2.1). A considerable amount of the applied portion of salt during the winter season is flushed away from the roads by runoff and overland flow, but a portion may also be retained in the basin each season and cause a continuous degradation of the groundwater quality, resulting in increased salinity levels (Howard and Haynes, 1993). Salinization of groundwater does appear to be related to the amount of nearby impervious surfaces where chemical road salts (de-icing) are applied. This finding is also reported by Rosenberry et al. (1999), where high chloride concentration was measured in deep groundwater wells. The results indicated that the road-salt contamination of groundwater had penetrated at least 123 meters into the bedrock beneath the road (Rosenberry et al., 1999). The high chloride and sodium concentrations in the groundwater samples form Torshovdalen is, therefore, likely related to infiltration of road salt.

6.5.4. Trace elements

Both strontium and calcium show relatively high concentrations in the groundwater samples, which is likely due to the same processes as the one referred in section 6.2.2 for Akerselva and Grefsen. Another minor source of strontium in the groundwater can be infiltration of precipitation (Bain and Bacon, 1994)

Iron and manganese are two examples of redox-sensitive elements, and elevated concentration of these elements are typically found in reducing environments (Frengstad et al., 2002).

The concentration of dissolved iron in the groundwater samples can, to some extent, be explained by the XRF analysis. The sediment samples representing the bedrock close to the groundwater wells in Torshovdalen contained between 3.7 – 6.6 % (in weight percentage) of Fe_2O_3. This combination of findings, a high concentration of dissolved iron and the amount of Fe_2O_3, suggest that dissolution of the iron-containing minerals such as biotite and iron-rich carbonates is a possible explanation for iron in the groundwater samples. Dissolved iron can also be derived from anthropogenic sources, such as mining and metals corrosion (Minear and Keith, 1982). Metal corrosion can occur in the area surrounding Torshovdalen, but it can also occur in the unsaturated zone due to oxidation of iron-containing materials, where iron is released into the environment and groundwater.

High concentration of manganese is also found in the groundwater samples from the wells W1 and W3. It is difficult to explain this result, but it might be related to anthropogenic inputs, such as municipal waste and sewage and emission from steel and iron production (c.f. section 6.4.2) (Howe et al., 2004) or natural sources. Results from Grefsen and the ephemeral spring shows a significantly lower concentration of manganese compared to the groundwater samples. Therefore, it seems unlikely that this stream and spring are responsible for the high manganese concentration in the groundwater, especially since metals are assumed to not migrate through sediments, but are adsorbed in the soil, or the first decimeters of a river (Jaudon et al., 1989). Also, XRF results from the bedrock samples showed a low weight percentage of MnO. The MnO values varied from 0.05 – 0.15 % and suggestes that dissolution of the manganese oxide is not the main source for manganese in the groundwater. There are some natural atmospheric sources for manganese in groundwaters, such as ocean spray, vegetation and igneous rocks (Howe et al., 2004). It is, however, difficult to decide if these natural sources affect the groundwater quality in Torshovdalen, and if they are, to what extent.

6.5.5. Field parameters

High values were measured for pH, EC and alkalinity in the groundwater. Low and stable temperatures between 5.5 to 5.6 °C were measured during the two days of sampling.

The pH measured in the three groundwater samples varied between 7.95 to 8.08 and was the highest measured pH compared to the other water samples collected in Torshovbekken watershed.

The host rock to the groundwater samples is limestone and shale (sedimentary rocks), dominated by carbonate and silicate minerals, respectively. Chemically, these minerals can act as bases and give an increased pH as water-rock interactions occur and chemical weathering proceeds (Frengstad et al., 2001). According to Frengstad et al. (2002), pH in groundwater is only limited to the aquifer lithology to a certain extent. The groundwater "maturity" and the state of equilibrium relative to the calcium carbonate system are also important factors controlling the pH in groundwater. Mature groundwater is normally Ca-HCO_3 water and has acquired a geological signature, probably due to calcium carbonate dissolution (Banks et al., 1998b).

Given that the groundwater samples collected in this study are classified as calcium-chloride water (Figure 5.2), there are most likely other explanations for the high pH values. Frengstad et al. (2002) also argue that there is a slight tendency towards elevated pH values in bedrock groundwater near the coast. One of the theories is that leaching of high-pH pore waters from marine clays deposited and raised above the postglacial shoreland due to isostatic rebound can result in the pH values measured in the groundwater samples in this study. Also, the high pH can be explained by ion exchange of calcium against sodium derived from these marine environments below the postglacial marine limit (Appelo and Postma, 2005, Frengstad et al., 2002). The alkalinity values broadly mirror the pH, especially in the two samples from the groundwater well W3 (W3-1 and W3-2). The high alkalinity can be explained due to silicate and carbonate weathering by carbon dioxide, which consumed protons and produces base cations, in addition to alkalinity (Frengstad et al., 2002).

As mentioned, relatively high electrical conductivity was measured in the groundwater, ranging from 1219 to 1300 µS/cm. By comparing the in-situ measurements of EC against the calculated (Eq. 4.1), the EC in the two samples from well 3 (W3-1 and W3-2) is lower (1219 and 1300 µS/cm) compared to the calculated EC values (ranging from 1371-1533 µS/cm). The sample from groundwater well W1 (W1-1) shows the opposite trend. A higher value was measured in the field (1253 µS/cm) compared to the calculated EC values (412.5 – 442.1 µS/cm, depending on the cation and anion concentration). Since the EC is dependent on the temperature (Hayashi, 2004), and equation 4.1 is only valid at 25 °C, it is possible to assume that the low groundwater temperature has resulted in lower electrical conductivity in the samples from the groundwater well W3 compared to the calculated EC values. However, the explanation cannot be used for the values obtained in the groundwater well W1. The electrical conductivity is primarily dependent on the concentration of ionic species (Hayashi, 2004). Based on the

concentration of major ions in the groundwater (sum anions and cations, Table 5.3), the calculated values appear most accurate. The high EC values in the groundwater sample W1-1 can be related to contamination of the water from drilling fluids, bentonite pellets and casing materials influencing the water, resulting in the greyish color of the water sample.

6.5.6. Bacterial characterization

E. coli bacteria can enter the groundwater via several sources, including percolation from surface water, septic systems, sewage leaking or direct injection of wastewater effluent of surface water through wells (John and Rose, 2005). In this study, percolation from surface water and sewage leaking are believed the be the primary sources of *E. coli* into the groundwater in Torshovdalen.

Since Torshovbekken today is a part of the combined sewage system in Oslo, contamination of groundwater from sewage leaking can occur and degrade the water quality. *E. coli* bacteria was used as an indicator of microbial water quality. This is based on the premise that these bacteria are present in high numbers in the faeces of humans and other warm-blooded animals. If faecal bacteria enters the groundwater they would likely be flowing in the groundwater, still after significant dilution (Mor et al., 2006). The presence of *E. coli* bacteria in the groundwater is therefore used as an indicator for faecal pollution and can often be related to sewage leaking.

E. coli can also reach the groundwater from the surface soil (Van Elsas et al., 2011). Given the location of the groundwater well W3, which is only centimeters from a walking path, faecal pollution from animals, in particular dogs, will most likely increase the concentration of *E. coli* bacteria around the groundwater well W3. During and after heavy rainfall, the bacteria can infiltrate into the unsaturated zone before reaching the groundwater.

Surprisingly, no *E. coli* bacteria were found in any of the three groundwater samples from the wells W1 and W3. If *E. coli* infiltrates from the surface soil, they are most likely to be removed by percolating through the unsaturated zone before reaching the groundwater (John and Rose, 2005). It is also thinkable that there is no leaking from the sewage system or leachate the surface soil, below a certain depth that is deeper than the ephemeral spring where *E. coli* are present. However, there are some other factors that can result in short survival time in aquatic environments, which could explain the absence of *E. coli* bacteria in the groundwater.

E. coli bacteria in waters are, among other factors, dependent on the temperature and the sunlight intensity (Blaustein et al., 2013). Previous work by Sampson et al. (2006), showed that cooler water temperature could increase the ability for *E. coli* to survive in a variety of aquatic conditions. In this study, the absence of *E. coli* bacteria in the groundwater makes the explanation somewhat week as the groundwater temperature were relatively low.

Another factor affecting the concentration of *E. coli* bacteria is the presence of sunlight. UV radiation causes significant damage to *E. coli* and is considered to be an important factor leading to inactivation or killing of the bacteria in environmental waters (Whitman et al., 2004). Since the groundwater is located below the surface, the absence of *E. coli* in the groundwater is likely not caused by the presence of sunlight or the low temperature.

According to these findings, it could be argued that the positive results (absence of *E. coli* in the groundwater) are mainly due to a reduction in *E. coli* as the surface water percolate the unsaturated zone or the non-leaking sewage pipes. The groundwater in Torshovdalen might also have a significant contribution of groundwater flowing from the upstream area (Grefsen), where the *E. coli* contamination is very low (26 *E. coli*/100ml). Subsequently, dilution from pristine groundwater might be another factor controlling the groundwater quality in Torshovdalen.

6.6. Bivariate analysis of water samples

The calculated Person's coefficient based on the samples A1-2, A2-2, T1-2, G1-1, W3-1, W3-2 and W1-1 (c.f. section 5.2.7) displayed a high correlation coefficient between several major and trace elements (Appendix B6).

Arsenic has not been discussed so far as it occurred in relatively low concentration compared to other trace elements in each water sample, but has a positively high correlation against sodium, calcium and chloride in the water samples. Arsenic is a toxic element and a global concern as a pollutant of groundwater (Jiang et al., 2012). Based on drinking water regulation from the Ministry of health and care service, and the world health organization (WHO), the limit of arsenic in drinking water are set to 10 µg/l (WHO, 2011). The concentration of arsenic is higher than 10 µg/l in the two groundwater samples from well W3 (W3-1 and W3-2), and in the ephemeral spring (T1-2). The main origin of arsenic in soils is the parent material from which the soil is derived. The concentration depends on the rock type, and sedimentary rock usually contains much higher concentrations compared to igneous rock. Additionally, shales and clays are assumed to exhibit a high concentration of arsenic (Adriano, 2001). The high concentration of arsenic in the groundwater samples (W3-1 and W3-2), and the ephemeral spring (T1-2), can be connected to the composition of the unsaturated zone and bedrock, mainly since the high concentration of arsenic are found together with a high concentration of sodium, chloride and calcium. However, anthropogenic sources, e.g. agriculture and mining, can also elevate the concentration of arsenic (Adriano, 2001)

A high correlation coefficient (>0.9) was also found in the relationship between Na/Cl and Ca/Cl. The result is not unexpected when knowing the results of the major inorganic elements in Torshovbekken watershed. Sodium, chloride and calcium are the dominating ions in the water samples, and the concentration is considered to increase and decrease proportional. The correlation among these elements

does also reflect some of the processes discussed in this chapter, i.e. infiltration of rainwater, dissolution and weathering of minerals and leachate of marine clays.

Infiltration of rainwater releases an equal concentration of sodium and chloride into the solution (Tiwari and Singh, 2014). The process results in a Pearson's coefficient, the Na/Cl ratio, near one. Infiltration might also lead to cation exchange when precipitation or runoff (both containing NaCl) percolates into the soil, assuming calcium-rich clays, a process which might explain the positive high coefficient factor between calcium and chloride.

A high positive correlation coefficient (0.991) was also observed between sodium and calcium. If rainwater and runoff are the main sources of sodium in the water samples and cation exchange from clays enriched in calcium, together with the dissolution of carbonate rocks containing calcite, are the main sources of calcium in the water samples. Then, the high correlation coefficient between these two elements (sodium and calcium) might reveal that the processes explained in this section, co- occur, or are the primary processes within the watershed, resulting in a concentration of sodium and calcium which increases and decreases proportionalyl.

Same as for arsenic, nickel has not been discussed so far as it occurred in relatively low concentration compared to other trace elements in the water samples, but shows a negatively high correlation against iron, potassium, magnesium, manganese and strontium (-0.887 to -0.971). Igneous rocks, upon weathering, are usually the main source of nickel in soils (Adriano, 2001). Igneous rocks are present in the upper catchment area (Grefsen) and could be a possible source for nickel. Moving down the watershed, there is a change in lithology from the igneous rock near Grefsen to sedimentary rock in Torshovdalen and the area surrounding the lower part of Akerselva. The concentration of nickel will, therefore, theoretically change from relatively high in Grefsen to low in the lower catchment area. The decrease in nickel and increase in potassium, magnesium, manganese and strontium as a result of changing lithology within the watershed could be an explanation for the negatively high correlation coefficient. Nevertheless, based on the results from ion chromatography and QICPMS, the concentrations do not change from the upper to the lower area of the catchment. Results showed that the highest concentration of nickel, potassium, magnesium, manganese and strontium are mainly found in the groundwater in Torshovdalen. These finding indicates that there are other factors, possibly anthropogenic, affecting the water quality, contributing to an elevated concentration of nickel in the groundwater and the negatively high correlation coefficients.

6.7. Geophysical logging

The geophysical logging, in particular the resistivity and the natural gamma log, together with results from X-ray diffraction, X-ray fluorescence and reports from the study area, e.g. Bjørlykke (1974), Bjørlykke (2004), can be used to identify and confirm that the bedrock in Torshovdalen is a part of the Cambro-Silurian strata. Results from natural gamma log varied between 60-80 cps in the bedrock in both groundwater wells (W1 and W3), with some deviations. These gamma-ray values do correspond well to those reported by Elvebakk (2008), where similar values were registered in logging performed in Cambro-Silurian bedrocks.

The deviations that were observed in the natural gamma ray log (observed as decreasing peaks), co-occurred as there was a registered increasing peak in the resistivity log. According to Guyod (1966), the resistivity normally increases when porosity or water salinity, or both, decreases, which are properties often seen in shale formations. The peaks in the resistivity log might, therefore, be an indication of shale. The lower values in resistivity and higher gamma-ray values will then represent the limestone formation, which is assumed to have higher porosity and waterfilled pore space compared to shale. It is, however, important to mention that these properties are also found in sandstone (Elvebakk, 2008).

6.8. Daylighting of Torshovbekken

The result of this study shows a great variation regarding the water quality within Torshovbekken watershed. Although this thesis has not focused on the daylighting of Torshovbekken, the finding in this study will be of importance if the waterway is considered to be reopened in the future. This section will, therefore, discuss the possibilities for daylighting of Torshovbekken, with the main focus on the opening of a new waterway in Torshovdalen, based on water samples collected within the Torshovbekken watershed.

It is evident that daylighting of Torshovbekken will reduce the risk of flooding and contribute to the achievement of a blue-green city. It will also increase biodiversity and better air quality for the population (Oslo Municipality, 2018). The City of Oslo aims to open waterways in a way that takes into consideration the nature of the area and make the waterway accessible for the general public (Oslo Municipality, 2018). However, concerning the access for the general public, analyzes of the water samples indicate that the water quality within Torshovbekken watershed might limit the use of the reopened waterway.

The first concern regarding a reopened waterway in Torshovdalen is related to the high *E. coli* concentrations measured in the ephemeral spring (T1), during periods without rain (the samples T1-1 and T1-2). If Torshovbekken is reopened in Torshovdalen, it is possible to assume that the relatively high amount of bacteria observed in the shallow subsurface flow, here represented by the ephemeral

spring, is likely to be transported into the future open waterways, resulting in a degradation of the water quality with respect to EU bathing water directive (EU, 2006).

Another important factor is the absence of *E. coli* in the groundwater which is probably related to the natural depuration processes occurring in the unsaturated zone. Before the process of reopening streams and rivers in an urban area, an evaluation of the soils and sediments must be performed. The evaluation is necessary in order to predict how the soil, in addition to the natural processes occurring in the unsaturated zone and the groundwater quality are affected by the construction of the new waterway. The construction of a new waterway in Torshovdalen can disturb the clay minerals which are assumed to hinder runoff infiltration and absorb bacteria and inorganic elements from the infiltrated urban runoff. A result might be that these bacteria and inorganic elements are leached into the groundwater which will lead to a degradation of the groundwater quality.

Daylighting of Torshovbekken is an example of the third step in the stormwater three-step approach, which will reduce the amount of runoff going into the combined sewage systems. Watersamples analyzed for *E. coli* in Akerselva after heavy rainfall (c.f. section 5.3.2.) contained extremely high concentrations of *E. coli*, probably due to sewage overflows or structural problems leading to sewage leaking. Assuming that the high *E. coli* concentrations are a result of sewage overflow, a reopened waterway in Torshovdalen will result in fewer sewage overflows and flooding events after heavy rainfall, which might have a positive effect on the water quality running into Akerselva. However, if Torshovbekken again becomes a tributary to Akerselva, any form of contamination in this stream, e.g. *E. coli* contamination from animals, inorganic elements from high traffic roads and road salt, will be transported into Akerselva and eventually end up in the Oslo Fjord.

7. Conclusion

In this thesis, the water quality in an urban environment has been investigated, within the Torshovbekken watershed in Oslo. The project aim was to assess the change in water quality from rainwater to groundwater, including natural and anthropogenic inputs. These results were further used to determine geochemical processes in the unsaturated zone and how the Cambro-Silurian bedrock affects the distribution of major and trace ions in the groundwater. In addition, natural and anthropogenic sources of *E. coli* into waterbodies were also assessed.

There is an apparent change in the quality of the water samples, starting with a highly diluted and slightly acidic sodium-chloride type of rainwater, and evolving into a more mineralized, circum-neutral calcium-chloride type of water in the ephemeral spring, open waterways and groundwater of Torshovdalen. The rainwater, representing the least affected by water-rock interactions (although some dust from the erosion of rocks may affect rainwater chemistry), appears to be strongly influenced by air pollution when compared to the result of the rainwater from other stations in Norway. However, the conclusion is somewhat limited by the few samples available from the Oslo region, including this and previous studies.

The main natural processes affecting the water quality in the study area occurs during water-rock interactions, i.e. mineral weathering of calcium-, and silica containing rocks. These are also essential processes affecting the groundwater composition in Torshovdalen. Since rainwater is diluted and slightly acidic, it is expected that calcite dissolution is the main process occurring in the Cambro-Silurian bedrock in Torshovdalen, consisting of nodular limestone and shale. The process is assumed to have a major influence on the groundwater quality were calcium is the main cation. Weathering of silicates, in particular albite, followed by muscovite and chlorite has resulted in a higher concentration of especially sodium and silica, from rainwater to groundwater. Taken togheter, these results suggest that the Cambro-Silurian bedrock in Torshovdalen affects the groundwater quality.

The composition of the groundwater reveals additional geochemical processes. Assuming that the loose sediments in Torshovdalen consist partially of marine clay, leaching of old seawater from these clay layers, deposited below the marine limit, might result in an increasing concentration of chloride in the groundwater. The high chloride concentration is also believed to be derived from anthropogenic sources, including leachate from septic systems and infiltration of road salts, both resulting in high salinity values.

The effect of added road salt during the winter is also observed in the open waterways, especially after heavy rainfall. The rain event resulted in a higher concentration of the major ions in Akerselva and can therefore be associated with the increasing population and urbanization in Oslo. Additionally, climate changes lead to more intense and frequent rainfall. Road salts can also contribute to high sulphate concentration. Sulphate from road salting can dissolve during snow melting and accumulate in the soil and unsaturated zone, where it stays and continuously degrades the water quality and causes high salinity values. As the rainwater infiltrates into the soil, sulphate is dissolved and released in the water, as was seen in the ephemeral spring in the sampling campaign in November 2018.

Nitrification of wastewater containing urea, plants and organic matter are sources of nitrate in the water bodies. Similar to sulphate, nitrate accumulated in the unsaturated zone can then be leached out during the next rainfall. The result is elevated nitrate concentration, which was seen in the samples collected in Akerselva and the ephemeral spring during the sampling campaign on November 12th,2018.

This thesis has also provided a deeper insight into the occurrence of *E. coli* bacteria in an urban setting, where both natural and anthropogenic inputs appear to have a significant impact on the water quality.

The natural sources of *E. coli* in Torshovbekken watershed are most likely from warm-blooded animals such as dogs, birds and cats. These are the main sources for *E. coli* in a non-urban environment, i.e. in Grefsen (G1), where the concentration was relatively low. Moving down the watershed, into more urbanized areas, including Torshovdalen (T1) and the lower part of Akerselva (A1, A2, A3), it is evident that the *E. coli* concentration is strongly affected by anthropogenic factors. The effect of increased impervious surfaces and rain events are believed to be essential as it contributes to more *E. coli* bacteria into the receiving rivers and fjords, i.e. Akerselva and the Oslo Fjord. During these heavy rain events, the existing sewage system is not capable of handling a large amount of rain and runoff, and the result is sewage overflow. There also might be structural problems of the existing pipelines, resulting in sewage leaking. The consequence of both hypotheses is an overflow of untreated wastewater as seen on September 10th, 2018, when a large amount of *E. coli* bacteria was measured in Akerselva. During these periods with heavy rain, and high concentration of E coli is measured, the water quality is classified as "poor", according to the EU bathing water directive.

One of the more surprisingly, but positive, finding was the absence of *E. coli* in the groundwater. The results can be linked to the processes occurring in the unsaturated zone and the high clay content.

The relatively high clay content in the unsaturated zone in Torshovdalen explains the low infiltration capacity. These clay minerals are also assumed to be partially responsible for the removal of *E. coli* bacteria as they infiltrate into the unsaturated zone. The clay-rich soil will firstly hinder surface water infiltration, and the bacteria is leached into the surface water bodies, i.e. Akerselva. However, assuming infiltration of bacteria-rich surface water and runoff, the clay minerals can act as a filter for the bacteria

and retain contaminants, contributing to the natural depuration of the groundwater, where no *E. coli* bacteria were observed.

Importantly, this study has provided information regarding the main factors contributing to the water quality in the urban area of Oslo. The water quality within Torshovbekken watershed should not hinder daylighting of Torshovbekken, although bathing is not advised based on the results obtained in this study. Additionally, the installation of the groundwater wells in Torshovdalen has made it possible to assess the groundwater conditions in Torshovdalen, providing a better understanding of the biogeochemical processes that take place in an urban hydrological cycle.

7.1. Recommendations for further work

This study generates several questions regarding the different elements in an urban hydrological cycle.

A natural progression of this work, which is investigated by Uglum (in press), is to calculate the water budget in Torshovbekken watershed, as it will give a profound understanding concerning an urban watershed.

Further research is also required to determine the groundwater flow rates and average residence time. These are two important parameters for the description of contaminant transport. Groundwater samples and samples from the urban soil will provide valuable information and a better understanding of the short and long-term effect of road salting and de-icing during the winter.

Additionally, further work needs to be done to establish a better understanding of the groundwater level, which could be done by frequently monitoring the groundwater level throughout the year. The snow melting during the spring, dry and warm period during the summer and (often) wet autumn would be important periods to study the seasonal variability of groundwater levels and quality.

Finally, an important issue for further work would be to assess the capacity of the sewage pipes, especially the combined sewage pipes, as faecal contamination in Akerselva will result in contamination in Sørenga, a popular bathing area in Oslo.

References

AAS, W. 2018. Monitoring of long-range transported air pollutants in Norway, Annual Report 2017. *NILU Rapport m-1064*.

ADRIANO, D. C. 2001. Trace elements in terrestrial environments: Biogeochemistry, bioavailability, and risks of metals, 2nd. Springer-Verlag, New York.

AHMED, F., GULLIVER, J. & NIEBER, J. A new technique to measure infiltration rate for assessing infiltration of BMPs. 12th International Conference on Urban Drainage, 2011a.

AHMED, F., GULLIVER, J. S. & NIEBER, J. L. Rapid infiltration measurement of LID best management practices. World Environmental and Water Resources Congress 2011: Bearing Knowledge for Sustainability, 2011b. 4379-4388.

AMUNDSEN, C., HÅLAND, S., FRENCH, H., ROSETH, R., KITTERØD, N., PEDERSEN, P. & RIISE, G. 2012. Environmental Damages Caused By Road Salt: A Literature Review. *Technology Report*, 2587.

ANDERSEN, T. 2017. Mass spectrometry - Inductively Coupled Plasma Mass Spectrometer *In:* WORK, U. (ed.). Oslo: University of Oslo.

APPELO, C. A. J. & POSTMA, D. 2005. *Geochemistry, groundwater and pollution*, Leiden, Balkeman.

ASA RANI, L. & BABU, D. 2008. A statistical evaluation of ground water chemistry from the west coast of Tamil Nadu, India.

ASQUITH, G. & KRYGOWSKI, D. 2004. AAPG Methods in Exploration, No. 16, Chapter 1: Basic Relationships of Well Log Interpretation.

BAIN, D. & BACON, J. 1994. Strontium isotopes as indicators of mineral weathering in catchments. *Catena,* 22**,** 201-214.

BANKS, D., FRENGSTAD, B., KROG, J., MIDTGÅRD, A., STRAND, T. & LIND, B. 1998a. Kjemisk kvalitet av grunnvann i fast fjell i Norge [The chemical quality of groundwater in bedrock in Norway: in Norwegian]. *Nor Geol Unders report,* 98**,** l998b.

BANKS, D., MIDTGÅRD, A. K., FRENGSTAD, B., KROG, J. R. & STRAND, T. 1998b. The chemistry of Norwegian groundwaters: II. The chemistry of 72 groundwaters from Quaternary sedimentary aquifers. *Science of the total environment,* 222**,** 93-105.

BANKS, D., SÆTHER, O. M., RYGHAUG, P. & REIMANN, C. 2001. Hydrochemical distribution patterns in stream waters, Trøndelag, central Norway. *Science of the total environment*, 267**,** 1-21.

BASBERG, L., BANKS, D. & SÆTHER, O. M. 1998. Redox processes in groundwater impacted by landfill leachate. *Aquatic Geochemistry,* 4**,** 253-272.

BECKER, M. A. 2016. *Assessment of Downspout Disconnection by Modeling Infiltration Potential in Urban Areas.* NTNU.

BECKER, M. A., MUTHANNA, T. M. & BRASKERUD, B. C. 2016. Trinn 1: Reduser overvannet i avløpsnettet ved å frakoble taknedløp.

BJØRLYKKE, K. 1974. Geochemical and mineralogical influence of Ordovician Island Arcs on epicontinental clastic sedimentation. A study of Lower Palaeozoic sedimentation in the Oslo Region, Norway. *Sedimentology,* 21**,** 251-272.

BJØRLYKKE, K. 2004. *A short introduction to the geology around the inner part of the Oslo fjord.* [Online]. Department of geoscience, University of Oslo. Available: https://www.mn.uio.no/geo/tjenester/kunnskap/geology-oslo-area/osloarea-bjorlykke.pdf [Accessed 13.09 2018].

BJØRLYKKE, K. 2012. *Oslo-områdets geologi.* [Online]. Department of geoscience, University of Oslo. Available: https://www.mn.uio.no/geo/tjenester/kunnskap/geologi-oslofeltet/geologi-slofeltet.k.b.pdf [Accessed 12.09 2018].

BLAUSTEIN, R., PACHEPSKY, Y., HILL, R., SHELTON, D. & WHELAN, G. 2013. Escherichia coli survival in waters: temperature dependence. *Water research,* 47**,** 569-578.

BOGÁRDI, I., KUZELKA, R. D. & ENNENGA, W. G. 2013. *Nitrate contamination: exposure, consequence, and control*, Springer Science & Business Media.

BOUCHALOVÁ, M., WENNBERG, A. & TRYLAND, I. 2013. Impact of rainfall on bathing water quality–a case study of Fiskevollbukta, Inner Oslofjord, Norway. *Vann,* 4**,** 491-498.

BOULDING, J. R. & GINN, J. S. 2016. *Practical handbook of soil, vadose zone, and ground-water contamination: assessment, prevention, and remediation*, CRC Press.

BRAND, U., MORRISON, J. O. & CAMPBELL, I. T. 1998. Strontium in sedimentary rocks. *Geochemistry.* Dordrecht: Springer Netherlands.

BRATINA, B. J., STEVENSON, B. S., GREEN, W. J. & SCHMIDT, T. M. 1998. Manganese reduction by microbes from oxic regions of the Lake Vanda (Antarctica) water column. *Applied and environmental microbiology,* 64**,** 3791-3797.

BROUWER, P. 2006. Theory of XRF. *Almelo, Netherlands: PANalytical BV*.

BRUTON, D. L., GABRIELSEN, R. H. & LARSEN, B. T. 2010. The Caledonides of the Oslo Region, Norway–stratigraphy and structural elements. *Norwegian Journal of Geology/Norsk Geologisk Forening,* 90.

BÖHLKE, J.-K. 2002. Groundwater recharge and agricultural contamination. *Hydrogeology Journal,* 10**,** 153-179.

CASSIANI, G., BINLEY, A. & FERRÉ, T. P. 2006. Unsaturated zone processes. *Applied hydrogeophysics.* Springer.

COULTER, B. 2011. LS 13 320 Laser Diffraction Particle Size Analyzer: Instructions for use. *Backman Coulter Inc*.

COUNTY, P. G. 1999. *Low-impact development hydrologic analysis,* Department of Environmental Resources.

DALEY, M. L., POTTER, J. D. & MCDOWELL, W. H. 2009. Salinization of urbanizing New Hampshire streams and groundwater: effects of road salt and hydrologic variability. *Journal of the North American Benthological Society,* 28**,** 929-940.

DAVIES, P. J., WRIGHT, I. A., JONASSON, O. J. & FINDLAY, S. J. 2010. Impact of concrete and PVC pipes on urban water chemistry. *Urban Water Journal,* 7**,** 233-241.

DAVIS, S. N. 1964. Silica in streams and ground water. *American Journal of Science,* 262**,** 870-891.

DEAN, W. E. 1974. Determination of carbonate and organic matter in calcareous sediments and sedimentary rocks by loss on ignition; comparison with other methods. *Journal of Sedimentary Research,* 44**,** 242-248.

DOMAGALSKI, J. L. & JOHNSON, H. 2012. Phosphorus and groundwater: establishing links between agricultural use and transport to streams. *US Geological Survey Fact Sheet,* 3004**,** 2012.

DUTROW, B. L. & CLARK, C. M. 2016. *X-ray Powder Diffraction (XRD)* [Online]. Available: https://serc.carleton.edu/research_education/geochemsheets/techniques/XRD.html [Accessed 29.08 2018].

ECKNER, K. F. 1998. Comparison of membrane filtration and multiple-tube fermentation by the Colilert and Enterolert methods for detection of waterborne coliform bacteria, Escherichia coli, and enterococci used in drinking and bathing water quality monitoring in southern Sweden. *Applied and Environmental Microbiology,* 64**,** 3079-3083.

EDBERG, S., RICE, E., KARLIN, R. & ALLEN, M. 2000. Escherichia coli: the best biological drinking water indicator for public health protection. *Journal of Applied Microbiology,* 88**,** 106S-116S.

ELVEBAKK, H. 2008. Borehullslogging, ny jernbanetunnel Sandvika-Lysaker, Bærum kommune, del 2. *NGU rapport 2008.065*.

ELVEBAKK, H. 2010. Results of borehole logging in well LYB CO2, Dh4 of 2009, Longyearbyen, Svalbard. *NGU, Trondheim, Norway,* 35.

ELVEBAKK, H. 2011. Sammenstilling av resistivitet, seismiske hastigheter og naturlig gammastråling i norske bergarter. *NGU rapport 2011.042*.

ENGLUND, J.-O. & MYHRSTAD, J. A. 1980. Groundwater chemistry of some selected areas in southeastern Norway. *Hydrology Research,* 11**,** 33-54.

ERIKSSON, I., BORCHGREVIK, J., SÆTHER, M., DAVIKNES, K., ADAMOU, S. & ANDRESEN, L. 2016a. *COST TU1206 Sub-Urban Report* [Online]. Available: https://static1.squarespace.com/static/542bc753e4b0a87901dd6258/t/5707869ae707eb820b4118a5/1460111042910/TU1206-WG1-012+Oslo+City+Case+Study.pd [Accessed 17.09 2018].

ERIKSSON, I., BORCHGREVINK, J., SÆTHER, M. M., DAVIKNES, H. K., ADAMOU, S. & ANDRESEN, L. 2016b. OSLO. *COST TU1206 Sub-Urban Report* TU1206-WG1-012.

EU 2006. Directive 2006/7/EC of the European parliament and of the council of 15 February 2006 concerning the management of bathing water quality and repealing Directive 76/160/EEC.

EWING, J. M. & VEPRASKAS, M. J. 2006. Estimating primary and secondary subsidence in an organic soil 15, 20, and 30 years after drainage. *Wetlands,* 26**,** 119-130.

FHI. 2012. *Mikrobiologiske drikkevannsanalyser - hva forteller de?* [Online]. Folkehelseinstituttet. Available: https://www.fhi.no/ml/drikkevann/nasjonal-vannvakt/mikrobiologiske-drikkevannsanalyser/ [Accessed 11.10 2018].

FHI. 2015. *Kontroll av badevannskvalitet* [Online]. Available: https://www.fhi.no/ml/badevann/badevann--forurensning-og-regler/ [Accessed 31.10 2918].

FLETCHER, T. D., ANDRIEU, H. & HAMEL, P. 2013. Understanding, management and modelling of urban hydrology and its consequences for receiving waters: A state of the art. *Advances in water resources,* 51**,** 261-279.

FRENGSTAD, B., BANKS, D. & SIEWERS, U. 2001. The chemistry of Norwegian groundwaters: IV. The pH-dependence of element concentrations in crystalline bedrock groundwaters. *Science of the Total Environment,* 277**,** 101-117.

FRENGSTAD, B., BANKS, D., SKREDE, A. M., KROG, J., SIEWERS, U. & STRAND, T. 2002. The hydrochemistry of crystalline bedrock groundwater in Norway. *NGU Bulletin***,** 87-98.

GLAZOVSKY, N. & ZAITSEVA, N. 2009. *ENVIRONMENTAL STRUCTURE AND FUNCTION: EARTH SYSTEM*, EOLSS Publications.

GULDE, K. T. 2017. Dammer og våtmarker renser den nyåpnede Hovinbekken.

GULLIVER, J. S. & ANDERSON, J. L. 2008. *Assessment of stormwater best management practices*, University of Minnesota.

GUYOD, H. 1966. Interpretation of electric and gamma ray logs in water wells. *The Log Analyst,* 6.

HAKALEHTO, E., HEITTO, A. & HEITTO, L. 2013. Fast coliform detection in portable microbe enrichment unit (PMEU) with Colilert® medium and bubbling. *Pathophysiology,* 20**,** 257-262.

HANSSEN-BAUER, I., FØRLAND, E., HADDELAND, I., HISDAL, H., MAYER, S., NESJE, A., NILSEN, J., SANDVEN, S., SANDØ, A. & SORTEBERG, A. 2015. Klima i Norge 2100 Kunnskapsgrunnlag for klimatilpasning oppdatert i 2015. *NCCS report, NCCS, Oslo, Norway***,** 203.

HAYASHI, M. 2004. Temperature-electrical conductivity relation of water for environmental monitoring and geophysical data inversion. *Environmental monitoring and assessment,* 96**,** 119-128.

HEALY, R. W. 2010. *Estimating groundwater recharge*, Cambridge University Press.

HEALY, R. W. & COOK, P. G. 2002. Using groundwater levels to estimate recharge. *Hydrogeology journal,* 10**,** 91-109.

HEALY, R. W., WINTER, T. C., LABAUGH, J. W. & FRANKE, O. L. 2007. *Water budgets: foundations for effective water-resources and environmental management*, US Geological Survey Reston, Virginia.

HEIER, K. 1962. Trace elements in feldspars—a review. *Norsk geol. tidsskr,* 42**,** 415-454.

HEIRI, O., LOTTER, A. F. & LEMCKE, G. 2001. Loss on ignition as a method for estimating organic and carbonate content in sediments: reproducibility and comparability of results. *Journal of paleolimnology,* 25**,** 101-110.

HELLSTEN, S., LOON, M., TARRASON, L., VESTRENG, V., TORSETH, K., KINDBOM, K. & AAS, W. 2017. Base cations deposition in Europe. *IVL Report B1722*.

HIBBINS, S. G. & STAFF, U. B. 2000. Strontium and strontium compounds. *Kirk-Othmer Encyclopedia of Chemical Technology***,** 1-10.

HOLDEN, P. A. & FIERER, N. 2005. Microbial processes in the vadose zone. *Vadose Zone Journal,* 4**,** 1-21.

HONGVE, D. 1977. The ionic composition of lakes fed by ground water and precipitation in the Upper Romerike District. *Hydrology Research,* 8**,** 141-162.

HOWARD, K. W. & HAYNES, J. 1993. Groundwater contamination due to road de-icing chemicals—salt balance implications. *Geoscience Canada,* 20.

HOWE, P., MALCOLM, H. & DOBSON, S. 2004. *Manganese and its compounds: environmental aspects*, World Health Organization.

IDEXX. 2006. *Colilert-18, Colilert*-18 Test Kit* [Online]. Available: https://www.idexx.com/en/water/water-products-services/colilert-18/ [Accessed 28.12 2018].

ISHII, S. & SADOWSKY, M. J. 2008. Escherichia coli in the environment: implications for water quality and human health. *Microbes and Environments,* 23**,** 101-108.

JAUDON, P., MASSIANI, C., GALEA, J., REY, J. & VACELET, E. 1989. Groundwater pollution by manganese. Manganese speciation: application to the selection and discussion of an in situ groundwater treatment. *Science of the total environment,* 84**,** 169-183.

JIANG, J.-Q., ASHEKUZZAMAN, S., JIANG, A., SHARIFUZZAMAN, S. & CHOWDHURY, S. R. 2012. Arsenic contaminated groundwater and its treatment options in Bangladesh. *International journal of environmental research and public health,* 10**,** 18-46.

JOHANNESSEN, M., DALE, T., GJESSING, E., HENRIKSEN, A. & WRIGHT, R. 1977. Acid precipitation in Norway: the regional distribution of contaminants in snow and the chemical concentration processes during snowmelt. *IAHS Publ,* 118**,** 116-120.

JOHN, D. E. & ROSE, J. B. 2005. Review of factors affecting microbial survival in groundwater. *Environmental science & technology*, 39**,** 7345-7356.

JØRGENSEN, P., STUANES, A. & ØSTMO, S. 1991. Aqueous geochemistry of the Romerike area, southern Norway. *Norges Geologiske Undersøkelse Bulletin,* 420**,** 57-67.

KEAREY, P., BROOKS, M. & HILL, I. 2013. *An introduction to geophysical exploration*, John Wiley & Sons.

KREITLER, C. W. 1974. *Determining the source of nitrate in groundwater by nitrogen isotope studies.*

LANCE, J. 1972. Nitrogen removal by soil mechanisms. *Journal (Water Pollution Control Federation)***,** 1352-1361.

LARSEN, B. T., OLAUSSEN, S., SUNDVOLL, B. & HEEREMANS, M. 2008. The Permo-Carboniferous Oslo Rift through six stages and 65 million years. *Episodes,* 31**,** 52-58.

LENG, Y. 2009. *Materials characterization: introduction to microscopic and spectroscopic methods*, John Wiley & Sons.

LENG, Y. 2010. *X-Ray Diffraction Methods,* Chichester, UK, Chichester, UK: John Wiley & Sons, Ltd.

LINDHOLM, O. 2008. Veiledning i klimatilpasset overvannshåndtering. *Hamar: Norsk Vann BA*, vol. 162.

LINDHOLM, O., ENDRESEN, S., THOROLFSSON, S., SÆGROV, S., JAKOBSEN, G. & AABY, L. 2008. Veiledning i klimatilpasset overvannshåndtering. *Rapport,* 162**,** 2008.

MARSALEK, J., KARAMOUZ, M., CISNEROS, B. J., MALMQUIST, P.-A., GOLDENFUM, J. A. & CHOCAT, B. 2014. *Urban Water Cycle Processes and Interactions: Urban Water Series-UNESCO-IHP*, CRC Press.

MAYHEW, S. 2015. *A dictionary of geography,* Oxford University Press, USA.

MILJØDIREKTORATET 2016. Treleddsstrategi for overvann og grønnstruktur i arealplanlegging.

MINEAR, R. & KEITH, L. 1982. Water Analysis, Vol. 1, Inorganic Species, Part. 1. Academic Press, New York.

MOR, S., RAVINDRA, K., DAHIYA, R. & CHANDRA, A. 2006. Leachate characterization and assessment of groundwater pollution near municipal solid waste landfill site. *Environmental monitoring and assessment,* 118**,** 435-456.

MUÑOZ-CARPENA, R., REGALADO, C. M., ÁLVAREZ-BENEDI, J. & BARTOLI, F. 2002. Field evaluation of the new Philip-Dunne permeameter for measuring saturated hydraulic conductivity. *Soil Science,* 167.

NAOROZ, M. 2016a. Ion Chromatography of Fluoride, Chloride, Bromide, Nitrate, Sulfate, and Phosphate with Suppression of Eluent. *Unpublished user manual.*

NAOROZ, M. 2016b. Ion Chromatography of Sodium, Magnesium, Potassium and calsium with Suppression of Eluent. . *Unpublished user manual.*

NAOROZ, M. 2017. Determination of soluble silicate in water by Seal AutoAnalyzer (AA3). *University of Oslo, Department of Geosciences.*

NAYAK, P. S. & SINGH, B. 2007. Instrumental characterization of clay by XRF, XRD and FTIR. *Bulletin of Materials Science,* 30**,** 235-238.

NEUMANN, E.-R., OLSEN, K., BALDRIDGE, W. & SUNDVOLL, B. 1992. The Oslo rift: A review. *Tectonophysics,* 208**,** 1-18.

NGU. 2016. *Borehole Geophysics* [Online]. Available: https://www.ngu.no/en/topic/borehole-geophysics [Accessed 18.10 2018].

NGU. 2017. *Damage due to subsidence* [Online]. Available: https://www.ngu.no/en/topic/damage-due-subsidence [Accessed 15.12 2018].

NIELSEN, D., TH. VAN GENUCHTEN, M. & BIGGAR, J. 1986. Water flow and solute transport processes in the unsaturated zone. *Water resources research,* 22**,** 89S-108S.

NIELSEN, E. & LADEFOGED, O. 2013. Barium, inorganic water-soluble compounds. Evaluation of health hazards and proposal of health based quality criteria for soil and drinking water *In:* AGENCY, T. D. E. P. (ed.). Copenhagen.

NIEMCZYNOWICZ, J. 1999. Urban hydrology and water management–present and future challenges. *Urban water,* 1**,** 1-14.

NIKANOROV, A. & BRAZHNIKOVA, L. 2009. Water chemical composition of rivers, lakes and wetlands. *Types and properties of water,* 2**,** 42-80.

NOU 2010. Adapting to a changing climate. *Norway's vulnerability and the need to adapt to the impacts of climate change,* Official Norwegian Reports NOU 2010: 10.

OLAUSSEN, S., LARSEN, B. T. & STEEL, R. 1994. The Upper Carboniferous-Permian Oslo Rift; basin fill in relation to tectonic development.

OPPONG-ANANE, A. B., QUIÑONES, K. Y. D., HARRIS, W., TOWNSEND, T. & BONZONGO, J.-C. J. 2018. Iron reductive dissolution in vadose zone soils: Implication for groundwater pollution in landfill impacted sites. *Applied Geochemistry,* 94**,** 21-27.

OSLO MUNICIPALITY 2015. Prinsipper for gjenåpning av elver og bekker i Oslo.

OSLO MUNICIPALITY. 2018. *Reopening waterways* [Online]. Available: https://www.oslo.kommune.no/english/politics-and-administration/green-oslo/best-practices/reopening-waterways/ [Accessed 12.12 2018].

PALMER, M. & EDMOND, J. 1992. Controls over the strontium isotope composition of river water. *Geochimica et Cosmochimica Acta,* 56**,** 2099-2111.

PANSU, M. & GAUTHEYROU, J. 2006. Water content and loss on ignition. *Handbook of Soil Analysis: Mineralogical, Organic and Inorganic Methods***,** 3-13.

PARUCH, A. 2011. Long-term survival of Escherichia coli in lightweight aggregate filter media of constructed wastewater treatment wetlands. *Water Science and Technology,* 63**,** 558-564.

PATIL, D. S., CHAVAN, S. M. & OUBAGARANADIN, J. U. K. 2016. A review of technologies for manganese removal from wastewaters. *Journal of Environmental Chemical Engineering,* 4**,** 468-487.

PERLMAN, H. 2016. *Water properties: Temperature* [Online]. Available: https://water.usgs.gov/edu/temperature.html [Accessed 28.12 2018].

PHILLIPS, F. M. & CASTRO, M. C. 2003. Groundwater dating and residence-time measurements. *Treatise on geochemistry,* 5**,** 605.

PIDWIRNY, M. 2006. *The hydrologic cycle* [Online]. Available: http://www.physicalgeography.net/fundamentals/8b.html [Accessed 12.01 2019].

PINKHAM, R. 2000. *Daylighting: new life for buried stream,* Colorado, Rocky Mount ocky Mountain Institute, ain Institute, Old Snowmass.

PITT, R., CHEN, S.-E. & CLARK, S. 2002. Compacted urban soils effects on infiltration and bioretention stormwater control designs. *Global Solutions for Urban Drainage.*

POPPE, L., PASKEVICH, V., HATHAWAY, J. & BLACKWOOD, D. 2001. A laboratory manual for X-ray powder diffraction. *US Geological Survey Open-File Report,* 1**,** 1-88.

PROVIN, T. & PITT, J. L. 2001. Managing soil salinity. *Texas FARMER Collection*.

REDDY, D., NAGABHUSHANAM, P. & PETERS, E. 2011. Village environs as source of nitrate contamination in groundwater: a case study in basaltic geo-environment in central India. *Environmental monitoring and assessment,* 174**,** 481-492.

REIMANN, C., FINNE, T. E., NORDGULEN, Ø., SÆTHER, O. M., ARNOLDUSSEN, A. & BANKS, D. 2009. The influence of geology and land-use on inorganic stream water quality in the Oslo region, Norway. *Applied Geochemistry,* 24**,** 1862-1874.

ROALD, B. 2018. *Sørenga stengt for bading* [Online]. Available: https://www.nrk.no/nyheter/sorenga-stengt-for-bading-1.14062776 [Accessed 02.11 2018].

ROLLINSON, H. R. 2014. *Using geochemical data: evaluation, presentation, interpretation*, Routledge.

ROSENBERRY, D., BUKAVECKAS, P., BUSO, D., LIKENS, G., SHAPIRO, A. & WINTER, T. 1999. Movement of road salt to a small New Hampshire lake. *Water, Air, and Soil Pollution,* 109**,** 179-206.

ROSSELAND, B., ELDHUSET, T. D. & STAURNES, M. 1990. Environmental effects of aluminium. *Environmental Geochemistry and Health,* 12**,** 17-27.

SAMPSON, R. W., SWIATNICKI, S. A., OSINGA, V. L., SUPITA, J. L., MCDERMOTT, C. M. & KLEINHEINZ, G. 2006. Effects of temperature and sand on E. coli survival in a northern lake water microcosm. *Journal of water and health,* 4**,** 389-393.

SOLHEIM, E. B., FRENCH, H. K. & BRASKERUD, B. C. 2017. Måling av infiltrasjon fra overflaten for bruk av åpen LOD i praksis. VANN 03-2017.

SSB. 2018. *Kommunefakta* [Online]. Available: https://www.ssb.no/kommunefakta/oslo [Accessed 20.02 2019].

SUNDARAM, B., FEITZ, A., DE CARITAT, P., PLAZINSKA, A., BRODIE, R. S., CORAM, J. & RANSLEY, T. 2009. Groundwater sampling and analysis–a field guide. *Geoscience Australia, Record,* 27**,** 104.

SÆTHER, O., MISUND, A., ØDEGÅRD, M., ANDREASSEN, B. T. & VOSS, A. 1992. Groundwater contamination at Trandum landfill, southeastern Norway. *Norges Geologiske Undersøkelse Bulletin,* 422**,** 83-95.

THOMAS, R. 2001. A beginner's guide to ICP-MS. *Spectroscopy,* 16**,** 38-42.

TIWARI, A. K. & SINGH, A. K. 2014. Hydrogeochemical investigation and groundwater quality assessment of Pratapgarh district, Uttar Pradesh. *Journal of the Geological Society of India,* 83**,** 329-343.

TORGERSEN, G., BJERKHOLT, J. T. & LINDHOLM, O. G. 2014. Addressing flooding and suds when improving drainage and sewerage systems—A comparative study of selected Scandinavian cities. *Water,* 6**,** 839-857.

TRICE, A. 2013. Daylighting streams: breathing life into urban streams and communities. *American Rivers, Washington*.

UGLUM, M. in press. Considering groundwater recharge and flow in urban development planning – A case study from Torshovdalen, Oslo. *To be defended in 2019*.

UN 2018. The speed of urbanization around the world. *In:* 2018/1, N. (ed.) *United Nations.*

VAN ELSAS, J. D., SEMENOV, A. V., COSTA, R. & TREVORS, J. T. 2011. Survival of Escherichia coli in the environment: fundamental and public health aspects. *The ISME journal,* 5**,** 173.

WHITMAN, R. L., NEVERS, M. B., KORINEK, G. C. & BYAPPANAHALLI, M. N. 2004. Solar and temporal effects on Escherichia coli concentration at a Lake Michigan swimming beach. *Applied and environmental microbiology,* 70**,** 4276-4285.

WHO 2011. Guidelines for drinking-water quality. *WHO chronicle,* 38**,** 104-8.

WILLIAMS, J. H. & JOHNSON, C. D. 2004. Acoustic and optical borehole-wall imaging for fractured-rock aquifer studies. *Journal of Applied Geophysics,* 55**,** 151-159.

ZHANG, Y., SUN, T., LI, F., WANG, J. & OH, K. 2013. Effect of decing salts on ion concentrations in urban stormwater runoff. *Procedia Environmental Sciences,* 18**,** 567-571.

Appendix A: Groundwater wells

A1: Depth of the groundwater wells

A2: Well configuration

A1: The depth of the three installed groundwater wells in Torshovdalen, including depth drilled in the loose sediments and in the bedrock, all given in meters below the surface

Well	Depth drilled in loose sediment (depth to bedrock)	Depth drilled in bedrock
1	3.36 meters	1.12 meters
2	2.40 meters	5.04 meters
3	12.40 meters	5.20 meters

A2: Well configuration of the three groundwater wells installed in Torshovdalen (W1, W2, W3) Depth are in meters below the surface (notice the different in depth to bedrock). The filter PVS pipes are marked with stripes. Depth of sediment and bedrock are shown to the left side of each well

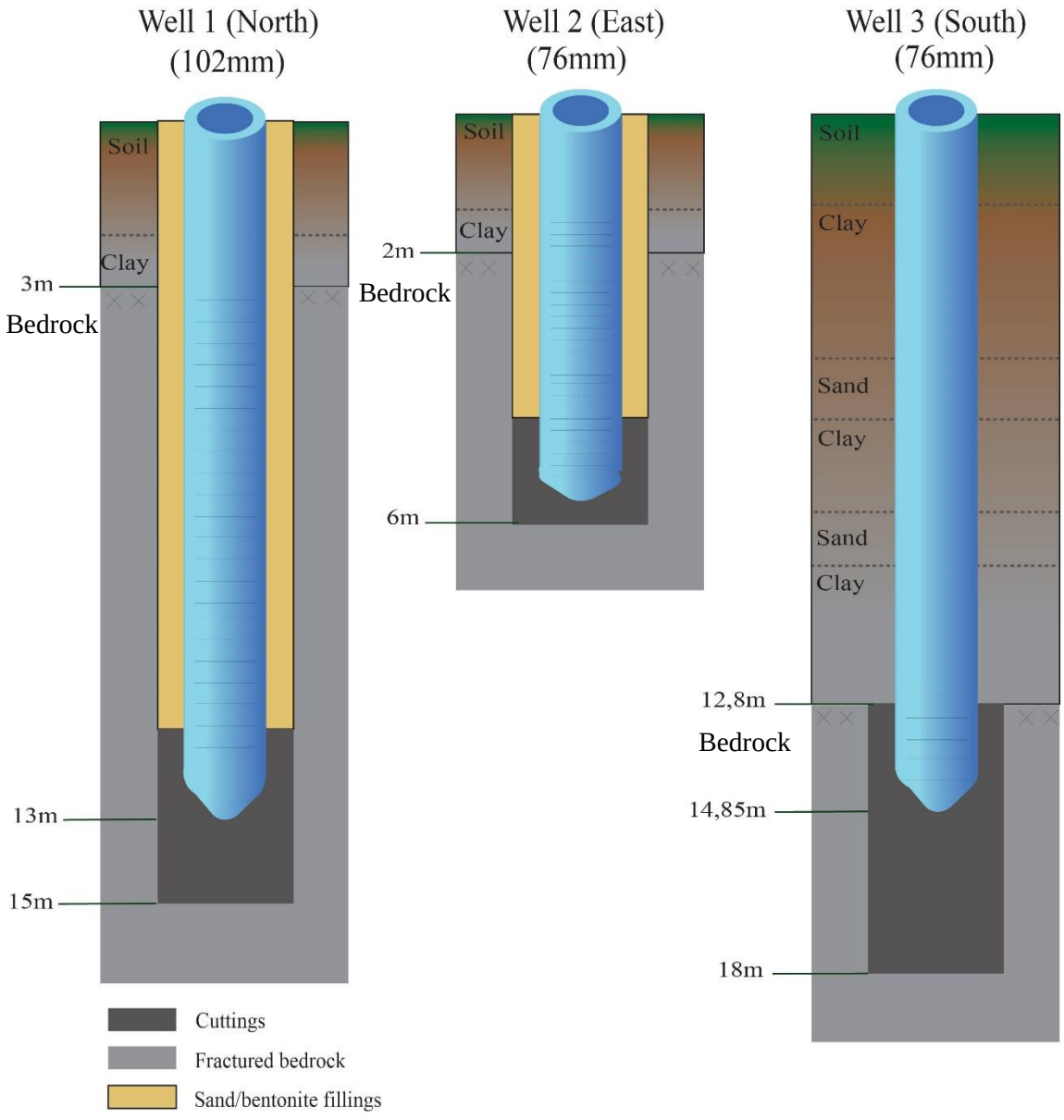

Appendix B: Chemical data of water samples

B1: Field parameters; pH, temperature and EC

B2: Major cations and anions

B3: Soluble silicates

B4: Trace elements (B, Al, Cr, Mn, Fe)

B5: Trace elements (Ni, Cu, Zn, As, Se, Sr, Pb)

B6: Pearson's correlation coefficient

B7: *E. coli* concentration, coliform bacteria, precipitation and snow depth

B8: *E. coli* concentration, coliform bacteria, precipitation and snow depth

B1: Field parameters; pH, temperature (°C) and electrical conductivity (EC, uS/cm).

Date	Sample	pH	Temperature	EC
10.05.18	A1-1	6.8	4.8	22.3
23.05.18	A1-2	7.5	12	35
12.11.18	A1-3	7.4	8.5	67
10.05.18	A2-1	7.0	5.2	22.3
23.05.18	A2-2	6.9	11.9	34
12.11.18	A2-3	7.3	8.6	65
10.05.18	T1-1	6.8	15.4	1859
23.05.18	T1-2	7.5	18.3	1900
12.11.18	T1-3	7.6	8.9	1395
22.09.18	G1-1	7.7	8.2	229
12.11.18	G1-2	7.3	7.7	246
21.09.18	R1	6.4	7.2	18.5
26.09.18	W3-1	8.08	5.5	1300
10.10.18	W3-2	7.95	5.6	1219
10.10.18	W1	8.05	5.5	1253

B2: Results from the ion chromatography, giving the concentration of the major ions in mg/l in all of the water samples. RSD = Relative standard deviation (%), NA = Not detected.

Date	Sample	Na	RSD%	K	RSD%	Mg	RSD%	Ca	RSD%	F	RSD%	Cl	RSD%	SO_4	RSD%	Br	RSD%	NO_3	RSD%	PO4	RSD%	HCO_3	RSD%
		mg/l		mg/l		mg/l		mg/l		mg/l		mg/l		mg/l		mg/l		mg/l		mg/l		meq/L	
10.05.18	A1-1	2.37	0.5	0.39	0.3	0.80	4.7	3.82	0.6	NA	6.7	3.41	3.8	2.25	1.9	NA	4.6	1.15	0.6	NA	NA	0.18	NA
23.05.18	A1-2	3.35	0.3	0.41	0.1	0.87	4.8	3.86	0.1	NA	3.2	4.85	1.1	3.06	1.3	0.38	1.4	0.89	0.3	NA	NA	0.17	NA
12.11.18	A1-3	4.12	0.9	0.73	0.9	1.06	3.5	6.49	0.3	0.05	2.2	5.61	1.2	5.41	1.4	NA	1.4	1.82	0.0	NA	NA	0.33	NA
10.05.18	A2-1	2.42	0.5	0.43	0.3	0.80	4.7	3.31	0.6	NA	6.7	3.32	3.8	2.29	1.9	NA	4.6	1.09	0.6	NA	NA	0.20	NA
23.05.18	A2-2	3.05	0.3	0.38	0.1	0.86	4.8	3.72	0.1	NA	3.2	4.54	1.1	2.90	1.3	0.38	1.4	0.88	0.3	NA	NA	0.17	NA
12.11.18	A2-3	4.21	0.9	0.71	0.9	1.05	3.5	6.51	0.3	0.05	2.2	5.67	1.1	5.40	1.4	NA	1.4	1.78	0.0	NA	NA	0.27	NA
10.05.18	T1-1	191.1	0.5	7.64	0.3	25.63	4.7	200.72	0.6	0.07	6.7	446.33	3.8	114.23	1.9	0.50	4.6	10.98	0.6	0.37	1.6	5.12	1.6
23.05.18	T1-2	210.6	0.3	8.37	0.1	25.72	4.8	196.52	0.1	0.04	3.2	518.92	1.1	102.28	1.3	0.63	1.4	7.11	0.3	NA	NA	6.00	NA
12.11.18	T1-3	147.82	0.9	9.91	0.9	21.30	3.5	177.21	0.3	0.17	2.2	331.20	1.1	136.10	1.4	0.48	1.4	19.83	0.0	NA	NA	3.51	NA
22.09.18	G1-1	14.61	0.5	0.92	0.3	2.90	7.5	31.90	0.5	0.02	2.9	32.20	1.0	21.13	0.7	NA	1.3	3.02	0.4	NA	NA	0.92	NA
12.11.18	G1-2	14.75	0.9	1.58	0.9	2.65	3.5	31.61	0.3	0.14	2.2	30.58	1.2	16.53	1.7	0.41	1.4	4.47	0.0	NA	NA	1.05	NA
21.09.18	R1	1.24	0.5	0.83	0.3	0.91	7.5	0.69	0.5	0.29	2.9	2.44	1.0	1.14	0.7	0.39	1.3	1.67	0.4	0.89	1.6	0	1.6
26.09.18	W3-1	113.72	0.5	17.34	0.3	36.78	7.5	106.25	0.5	0.20	2.9	236.28	1.0	113.70	0.7	0.28	1.3	0.23	0.4	NA	NA	4.8	NA
10.10.18	W3-2	130.71	0.7	13.96	0.4	44.65	0.9	109.21	0.5	0.14	3.2	285.08	1.2	130.44	1.7	0.49	1.4	0.23	0.4	NA	NA	4.56	NA
10.10.18	W1	22.53	0.7	10.34	0.4	10.72	0.9	40.03	0.5	0.71	3.2	90.37	1.2	19.71	1.7	NA	1.4	0.24	0.4	NA	NA	1.42	NA

B3: Concentration of soluble silicates (mg/l) in seven water samples. RSD = Relative standard deviation

Date	Sample	SiO_2	RSD%
		mg/l	
23.05.18	A1-2	3.49	1.07
23.05.18	A2-2	3.48	1.07
23.05.18	T1-2	9.34	1.07
22.09.18	G1-1	9.65	1.07
26.09.18	W3-1	11.78	1.07
10.10.18	W3-2	11.96	1.07
10.10.18	W1	5.31	1.07

B4: Results from QICPMS, showing the concentration of the trace elements (in ppb) together with the relative standard deviation (RSD)

Date	Sample name	B	RSD	Al	RSD	Cr	RSD	Mn	RSD	Fe	RSD
		ppb		ppb		ppb		ppb		ppb	
23.05.18	A1-2	4.6925	7.39	132.2401	1.47	0.1099	31.03	8.8082	0.83	41.9498	1.61
23.05.18	A2-2	3.9494	8.69	129.5506	0.85	0.1158	12.63	11.4447	0.78	41.9296	1.78
23.05.18	T1-2	136.8148	1.21	8.2892	3.84	0.9881	8.15	22.5568	0.77	265.3288	1.02
22.09.18	G1-1	11.077	4.41	18.5813	1.89	0.4195	13.59	0.1913	7.63	34.0887	2.95
26.09.18	W3-1	147.773	0.9	2.5774	8.05	0.2406	23.22	321.9663	0.44	470.1078	1.62
10.10.18	W3-2	158.0788	2.26	25.9661	3.12	0.3454	17.19	255.5822	0.41	341.2713	0.67
10.10.18	W1	201.9785	1.41	115.6087	1.75	0.4104	12.55	56.4066	0.83	237.4923	1
	Detection limit	7.10		0.27		0.05		0.04		0.24	

Below detection limit of method/instrument detection limit

RSD = Standard deviation in percentage (%)

B5: Results from QICPMS, showing the concentration of the trace elements (in ppb) together with the relative standard deviation (RSD)

Date	Sample name	Ni	RSD	Cu	RSD	Zn	RSD	As	RSD	Se	RSD	Sr	RSD	Pb	RSD
		ppb		ppb		ppb		ppb		ppb		ppb		ppb	
23.05.18	A1-2	0.3323	7.41	0.7216	4.6	4.8721	5.38	0.9711	7.99	0.0416	79.3	31.0049	5.45	0.0762	2.56
23.05.18	A2-2	0.3337	6.23	0.8544	2.49	5.4905	2.27	0.7017	13.9	0.0235	97.61	29.4436	3.94	0.0721	4.35
23.05.18	T1-2	4.1718	1.93	13.4218	1.48	329.4432	0.68	27.183	1.73	0.1569	42.3	2097.691	1.55	0.1157	4
22.09.18	G1-1	0.6546	6.09	0.4885	7.37	4.8068	5.85	2.4031	14.32	0.0783	75.47	168.9561	4.93	0.0134	16.98
26.09.18	W3-1	2.1033	3.43	0.0908	25.65	2.5879	7.08	18.8824	5.18	0.0564	44.49	3785.498	1.77	0.0244	8.21
10.10.18	W3-2	2.3904	2.98	0.4641	6.34	23.0265	2.33	16.4269	2.29	0.0248	109.7	3343.549	1.44	0.0949	4.6
10.10.18	W1-1	4.399	0.88	0.5599	3.47	1.6118	10.83	4.3689	4.98	0.3392	5.72	1209.47	1.67	0.0633	4.74
	Detection limit	0.04		0.03		0.04		0.32		0.1		0.07		0.05	

Below detection limit of method/instrument detection limit

RSD = Standard deviation in percentage (%)

B6: Pearson's correlation coefficient between major and minor elements together with field parameters (pH, temperature and EC), based on the samples; A1-2. A2-2, T1-2, G1-1, W3-1, W3-2 and W1-1. Selenium (Se) and Lead (Pb) are not included since the concentration is below the detection limit in more than two of the water samples used to calculate the Pearson coefficient.

	Na	K	Mg	Ca	F	Cl	SO4	Br	NO_3	HCO_3	B	Al	Mn	Fe	Ni	Cu	Zn	As	Sr	pH	EC	Temp	SiO_2
Na	1.000																						
K	0.625	1.000																					
Mg	0.789	0.900	1.000																				
Ca	0.991	0.618	0.747	1.000																			
F	-0.471	0.252	-0.231	-0.453	1.000																		
Cl	0.992	0.591	0.734	0.994	-0.395	1.000																	
SO_4	0.881	0.833	0.977	0.847	-0.444	0.829	1.000																
Br	0.149	0.677	0.423	0.168	0.755	0.084	0.399	1.000															
NO_3	0.575	-0.192	-0.021	0.627	-0.527	0.627	0.173	-0.297	1.000														
HCO_3	0.974	0.773	0.882	0.967	-0.423	0.952	0.947	0.349	0.421	1.000													
B	0.276	0.750	0.476	0.254	0.683	0.313	0.319	0.009	-0.342	0.354	1.000												
Al	-0.735	-0.555	-0.694	-0.758	0.938	-0.690	-0.796	-0.500	-0.432	-0.794	0.508	1.000											
Mn	0.428	0.881	0.863	0.376	-0.035	0.342	0.781	0.728	-0.438	0.601	0.388	-0.515	1.000										
Fe	0.696	0.988	0.909	0.684	0.118	0.658	0.867	0.714	-0.103	0.830	0.684	-0.599	0.875	1.000									
Ni	-0.111	-0.926	-0.887	0.018	0.463	0.076	-0.751	-0.600	0.510	-0.364	0.418	0.602	-0.981	-0.908	1.000								
Cu	-0.360	-0.444	-0.401	-0.404	-0.347	-0.365	-0.411	-0.262	-0.146	-0.424	0.043	0.089	-0.371	-0.286	-0.418	1.000							
Zn	0.779	0.079	0.235	0.805	-0.378	0.830	0.393	-0.261	0.916	0.636	0.050	-0.407	-0.221	0.171	0.485	-0.157	1.000						
As	0.984	0.489	0.702	0.977	-0.433	0.963	0.837	-0.291	0.477	0.989	0.314	-0.581	0.335	0.625	-0.202	0.427	0.735	1.000					
Sr	0.748	0.959	0.975	0.719	-0.114	0.694	0.946	0.614	-0.073	0.870	0.539	-0.684	0.908	0.974	-0.971	-0.453	0.184	0.681	1.000				
pH	0.380	0.797	0.645	0.435	0.610	0.372	0.591	0.612	-0.120	0.540	0.444	-0.627	0.626	0.733	-0.465	-0.318	-0.053	-0.399	0.699	1.000			
EC	0.866	0.789	0.748	0.898	0.134	0.893	0.775	0.285	0.388	0.895	0.736	-0.593	0.447	0.809	0.488	-0.477	0.631	0.822	0.767	0.651	1.000		
Temp	0.325	-0.470	-0.279	0.324	-0.457	0.371	-0.113	-0.534	0.810	0.120	-0.157	0.049	-0.600	-0.358	0.506	0.227	0.792	0.609	-0.336	-0.638	0.056	1.000	
SiO2	0.683	0.706	0.829	0.686	-0.762	0.623	0.870	0.505	0.167	0.786	-0.276	-0.950	0.710	0.716	-0.880	-0.520	0.203	0.481	0.810	0.745	0.594	-0.302	1.000

B7. Concentration of coliform and *E. coli* bacteria per 100 ml water samples. All results were obtained at the Oslo City Water and Sewerage Work Agency (VAV) laboratory using Colilert-18. Data regarding the precipitation were modified form eklima.met.no.

Sample	Date	E.coli/100 ml	Coliform/100ml	Precipitation (mm/day)	Snowdepth (cm)	Comment
A3	19.02.18	246.0		1.2	55	
A3	26.02.18	520.0		2.5	57	
A3	05.03.18	120.0		0.0	53	Dry cold period
A3	12.03.18	384.0		0.0	53	Dry cold period
A3	19.03.18	75.0		0.0	55	Dry cold period
A3	26.03.18	119.0		0.0	46	Snowmelting
A3	03.04.18	63.0		0.0	42	Snowmelting
A3	09.04.18	754.0		0.0	34	Snowmelting
A3	16.04.18	480.0		0.0	2	
A3	23.04.18	75.0		0.0	0	Dry warm period
A3	07.05.18	75.0		0.0	0	Dry warm period
A3	14.05.18	30.0		0.0	0	Dry warm period
A3	22.05.18	63.0		0.1	0	
A3	28.05.18	211.0		0.0	0	
A1	30.05.18	474.5	1980.5	0.5	0	
A2	30.05.18	441.5	1346.0	0.5	0	
T1	30.05.18	4097.5	36518.0	0.5	0	
A3	04.06.18	368.0		0.0	0	
A3	12.06.18	1872.0		10.4	0	Heavy rainfall
A1	12.06.18	769.0	4075.0	0.0	0	
A2	12.06.18	728.5	6035.0	0.0	0	
T1	12.06.18	4356	37653.0			
A1	18.06.18	3229.0	10254.0	4.8	0	
A2	18.06.18	2459.5	11159.5	4.8	0	
A3	18.06.18	1223.0		4.8	0	
T1	18.06.18	7628.5	52918.0	4.8	0	
A3	25.06.18	288.0		0.0	0	Dry period. high temp
A3	02.07.18	379.0		0.0	0	Dry period. high temp
A3	09.07.18	529.0		0.0	0	Dry period. high temp
A3	16.07.18	441.0		0.0	0	Dry period. high temp
A1	26.07.18	2177.0	2317.0	0.0	0	High temperatur. 34 °C
A2	26.07.18	563.0	4671.0	0.0	0	

B8. Concentration of coliform and *E. coli* bacteria per 100 ml water samples. All results were obtained at the Oslo City Water and Sewerage Work Agency (VAV) laboratory using Colilert-18. Data regarding the precipitation were modified form eklima.met.no.

Sample	Date	*E. coli*/100 ml	Coliform/100ml	Precipitation (mm/day)	Snowdepth (cm)	Comment
T1	26.07.18	2444.0	52918.0	0.0	0	
A3	30.07.18	420.0		9.6	0	
A3	06.08.18	1050.0		0.0	0	
A3	13.08.18	988.0		1.2	0	
A3	20.08.18	884.0		0.1	0	
A3	27.08.18	591.0		0.0	0	
A3	03.09.18	327.0		0.0	0	
A3	10.09.18	20460.0		8.5	0	21.5 mm last 48h
A3	17.09.18	630.0		0.0	0	
A3	24.09.18	630.0		0.1	0	
A3	01.10.18	624.0		0.1	0	
W3	09.10.10	0	389.0	1.3	0	
A3	08.10.18	457		0.0	0	
A3	15.10.18	359		0.0	0	
A3	22.10.18	933		0.0	0	
A3	29.10.18	383		0.3	0	
A3	05.11.18	213		1.0	0	
G1	12.11.18	26		25.8	0	Heavy rainfall
T1	12.11.18	5.2		25.8	0	Heavy rainfall
W3	12.11.18	0	520	25.8	0	Heavy rainfall
W1	12.11.18	0	480	25.8	0	Heavy rainfall

Appendix C: XRD analysis

C1: XRD Clay mineral identification flow diagram

C2: W1-L1.5 (raw file and results from DIFFRACT.EVA)

C3: W1-L2.5 (raw file and results from DIFFRACT.EVA)

C4: W1-L3.5 (raw file and results from DIFFRACT.EVA)

C5: W1-B1 (raw file and results from DIFFRACT.EVA)

C6: W1-B.15 (raw file and results from DIFFRACT.EVA)

C7: W1-B4 (raw file and results from DIFFRACT.EVA)

C8: W2-L1 (raw file and results from DIFFRACT.EVA)

C9: W2-B1 (raw file and results from DIFFRACT.EVA)

C10: W2-B4 (raw file and results from DIFFRACT.EVA)

C11: W3-L4 (raw file and results from DIFFRACT.EVA)

C1: XRD Clay mineral identification flow diagram. Photo modified from Poppe et al., (2009).

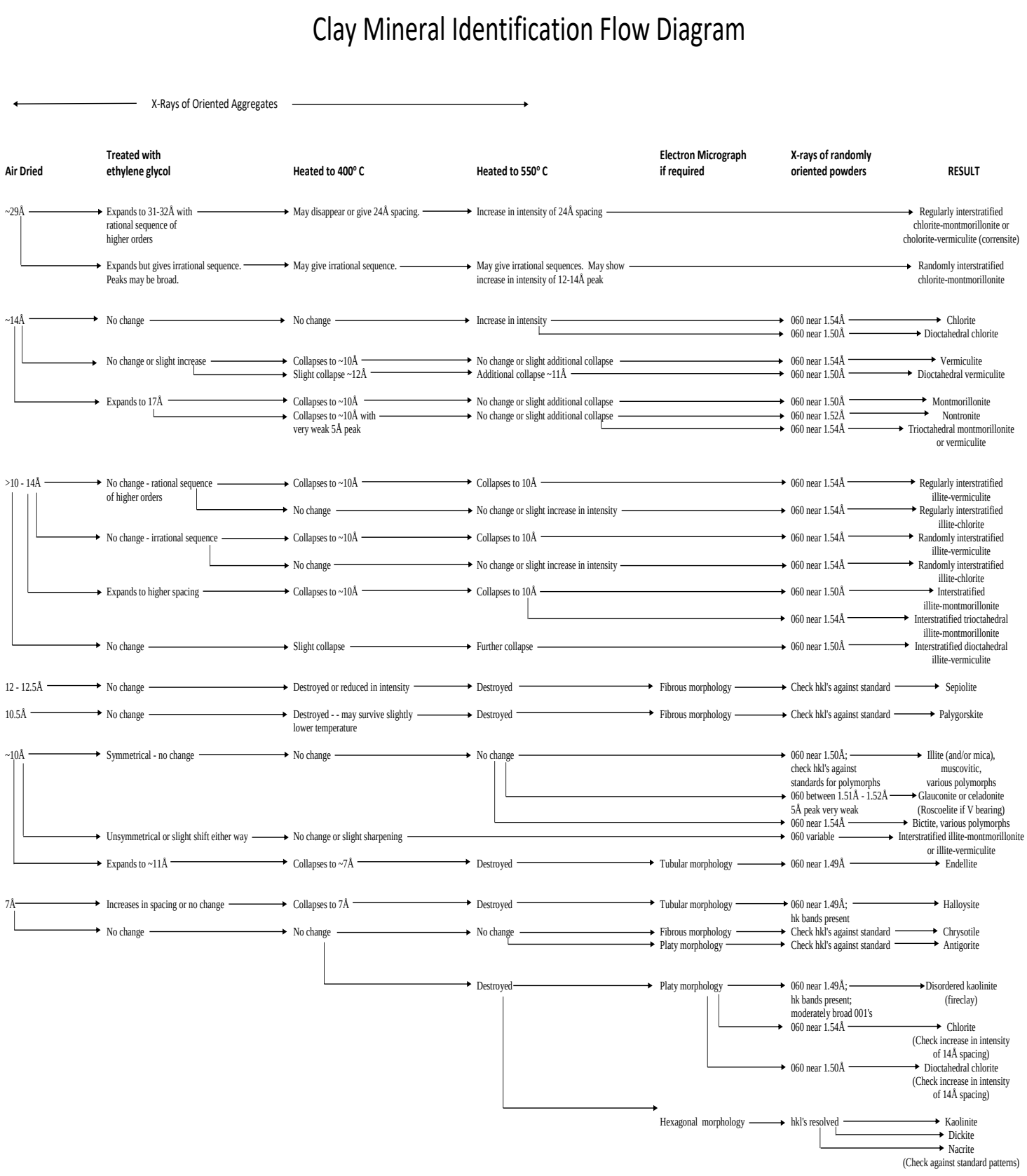

C2: W1-L1.5

W1-L1.5

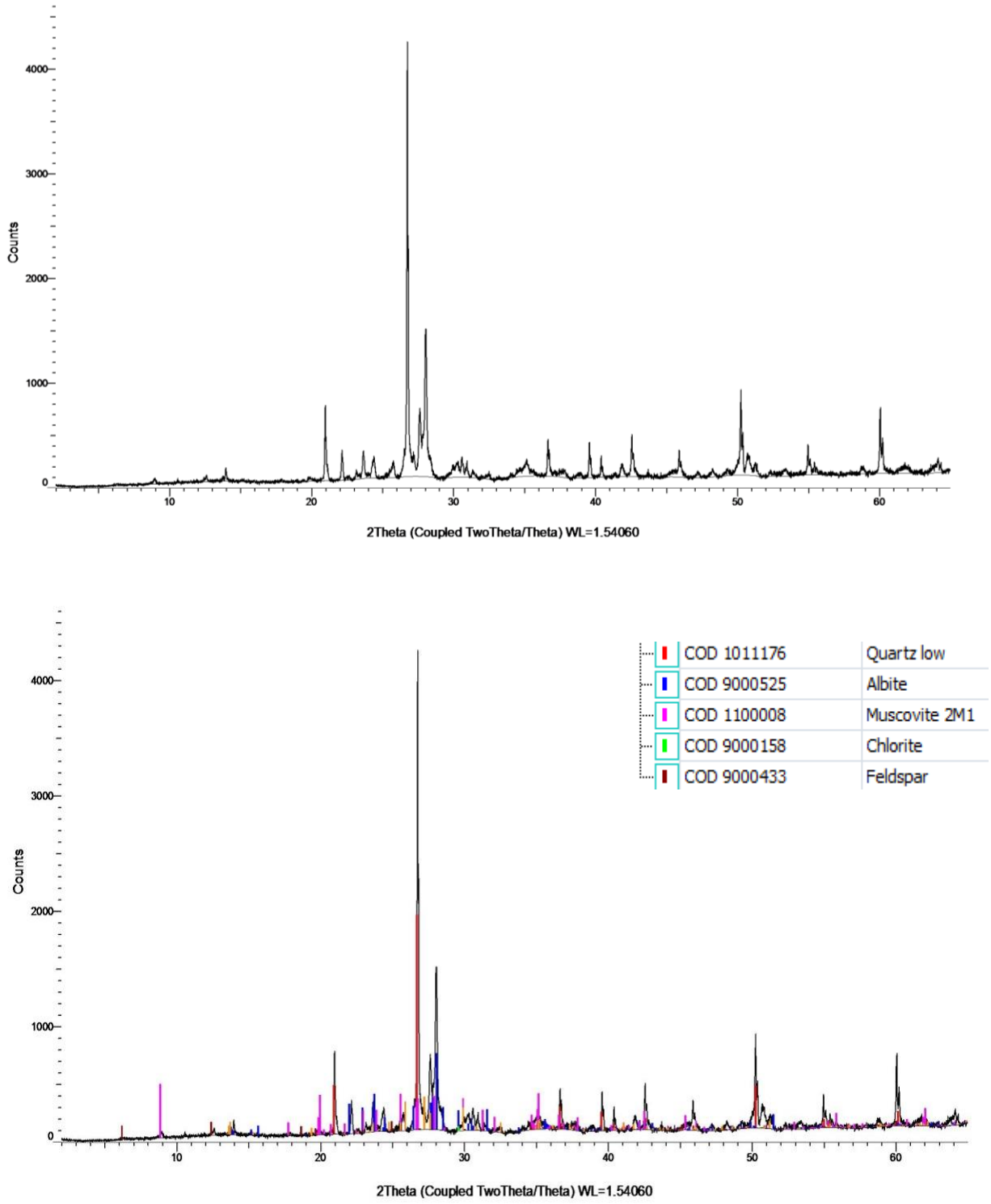

C2: W1-L2.5

W1-L2.5

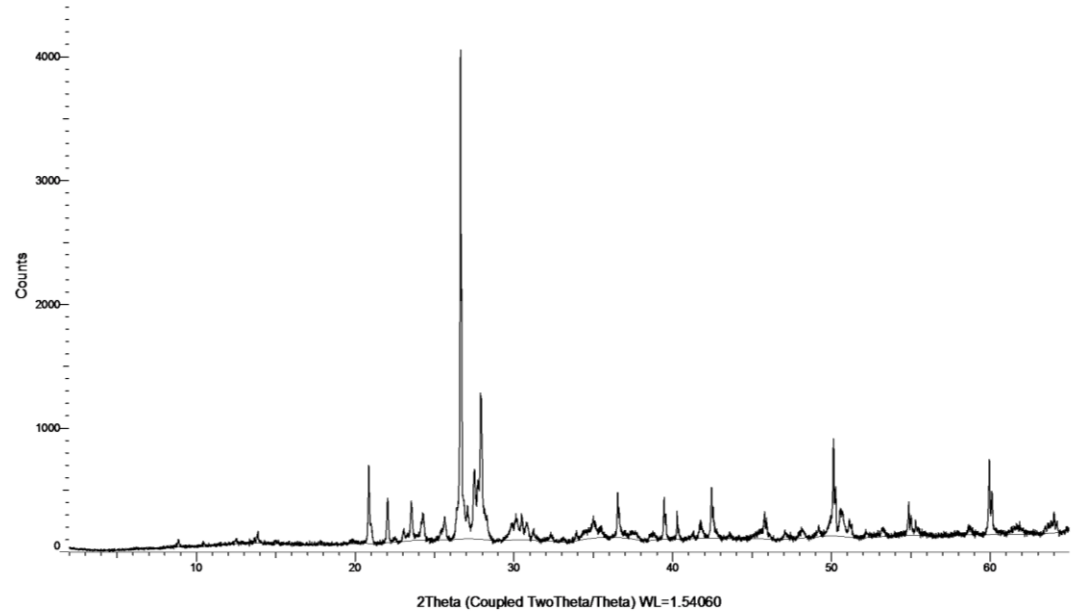

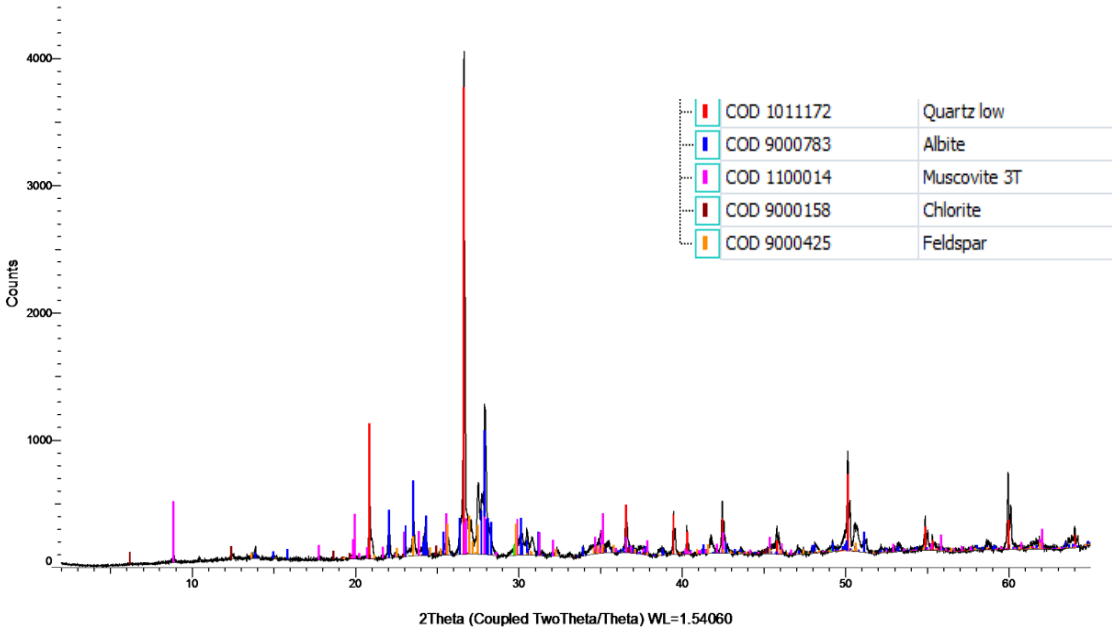

C3: W1-L3.5

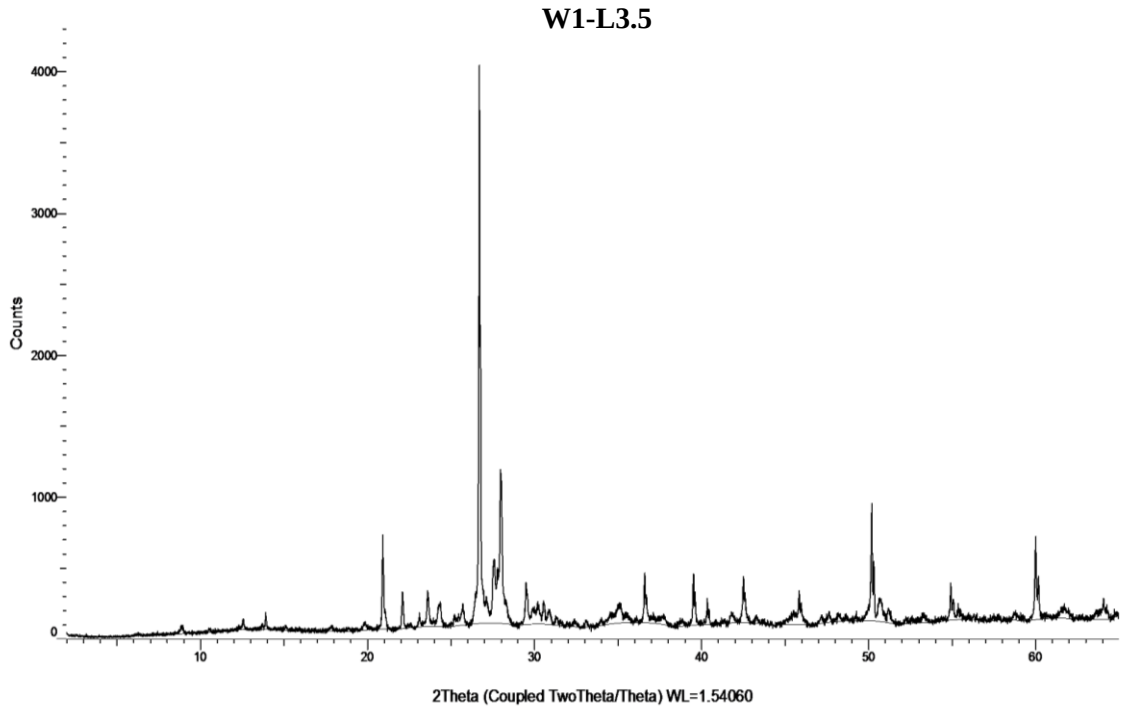
W1-L3.5
Counts
4000
3000
2000
1000
0
10
20
30
40
50
60
2Theta (Coupled TwoTheta/Theta) WL=1.54060

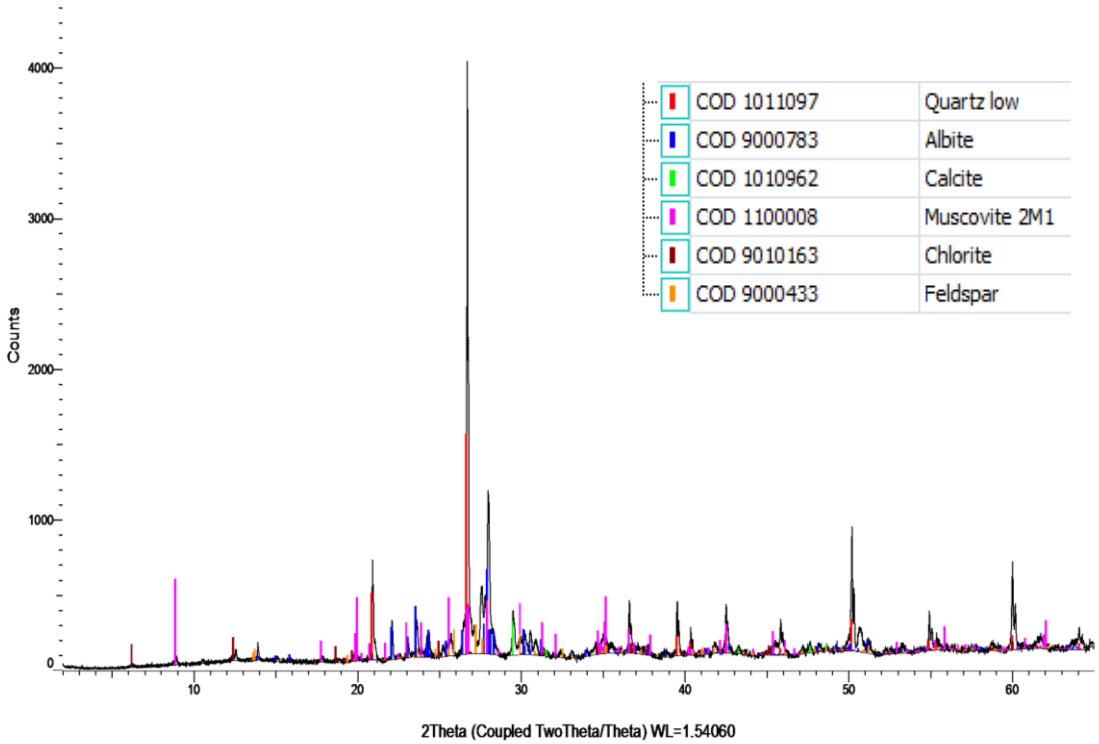
Counts
4000
3000
2000
1000
0
10
20
30
40
50
60
2Theta (Coupled TwoTheta/Theta) WL=1.54060
COD 1011097
Quartz low
COD 9000783
Albite
COD 1010962
Calcite
COD 1100008
Muscovite 2M1
COD 9010163
Chlorite
COD 9000433
Feldspar

C4: W1-B1

W1-B1

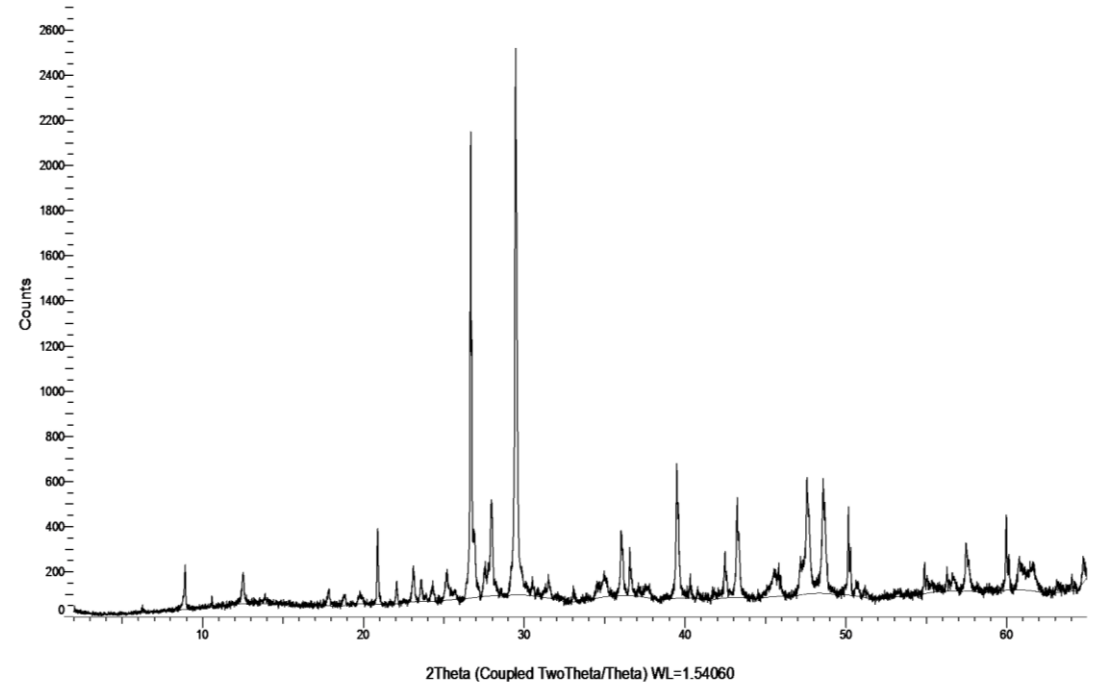
Counts
2600
2400
2200
2000
1800
1600
1400
1200
1000
800
600
400
200
0
10
20
30
40
50
60
2Theta (Coupled TwoTheta/Theta) WL=1.54060

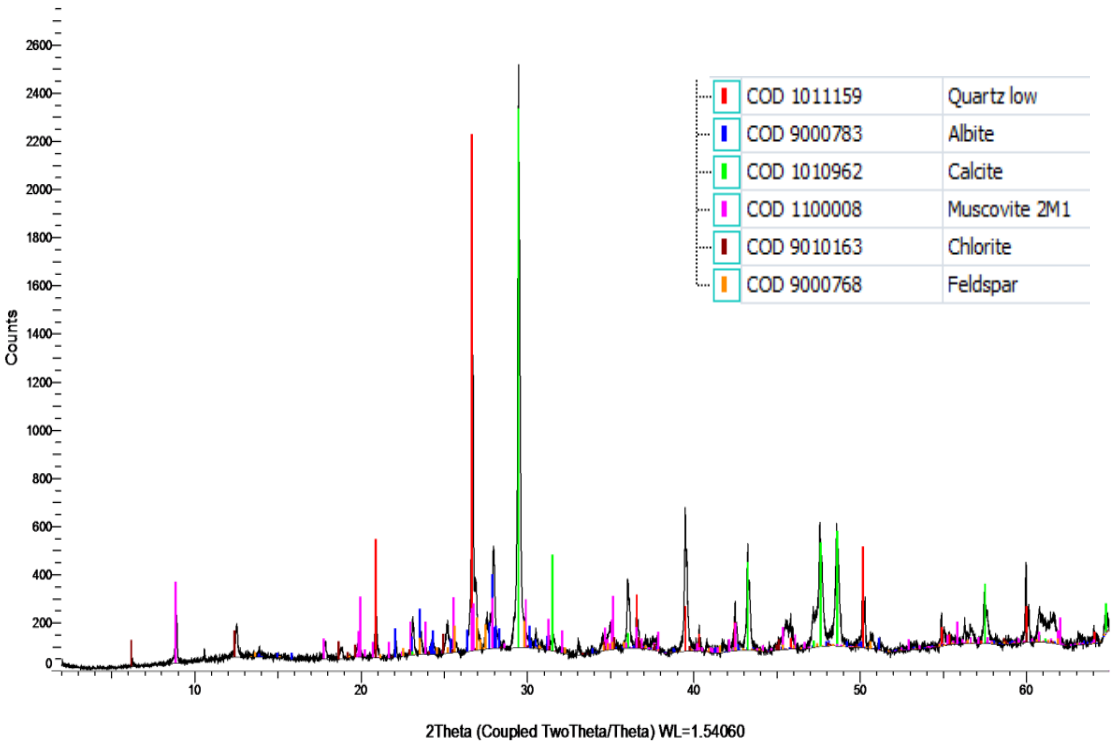
Counts
2600
2400
2200
2000
1800
1600
1400
1200
1000
800
600
400
200
0
10
20
30
40
50
60
2Theta (Coupled TwoTheta/Theta) WL=1.54060
COD 1011159
Quartz low
COD 9000783
Albite
COD 1010962
Calcite
COD 1100008
Muscovite 2M1
COD 9010163
Chlorite
COD 9000768
Feldspar

C5: W1-B1.5

W1-B1.5

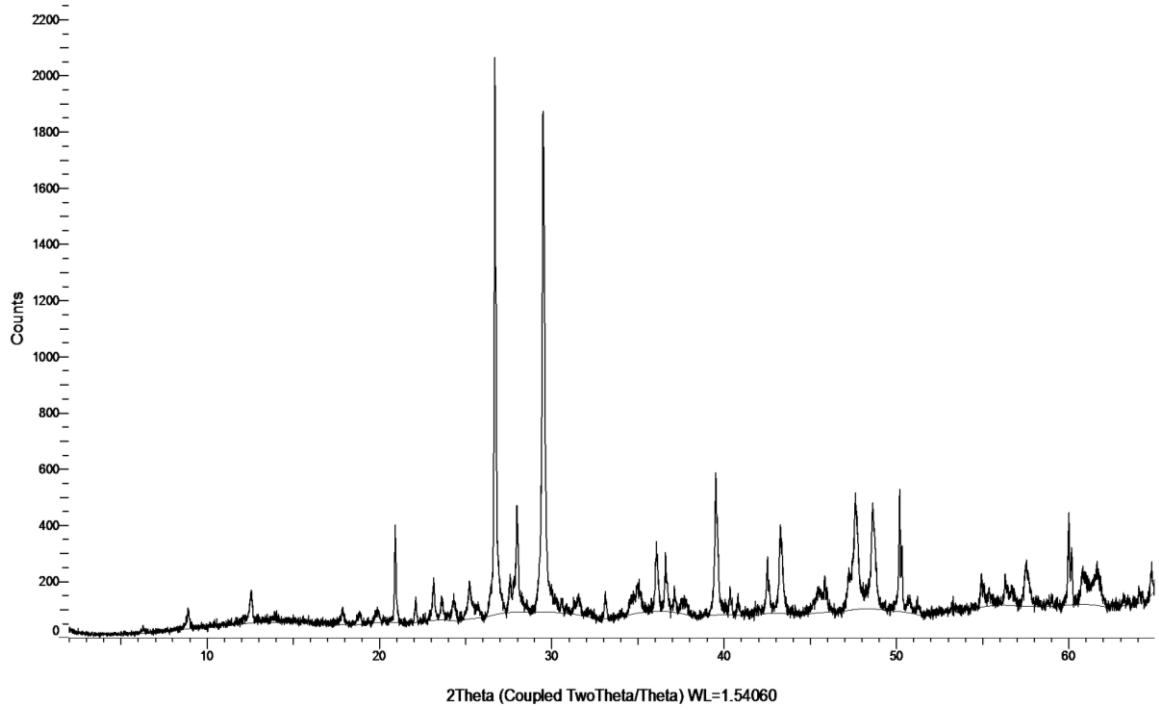

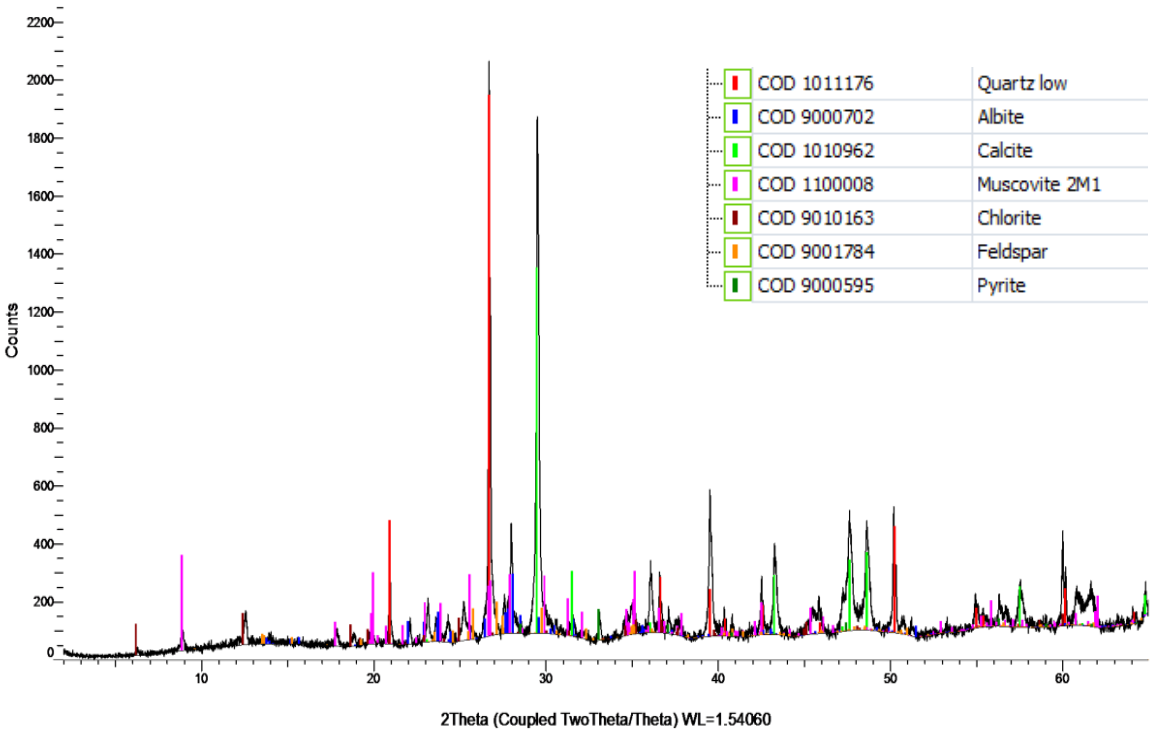

C6: W1-B4

W1-B4

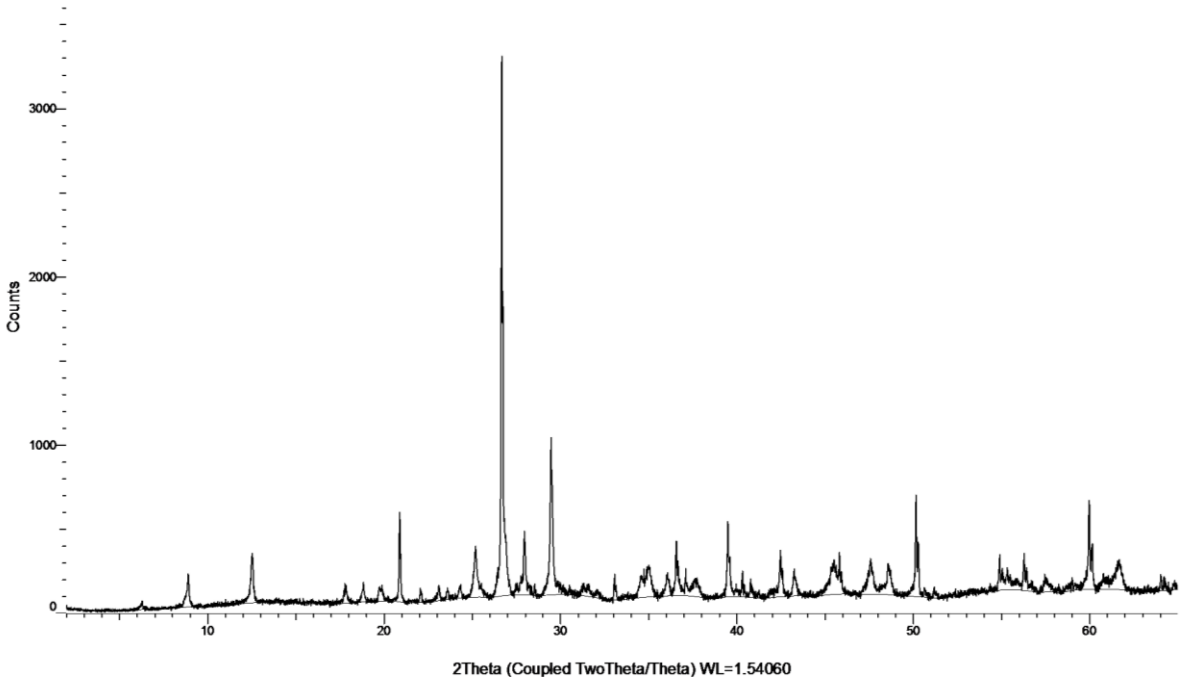
Counts
3000
2000
1000
0
10
20
30
40
50
60
2Theta (Coupled TwoTheta/Theta) WL=1.54060

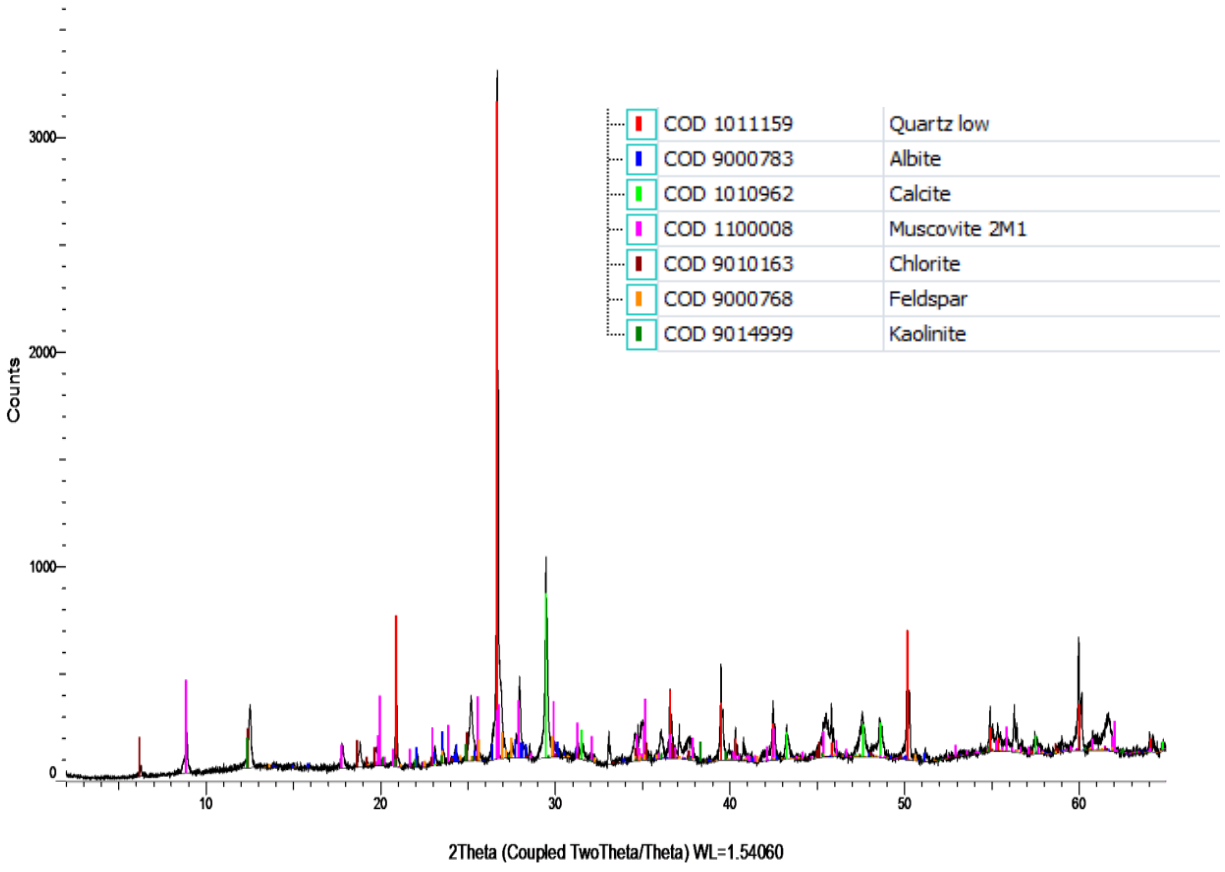
COD 1011159 Quartz low
COD 9000783 Albite
COD 1010962 Calcite
COD 1100008 Muscovite 2M1
COD 9010163 Chlorite
COD 9000768 Feldspar
COD 9014999 Kaolinite
Counts
3000
2000
1000
0
10
20
30
40
50
60
2Theta (Coupled TwoTheta/Theta) WL=1.54060

C7: W2-L1

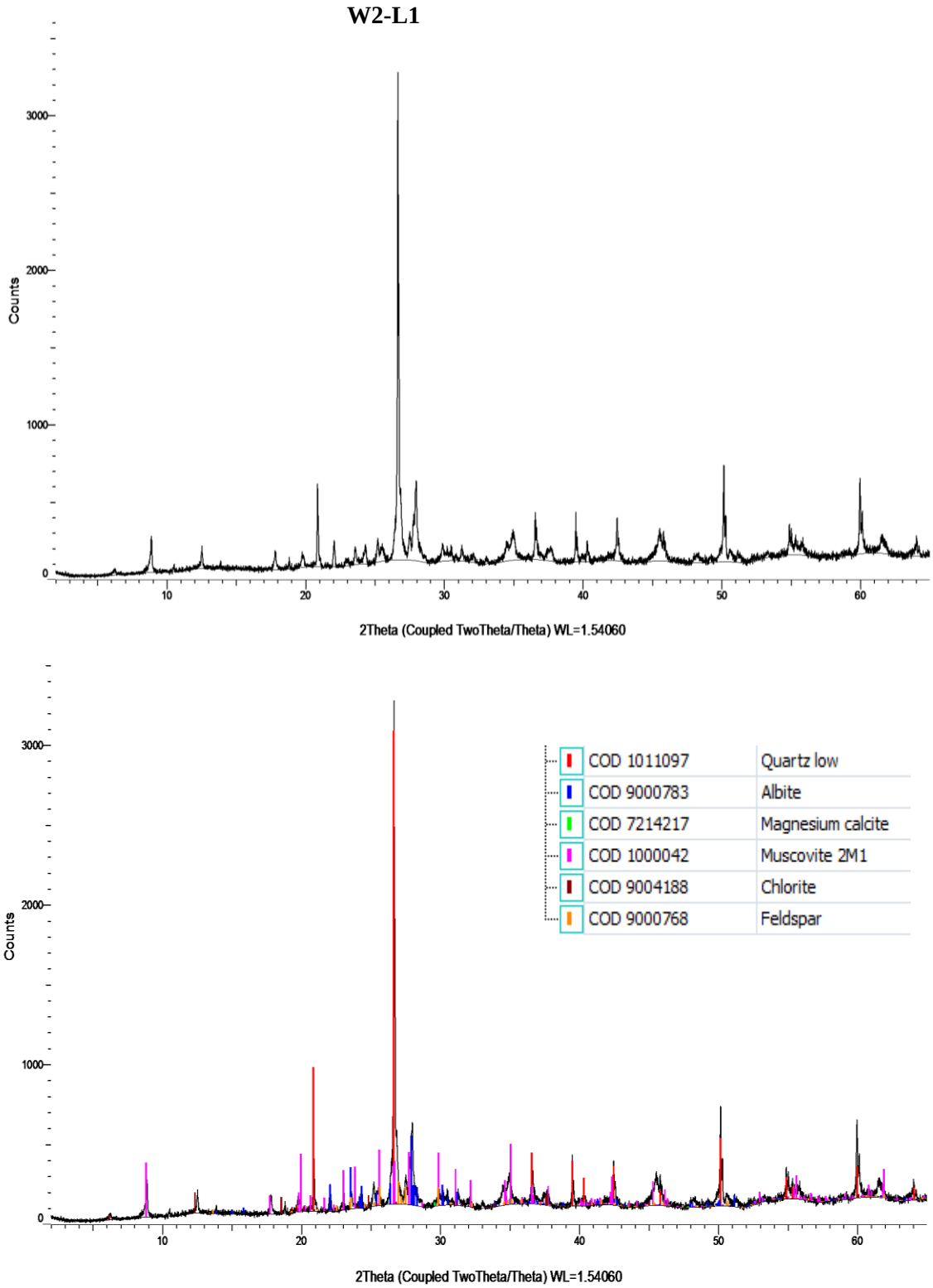
W2-L1
Counts
3000
2000
1000
0
10
20
30
40
50
60
2Theta (Coupled TwoTheta/Theta) WL=1.54060
COD 1011097
Quartz low
COD 9000783
Albite
COD 7214217
Magnesium calcite
COD 1000042
Muscovite 2M1
COD 9004188
Chlorite
COD 9000768
Feldspar

C8: W2-B1

W2-B1

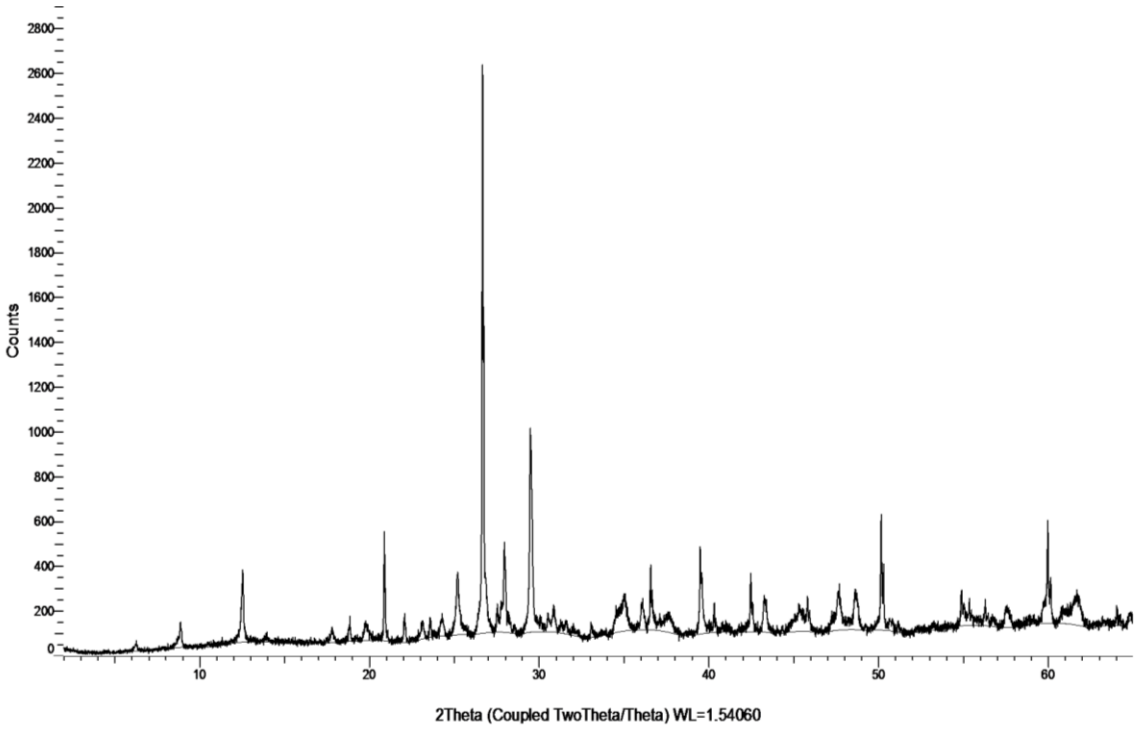
Counts
2Theta (Coupled TwoTheta/Theta) WL=1.54060

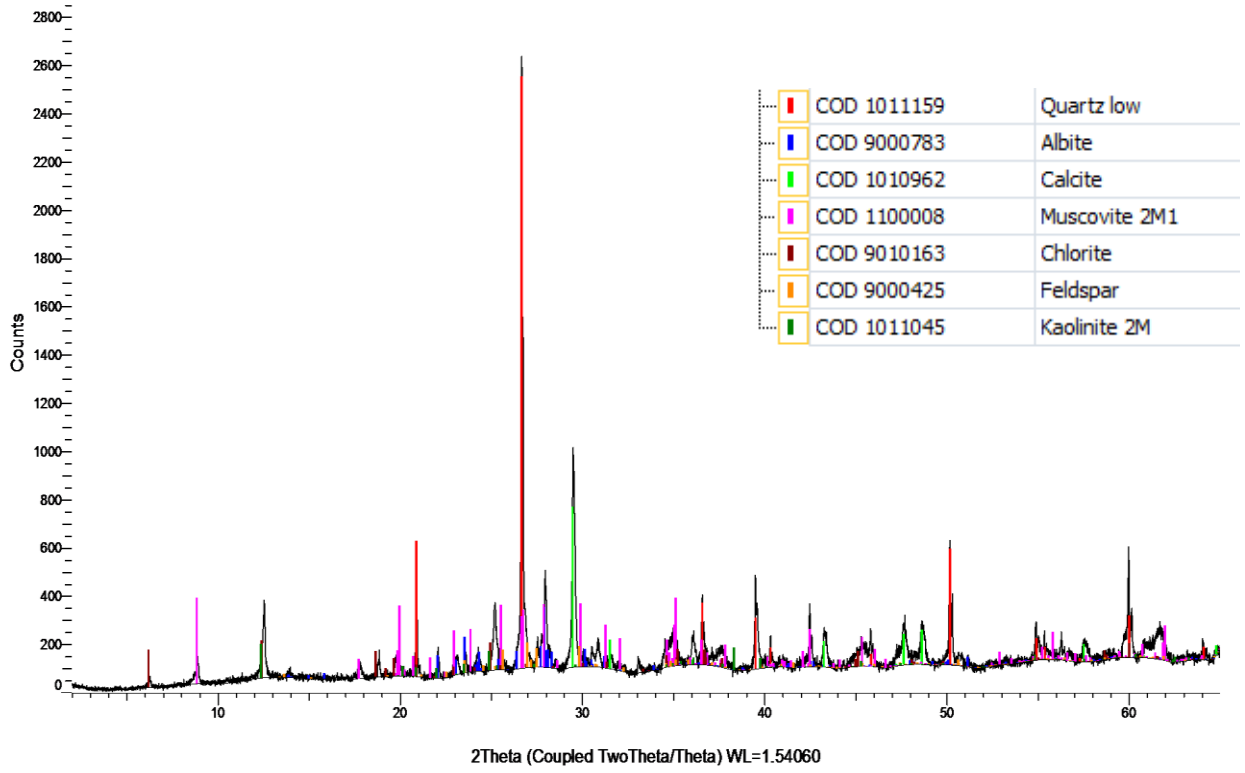
COD 1011159 Quartz low
COD 9000783 Albite
COD 1010962 Calcite
COD 1100008 Muscovite 2M1
COD 9010163 Chlorite
COD 9000425 Feldspar
COD 1011045 Kaolinite 2M
Counts
2Theta (Coupled TwoTheta/Theta) WL=1.54060

C9: W2-B4

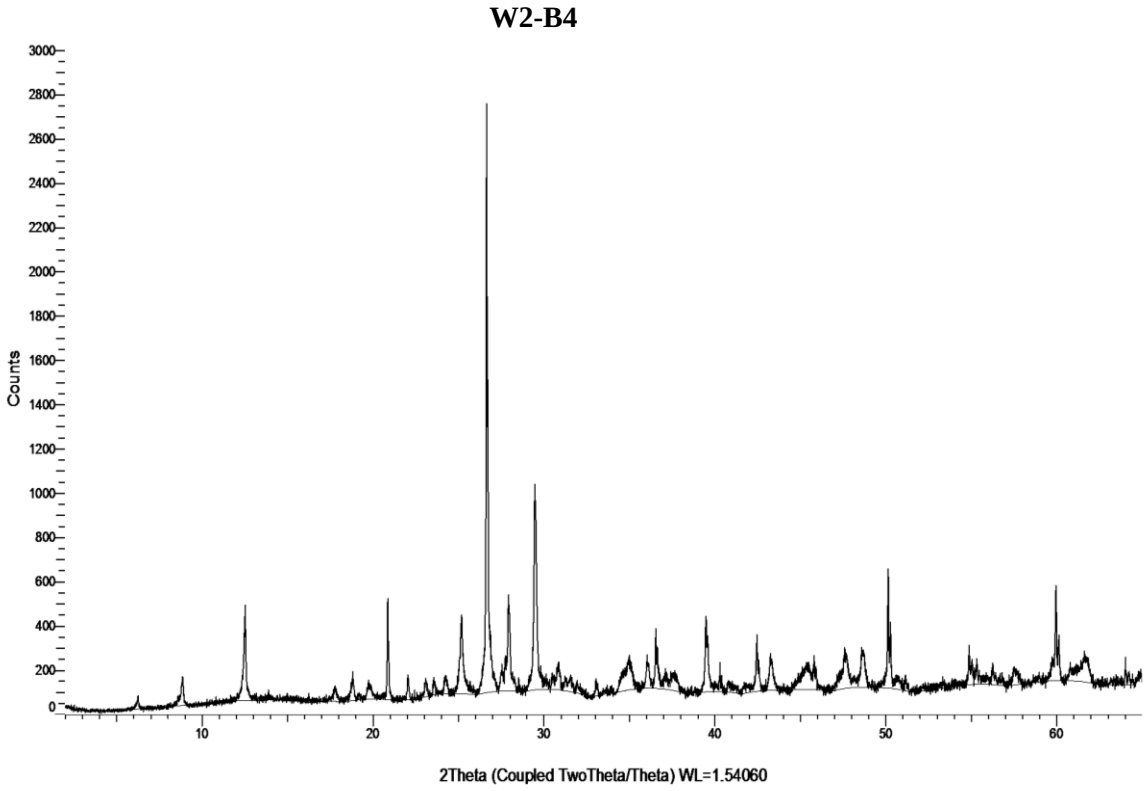
W2-B4
Counts
2Theta (Coupled TwoTheta/Theta) WL=1.54060

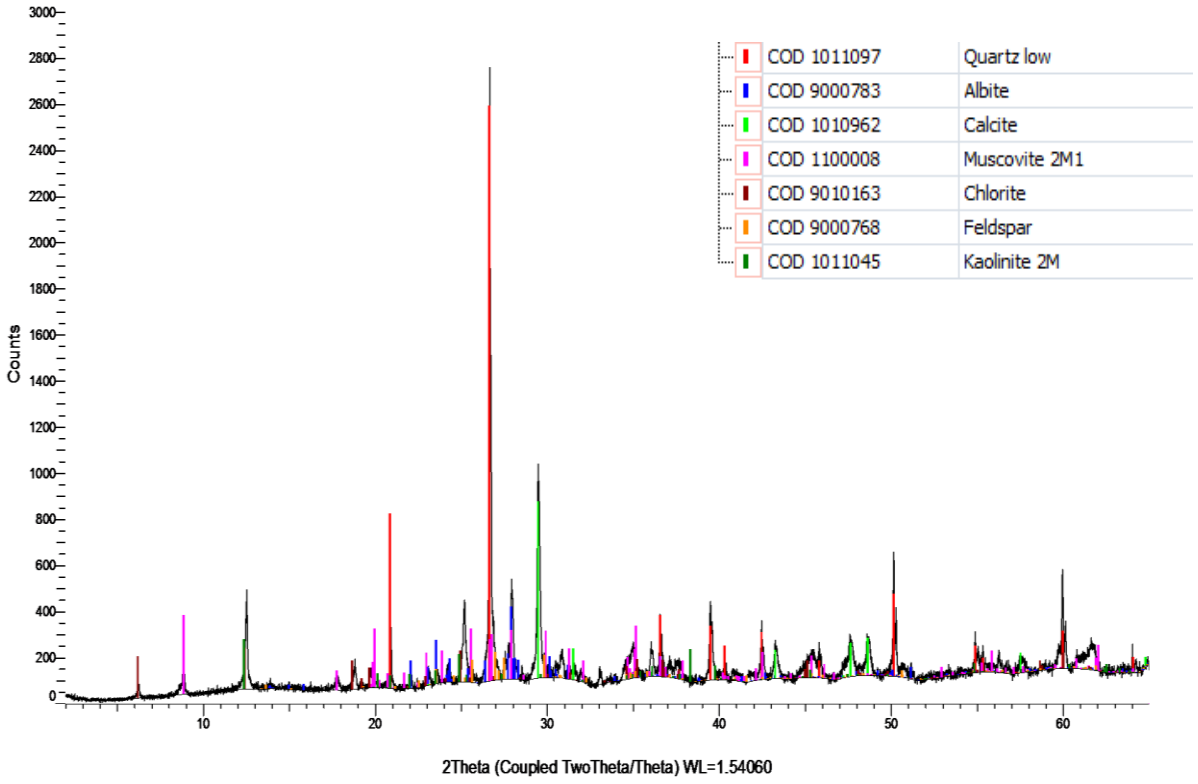
COD 1011097 Quartz low
COD 9000783 Albite
COD 1010962 Calcite
COD 1100008 Muscovite 2M1
COD 9010163 Chlorite
COD 9000768 Feldspar
COD 1011045 Kaolinite 2M
Counts
2Theta (Coupled TwoTheta/Theta) WL=1.54060

C10: W3-L4

W3-L4

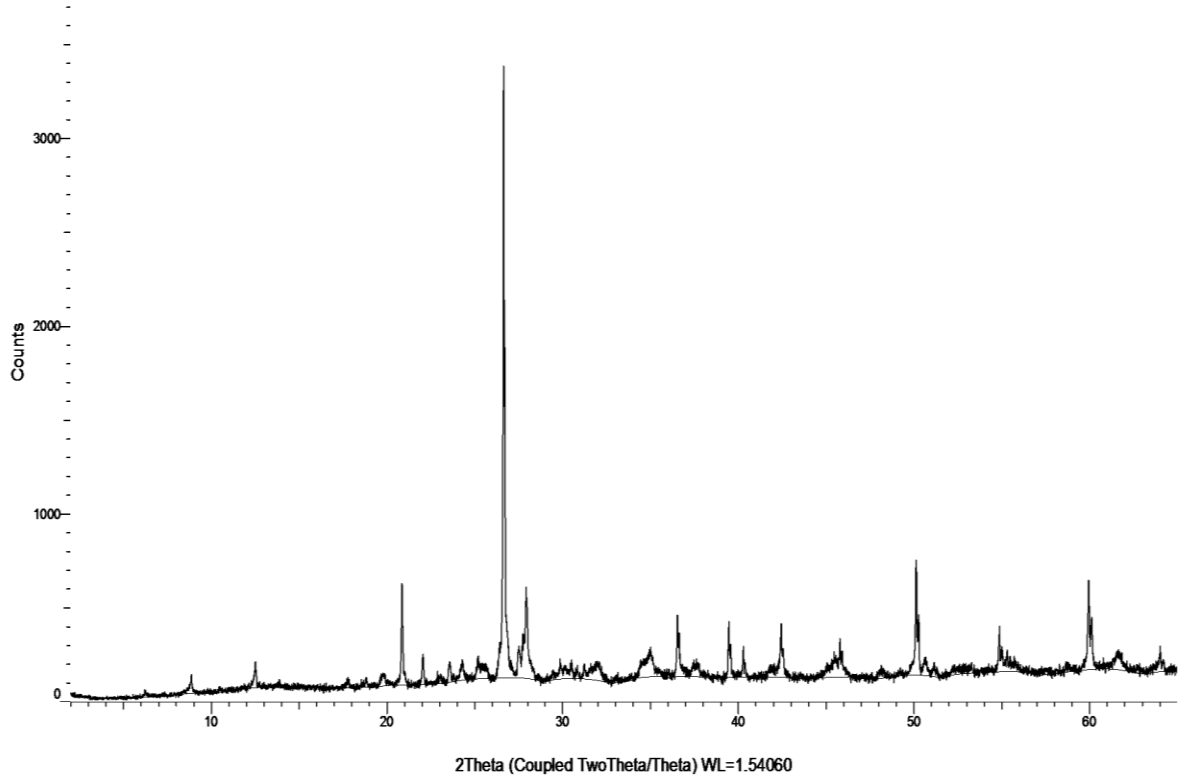

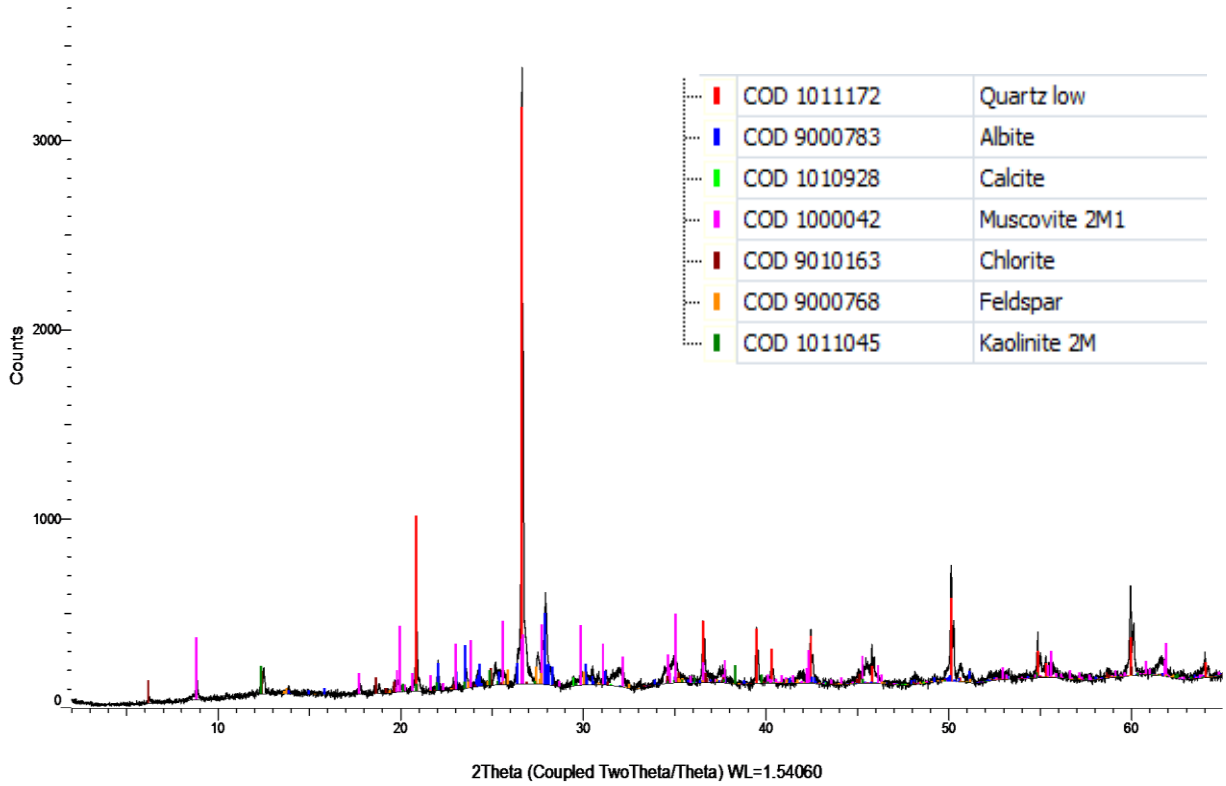

Appendix D: XRF data

D1: Chemical composition of fusion beads

D2: Chemical composition of pressed powder pellets - 1

D3: Chemical composition of pressed powder pellets - 2

D1. Chemical composition obtained from XRF analysis of fusion beads. NA = Not detected

Sample	SiO_2 (%)	Al_2O_3 (%)	Fe_2O_3 (%)	CaO (%)	K_2O (%)	MgO (%)	Na_2O (%)	MnO (%)	P_2O_5 (%)	Cl (%)	CuO (%)	ZnO (%)	TiO_2 (%)	SO_3 (%)
W1-L1.5	67.82	15.47	4.39	1.06	4.13	1.16	3.07	0.15	0.15	0.04	NA	NA	0.60	0.02
W1-L2.5	68.55	15.26	3.93	1.04	4.33	1.00	3.51	0.13	0.14	NA	NA	NA	0.67	0.02
W1-L3.5	64.54	14.97	4.69	3.03	3.97	1.50	2.85	0.12	0.12	NA	NA	NA	0.68	0.44
W1-B1	39.06	11.43	3.73	20.52	2.80	2.12	1.22	0.09	0.09	NA	NA	NA	0.47	0.68
W1-B1.5	43.73	11.95	4.12	17.20	3.01	2.01	1.41	0.09	0.10	NA	NA	NA	0.52	0.75
W1-B4	51.87	16.00	6.66	6.98	3.88	3.37	0.86	0.05	0.08	0.04	NA	NA	0.67	0.90
W2-L1	59.63	18.13	7.06	1.46	4.26	2.78	1.73	0.10	0.20	0.04	NA	NA	0.80	0.07
W2-B1	47.52	15.99	6.76	9.29	3.32	3.53	1.26	0.14	0.26	NA	NA	NA	0.64	0.56
W2-B4	46.90	15.87	6.83	9.72	3.34	3.58	1.23	0.14	0.28	NA	NA	NA	0.65	0.61
W3-L4	53.36	14.76	8.78	1.98	3.28	2.06	1.63	0.14	0.52	NA	0.08	0.14	0.64	0.16

D2. Chemical composition obtained from XRF analysis of press pellets. All elements are given in ppm (parts per million). Sample W2-L1 and W3-L4 were not analyzed for trace elements due to lack of sample material (used for clay diffraction, XRD). NA = Not detected.

Sample	Ag	As	Ba	Bi	Br	Cd	Ce	Co	Cr	Cr	Cs	Cu	Ga	Hf	La	Mo	Nb	Nd
W1-L1.5	15.2	35.0	508.7	13.7	6.8	11.7	131.9	12.1	56.8	56.8	6.1	12.9	19.8	7.4	56.8	4.3	53.3	44.8
W1-L2.5	14.3	35.8	491.4	13.1	6.0	7.6	130.6	8.5	46.3	46.3	6.9	11.2	20.1	5.6	65.7	2.3	61.4	43.2
W1-L3.5	15.3	40.7	542.1	14.6	6.2	7.1	125.1	10.4	81.4	81.4	7.0	12.6	20.9	9.2	65.8	2.3	56.4	44.7
W1-B1	18.6	43.0	457.6	17.1	6.7	9.0	56.9	7.5	88.1	88.1	8.5	6.5	12.2	2.8	26.4	0.5	14.4	20.7
W1-B1.5	18.7	48.0	652.9	17.2	6.4	5.8	64.8	18.1	152.4	152.4	9.7	18.0	20.2	4.2	37.3	0.6	14.7	23.9
W1-B4	17.4	44.5	419.2	16.6	6.4	9.2	54.6	10.0	87.6	87.6	7.5	10.1	14.3	4.7	31.1	0.8	21.2	20.9
W2-B1	22.3	44.1	859.2	15.2	6.9	9.6	63.3	23.9	146.6	146.6	11.0	34.7	17.6	1.7	34.6	0.9	15.8	20.6
W2-B4	17.4	42.6	831.3	15.1	6.1	9.6	63.8	25.0	136.1	136.1	10.1	29.8	16.6	3.9	41.0	0.9	18.0	21.4

D3. Chemical composition of minor element obtained from XRF analysis of press pellets. All elements are given in ppm (parts per million). Sample W2-L1 and W3-L4 were not analyzed for trace elements due to lack of sample material (used for clay diffraction, XRD). NA = Not detected

Sample	Ni	P	Pb	Rb	Sc	Se	Sm	Sn	Sr	Ta	Th	Tl	U	V	W	Y	Yb	Zn	Zr
W1-L1.5	29.3	689.6	28.2	123.5	9.5	5.6	10.8	3.5	124.6	3.2	10.9	18.5	2.8	94.6	2.4	28.5	1.7	67.7	283.3
W1-L2.5	28.8	630.2	23.7	126.6	9.1	6.0	3.2	2.4	111.1	3.9	11.2	18.3	2.9	81.9	2.2	33.1	2.0	68.8	325.0
W1-L3.5	41.8	634.2	21.6	128.4	10.1	5.7	6.9	5.4	164.5	2.7	13.0	20.5	2.0	89.1	NA	33.7	4.7	70.7	363.6
W1-B1	40.6	405.1	13.5	85.6	5.7	7.1	2.0	1.1	369.2	0.3	6.7	22.2	2.1	69.7	2.7	17.8	NA	40.4	120.1
W1-B1.5	94.3	329.6	18.8	152.9	15.9	7.3	5.8	1.9	237.5	0.1	10.3	23.0	3.8	137.8	1.1	22.6	2.8	75.4	144.7
W1-B4	44.2	413.7	15.3	101.5	8.2	7.7	0.4	NA	320.7	0.6	8.5	22.6	3.4	77.3	1.6	21.4	1.1	46.3	170.5
W2-B1	98.6	969.7	35.9	120.2	17.4	7.5	8.5	2.4	404.3	NA	7.5	24.2	4.8	125.8	2.1	24.5	0.9	87.5	136.5
W2-B4	92.7	946.6	24.5	108.5	17.3	6.7	2.4	2.0	392.7	1.5	7.3	20.8	4.0	116.2	1.8	23.8	1.4	83.1	158.3

Appendix E: Unsaturated zone

E1: Major cations and anions

E2: Trace elements

E3: Grain size distribution analysis

E4: Infiltration test; TD1, TD2, TD3

E5: Infiltration test; TD1, TD2, TD3

E6: Infiltration test; TD4, TD5, TD6, TD7

E7: Infiltration test; TD4, TD5, TD6, TD7

E8: Infiltration test; TD8, TD9, TD10, TD11

E9: Infiltration test; TD8, TD9, TD10, TD11

E1. Major cation and anion concentration in the unsaturated zone (mg/g dry weight). NA = Not detected

Sample	Na	K	Mg	Ca	F	Cl	SO_4	Br	NO_3	PO_4
W1-L1.5	0.018	0.008	0.008	0.056	0.004	0.013	0.014	0.004	0.003	0.006
W1-L2.5	0.008	0.017	0.010	0.096	0.005	0.003	0.009	0.004	N.A.	0.008
W1-L3.5	0.008	0.018	0.010	0.035	0.010	0.006	0.007	0.004	0.004	0.009
W2-L1	0.149	0.030	0.014	0.140	0.005	0.008	0.150	0.009	0.003	0.012
W2-L2	0.022	0.012	0.012	0.044	0.012	0.022	0.019	0.004	0.003	0.009
W3-L1	0.017	0.022	0.009	0.224	0.006	0.003	0.041	0.009	0.011	0.010
W3-L2	0.017	0.032	0.009	0.248	0.005	0.006	0.186	0.008	0.031	0.009
W3-L4	0.042	0.059	0.024	0.332	0.003	0.096	0.127	0.038	0.002	0.013

E2. Trace element concentration in the unsaturated zone (µg/g dry weight)

Sample	B	Al	Cr	Mn	Fe	Ni	Cu	Zn	As	Se	Sr	Pb
W1-L1.5	0.539	2.110	0.005	1.088	2.660	0.063	0.156	0.024	0.047	0.006	0.973	0.002
W1-L2.5	0.747	0.408	0.005	11.284	2.295	0.095	0.302	0.038	0.098	0.016	2.396	0.003
W1-L3.5	0.289	2.519	0.008	0.530	1.463	0.033	0.024	0.025	0.013	0.001	0.492	0.001
W2-L1	0.277	0.241	0.007	0.556	0.776	0.036	0.158	0.026	0.031	0.004	2.421	0.001
W3-L1	0.288	0.214	0.007	0.519	0.752	0.037	0.189	0.016	0.031	0.003	2.485	0.000
W3-L4	2.255	1.054	0.042	9.368	5.885	0.230	0.245	0.510	0.115	0.005	3.087	0.010

E3: Grain size distribution analysis

Sample	Weight (g)	< 2 µm	> 2 µm	> 63 µm	> 125 µm	> 250 µm	> 500 µm	> 1 mm	> 2 mm	> 4 mm	> 8 mm
T1	163.3	5.3	25.88	22.77	23.61	11.43	6.59	1.45	0.13	0.35	0.00
T2	133.10	5.58	33.08	25.58	11.69	7.42	6.95	4.00	1.32	0.31	0.26
T3	212.7	1.41	6.69	6.87	9.74	12.66	12.28	12.27	9.56	11.19	14.59
T4	232.6	1.14	6.6	6.81	7.85	10.47	14.84	14.45	13.06	12.52	12.25
T6	224.1	0.41	3.55	2.56	3.20	3.89	5.93	9.71	11.26	12.45	46.36
T9	183.3	1.23	5.48	10.43	5.23	12.01	5.68	24.81	23.26	4.02	6.82
T11	188.5	1.7	10.51	5.99	11.44	15.63	26.94	14.41	10.83	0.94	0.79

E4: Infiltration test; TD1, TD2, TD3

TD1 Time (min)	Height(m)	Infiltration (cm/h)	TD2 Time (min)	Height(m)	Infiltration (cm/h)	TD3 Time (min)	Height(m)	Infiltration (cm/h)
0	45		0	45		1	45	
0.5	42	600.0	0.5	37.7	1460.0	2	30.5	1450.0
1.5	38.5	350.0	1.5	29	870.0	3	22.4	810.0
3	35.6	193.3	3	21	533.3	4	16.7	570.0
3.5	34.7	180.0	3.5	18.6	480.0	5	12.5	420.0
4.5	33	170.0	4.5	15.4	320.0	6	9.5	300.0
6	31	133.3	6.5	10.2	260.0	6.5	8	300.0
8	29	100.0	8	7.5	180.0	7.5	6	200.0
10	27	100.0	9	5.9	160.0	8	5	200.0
12	25.2	90.0	10	4.4	150.0	8.5	4	200.0
14	23.9	65.0	11	3.2	120.0	9	3.1	180.0
16	22.5	70.0	11.5	45	-	9.5	2.4	140.0
18	21.4	55.0	12.5	41.1	390.0	10	1.7	140.0
20	20.3	55.0	13.5	37.5	360.0	10.5	45	-
22	19.2	55.0	14.5	34.2	330.0	12	38.5	433.3
24	18.2	50.0	15.5	31.4	280.0	13	34.2	430.0
26	17.3	45.0	17	27.5	260.0	14	30	420.0
28	16.5	40.0	19	23	225.0	15	27	300.0
30	15.8	35.0	21	19.2	190.0	16	24	300.0
34	14.3	37.5	23	16	160.0	18	19	250.0
38	12.9	35.0	25	13.3	135.0	20	14.8	210.0
42	11.5	35.0	27	10.8	125.0	22	11.5	165.0
46	10.1	35.0	29	8.6	110.0	24	8.6	145.0
50	8.9	30.0	32	5.8	93.3	26	6	130.0
54	7.9	25.0	34	4	90.0	28	4	100.0
58	6.9	25.0	34.5	45	-	30	2	100.0

E5: Infiltration test; TD1, TD2, TD3

TD1 Time (min)	Height(m)	Infiltration (cm/h)	TD2 Time (min)	Height(m)	Infiltration (cm/h)	TD3 Time (min)	Height(m)	Infiltration (cm/h)
70	4.2	22.5	40	33.7	200.0	34	34.5	300.0
70.5	45		42	30	185.0	36	29.5	250.0
74	41.8	91.4	44	26.8	-7.6	38	25	225.0
78	38.5	82.5	46	24	140.0	40	21.5	175.0
82	35.5	75.0	48	21.4	130.0	42	18.2	165.0
86	33	62.5	50	19	120.0	44	15.5	135.0
90	30.6	60.0	52	16.8	110.0	46	13	125.0
94	28.4	55.0	54	14.7	105.0	48	10.8	110.0
96	27.4	50.0	56	12.8	95.0	50	8.5	115.0
100	26	35.0	58	11	90.0	52	6.6	95.0
104	25	25.0	60	9.2	90.0	54	4.8	90.0
108	24.1	22.5	62	7.8	70.0	56	3	90.0
112	23.2	22.5	64	6.4	70.0	56.5	45	-
			66	5	70.0	58	41	266.7
			68	3.6	70.0	60	36	250.0
			68.5	45		62	31.6	220.0
			70	42	200.0	64	27.6	200.0
			73	36.7	176.7	66	24.4	160.0
			74	35	170.0	68	21.4	150.0
			76	32	150.0	70	18.6	140.0
			78	29.2	140.0	73	15	120.0
			80	26.8	120.0	74	14	100.0
			82	24.4	120.0	76	12	100.0
			84	22.3	105.0	78	10	100.0
			86	20.2	105.0	80	8	100.0
			88	18.4	90.0	82	6.5	75.0
			90	16.7	85.0	84	5	75.0
			92	15.2	75.0	86	3.5	75.0
			94	13.8	70.0	88	2.1	70.0
			96	12.5	65.0	89	1.4	70.0
			98	11.2	65.0	90	0.7	70
			100	9.9	65.0			

E6: Infiltration test; TD4, TD5, TD6

TD4 Time (min)	Height(m)	Infiltration (cm/h)	TD5 Time (min)	Height(m)	Infiltration (cm/h)	TD6 Time (min)	Height(m)	Infiltration (cm/h)	TD7 Time (min)	Height(m)	Infiltration (cm/h)
0	45		0	45		0	45		0	45	
4	27.3	266	4	32	198	5	44.8	2	5	27	216.0
8	18.3	135	8	23	140	10	44.6	2	10	15	144.0
12	12.5	87	12	16	105	15	44.3	4	15	7	96.0
16	8.5	60	16	10	86	20	44	4	18	3	80.0
20	5	53	20	5	72	32	43.2	4	18.5	45	-
20.5	45	-	21	45	-	36	43	3	20	41	160.0
24	38.8	106	24	37	137	41	42.8	2	25	29	144.0
28	32	102	28	29	120	51	42.6	1	32	17	102.9
32	26	90	32	22	101	55	42.5	2	36	11.5	82.5
36	20.7	80	36	17	87	60	42.4	1	41	5	78.0
40	15.3	81	40	12	75				43.5	2	72.0
45	9	76	45	7	56				44	45	-
45.5	45	-	46	45	-				51	31.5	115.7
49	38	120	49	38	120				55	25	97.5
53	30	120	53	31	105				62	16	77.1
57	22	120	57	25	86						
60	16.5	110	60	22	66						
65	8.5	96	65	18	54						

E7: Infiltration test; TD4, TD5, TD6

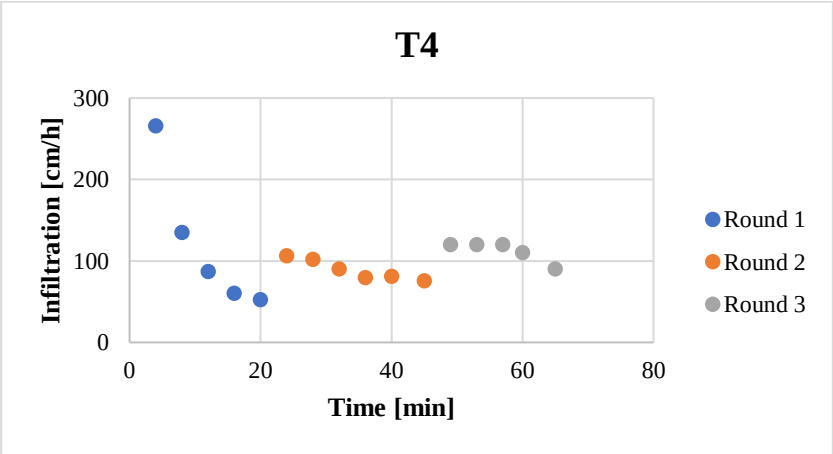

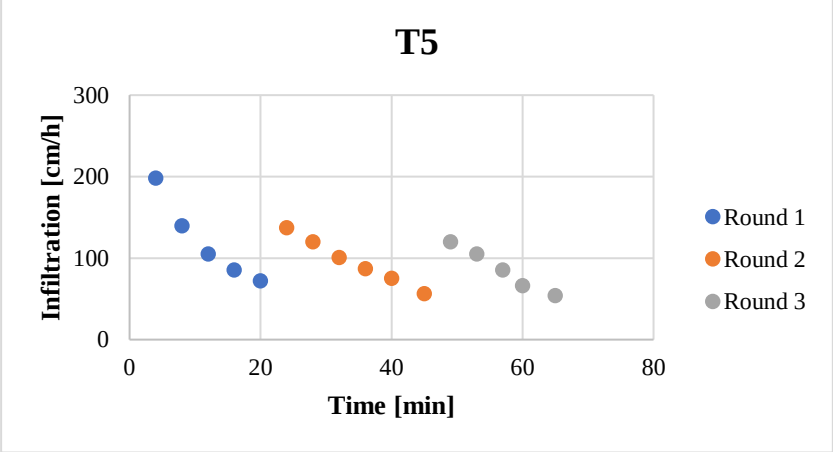

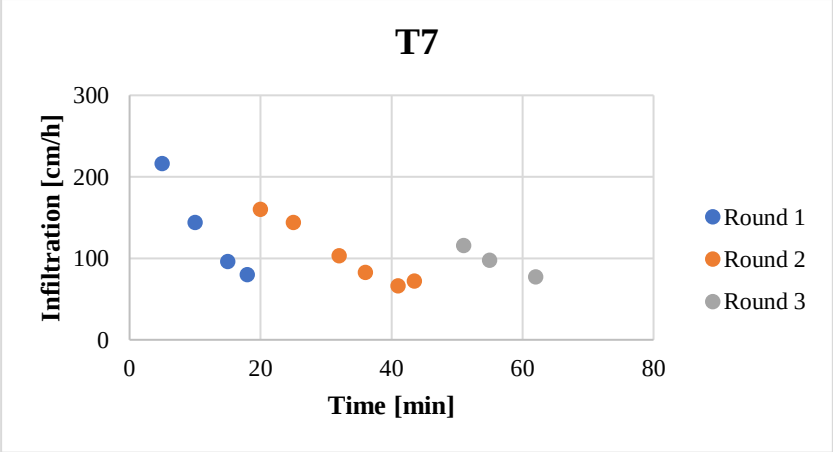

E8:Infiltration test; TD8, TD9, TD10, TD11

TD8 Time (min)	Height(m)	Infiltration (cm/h)	TD9 Time (min)	Height(m)	Infiltration (cm/h)	TD10 Time (min)	Height(m)	Infiltration (cm/h)	TD11 Time (min)	Height(m)	Infiltration (cm/h)
0	45		0	45		0	45		0	45	
4	25.5	293	4	31	210	4	37.7	110	4	41	60
8	14	173	8	22.3	131	8	33	71	8	37.5	52.5
12	7.5	98	12	16	95	12	29	60	12	34.3	48
12.5	45	-	16	11	75	16	26	45	16	31.7	39
16	33.8	192	20	7	60	20	23.6	36	20	29.2	37.5
20	23.8	150	24	4	45	24	21.2	36	24	27	33
24	16.3	113	24.5	45	-	28	19.2	30	28	25	30
28	11	80	28	37.8	123	32	17.5	26	32	23.1	28.5
32	6.5	68	32	31	102	36	15.8	26	36	21.4	25.5
32.5	45	.	36	26	75	40	14	27	40	19.9	22.5
36	37.3	132	40	21.5	68	44	12.8	18	44	18.4	22.5
40	29.8	113	44	17.8	56	48	11.4	21	48	17	21
44	23.8	90	48	14.3	54	52	10	21	52	15.9	16.5
48	18	87	52	11	52	56	9	17	56	15	13.5
52	15	45	56	8.5	50	60	8	15	60	14.2	12
56	11.5	53	60	6	48				65	13.2	12
60	8.3	48							70	12.2	12

E9:Infiltration test; TD8, TD9, TD10, TD11